Norway Lobster and *Hematodinium sp.* in the Clyde: modelling the population dynamics of a commercially important host-parasite system

Hazel Smith

January 2021

This thesis is submitted to the University of Strathclyde for the degree of Doctor of Philosophy in the Faculty of Science

Copyright Declaration

Signed:

Date:

Abstract

The Norway lobster, *Nephrops norvegicus*, also commonly known as the Dublin Bay prawn, langoustine or scampi, is a burrow-dwelling crustacean abundant in muddy areas across the North-East Atlantic. The species has a high commercial value for human consumption. Trawl and creel fisheries for *Nephrops* are among the most valuable in the UK, especially in Scotland. The Clyde Sea Area, on the west coast of Scotland, supports a particularly productive *Nephrops* fishery. In recent years, over 5000 tonnes of *Nephrops* have been landed annually in this region. However, *Nephrops* in the Clyde Sea Area carry a particularly high prevalence of a parasitic dinoflagellate species (*Hematodinium sp.*). This parasite causes drastic changes in the organs, tissues and haemolymph of infected individuals and is ultimately fatal. The overall meat quality of infected animals is also significantly reduced which leads to a drop in commercial value. Understanding the dynamics of the host-parasite relationship between *Nephrops* and *Hematodinium* and how this may change over time is therefore important for assessing the economic potential of *Nephrops* fisheries in the Clyde Sea Area.

This thesis describes the development of a *Nephrops-Hematodinium* population model which simulates the coupled dynamics of *Nephrops* and *Hematodinium* in the Clyde Sea Area. This includes a representation of harvesting by fisheries. The model involves a dynamic energy budget approach to modelling the moult cycle of *Nephrops*, embedded in an Escalator-Box-Car type representation of the development of annual cohorts of individuals. Resolving the moult cycle is critical since the life-cycle of the parasite is synchronised with moulting. *Nephrops* are vulnerable to infection by *Hematodinium* spores immediately following a moult event whilst their shell is still in a soft, post-moult condition. Furthermore, the *Nephrops* moult hormone, methyl farnesoate, is thought to cause *Hematodinium* to switch from the growth phase into the spore production phase. This ultimately leads to the mass release of parasitic spores which in turn leads to the death of the infected host.

Observational detection of *Hematodinium* in sampled *Nephrops* is a complex process. Visual effects of infection only manifest once the host is heavily-infected. In the early stages of infection, molecular and immunological tests are required to detect the parasite.

The *Nephrops-Hematodinium* population model is designed to mimic the detection thresholds for the various tests, so that the model can be directly tested against field data on *Hematodinium* prevalence collected by field surveys.

Analysis of the performance of the *Nephrops-Hematodinium* population model relative to observational data leads to a paradigm-shift regarding understanding of the parasite life-cycle within the host. The existing assumption that infection to sporulation must occur within a single year is shown to be unsustainable. The parasite life-cycle can take up to 2 years or more, depending on the moulting rate of the host – which in turn depends on its size at infection. Inter-moult intervals increase with size, but follow different schedules for males and females. As a result, *Hematodinium* prevalence is strongly dependent on size and sex, with females and smaller individuals more vulnerable to infection. This is an emergent property of the *Nephrops-Hematodinium* population model and is also replicated in field observations. As a corollary of this, population-level prevalence estimates obtained from the various diagnostic tests are dependent on the size-selectivity of fishing gears used to sample animals in the field.

Furthermore, the *Nephrops-Hematodinium* population model is also used to conduct scenario experiments on the effects of parasite prevalence for fishery yields. The presence of the parasite in the Clyde Sea Area was estimated to cause a 10-15% reduction in potential yields. In the actual fishery, visually infected animals are typically discarded at sea since they detract from the value of the catch. However, it is estimated that a proportion of these survive and go on to release spores and perpetuate the infection. The *Nephrops-Hematodinium* population model was used to assess the consequences of ceasing this discarding practice and instead bringing infected animals ashore for disposal. The results showed that this operation change could lead to a small reduction in overall prevalence alongside a small increase in yield.

Supporting investigations in this thesis include the development of a new method for predicting suitable *Nephrops* habitat in the Clyde Sea Area. Larval-transport connectivity between patches of suitable sediment is investigated using particle tracking methodology, driven by output from a high resolution hydrodynamic model of the region. The results show a high rate of larval retention from patches in the northern regions of the Firth of Clyde. Patches of suitable sediment in the southern regions of the Firth of Clyde, on the other hand, were found to export a greater proportion of larvae, with some larvae from this region settling on suitable sediment in the Sound of Jura. These results provide a basis for a future implementation of the *Nephrops-Hematodinium* population model in spatially discrete patches, interconnected by the larval transport simulations.

Acknowledgements

Firstly I would like to thank my supervisors - Douglas Speirs, Mike Heath, Douglas Neil and Helen Dobby - for their guidance and support throughout this project. Secondly, I would also like to thank my friends, office mates and other members of the marine group who have all helped to make the PhD process as enjoyable as possible. A special mention must go to Hoa Nguyen - your 1 o'clock knock on my office door was always the highlight of my time in the office. Thank you for your friendship, support and daily dose of encouragement, without which this thesis would never have reached completion.

Furthermore, I am thankful to have had a number of memorable experiences throughout the course of my PhD. Particular thanks must go to Douglas Neil for allowing me to help with lab-work at Glasgow University. This provided me with the opportunity to gain valuable first hand experience in *Hematodinium* sampling techniques. During my time as a PhD student, I was also lucky enough to participate in two separate trips aboard Marine Scotland research vessels. In June 2016 I spent four days on FRV Scotia as part of the *Nephrops* Underwater TV Survey. Thanks to Helen Dobby and Ade Weetman for helping to organise this. Thanks also to Matt Pace for allowing me to help with his sediment sampling fieldwork aboard FRV Alba in October 2017.

Another highlight of my time as a PhD student was completing a three month internship with Scottish Natural Heritage, based in Battleby, Perth. This internship allowed me to delve briefly into a completely new research area looking at the population-level consequences of underwater noise from offshore windfarm construction on marine mammals. Thanks to Caroline Carter, Fiona Manson and Erica Knott for making this such an enjoyable experience.

Finally, thanks to Mum, Dad and Jillian for their support and encouragement throughout the course of this PhD. Thanks especially to Mum and Dad for having me home during the final months of thesis writing - the timing of which coincided with the coronavirus pandemic. I am grateful for the unexpected extra time we have had together. Thank you

for making this unusual time as enjoyable as possible and ensuring that hours of thesis writing were accompanied by an equal amount of fun. Thanks in particular for a summer filled with long ‘adventurous’ cycle rides and ice cream!

Contents

List of Figures

List of Tables

List of Abbreviations

alrg	Additive Log-Ratio Gravel
alrs	Additive Log-Ratio Sand
BGS	British Geological Survey
CL	Carapace Length
CSA	Clyde Sea Area
DEB	Dynamic Energy Budget
DVM	Diel Vertical Migration
ELISA	Enzyme Linked Immunoassay
FVCOM	Finite Volume Community Ocean Model
GAM	Generalised Additive Model
ICES	International Council for the Exploration of the Sea
MCRS	Minimum Conservation Reference Size
MI	Moult Increment
ODE	Ordinary Differential Equation
PCR	Polymerase Chain Reaction
UWTV	Underwater Television
VMS	Vessel Monitoring System

Chapter 1

Introduction

1.1 *Nephrops norvegicus*

Nephrops norvegicus (henceforth *Nephrops*) is a benthic crustacean belonging to the order Decapoda. *Nephrops* have the appearance of a typical clawed lobster, but can be easily distinguished by their slender body, long claws, and large, dark, kidney-shaped eyes, as shown in Figure 1.1. *Nephrops* are known by a number of alternative names, the most common of which is the Norway Lobster. Other names relate to the commercial processing of this species and include langoustine, scampi and Dublin Bay prawn.

Nephrops are widely distributed across the continental shelves of the north-east Atlantic and the Mediterranean (Bell et al., 2013). The distribution of the species is restricted to areas of muddy seabed sediment suitable for the construction of burrows. As a result, the overall distribution of *Nephrops* is highly discontinuous. More than 30 distinct *Nephrops* populations are located across European waters, the vast majority of which are physically isolated by large stretches of unsuitable sediment (Bell et al., 2013).

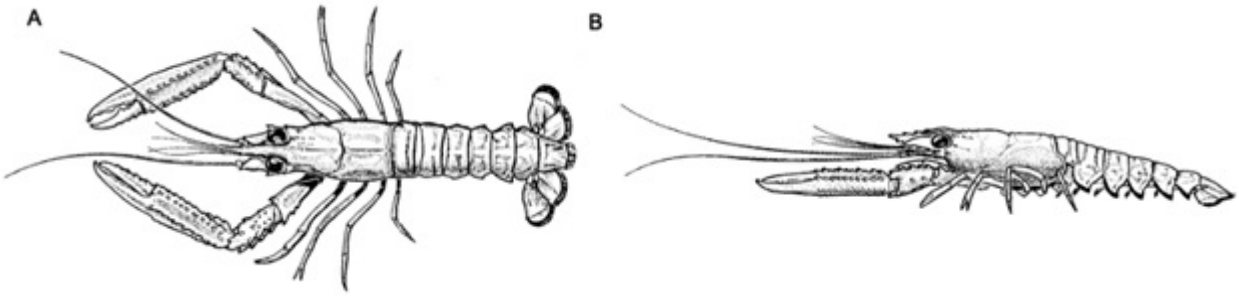

Figure 1.1: Dorsal (A) and lateral (B) view of *Nephrops norvegicus* (adapted from Howard (1989)).

Nephrops are fished extensively across their geographic range. Fisheries for the species can be found in the Mediterranean, the Skagerrak and Kattegat, the Bay of Biscay, the Irish Sea and the North Sea (Bell et al., 2013). One of the largest *Nephrops* fisheries is located in the Clyde Sea Area (CSA) on the west coast of Scotland. *Nephrops* caught in the CSA contribute around 20% of the total Scottish catch, and over 7% of the entire European catch (McIntyre et al., 2012).

The life-cycle of *Nephrops* differs significantly across its geographic range. Populations dwelling in the CSA (alongside populations in the Mediterranean, the Iberian Peninsula, the Bay of Biscay, the Irish Sea and the majority of the North Sea) follow an annual breeding cycle. The timing of key events in the reproductive cycle of *Nephrops* in the CSA are shown in Figure 1.2. In order for mating to occur, the outer cuticle of females must be in the soft, immediate post-moult condition (Bell et al., 2013). In the CSA, mature females moult in late spring (Field et al., 1992), with mating assumed to occur shortly afterwards. The ovaries of females then mature throughout the spring and summer months before egg laying occurs in late summer and early autumn. The eggs are incubated externally for approximately 9 months before the planktonic larvae hatch (Dickey-Collas et al., 2000). Shortly after releasing their eggs, the females moult, and mate again, thereby continuing the cycle.

However, populations dwelling in colder waters around Iceland and the Faroe Islands undertake a biennial breeding cycle (Bell et al., 2013). The lower temperatures in these regions significantly increase the length of the egg incubation period. This delays the hatching season and causes it to overlap with the spawning season. As a result, females dwelling in colder waters have insufficient time to complete the reproductive cycle within a single year.

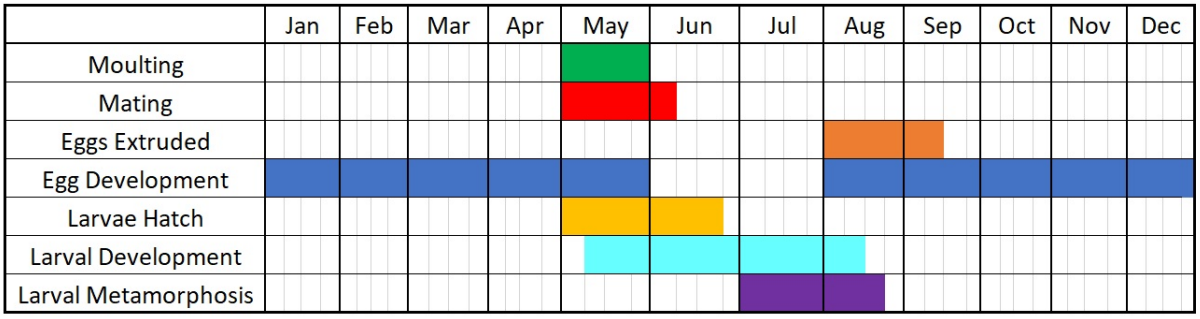

Figure 1.2: Diagram showing the timing of key events in the reproductive cycle of *Nephrops* in the CSA.

Nephrops larvae pass through three developmental zoeal stages, as shown in Figure 1.3. *Nephrops* zoea show minimal swimming ability and are dispersed primarily by the water currents. Towards the end of the third larval stage, the zoea become negatively phototactic and descend to the bottom of the water column where they then metamorphose into the adult form (Smith, 1987). Larval development in the CSA is thought to take around 70 days (Dickey-Collas et al., 2000). Larvae in this region therefore reach the point of metamorphosis around the month of July.

Individuals dispersed to patches of unsuitable sediment are unable to survive into adulthood. Individuals dispersed to patches of suitable *Nephrops* habitat are subject to a number of density dependent factors. This includes direct competition for space as well as cannibalism of younger individuals (ICES, 2000). Individuals which manage to successfully reach adulthood assume a relatively stationary life on the seabed, only leaving their burrows during periods of low light to undertake short foraging excursions. *Nephrops* are opportunistic predators and consume a wide variety of prey species including crustaceans, polychaetes, molluscs and echinoderms (Bell et al., 2013).

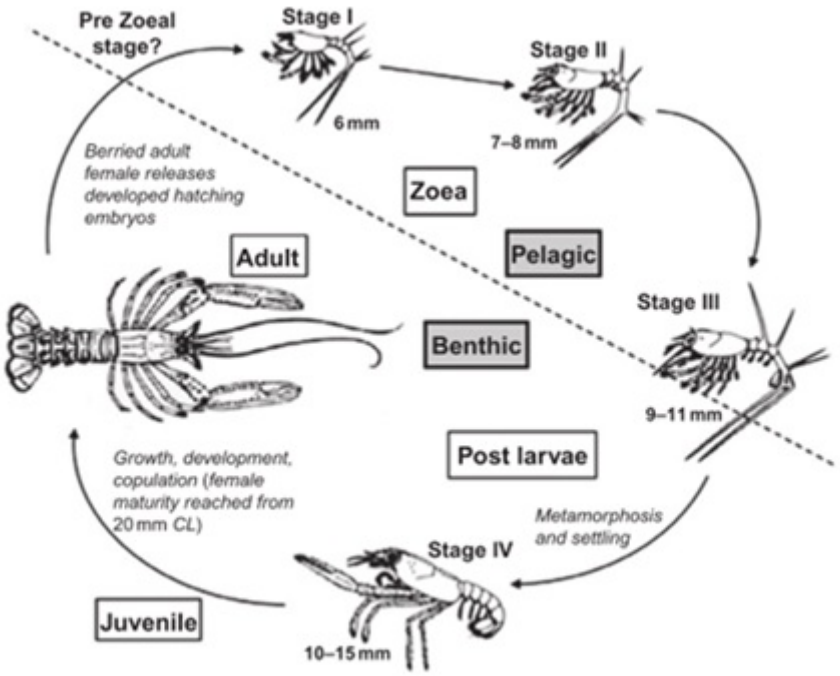

Figure 1.3: Life cycle of *Nephrops norvegicus* (Powell and Erikkson, 2013).

1.2 *Nephrops* Fisheries in the Clyde Sea Area

The Clyde Sea Area (CSA) on the west coast of Scotland encompasses an area of around 3600 km^2 (McIntyre et al., 2012). The region includes the Firth of Clyde and the Clyde Estuary as well as a number of fjordic sea lochs. The boundary of the CSA extends from the southern tip of the Mull of Kintyre to Corsewall Point, as shown in Figure 1.4.

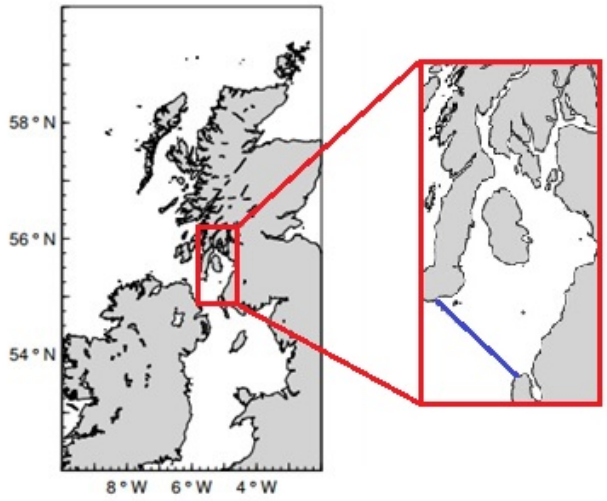

Figure 1.4: Map of the CSA on the west coast of Scotland. The blue line between the southern tip of the Mull of Kintyre and Corsewall Point represents the boundary of the CSA.

The CSA has a rich fishing heritage with evidence of fishing activity dating as far back as medieval times. Since this time the CSA has supported a number of important fisheries, including herring, haddock and cod. However, in recent years the region has witnessed a substantial shift in the composition of species caught. The CSA recently attracted media and scientific attention following the rapid decline of landings of demersal fish such as haddock, cod, saithe and whiting (see Figure 1.5). It was claimed that decades of overfishing had depleted fish stocks to such an extent that the region was now effectively a "marine desert" (Thurstan and Roberts, 2010). These claims were later found to be misleading since the total biomass of fish in the CSA has remained fairly stable over time. Overfishing has, however, caused a substantial decrease in the mean size of demersal fish (Heath and Speirs, 2012). As a result, demersal fish stocks in the CSA are currently unable to sustain commercial catches due to the lack of large marketable individuals in the population.

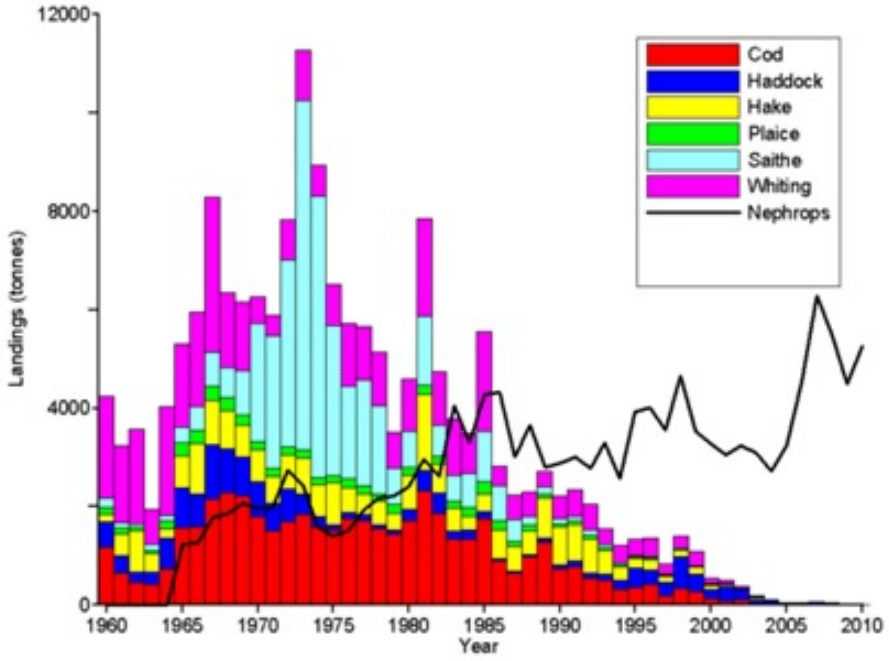

Figure 1.5: Landings of the main demersal fish species and *Nephrops* in the CSA since 1960 (McIntyre et al., 2012).

The reduction in the number of large predatory fish has been accompanied by a dramatic increase in landings of *Nephrops* and other benthic invertebrates. This pattern is typical of many heavily exploited marine ecosystems (Howarth et al., 2014). *Nephrops* are now the most commercially important species landed in the CSA and make up around 84% of landings by weight and 87% by value (Howarth et al., 2014). The remaining percentages are composed solely of other invertebrates such as scallops, crabs and lobster. Since 2003, the only landings of demersal fish in the CSA have been by-catch from the *Nephrops* fishery (Heath and Speirs, 2012). *Nephrops* contribute several million pounds of revenue to the local economy and, paradoxically, now provide a resource which is economically more valuable than the multi-species fisheries which existed before.

Nephrops in the CSA are caught using two main methods: demersal otter trawling and creeling (baited traps). These two methods target different markets, with smaller trawl-caught *Nephrops* generally sold as scampi (the separated tails, de-shelled and coated) and larger creel-caught individuals generally sold as langoustine (the whole animal, fresh or frozen). Creel caught *Nephrops* are usually of higher quality and therefore attract a much higher price at market. Creeling, however, is restricted to the upper sea-lochs of the CSA. Creel-caught *Nephrops* therefore only make up a small proportion of the overall catch (< 5 %) (ICES, 2015).

A major problem affecting *Nephrops* fisheries in the CSA is infection by the parasitic dinoflagellate *Hematodinium*. *Hematodinium* infections were first reported in the CSA in the early 1980s (Field et al., 1992). Recent surveys conducted in 2018-19 have revealed that *Hematodinium* infections are still present in the region (I. Molto-Martin and A. Albalat, pers com.). *Hematodinium* causes a reduction in overall meat quality and leads to an increase in overall mortality rates. *Hematodinium* infections therefore have important economic implications for fisheries in the CSA, the majority of which now rely solely on *Nephrops* as their main source of income.

1.3 *Hematodinium*

Hematodinium is a genus of parasitic dinoflagellate which primarily infects crustaceans (Shields, 1994). The parasite was first discovered in *Carcinus maenas* (green shore crab) and *Liocarcinus depurator* (harbour crab) off the coast of France (Chatton and Poisson, 1931). *Hematodinium* infections have since been reported in over 40 species of marine crustaceans worldwide (Rowley et al., 2015). This includes *Callinectes sapidus* (blue crab) and *Chionoecetes bairdi* (tanner crab) in North America, *Portunus armatus* (sand crab) in Australia and *Portunus trituberculatus* (Chinese swimming crab) in northern Asia. *Hematodinium* infections have also been recorded in *Nephrops* populations across Europe including the west coast of Scotland (Field et al., 1992, 1998; Stentiford et al., 2001c), the Irish Sea and the Skaggerak and Kattegat (Briggs and McAliskey, 2002).

Only two species of the genus *Hematodinium* have been identified to date: *Hematodinium perezi* and *Hematodinium australis*. The parasite associated with *Nephrops* is considered to be a separate species (Stentiford and Shields, 2005). This species, however, is yet to be formally identified and is therefore referred to as *Hematodinium sp.* However, for simplicity I will refer to it solely as *Hematodinium* for the remainder of this thesis.

Advanced stages of *Hematodinium* infections cause a characteristic change in the colour of infected hosts, with heavily-infected individuals often described as 'chalky' or 'milky-white'. Heavily-infected individuals can therefore be easily identified, as shown in Figure 1.6. These characteristic colour changes are accompanied by a reduction in overall meat quality. The muscle tissue of heavily-infected individuals enters into a state of advanced autolysis which renders it bland in taste (Albalat et al., 2012). This reduces the market value of heavily-infected individuals and often leads to the selective discarding of visibly-infected individuals.

Hematodinium infections also cause a significant increase in mortality rates. *Hematodinium* is able to evade the immune system of the host (Rowley et al., 2015). This prevents infected individuals from recovering from the infection (Stentiford et al., 2001b). Consequently, it is thought that all *Hematodinium* infections eventually result in the death of infected individuals. *Hematodinium* infections therefore have important implications for fisheries operating within infected regions.

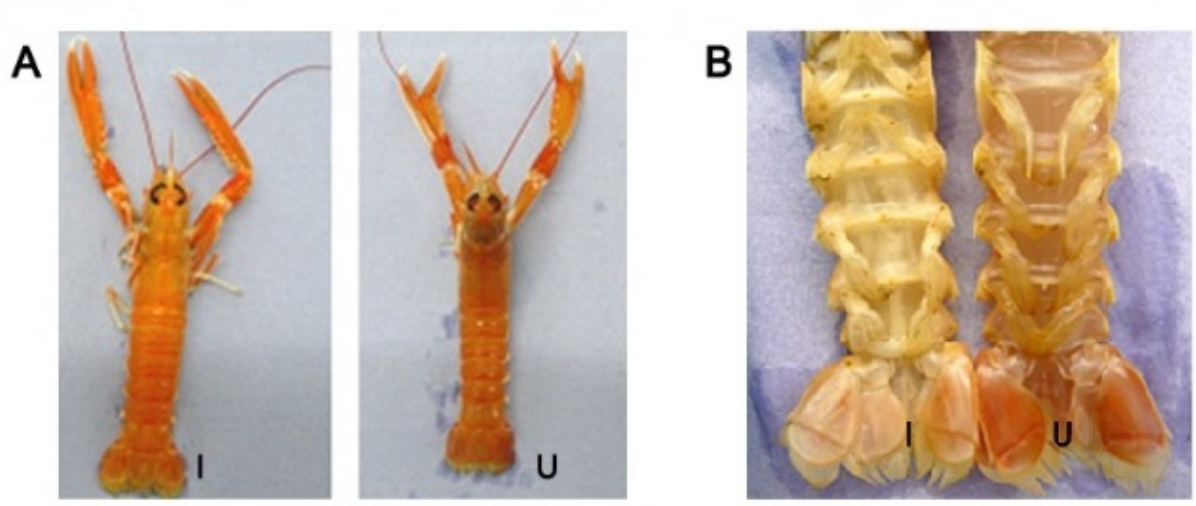

Figure 1.6: Dorsal (A) and ventral (B) view of uninfected *Nephrops* (U) and infected *Nephrops* (I) from the CSA (Beevers, 2010).

1.4 *Hematodinium* Transmission

Hematodinium passes through a characteristic life-cycle with alternating trophont and sporont stages, as shown in Figure 1.7 (Appleton and Vickerman, 1998). Vegetative trophont cells grow and proliferate before developing into sporonts. Sporonts, in turn, give rise to biflagellate zoospores, known as dinospores. Dinospores are classified as either macrospores (16–20 μm long) or microspores (11–14 μm long) depending on size (Appleton, 1996). Both macro and micro- spores are capable of surviving outside of the host and are thought to act as free-living agents of the infection.

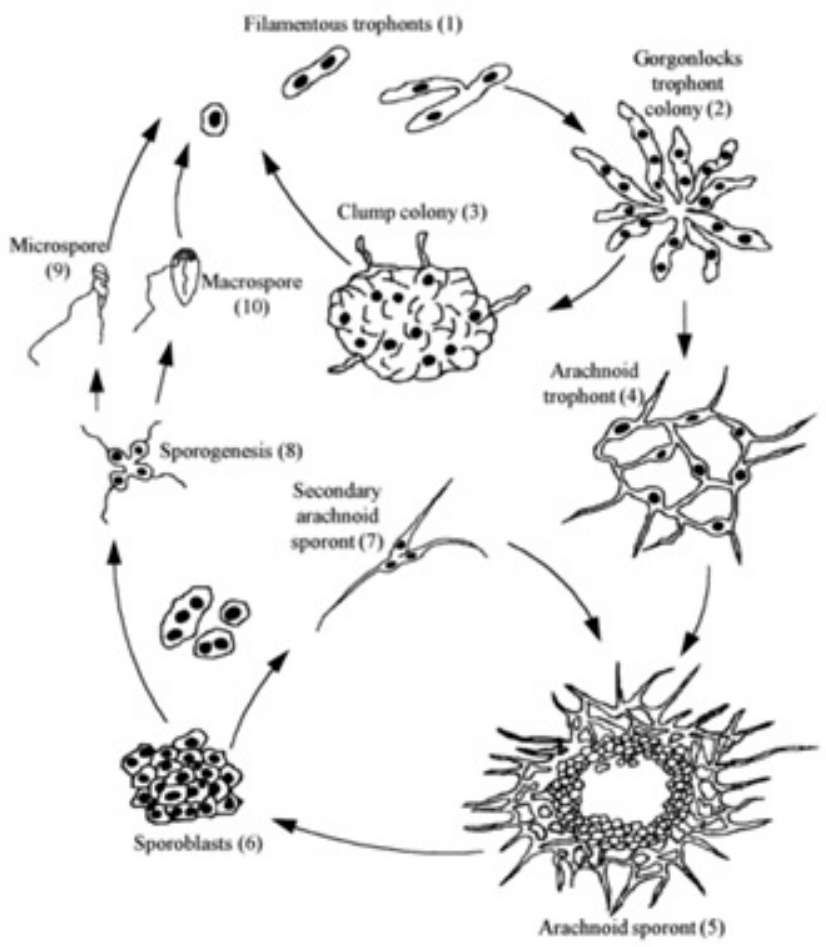

Figure 1.7: Developmental cycle of *in vitro*-cultured *Hematodinium sp.* derived from *Nephrops norvegicus* (Appleton and Vickerman, 1998).

Dinospores are released from infected individuals via the gills in a mass sporulation event (see Figure 1.8). The exact process responsible for triggering sporulation remains unknown. In the CSA, a distinct peak in sporulation activity occurs in late spring – a time which coincides closely with the main moulting season of *Nephrops* in this region (Field et al., 1992, 1998; Stentiford et al., 2001b). This led researchers to believe that moulting must play an important role in parasite transmission. This theory has gained further traction following recent experimental work by Gornik et al. (2015) which alluded to the importance of the *Nephrops* moult hormone, methyl farnesoate, in the life cycle of *Hematodinium*. *Hematodinium* lacks an essential isoprenoid pathway and must therefore scavenge isoprenoids directly from the host haemolymph. The moult hormone, methyl farnesoate, is thought to be the most likely source of essential isoprenoids. It is therefore postulated that increases in the level of methyl farnesoate prior to moulting stimulate a final growth burst of parasite cells and consequently trigger the formation of spores.

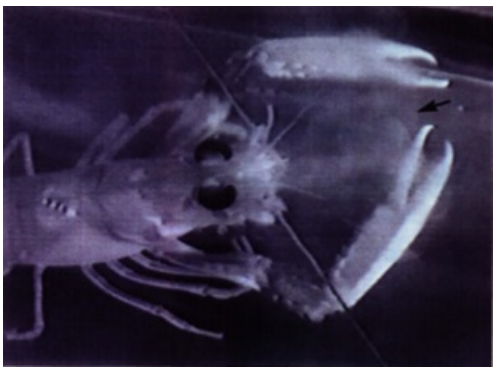

Figure 1.8: Image of spores being released from an infected individual during sporulation (Appleton, 1996).

Following release, the dinospores remain viable for a short period of time (approximately 73 and 52 days for macrospores and microspores respectively (Meyers et al., 1987)). During this time, dinospores act as water-borne transmission agents of the disease (Frischer et al., 2006). However, despite extensive research, the exact mode of *Hematodinium* transmission remains unknown. Dinospores may enter *Nephrops* via the gills or via breaks in integument (Hanif et al., 2013). Alternatively, dinospores may penetrate the softened exoskeleton of recently moulted individuals (Pagenkopp-Lohan et al., 2012). Distinctive patterns in *Hematodinium* prevalence point to this as the most likely source of parasite transmission. For example, prevalence levels of *Hematodinium* are higher amongst smaller individuals which are known to moult more frequently (see Section 1.6.4 for more details).

A number of other transmission routes have also been proposed. This includes ingestion of dinospores via suspension feeding (Briggs and McAliskey, 2002) or via the direct ingestion of infected individuals. Walker et al. (2009) carried out experiments in which blue crabs (*Callinectes sapidus*) were fed the tissues of crabs heavily infected with *Hematodinium*. Shortly after consumption of the infected tissues, 63% of crabs were found to have developed the infection (Walker et al., 2009). However, the speed at which infections developed indicate that undetected infections may have been present in the crabs prior to the start of the experiment (Li et al., 2011). Similar experiments have since been carried out, all of which have been unsuccessful in transmitting the infection by this method (Li et al., 2011; Butler et al., 2014). Ingestion of infected individuals is therefore unlikely to be a viable means of *Hematodinium* transmission. Contact between individuals during copulation has also been suggested as a possible route of *Hematodinium* transmission. During copulation, the soft cuticle of the female is disrupted, which may allow motile parasitic spores to enter the body (Field et al., 1992). However, this fails to explain transmission to male *Nephrops*.

Alternate host species may also play an important role in parasite transmission. *Hema-*

todinium is known to infect a wide range of other species in addition to *Nephrops*, as discussed in Section 1.3. Alternate hosts may be responsible for harbouring the infection when prevalence levels of *Hematodinium* in *Nephrops* are at their lowest (Tew et al., 2011). Alternate host species may therefore aid *Hematodinium* transmission by acting as a reservoir for the parasite.

1.5 Diagnosing *Hematodinium* Infection in *Nephrops*

A number of different diagnostic methods are used to test for the presence of *Hematodinium* infection in *Nephrops*. Each diagnostic method has a different detection threshold, as shown in Table 1.1. The simplest, but least sensitive, diagnostic test, known as the body colour method, involves examining individuals for characteristic changes in cuticle colour, as shown in Figure 1.6. The body colour method can be performed rapidly in the field but is extremely simple and lacks a great deal of sensitivity. As a result, a number of more sensitive diagnostic tests have been developed.

The next simplest method of *Hematodinium* diagnosis is the pleopod method. This method involves observing aggregations of parasites in the haemal spaces of the abdominal pleopods using low-magnification light microscopy (Field et al., 1992). Individuals are assigned a severity grade based on the number of parasites present in the pleopod blade. This scale ranges from '0' for uninfected individuals to '4' for the most severely infected individuals. The pleopod method therefore provides an arbitrary measure of intensity and can be used to monitor the progression of the infection over time. The pleopod method is relatively simple to perform and has been widely used in a number of different studies (Field et al., 1992, 1998; Stentiford et al., 2001b; Beevers et al., 2012).

The pleopod method shows a marked improvement in sensitivity over the body colour method. The body colour method is only able to detect infection in individuals with a parasite burden greater than 5×10^7 parasites per ml haemolymph (Field et al., 1992). The pleopod method, on the other hand, is able to detect infection in individuals with a parasite burden greater than 2.4×10^6 parasites per ml haemolymph (Field and Appleton, 1995). However, despite this marked improvement, both methods are relatively insensitive and can only detect high-level (patent) infection.

In recent years, a number of more-sensitive diagnostic methods have been developed to detect low level (sub-patent) *Hematodinium* infection. These include a western blot immunoassay method (Stentiford et al., 2001c), enzyme-linked immunosorbent assays (ELISA) (Small et al., 2002) and polymerase chain reaction (PCR) based methods (Beev-

ers, 2010). PCR is the most sensitive method of diagnosis, capable of detecting infections in individuals with a parasite burden as low as 30 parasites per ml haemolymph (Beevers, 2010). However, methods for diagnosing sub-patent infection (western blot immunoassay, ELISA and PCR) are relatively difficult to perform in comparison to the body colour and pleopod methods. As a result, these methods have only been employed in a limited number of studies.

Test	**Detection Threshold** (No. of parasites per ml of haemolymph)	
Body Colour	5×10^7	(Field et al., 1992)
Pleopod - Level IV	8×10^7	(Field and Appleton, 1995)
Pleopod - Level III	5.2×10^7	(Field and Appleton, 1995)
Pleopod - Level II	1.4×10^7	(Field and Appleton, 1995)
Pleopod - Level I	2.4×10^6	(Field and Appleton, 1995)
Western Blot Immunoassay	2×10^5	(Stentiford et al., 2001c)
ELISA	5×10^4	(Small et al., 2002)
PCR	3×10^1	(Beevers, 2010)

Table 1.1: The detection thresholds of the main tests used to diagnose *Hematodinium* infection in *Nephrops*.

1.6 Infection Dynamics

Hematodinium infection was first reported in the CSA by fishermen in the late 1980s. The first data set of disease prevalence in the region was produced shortly afterwards (Field et al., 1992). Since this initial report, a considerable amount of research into the prevalence of *Hematodinium* in the CSA has followed (Field et al., 1998; Stentiford et al., 2001b,c; Beevers et al., 2012). The CSA is now one of the best studied *Hematodinium*-host systems. These studies have revealed a number of distinctive patterns in infection dynamics as described in Sections 1.6.1 - 1.6.4.

1.6.1 Patent Infection

Early studies of *Hematodinium* prevalence in the CSA were carried out using the body colour and pleopod methods of diagnosis (Field et al., 1992, 1998; Stentiford et al., 2001b,c). These studies found a distinct seasonality in infection prevalence, as shown in Figure 1.9. A peak in *Hematodinium* prevalence was found to occur in late winter/spring with an almost complete absence of infection throughout the summer and autumn months.

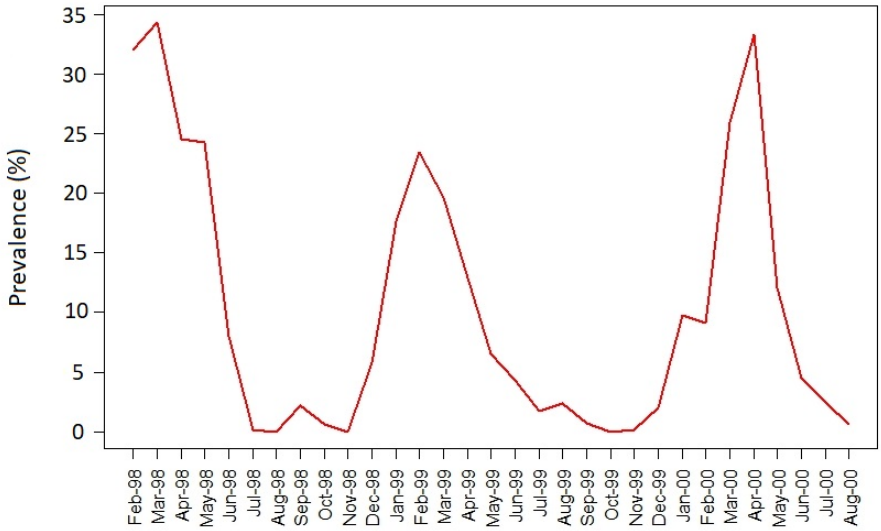

Figure 1.9: Pleopod-derived *Hematodinium* prevalence of *Nephrops* captured near Little Cumbrae in the CSA from February 1998 to August 2000 (Stentiford et al., 2001b).

Similar seasonal patterns in infection prevalence have also been observed in other *Hematodinium*-host populations across the world. The timing of peak infection prevalence, however, varies with geographical region. *Chionoecetes bairdi* populations in the sub-arctic showed a peak in *Hematodinium* prevalence between June and September (Meyers et al., 1987). *Necora puber* populations in French waters, on the other hand, showed a distinct peak in *Hematodinium* prevalence between September and November (Wilhelm and Mialhe, 1996).

However, it is important to note that all of these studies employ relatively insensitive methods of diagnosis, only capable of detecting *Hematodinium* infection once it has reached patent infection levels. As more sensitive diagnostic tests have been developed it has become clear that the seasonal peaks and troughs outlined above are not representative of the prevalence of low-level sub-patent *Hematodinium* infection.

1.6.2 Sub-patent Infection

The first study measuring sub-patent *Hematodinium* prevalence in the CSA was carried out by Stentiford et al. (2001c) using a western blot immunoassay technique. This study was the first to detect *Hematodinium* prevalence during the autumn. However, like previous studies, Stentiford et al. (2001c) also failed to detect infection during the summer months. Stentiford et al. (2001c) recorded a distinct peak in sub-patent level infections (i.e. those which were classified as positive by the western blot immunoassay method

but negative by the pleopod method) during late-autumn and winter, as shown in Figure 1.10. The amplitude of this sub-patent infection peak was found to be equivalent to the amplitude of the patent infection peak the following spring. This led researchers to believe that infection, sub-patency and patency all occurred within a single year.

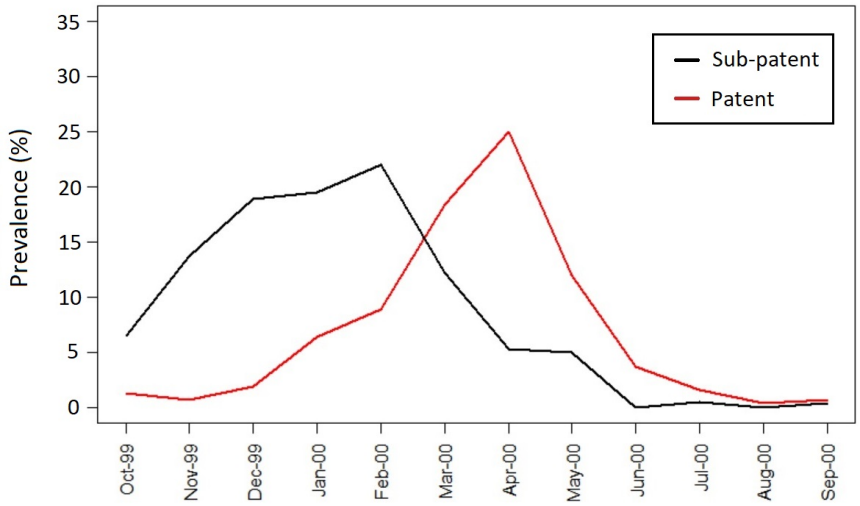

Figure 1.10: Plot showing the prevalence of patent *Hematodinium* infection (the percentage of individuals which were classified as positive by the pleopod method) and sub-patent *Hematodinium* infection (the percentage of individuals which were classified as positive by the western blot immunoassay method but negative by the pleopod method). Data is obtained from Stentiford et al. (2001c), with male and female prevalence combined into a single value.

However, despite being capable of detecting sub-patent infection, the western blot immunoassay method is still relatively insensitive, as shown in Table 1.1. A later study by Beevers et al. (2012), using highly sensitive PCR and ELISA methods of diagnosis, detected low level sub-patent infection in the CSA throughout the whole year, as shown in Figure 1.11. Consequently, only patent infection can be described as a seasonal phenomenon. The presence of low-level sub-patent infections during late winter/early spring (at the time of peak patent prevalence) challenged the previously held assumption that infection, sub-patency and patency all occur within a single year. This raised the possibility that infections may persist at a low level for a relatively long period (>1 year) before eventually manifesting as patent infection.

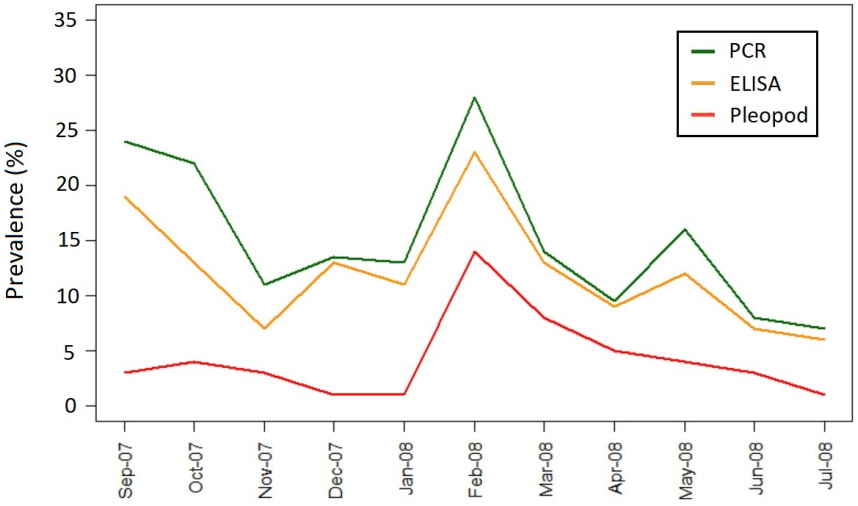

Figure 1.11: Plot showing the prevalence of *Hematodinium* infection in the CSA as determined by PCR, ELISA and pleopod methods of diagnosis (Beevers et al., 2012).

1.6.3 Time Series of Infection Prevalence

Studies recording the prevalence of *Hematodinium* in the CSA have been carried out sporadically since the late 1980s (Field et al., 1992, 1998; Stentiford et al., 2001b,c; Beevers et al., 2012). These studies focus specifically on the prevalence of *Hematodinium* in a region south of the island of Little Cumbrae. Records of *Hematodinium* prevalence in this region have been obtained using a number of different diagnostic methods ranging from the least sensitive body colour and pleopod methods to the most sensitive ELISA and PCR methods of diagnosis. Comparing estimates of *Hematodinium* prevalence obtained using different diagnostic methods is difficult due to the different detection thresholds of each diagnostic method (see Table 1.1). However, due to its relative ease and simplicity, many researchers have continued to use the pleopod method alongside the application of more sophisticated diagnostic techniques. Estimates of *Hematodinium* prevalence obtained using the pleopod method can therefore be combined to produce a long term time-series of *Hematodinium* prevalence, as shown in Figure 1.12.

The prevalence of *Hematodinium* in the CSA was highest in the early 1990s, just after records of the infection first began. During this period patent infection prevalence was found to be as high as 80% (Field et al., 1992). This initial epizootic period was followed by a period of relative stability. Records of *Hematodinium* prevalence in the CSA from 1998-2000 show a consistent peak in patent *Hematodinium* prevalence of 20-30% (Stentiford et al., 2001a). Following this, recorded levels of *Hematodinium* prevalence show

a slight fall, with patent *Hematodinium* infection reaching a peak of just 14% in 2008 (Beevers et al., 2012).

It is important to note, however, that the experimental methods used to obtain estimates of *Hematodinium* prevalence have changed substantially over the years. One change of particular importance is the use of trawl nets with different mesh sizes. Estimates of pleopod prevalence obtained prior to 1998 were made using trawl nets with a mesh size of 20 mm (Field et al., 1992, 1998). Estimates of pleopod prevalence covering the period 1998-2001, on the other hand, were obtained using trawl nets with a mesh size of 70 mm (Stentiford et al., 2001b). Finally, estimates of *Hematodinium* prevalence from 2007 onwards have been obtained using trawl nets with a mesh size of 80 mm (Beevers et al., 2012). Increasing the size of the mesh prevents the capture of small individuals which are more vulnerable to *Hematodinium* infection (Stentiford et al., 2001b). Mesh size therefore has important implications on reported levels of *Hematodinium*. Estimates obtained using smaller mesh sizes are more likely to report higher levels of *Hematodinium* prevalence in comparison to estimates made using larger mesh sizes. These differences must be taken into consideration when analysing the long term trend of *Hematodinium* prevalence in the CSA.

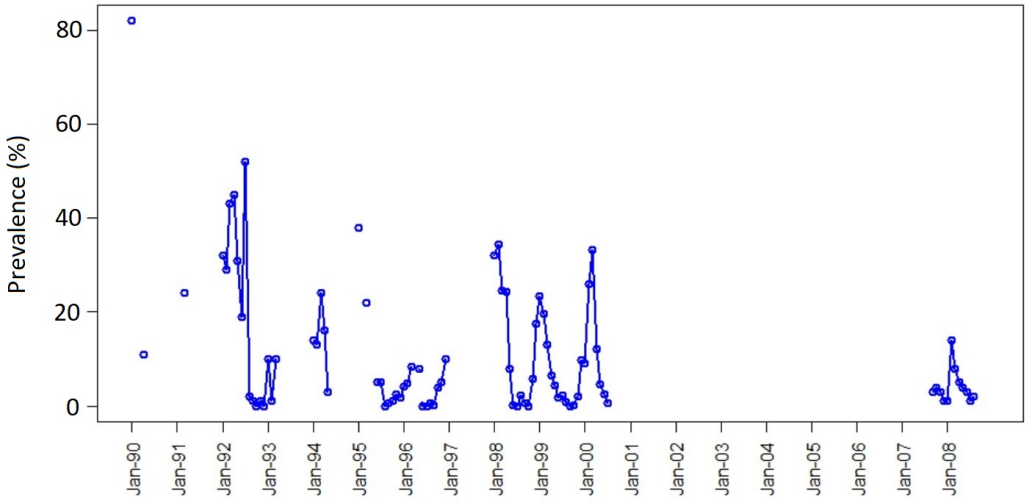

Figure 1.12: Pleopod-derived *Hematodinium* prevalence of *Nephrops* captured near Litttle Cumbrae in the CSA from 1990-2008. Data is obtained from multiple studies (Field et al., 1992, 1998; Stentiford et al., 2001b; Beevers, 2010). Consecutive monthly samples are linked together by lines.

1.6.4 Other Key Infection Dynamics

Other key features of *Hematodinium* infection dynamics include a higher rate of prevalence amongst females and smaller individuals (Field et al., 1992, 1998; Stentiford et al., 2001b,c; Briggs and McAliskey, 2002). These distinctive patterns in infection dynamics point to the important role of moulting in parasite transmission. Smaller individuals moult more frequently and are therefore more susceptible to contracting the infection (Field et al., 1992). Similarly, the increased prevalence of *Hematodinium* in female *Nephrops* can be explained by differences in the timing of the main moulting period between each sex. Female *Nephrops* moult before males, so that their cuticles are in the softened post-moult condition necessary to allow mating with hard shelled males. In the CSA, the main moulting period of females occurs in the spring (Field et al., 1992). This coincides with peak infection prevalence, putting these individuals at a much greater risk of contracting the infection. The moulting period of males, on the other hand, is much more variable. An increase in synchrony in the timing of moulting between males and females has been shown to cause a sharp peak in infection prevalence. However, if the moulting period of males and females occur completely separately, an extended lower-level 'plateau' of infection prevalence occurs (Stentiford et al., 2001b).

Hematodinium infection is also known to have a significant impact on the burrow emergence patterns of infected individuals. Infected individuals spend significantly more time outside of their burrows in comparison to uninfected individuals (Field et al., 1998; Stentiford et al., 2001a,c). This is thought to be caused by the high energy demands of *Hematodinium* infection, which force infected individuals to spend more time out of their burrow hunting for food. As a result, infected individuals are more susceptible to both natural and fishing mortality in comparison to their uninfected counterparts.

Finally, *Hematodinium* infection also causes a marked reduction in the swimming ability of infected individuals. Increases in infection severity are accompanied by a progressive reduction in the number of tail flips performed, the number of swimming bouts and the total distance travelled (Stentiford et al., 2000). Moreover, infected animals recover less efficiently from exhaustive swimming (Stentiford et al., 2015). This reduction in swimming ability makes it difficult for infected individuals to evade capture, and therefore further increases the susceptibility of infected individuals to both natural and fishing mortality.

1.7 Impact of Fishing Practices on Infection Prevalence

Current fishing practices may be contributing to the high level of *Hematodinium* infection in the CSA *Nephrops* population (Stentiford and Shields, 2005). One practice thought to contribute to the high levels of infection prevalence is the selective discarding of heavily-infected individuals which show visible signs of *Hematodinium* infection (see Figure 1.6). This increases the proportion of heavily-infected individuals in the population and hence increases the transmission rate of the parasite. Changing current discard policies to prevent the discarding of visibly-infected individuals will therefore have important consequences for *Hematodinium* transmission and is likely to lead to a reduction in overall infection prevalence.

Furthermore, fishermen in the CSA are also known to selectively discard smaller individuals including those which fall below the Minimum Conservation Reference Size (MCRS). Fish below the MCRS cannot be sold for human consumption and therefore have a reduced market value. Smaller individuals are known to be more vulnerable to *Hematodinium* infection (as discussed in Section 1.6.4). Populations with a greater proportion of smaller individuals are therefore more likely to have higher levels of infection prevalence. Changing discard practices to increase the numbers of small individuals removed from the population may therefore lead to a reduction in the overall prevalence of *Hematodinium*. This strategy, however, will increase the removal rate of immature females which have not yet had a chance to reproduce and could therefore have a detrimental effect on overall stock density.

Finally, altering the level of fishing intensity may also have a significant effect on *Hematodinium* prevalence. Increasing fishing intensity causes a reduction in the mean size of individuals (Stentiford et al., 2001a). This could lead to an increase in *Hematodinium* prevalence due to the increased susceptibility of smaller individuals to *Hematodinium* infection. However, increasing fishing intensity to relatively high levels also results in a decrease in the overall abundance of *Nephrops*. *Hematodinium* transmission is thought to be density dependent. Consequently, a decrease in the overall abundance of *Nephrops* caused by increasing fishing intensity may result in a reduction in the overall prevalence of *Hematodinium*.

Altering current fishing management practices in the CSA is therefore likely to have a significant impact on the overall prevalence of *Hematodinium*. However, predicting the exact effect of altering fishing management strategies on *Hematodinium* prevalence and

Nephrops population dynamics is difficult due to the large number of complex factors and feedback loops involved. Population modelling of *Nephrops* and *Hematodinium* is therefore needed to help explore the impact of fishing management practices on *Nephrops-Hematodinium* population dynamics.

1.8 Thesis Outline

Population modelling of *Nephrops* and *Hematodinium* in the CSA is urgently required to help further our understanding of the complex population dynamics of this commercially important host-parasite system. Furthermore, *Nephrops-Hematodinium* population modelling is also required to help predict the effect of altering fishing management strategies on *Nephrops-Hematodinium* population dynamics. However, despite this need, only limited modelling work has been undertaken in this area (Butler, 2007) with no full-scale models of *Nephrops-Hematodinium* population dynamics currently available. The lack of modelling work in this area is largely due to uncertainties surrounding the exact nature of *Hematodinium* transmission which have made it difficult to accurately model the host-parasite interaction. Recent studies have, however, pointed to the importance of moulting in two key areas of parasite transmission (see Section 1.4 for more detail):

i) the timing of spore release from infected individuals
ii) the time at which uninfected individuals are susceptible to contracting the infection.

In this thesis, a population model of *Nephrops* and *Hematodinium* in the CSA is developed based on these two key assumptions. Firstly, in **Chapter 2** a new model of *Nephrops* growth is developed which incorporates distinct moulting events crucial for accurately modelling parasite transmission. In **Chapter 3**, this newly developed *Nephrops* growth model is combined with information on mortality, reproduction and density-dependent larval settlement to create a population model of *Nephrops* and *Hematodinium*.

The *Nephrops-Hematodinium* population model is then parameterised in **Chapter 4** using data on the abundance of *Nephrops* in the CSA, the weights of *Nephrops* landed and discarded, the length distributions of *Nephrops* landed and discarded, and the prevalence of *Hematodinium* as determined by the pleopod method of diagnosis. Following this, **Chapter 5** examines the ability of the *Nephrops-Hematodinium* population model to replicate other sources of *Hematodinium* prevalence data which are not included in the parameterisation process. This includes the prevalence of sub-patent *Hematodinium* infection as measured by the western blot immunoassay, ELISA and PCR methods of di-

agnosis as well as data outlining distinct differences in *Hematodinium* prevalence between males and females and between individuals of different length classes.

The newly created *Nephrops-Hematodinium* population model is then used to help further our understanding of *Nephrops-Hematodinium* population dynamics in the CSA. **Chapter 6** focuses specifically on the estimation of key statistics which cannot be measured directly in the field. This includes the background level of *Hematodinium* prevalence in the population and the length of time it takes the parasite to reach patent infection levels within an individual host. Furthermore, the *Nephrops-Hematodinium* population model is also used to carry out a full exploration of the driving factors behind key infection dynamics, including the seasonal cycle in patent *Hematodinium* infection. In **Chapter 7**, the *Nephrops-Hematodinium* population model is used to assess the impact of altering current fishing management practices. This includes changes to current discard policies as well as changes to the current level of fishing intensity. The *Nephrops-Hematodinium* population model is used to explore the impact of these changes on a number of factors including the prevalence of *Hematodinium* as well as the overall abundance of *Nephrops* in the CSA.

The *Nephrops-Hematodinium* model developed in this thesis is strictly non-spatial. However, a number of factors are known to vary substantially across the CSA, including *Nephrops* growth rates, fishing intensity and *Hematodinium* prevalence. Fully understanding *Nephrops-Hematodinium* dynamics in the CSA therefore requires the development of a spatial population model, capable of accounting for these geographic variations. The final section of this thesis lays the groundwork for the creation of such a model. **Chapter 8** focuses on the development of a new method for predicting suitable *Nephrops* habitat, using a combined interpolation and random forest modelling approach. This new method is then used to create an updated high-resolution map of suitable habitat across the CSA. Furthermore, this chapter also explores the variability in *Nephrops* burrow density across areas of suitable habitat. Finally, **Chapter 9**, explores the movement of *Nephrops* larvae between areas of suitable habitat using a high-resolution hydrodynamic model. In addition to laying the groundwork for the creation of a spatial model, Chapters 8 and 9 also further our knowledge of the distribution and dispersal patterns of *Nephrops* in the CSA. Improving our understanding of these factors is essential for the effective management of this commercially important host-parasite system.

Part I

Nephrops-Hematodinium Population Model

Chapter 2

Modelling *Nephrops* Growth

2.1 Introduction

Nephrops, like all other arthropods, are encased within a hard, inelastic exoskeleton composed primarily of calcium carbonate. This prevents individuals from growing continuously. Instead growth occurs via a succession of moults, during which individuals shed their old exoskeleton before developing a new, larger outer shell. The discontinuous, 'stepwise' nature of *Nephrops* growth poses a number of challenges for modelling the growth of this species. One of the main challenges is caused by the absence of size-at-age data. During the moulting process, the entire outer shell is shed, leaving no permanent calcified exoskeletal structures suitable for age determination. Growth bands have been described in endoskeletal structures of *Nephrops* which persist across a moult, such as the gastric mill ossicles (Kilada and Driscoll, 2017) but these are thought unlikely to be suitable for aging purposes without further validation. The discontinuous nature of *Nephrops* growth, alongside the lack of size-at-age data, means that many commonly used growth models are not suitable for modelling the growth of this species.

However, moulting is thought to play an important role in *Hematodinium* transmission, as discussed in Section 1.4. Accurately modelling the discontinuous growth process of *Nephrops* is therefore vitally important for the creation of a realistic population model of *Nephrops* and *Hematodinium*. In this chapter I explore the moulting process of *Nephrops* in more detail. I then review currently available methods for modelling crustacean growth and assess their applicability to *Nephrops* in the CSA . Finally, I develop a new method for modelling *Nephrops* growth, based on the dynamic energy budget approach, and test this new approach against *Nephrops* growth data from the CSA.

2.2 The Moulting Process

A full overview of the crustacean moult process is provided by Chang and Mykles (2011). In brief, the moult process is characterised by ecdysis - the periodic shedding of the outer shell. Prior to ecdysis, the flesh of crustaceans becomes densely packed within the exoskeleton and a new, soft, flexible shell begins to form inside the original exoskeleton. Calcium is removed from the old exoskeleton and stored in special structures located in the stomach wall, called gastroliths. Ecdysis is facilitated by the rapid absorption of water, which causes the new shell to expand, pushing away the old exoskeleton. During ecdysis the membranes of the gastroliths are broken, releasing the stored calcium. The calcium is then absorbed by the new exoskeleton, causing it to harden. Over time, the rapidly absorbed seawater is gradually replaced by tissue, and the process repeats itself. Moulting can therefore be described by two main processes: the size increment at moult, known as the moult increment, and the length of time between successive moults, known as the intermoult period.

2.2.1 Moult Increment

Size increments at moult can be determined by (i) holding animals captive in laboratory tanks and measuring their length directly before and after moulting, or (ii) by carrying out mark-recapture experiments. Both methods, however, have a number of associated problems. Growth under laboratory conditions is not directly comparable to growth in the field due to differences in temperature, population density and food availability etc (Chang et al., 2012). Some doubts therefore surround the extrapolation of moult increment data determined under laboratory conditions. Mark-recapture experiments, on the other hand, often suffer from low recapture rates (typically around 5% (Bailey and Chapman, 1983)). It is also possible that more than one moult could occur between tagging and recapture.

Despite these difficulties, lab studies and tag-recapture experiments have provided valuable information on the relationship between moult increment and pre-moult size in *Nephrops* from a wide range of geographical locations including the west coast of Scotland (Bailey and Chapman, 1983; Chapman, 1982), the Irish Sea (Haynes et al., 2016), the Kattegat (Ulmestrand and Eggert, 2001) and Portugal (Castro, 1992). The results of these studies were combined by Gonzalez-Gurriaran et al. (1998), as shown in Figure 2.1. This revealed distinct patterns in the relationship between moult increment and pre-moult size. In general, males show an increase in moult increment with increasing pre-moult size. The pattern for females, on the other hand, is less clear, with some regions showing

a decrease in moult increment with increasing pre-moult size.

However, Gonzalez-Gurriaran et al. (1998) focus primarily on larger individuals, the majority of which have already reached sexual maturity. A growth study covering a wider range of sizes was carried out by Bailey and Chapman (1983). This study was based on *Nephrops* in the CSA and used a combination of mark-recapture experiments and observations of growth in captivity. Bailey and Chapman (1983) found that prior to sexual maturity, moult increment increased with increasing pre-moult size in both males and females. A clear change in growth pattern occurs in females at the point of sexual maturity, as shown in Figure 2.2. In females, pre-moult size and moult increment become inversely related at the point of sexual maturity (Bailey and Chapman, 1983). This is caused by the high energy cost of gonad development and egg production. After sexual maturity, females must divert some energy towards reproduction. As a result, less energy is spent on growth as size increases. Males, on the other hand, spend approximately the same amount of energy on growth throughout their lives.

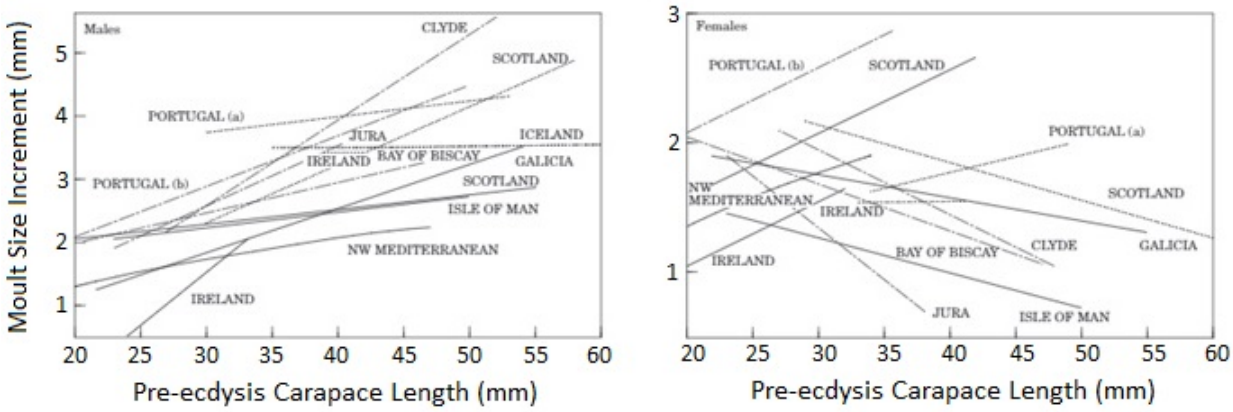

Figure 2.1: Graphs showing the relationship between moult increment and pre-moult carapace length in male and female *Nephrops* from a wide range of geographical areas (Gonzalez-Gurriaran et al., 1998).

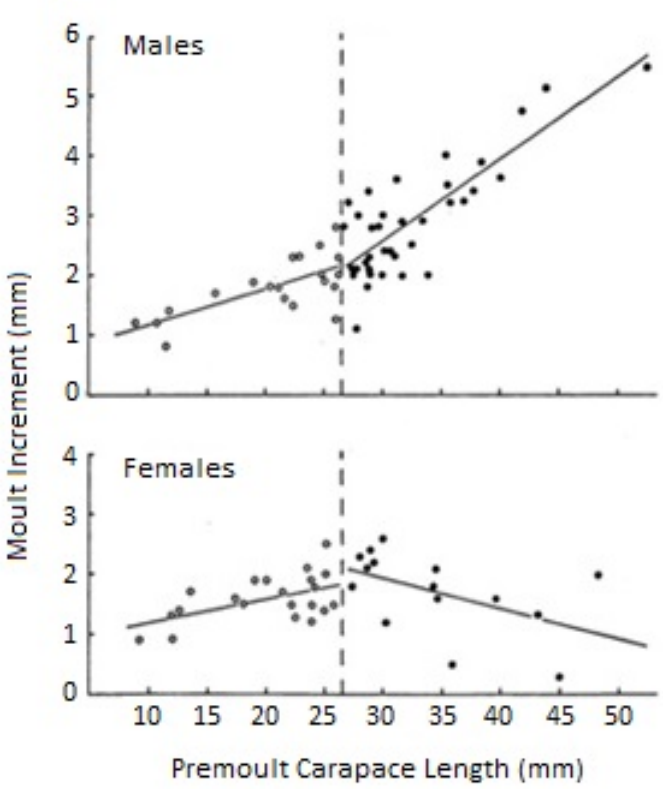

Figure 2.2: Graphs showing the relationship between moult increment and pre-moult carapace length according to sex, as determined by Bailey and Chapman (1983) for *Nephrops* in the CSA. Broken vertical line indicatess the size at sexual maturity. Separate linear regressions were fitted to immature and mature *Nephrops* (Bailey and Chapman, 1983).

2.2.2 Intermoult Period

The length of time between successive moults can be measured directly by observing animals reared in captivity or indirectly by examining the proportion of pre-moult and post-moult individuals in monthly samples (Bailey and Chapman, 1983). Juvenile *Nephrops* have a very short intermoult period and typically moult around once per month (Bell et al., 2013). The length of the intermoult period then increases as size and age increase (Bell et al., 2013).

Clear differences in the length of the intermoult period exist between geographical regions, especially amongst mature females. In mature females, the duration of the intermoult period is directly related to the length of the incubation period, since females cannot moult whilst carrying eggs. Mature females dwelling in the Mediterranean, the Iberian Peninsula, the Bay of Biscay, the Irish Sea and the majority of the North Sea therefore moult annually. Mature females dwelling in colder water around Iceland and the Faroe Islands, however, only moult on a biennial basis (see Section 1.1 for more detail).

2.2.3 Moult Pattern of Mature Females in the CSA

In order to reduce the risk of predation, mature females spend relatively more time inside their burrow whilst incubating eggs. Mature females in the CSA follow an annual reproductive cycle and must therefore moult/mate shortly after releasing their eggs. Consequently, the time of emergence of mature females from their burrows provides a proxy for the timing of the annual moult. In this section, I determine the timing of the annual moult of mature females in the CSA by analysing monthly sex prevalence and carapace length data collected near the Isle of Cumbrae in 2006 and 2009 (Milligan et al., 2009; Watts et al., 2016; Albalat et al., 2016a).

The proportion of females in the catch is lower than the proportion of males for the majority of the year, as shown in Figure 2.3. However, there is a clear increase in the proportion of females in the catch around April/May. This coincides with an increase in the mean carapace length of females. The increased prevalence of females can therefore be attributed to the emergence of mature females from their burrows in order to release their eggs. This points to April/May as the most likely timing of the annual moult of mature females in the CSA.

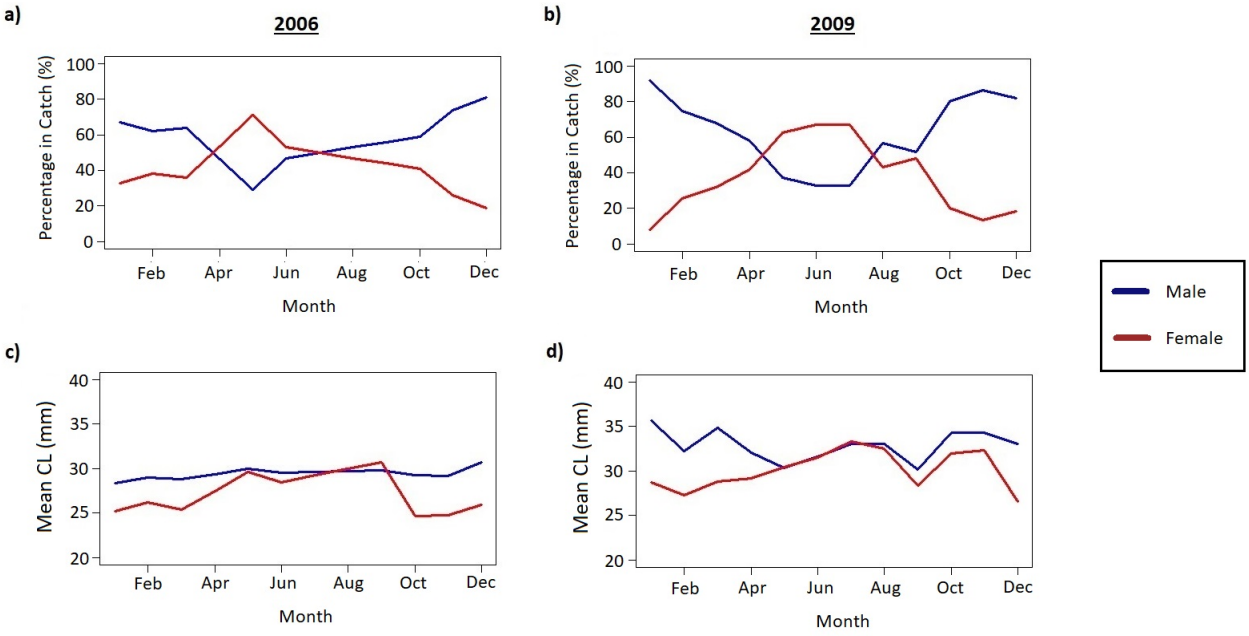

Figure 2.3: Plots (a) and (b) show the proportion of males and females in the catch for 2006 and 2009 respectively. Plots (c) and (d) show the mean carapace length of males and females in the catch for 2006 and 2009 respectively.

Further insight into the timing of the annual moult in mature females can be gained by examining the carapace hardness of individuals in the catch throughout the year. During 2009, the carapace of each individual in the sub-sample was classified as 'hard', 'soft' or 'jelly-like'. 'Jelly-like' animals were assumed to have moulted very recently. 'Soft' animals were assumed to either be very close to moulting or to have moulted relatively recently. 'Hard' animals, on the other hand, were assumed to be between moults.

'Jelly-like' males were present in low numbers throughout the entire year, with no sign of seasonality. This indicates asynchronous moulting patterns amongst males. Females, on the other hand show clear seasonality, with a peak in the proportion of 'jelly-like' individuals occurring around May. This peak is followed by a peak in 'soft-shelled' females around June, showing the progressive stages of carapace hardening following a moult. A high prevalence of 'soft' females was also observed in January. However, the number of females sampled in January was very low (< 10) and this value can therefore be regarded as an anomaly. Small numbers of 'jelly-like' females were present outside of the main moult peak. This is thought to be caused by immature females, which moult more frequently than mature females and do not yet follow an annual moult cycle (Bell et al., 2013).

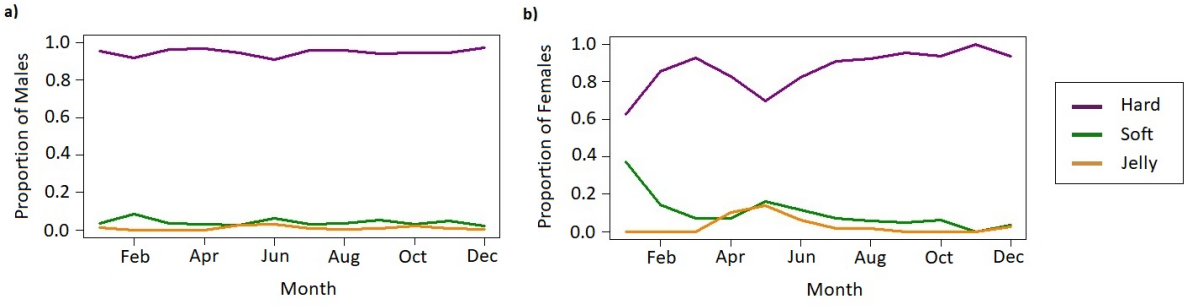

Figure 2.4: Plots showing the proportion of males (a) and females (b) in each carapace hardness category for 2009.

2.3 Crustacean Growth Models

A wide range of models have been developed to describe crustacean growth (see review by Chang et al. (2012)). In this section I explore three of the most commonly used models (i) the Von Bertalanffy growth model (ii) size transition matrix models and (iii) moult process models. These models range from simple continuous growth models to more complex growth models aimed at capturing the complex step-wise nature of crustacean growth. In this section I provide a brief overview of each model and assess the applicability of each method for modelling the growth of *Nephrops* in the CSA.

2.3.1 The Von Bertalanffy Growth Model

The Von Bertalanffy growth model assumes that growth rate declines with increasing age (Von-Bertalanffy, 1938). The length of an individual at age t (L_t) is calculated using the equation:

$$L_t = L_\infty \left(1 - e^{-k(t-t_0)}\right) \tag{2.1}$$

where L_∞ is the asymptotic length (the mean length an individual would reach if allowed to grow for an infinite number of years), k (yr^{-1}) is the rate at which L_∞ is approached, and t_0 is the age of individuals at zero length if they had always grown in the manner described by the equation.

The Von Bertalanffy growth model assumes that individuals grow continuously and therefore doesn't accurately describe the growth of individual crustaceans. The Von Bertalanffy growth curve can, however, be used to approximate population growth. This method is easily incorporated into traditional stock assessments and is therefore one of the most commonly used crustacean growth models. The Von Bertalanffy growth curve is currently used to model *Nephrops* growth in a number of ICES stock assessments (eg ICES (2009)).

Accurately estimating the Von Bertalanffy parameters in *Nephrops* is extremely difficult, since the age of individuals cannot be routinely determined. Growth studies therefore rely on the use of length frequency data. The growth of *Nephrops* is estimated by examining the progression of prominent length classes in length-frequency distributions (Chapman, 1982). This method gives a satisfactory estimate of annual growth for the first few year classes. However, reduced growth rates amongst sexually mature individuals, alongside high variability in individual growth rates, means that classes corresponding to older age groups are often difficult to detect.

The Von Bertalanffy growth parameters currently used by ICES are shown in Table 2.1 alongside a plot of the corresponding growth curves (Figure 2.5). Following the onset of sexual maturity, females spend less energy on growth and more on reproduction (Bailey and Chapman, 1983). The growth of mature females is therefore considerably slower than that of mature males. In order to account for this, the ICES Working Group on *Nephrops* stocks (2009) created a combined growth curve for females, whereby females follow the same growth curve as males until they reach the size at 50% maturity, assumed to be 27 mm CL in the CSA. At this point females switch to a slower growth curve.

	L_∞ (mm)	k (yr^{-1})
Males	73	0.16
Immature Females	73	0.16
Mature Females	60	0.06

Table 2.1: Table showing the Von Bertalanffy parameters for *Nephrops* in the CSA. The value of L_∞ and k are taken from the ICES Working Group (ICES, 2009).

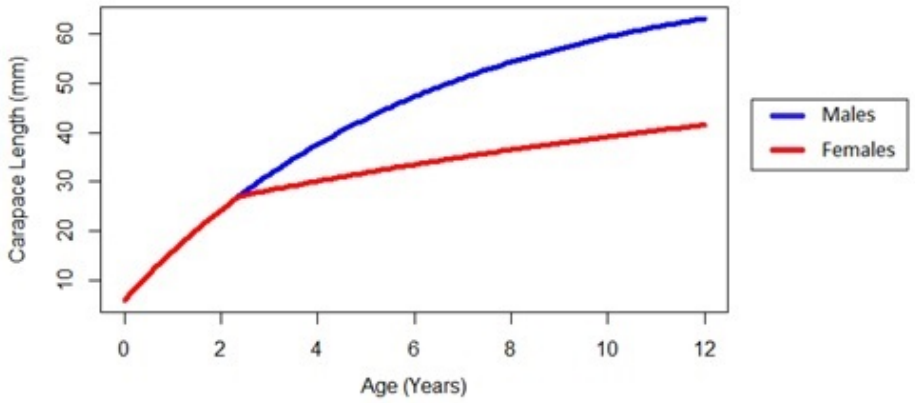

Figure 2.5: Von Bertalanffy growth curves for *Nephrops* in the CSA as determined by the ICES Working Group (ICES, 2009).

2.3.2 Size Transition Matrix Models

Due to the difficulties involved in ageing individuals, stock assessments for crustaceans are commonly based on size rather than age. Size structured stock assessment models have been developed for a wide range of crustacean species including red king crab (Zheng et al., 1994), rock lobsters (Punt et al., 2006), green tiger prawn (Punt et al., 2010), crayfish (Sadykova et al., 2009), and king crab (Siddeek et al., 2016). A size structured

approach has also been trialed for *Nephrops* in the Firth of Forth (Dobby, 2003, 2004).

Size structured models typically involve a growth transition matrix, which describes the probability of an organism growing from one size class to another within a given period of time. Growth transition matrices often contain sub-models which account for (i) size increment at moult and (ii) the likelihood of moulting within a given time step. An example of a size transition matrix is shown below, where m_i is the probability that an individual in size class 'i' moults in the given time step and $P_{i,j}$ is the probability that an individual in size class 'i' moves into size class 'j':

$$\text{Size Transition Matrix} = \begin{bmatrix} (1-m_1)+m_1P_{1,1} & 0 & \dots & 0 \\ m_1P_{1,2} & (1-m_2)+m_2P_{2,2} & \dots & 0 \\ m_1P_{1,3} & m_2P_{2,3} & \dots & 0 \\ \vdots & \vdots & \vdots & \vdots \\ m_1P_{1,n} & m_2P_{2,n} & \dots & 1 \end{bmatrix} \tag{2.2}$$

$P_{i,j}$ is assumed to be governed by a normal distribution,

$$P_{ij} = \int_{jmax}^{jmin} \frac{1}{\sqrt{2\pi\sigma_i}} e^{\frac{-(L-(L_i+\Delta L_i))^2}{(2\sigma_i)^2}} dL \tag{2.3}$$

where ΔL_i is the moult increment, σ is the variability in the growth increment, L_i is the midpoint of size class 'i' and jmin and jmax are the upper and lower bounds of size class j respectively.

Size transition matrix models are able to incorporate information on moult frequency in relation to size, sex and season. However, accurately parameterising such a model requires a large amount of data. Relatively little growth data is available for *Nephrops* in the CSA. Accurately parameterising a size transition model for *Nephrops* in the CSA would therefore be exceptionally difficult.

2.3.3 Moult-Process Models

Moult-process models simulate the succession of moults by the repeated application of equations relating moult increment and intermoult period to pre-moult size (Chang et al., 2012). Moult-process models require an initial starting length, L1. The length of the intermoult period is then calculated from L1, using a pre-determined relationship based on pre-moult size. The post-moult size, L2, is also calculated from L1, using a pre-determined

relationship between size increment at moult and pre-moult size. This process is then repeated with a new starting length, L2, and so on. Repeated application of this procedure simulates the step-wise growth of individual crustaceans (Chang et al., 2012).

Basic moult-process models are deterministic and do not take into account variation in moult increment and intermoult period between individual crustaceans. Stochastic moult-process models have since been developed to account for the uncertainty around these estimates. Stochastic moult-process models generate a distribution of step-wise growth curves by sampling the intrinsic variation in the raw data (Chang et al., 2012). A stochastic moult-process model for *Nephrops* in the Bay of Biscay was developed by Verdoit et al. (1999).

However, moult process models rely upon pre-determined, independent relationships between moult increment and pre-moult size and the length of the intermoult period and pre-moult size. In reality, moult increment and the length of the intermoult period are directly linked to each other. An increase in the length of the intermoult period allows an individual to accumulate more resources and therefore leads to a larger moult increment. Moult process models therefore do not provide the flexibility required to accurately model the growth of crustaceans.

2.4 Developing a Dynamic Energy Budget Based Model of *Nephrops* Growth

Accurately modelling the discontinuous growth of *Nephrops* is crucial for the creation of a realistic *Nephrops-Hematodinium* population model. However, there are currently no suitable models of *Nephrops* growth (see Section 2.3). In this section, I therefore develop a new model of *Nephrops* growth based upon the dynamic energy budget framework. Dynamic energy budget models consider the flow of energy through an organism. Energy consumed by an organism is either used for metabolism, invested in reproduction or transformed into growth. Dynamic energy budget models offer a flexible alternative to commonly used crustacean growth models. Traditional dynamic energy budget models, however, require a high level of experimental data. Consequently, only two dynamic energy budget models of crustacean growth have been created to date: one for blue crab (*Callincetes sapidus*) (Brylawski and Miller, 2006) and the other for swimming crab *Liocarcinus depurator* (Talbot et al., 2019).

In this section, I create a growth model for *Nephrops* in the CSA based on a simplified dynamic energy budget model. This model has less intensive data requirements in comparison to a traditional dynamic energy budget model. However, the model maintains a high level of biological realism, and is therefore able to accurately simulate the discontinuous growth process of *Nephrops*.

2.4.1 Model Overview

Energy consumed by an individual is split between a number of different processes as shown in Figure 2.6. In males and immature females, energy is used for metabolism and growth. Mature females, however, must also invest energy in reproduction. Any energy not used for metabolism or reproduction is transformed into muscle tissue, causing individuals to increase in weight.

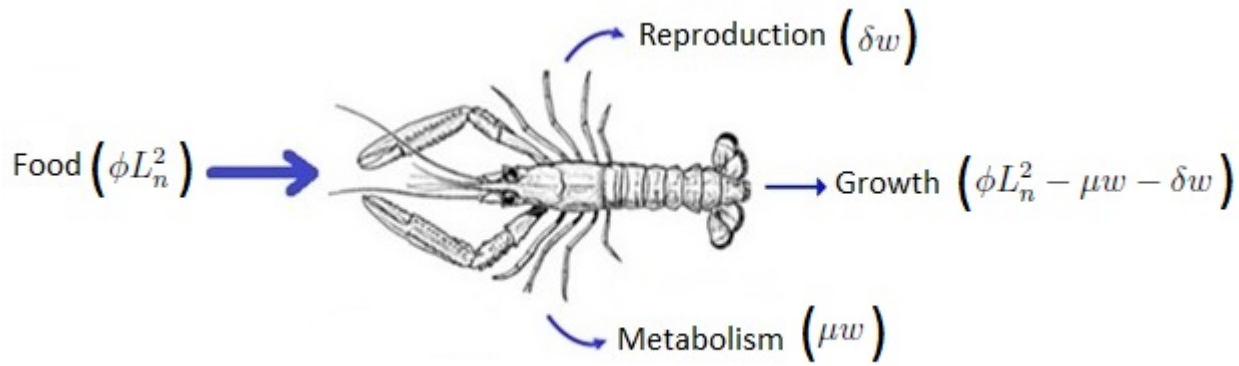

Figure 2.6: Diagram of *Nephrops* growth model.

Weight increase can therefore be described by the differential equation:

$$\frac{dw}{dt} = \phi L_n^2 - \mu w - \delta w \tag{2.4}$$

where ϕL_n^2 represents the assimilation rate, μw represents the basal metabolic rate and δw represents the rate at which energy is invested in reproduction. More detail about the form of this equation is provided by Gurney and Nisbet (1998). In brief, the assimilation rate is assumed to be length-dependent, with the rate of ingestion thought to scale with the surface area of the intestines. The amount of energy used for metabolism, on the other hand, is assumed to be weight dependent. The amount of energy invested in reproduction is also assumed to be weight dependent, and is given the constant of proportionality δ, where $\delta = 0$ for males and immature females.

Additional energy costs are experienced by individuals infected with *Hematodinium*. *Hematodinium*, like many other parasites, uses host derived energy to grow and therefore imposes additional energy requirements on infected individuals. This chapter, however, deals solely with the growth of non-infected individuals. An adapted version of this growth model, which includes the additional energy requirements imposed by the parasite, is shown in Chapter 3.

2.4.2 Moulting

Individuals cannot increase in weight continuously, due to the presence of a hard exoskeleton. At some point individuals must moult in order to continue growing. Moulting can be triggered by one of two events: (i) moulting occurs when the current exoskeleton becomes completely full or (ii) moulting is triggered by seasonal cues.

The asynchronous moult patterns of males and immature females, as discussed in Section 2.2.3, indicate that these individuals moult when their current exoskeleton is completely full. Moulting in males and immature females is therefore triggered by the reaching of a critical weight, w^*_{n+1}, where

$$w^*_{n+1} = cw^*_n. \tag{2.5}$$

where c is a constant of proportionality and w^*_n is the weight of the individual at the previous moult.

In mature females, the duration of the intermoult period is directly related to the length of the incubation period, since females cannot moult whilst carrying eggs. The switch from annual to biennial moulting in mature females (see Section 1.1) indicates that moulting in mature females is most likely triggered by seasonal cues eg increasing temperature / day length. For simplicity, a fixed annual date is used to trigger moulting in mature females within the model. The fixed annual date is taken to be May 1st as discussed in Section 2.2.3. It is important to note that mature females are still bound by the critical weight threshold. This prevents them from increasing their weight beyond the critical weight threshold within a single reproductive year.

Moulting causes individuals to shed their current exoskeleton and increase in size. The length of the new exoskeleton, L_{n+1}, is determined using a standard weight-length relationship:

$$L_{n+1} = \left(\frac{w}{a}\right)^{\frac{1}{b}}. \tag{2.6}$$

where w is current weight (g) and a and b are sex-specific parameters as shown in Table 2.2.

Sex	**a**	**b**	
Males	0.00028	3.24	(Howard and Hall, 1983)
Females	0.00074	2.91	(Howard and Hall, 1983)

Table 2.2: Table showing weight-length parameters for male and female *Nephrops* in the CSA.

The model therefore uses fixed moult increments for males and immature females. The length of time between moults, however, varies with pre-moult size. Smaller individuals have shorter intermoult periods, and therefore moult more frequently as required. Mature females, on the other hand, moult annually. As a result, the length of the intermoult period is fixed in mature females whilst moult increment varies with pre-moult size.

2.4.3 Model Implementation

The model was implemented in R (R Core Team, 2014). The model combines continuous weight increase with discontinuous length increase. In order to do this the model is run on a daily time step. At the end of each day the weight ODE (Equation 2.4) is temporarily paused. Length is then updated using the update rules shown in Equations 2.7 - 2.8. These rules summarise the moult information set out in Section 2.4.2. Following this, the weight ODE is restarted and allowed to run for a further daily time step before the system is paused and the process is repeated.

Males and Immature Females

$$L_{t+1} = \begin{cases} (\frac{w_t}{a})^{\frac{1}{b}} & \text{if } w_n > cw_{n+1} \\ L_t & \text{otherwise} \end{cases} \tag{2.7}$$

Mature Females

$$L_{t+1} = \begin{cases} (\frac{w_t}{a})^{\frac{1}{b}} & \text{if day of the year} = 121 \\ L_t & \text{otherwise} \end{cases} \tag{2.8}$$

2.5 Parameterisation of Growth Model

Growth data for *Nephrops* in the CSA were collected by Bailey and Chapman (1983). This includes data on the relationship between moult increment and pre-moult size, as discussed in Section 2.2.1. Bailey and Chapman (1983) also generated age-length data for *Nephrops* in the CSA, by examining prominent length classes in length frequency data. These two datasets provide the information necessary to parameterise the *Nephrops* DEB growth model.

2.5.1 Fixed Parameters

Parameter c (see Equation 2.5) describes the percentage weight increase which can occur in males and immature females, before individuals outgrow their current exoskeleton and are forced to moult. The value of this parameter was determined directly from data on moult increment and pre-moult size collected by Bailey and Chapman (1983). Linear regressions were carried out separately on the data for males and immature females, forcing the regression line to pass through the origin as shown in Figure 2.7. This produced the following set of regression equations:

$$\text{Males}: \text{MI} = 0.102104\, L_n \tag{2.9}$$

$$\text{Immature Females}: \text{MI} = 0.076293\, L_n \tag{2.10}$$

where MI is moult increment and L_n is the length of an individual at moult n. Data points corresponding to mature females were excluded from the data since moulting in mature females occurs annually and is therefore not governed by the parameter 'c'.

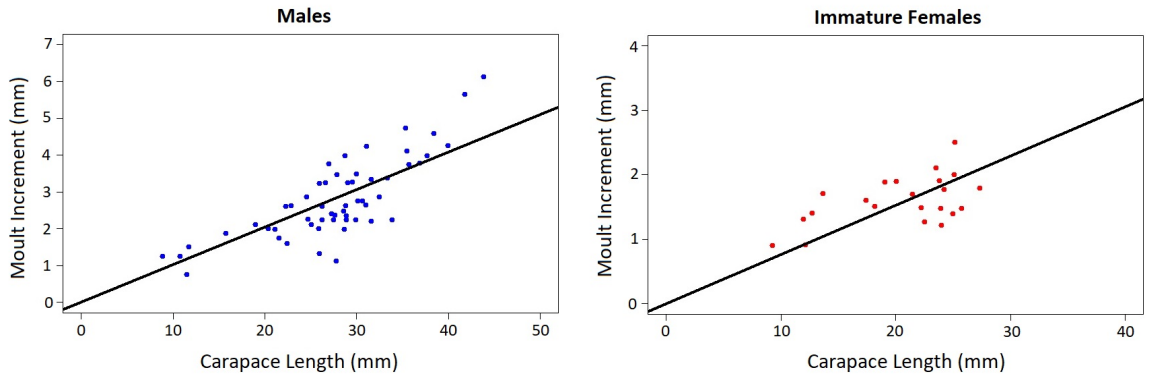

Figure 2.7: Data showing moult increment across a range of different pre-moult sizes collected by Bailey and Chapman (1983). Males are shown in blue and immature females are shown in red, with linear regression lines shown in black.

The length of an individual at moult 'n+1' can be calculated from its length at moult 'n' and corresponding moult increment using the equation:

$$L_{n+1} = L_n + \text{MI}. \tag{2.11}$$

Substituting the expressions for MI shown in Equations 2.9 and 2.10 gives us

$$\text{Males}: \; L_{n+1} = 1.102104 \, L_n \tag{2.12}$$

$$\text{Immature Females}: \; L_{n+1} = 1.076293 \, L_n. \tag{2.13}$$

The moult model states that males and immature females will moult upon reaching a critical weight w^*_{n+1}, where $w^*_{n+1} = cw^*_n$, as shown in Equation 2.5. Converting this equation from weight to length using the weight-length relationship parameters shown in Table 2.2 gives us

$$\text{Males}: \; L_{n+1} = c^{1/3.24} \, L_n \tag{2.14}$$

$$\text{Immature Females}: \; L_{n+1} = c^{1/2.91} \, L_n \tag{2.15}$$

Comparing these equations with equations 2.12 and 2.13 makes it possible to conclude that c equals 1.37 and 1.24 for males and immature females respectively. Male *Nephrops* can therefore increase in weight by 137% before they outgrow their current exoskeleton and are required to moult. Immature females, on the other hand, can increase in weight by 124% before they are required to moult.

It is important to note that the fit of the model for males could be improved by fitting separate linear regressions for immature and mature males, as shown in Bailey and Chapman (1983) - see Figure 2.2. However, the linear regression line for mature males would not pass through the origin. As a result, the critical weight threshold for mature males would become length dependent. This increases the complexity of the model as well as reducing its biological interpretability. For biological and mathematical simplicity, a single critical weight threshold is therefore used to trigger moulting in both immature and mature males.

2.5.2 Free-fitting Parameters

Parameters ϕ, μ, δ and L_0 were estimated by fitting the *Nephrops* DEB growth model to growth data collected by Bailey and Chapman (1983). Model fitting was carried out using the optim package in R (R Core Team, 2014). The best fit model was determined using minimum least squares regression, with separate model fitting processes applied to

males and females, as described below. Following the estimation of L_0, a corresponding value for initial weight, W_0, was then determined using the weight-length relationship, shown in Equation 2.6.

The moult increment of males and immature females is determined by parameter c as described in Section 2.5.1. As a result males are already pre-fitted to match the moult increment data collected by Bailey and Chapman (1983). The remaining parameters governing male growth were therefore optimised to fit the age-length data only. The moult increment of mature females, however, is not governed by parameter c. The growth parameters for females were therefore optimised simultaneously to the moult increment data and to the age-length data. The optimised values for ϕ, μ, δ, L_0 and W_0 are shown in Table 2.3.

Name	**Description**	**Males**	**Immature Females**	**Mature Females**
ϕ	Parameter determining the rate of energy consumption	0.00005	0.00007	0.00007
μ	Parameter determining the amount of energy spent on metabolism	0.00025	0.002	0.002
δ	Parameter determining the amount of energy invested in reproduction	0	0	0.0003
L_0	Initial Length (mm)	6	6	-
W_0	Initial Weight (g)	0.09	0.14	-

Table 2.3: Table showing optimised parameters for the *Nephrops* DEB growth model.

Examples of the growth curves produced under these optimised parameters are shown in Figure 2.8. The *Nephrops* DEB growth model shows a good fit to the age-length data of Bailey and Chapman (1983). The model produces growth curves which are roughly Von Bertalanffy in shape, and match up relatively well with the standard Von Bertalanffy growth curves used in ICES stock assessments. Furthermore, the model is also able to replicate the distinctive patterns in moult increment observed in experimental data. Moult increment increases with increasing size in males and immature females, with a clear switch to decreasing moult increments in mature females. The *Nephrops* DEB growth model is therefore able to accurately simulate the growth of both male and female *Nephrops* in the CSA.

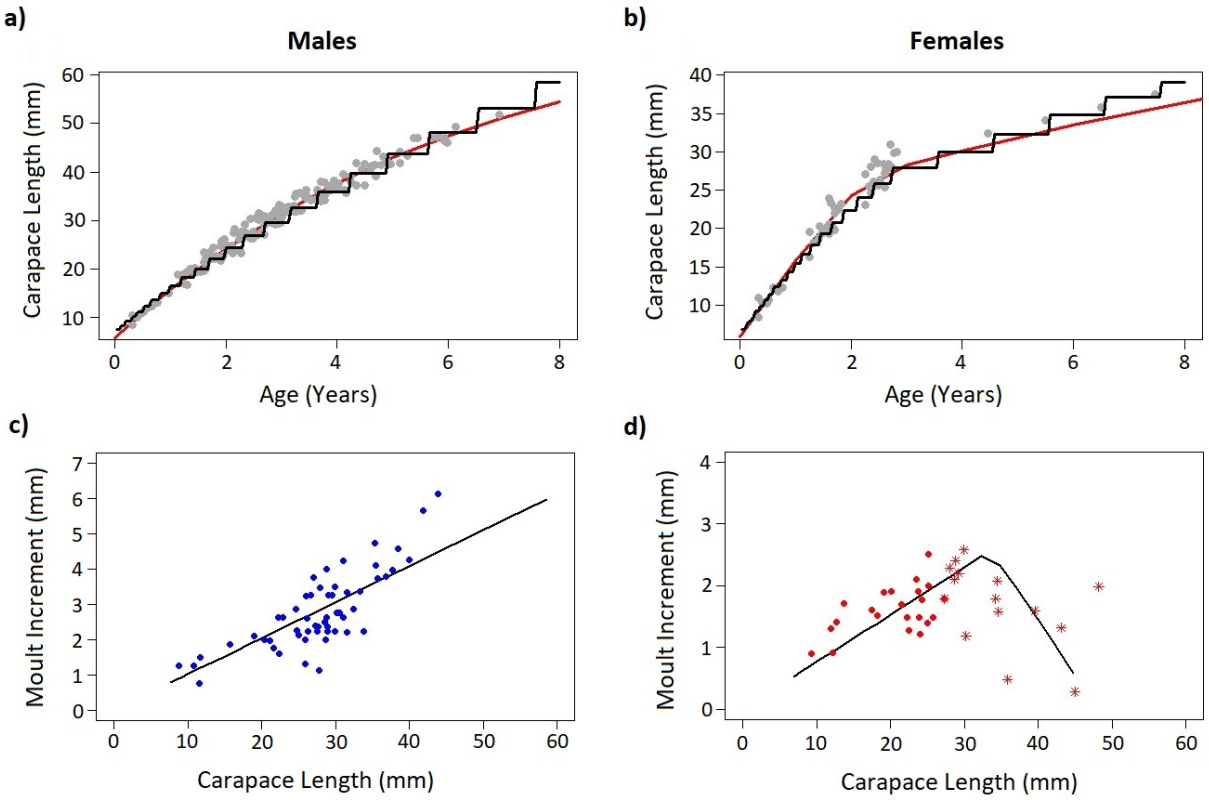

Figure 2.8: Plots (a) and (b) show the growth curves of males and females respectively. The black line shows the output of the *Nephrops* DEB growth model, the grey points are age-length data from Bailey and Chapman (1983) and the red line is the standard Von Bertalanffy curve used by ICES for *Nephrops* stock assessments. Plots (c) and (d) show moult increments at different lengths for males and females respectively. The black line shows the output of the *Nephrops* DEB growth model. The points show Bailey and Chapman (1983) experimental data, with males represented by blue dots, immature females by red dots, and mature females by red stars.

2.6 Conclusion

In conclusion, a new approach for modelling the growth of *Nephrops* in the CSA has been developed based on the dynamic energy budget framework. The *Nephrops* DEB growth model is able to accurately simulate *Nephrops* growth data from the CSA. Most importantly it also includes distinct moulting events crucial for correctly modelling *Hematodinium* transmission. This model can easily be adapted to model the growth of *Nephrops* in other geographical locations and could also be extended to model the growth of other crustaceans.

Chapter 3

Nephrops-Hematodinium Population Model

3.1 Introduction

In this chapter, I create a population model of *Nephrops* and *Hematodinium* in the CSA by combining our model of *Nephrops* growth set out in the previous chapter with key information on mortality, reproduction and parasite transmission. The model will be used to explore current knowledge gaps by examining the effect of contrasting model assumptions on the fit of the model to observational data. The model will also be used to improve our understanding of host-parasite dynamics and to explore the potential effects of altering current fishing management strategies on stock abundance and population health (i.e. the prevalence of *Hematodinium*).

This chapter focuses solely on model creation and outlines the key processes and equations which make up the *Nephrops-Hematodinium* population model. The model incorporates key aspects of the life cycle of *Nephrops* including growth, mortality, reproduction and density-dependent larval settlement. More detail on these processes can be found in Section 1.1. *Hematodinium* infection is incorporated into the model via two key assumptions. Firstly, we assume that parasitic spores are released into the environment by infected individuals whilst they are undergoing a moult. Although not yet fully proven, recent experimental work by Gornik et al. (2015) has alluded to the importance of the moult hormone, methyl farnesoate, in triggering the parasite to switch from the growth phase into the spore production phase (see Section 1.4 for more details). Secondly, we assume that uninfected individuals contract the infection by coming into contact with a spore whilst in a soft-shelled recently moulted condition. This is thought to be the most plausible method of parasite transmission, as discussed in Sections 1.4 and 1.6.4. The distinct

moulting events included in the Nephrops DEB growth model therefore play a crucial role in modelling parasite transmission, with sporulation and peak susceptibility both directly linked to moulting events.

3.2 Description of *Nephrops-Hematodinium* Population Model

3.2.1 Overview

The model tracks individuals from the first post-metamorphic stage onwards (see Figure 1.2). Individuals are partitioned into four distinct groups: uninfected females, uninfected males, infected females and infected males. Each group is comprised of a number of distinct cohorts, each of which contains individuals born within a relatively short time period. All individuals are assumed to be born healthy/uninfected. All individuals in the model therefore start out in an uninfected cohort. Uninfected individuals can, however, go on to develop infection. This occurs at distinct time points in the model, namely the time at which moulting occurs. This causes a proportion of the uninfected cohort to separate into a new infected cohort.

The model is based upon a classic modelling approach, known as an 'escalator boxcar train' model (see de Roos (1988) for more detail). This approach assumes that all individuals within a cohort develop at the same rate. Hence, individuals in a cohort are not only identical in age but are also assumed to be identical in weight, length etc. Individuals within a cohort are therefore said to move along 'characteristic lines'. This approach was adapted to allow for parasitic infection. The model therefore incorporates an extra dimension, in comparison to traditional 'escalator boxcar train' models. This allows uninfected cohorts to branch off into a number of infected 'sub-cohorts', as depicted in Figure 3.1. This creates a suite of 'characteristic lines' along which individuals can move.

The model stores key information about each cohort. This includes the number of individuals within the cohort (N). It also includes the weight (W), length (L), amount of energy invested in reproduction (E) and parasite burden (P) of individuals in each cohort. This information is tracked using a system of ODEs, as described in the following section.

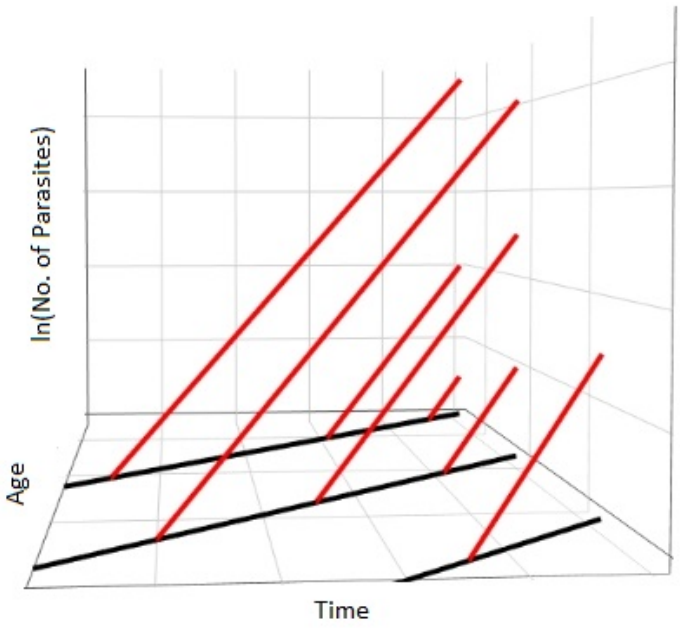

Figure 3.1: Schematic diagram of the extended 'escalator boxcar train' model approach. Cohorts move along characteristic lines, with uninfected cohorts branching off into infected cohorts. Branching occurs at distinct model time-steps, which correspond directly with the timing of moult events. Uninfected and infected individuals are represented by black and red lines respectively.

3.2.2 Cohort ODEs

Each cohort is marked with an identity marker i. The number of individuals in the i^{th} cohort, $\mathrm{N_i}$ is tracked using the equation

$$\frac{dN_i}{dt} = -Z^{l,s,p,t} N_i \tag{3.1}$$

where $Z^{l,s,p,t}$ is the mortality of individuals of length l, sex s and parasite burden p at time t. The overall mortality rate $Z^{l,s,p,t}$ is the sum of three separate components: natural mortality, fishing mortality and disease mortality. These processes are described in more detail in Section 3.2.5.

Secondly, the weight of individuals in the i^{th} cohort, $\mathrm{W_i}$, is tracked using the equation

$$\frac{dW_i}{dt} = \phi L_i^2 - \mu W_i - \delta W_i - \gamma P_i \tag{3.2}$$

This equation is an extension of the *Nephrops* DEB growth model outlined in the previous chapter (see Equation 2.4). An additional term has been added to describe the

energetic cost of parasitic infection. As before ϕL_i^2 represents energy acquired via feeding and μW_i and δW_i represent energy spent on metabolism and reproduction respectively. The additional cost associated with the disease is dependent on the number of parasites within the host (P_i) and an energy conversion factor (γ). Note that P=0 for individuals not infected with *Hematodinium*. 'Healthy' individuals therefore follow the same growth trajectories set out in the previous chapter.

Thirdly, the amount of energy invested in reproduction by individuals in the i^{th} cohort, E_i, is tracked using the equation

$$\frac{dE_i}{dt} = \delta W_i \tag{3.3}$$

The amount of energy invested in reproduction is reset to 0 following the production of eggs.

Finally, the number of parasites is assumed to grow exponentially. The parasite burden of each individual in the i^{th} cohort, P_i, is therefore tracked using the equation

$$\frac{dP_i}{dt} = gP_i \tag{3.4}$$

where g is a parameter describing the rate of parasite growth.

The length of individuals in each cohort is also tracked. However, due to the discontinuous 'step-wise' nature of *Nephrops* growth, this cannot be modelled using an ODE. Instead length increase is governed by a set of difference equations, as shown in Equations 3.5 and 3.6, and described fully in the previous chapter. Briefly, it is assumed that all mature females moult annually, regardless of infection status, whilst all males and immature females moult upon reaching a pre-specified critical weight threshold. More detail on this can be found in Section 2.4.2.

Males and Immature Females

$$L_{t+1} = \begin{cases} (\frac{W_t}{a})^{\frac{1}{b}} & \text{if } w_n > cw_{n+1} \\ L_t & \text{otherwise} \end{cases} \tag{3.5}$$

Mature Females

$$L_{t+1} = \begin{cases} (\frac{W_t}{a})^{\frac{1}{b}} & \text{if day of the year} = 121 \\ L_t & \text{otherwise} \end{cases} \tag{3.6}$$

The model is run on a daily time step. At the end of each time step the system of ODEs is temporarily paused. Each cohort is then systematically checked to determine whether or not moulting will take place. Length changes are then applied to the corresponding cohorts. Following this the ODEs are restarted and allowed to run for a further daily time step before the system is paused and the process is repeated.

3.2.3 Initiating New Uninfected Cohorts

New uninfected cohorts are introduced into the model via reproduction. The total number of annual recruits is calculated on a fixed date each year (1st July). This value is subsequently divided into 2 separate cohorts (1 male and 1 female). New male and female cohorts are then launched into the model. This coincides with the time at which *Nephrops* larvae in the CSA metamorphose into the adult form (see Figure 1.2). The total number of new recruits introduced into the model is determined using the equation:

$$\text{Total Annual Recruits} = \kappa_1\kappa_2 \text{ Potential Fecundity x Settlement Probability} \tag{3.7}$$

where 'Potential Fecundity' represents the total number of eggs produced during the preceding egg laying season (taken to be 1st August of the previous year), κ_1 and κ_2 represent the survival rates of eggs and larvae respectively, and 'Settlement Probability' represents a density dependent larval settlement rate.

Potential fecundity is dependent on the amount of energy invested in reproduction and is calculated using the equation:

$$\text{Potential Fecundity} = \sum_{i=1}^{\text{No. of Cohorts}} \frac{E_{i,t-334}}{c_e} N_{i,t-75} \tag{3.8}$$

where c_e is the energetic cost of producing a single egg, $E_{i,t-334}$ is the amount of energy invested in reproduction by individuals in the i^{th} female cohort at the time of egg production and $N_{i,t-75}$ is the number of individuals in the i^{th} female cohort at the point at which larvae begin to hatch.

Density dependent factors affect the survival rate of juveniles during the post-settlement period. This occurs via two main mechanisms: (1) a reduction in available space for burrow construction and (2) cannibalism of younger individuals (ICES 2000). In the model the probability of a juvenile settling, and therefore surviving, is density dependent and is described by the equation:

$$\text{Settlement Probability} = e^{\frac{\text{-Total Biomass}}{B_0}} \tag{3.9}$$

where B_0 is a constant determining the carrying capacity of the population and total biomass is the total weight of the population at the beginning of the settlement period (1st July) .

Total annual recruitment is assumed to be split evenly between males and females, i.e a 50:50 male female ratio is assumed. New cohorts are launched with an initial weight, W_0 and an initial length, L_0.

3.2.4 Initiating New Infected Cohorts

The creation of new infected cohorts in the model occurs when uninfected individuals come into contact with a parasitic spore whilst in the soft-shelled, recently moulted condition. For simplicity, individuals in the model can only become infected if they come into contact with a spore on the same day as the moult occurs. In reality, individuals remain in a soft shelled condition for a number of days following moult, and are therefore vulnerable to infection for a longer period. However, this period is relatively short (2-3 days) and therefore has no significant effect on the overall model results.

The number of newly infected individuals of sex s and length l at time t ($N^{s,l,t}$) is calculated using the equation

$$N^{l,s,t} = N_{rm}^{l,s,t}\left(1 - e^{-\beta X_t}\right) \tag{3.10}$$

where $N_{rm}^{l,s,t}$ is the number of uninfected 'recently moulted' individuals, X_t is the number of spores in the environment at time t, and β is the probability of coming into contact with a spore.

Newly infected cohorts take on the weight and length of their uninfected counterparts. Newly infected individuals are assumed to be infected by a single parasite cell i.e. $P_0 = 1$. After creation of a new infected cohort, the number of individuals in the corresponding uninfected cohort is adjusted to account for the removal of newly infected individuals.

3.2.5 Spore Release and Survival

The total number of spores in the environment, X_t, is calculated using the equation

$$X_t = e^{-\lambda} X_{t-1} + S_t \tag{3.11}$$

where λ is the decay rate of spores, and S_t is a pulse of spores caused by sporulation of infected individuals.

Sporulation of infected individuals is assumed to occur at distinct moulting events. Infected individuals can, however, moult successfully without the production of spores (e.g. if parasite cells are still in the growth stages and are relatively low in concentration). Here we assume that the probability of producing spores at moult is dependent on the parasite concentration and takes the form of the following logistic regression equation:

$$\text{Probability of Sporulating at Moult} = \frac{1}{1 + e^{(-k_c(C - C_{50}))}} \tag{3.12}$$

where k_c is a slope parameter and C_{50} is the parasite concentration at which 50% of individuals sporulate. C is the concentration of parasites in the haemolymph and is calculated using the equation

$$C = \frac{P}{V} \tag{3.13}$$

where P is the number of parasites and V is the volume of haemolymph. The total volume of haemolymph is assumed to be proportional to weight and is calculated using the equation:

$$\mathrm{V} = h\, W \tag{3.14}$$

The total number of spores released at time t, S_t, is the sum of all spores released from the subset of infected cohorts moulting at time t:

$$S_t = \sum_{i=0}^{\text{No. of infected cohorts moulting at time t}} \text{Probability of Sporulating at Moult} \;\; N_i \; P_i \tag{3.15}$$

where N_i is the number of individuals in the i^{th} cohort and P_i is the parasite burden of an individual in the i^{th} cohort. For simplicity, it is assumed that each spore is formed from a single parasite cell and that all spores are initially viable.

Sporulation ultimately results in the death of infected individuals. Infected individuals

are therefore removed from the model once sporulation has occurred. Following each sporulation event, the number of individuals in each infected cohort is recalculated to account for the number of individuals lost, according to the equation

$$N_{i,t+1} = N_{i,t} - \text{Probability of Sporulating at Moult x } N_{i,t} \tag{3.16}$$

3.2.6 Natural, Fishing and Disease Mortality

Total mortality, $Z^{l,s,p,t}$, is composed of three main components: natural mortality, M, fishing mortality $F^{l,s,p,t}$ and disease mortality D^p. Total mortality is therefore calculated using the equation:

$$Z^{\,\mathrm{l,s,p,t}} = M + F^{\mathrm{l,s,p,t}} + D^p \tag{3.17}$$

Natural mortality (M) is assumed to be the product of two main components: a constant mortality rate (m) and a quarterly catchability parameter $Q^{l,s,p,t}$. The quarterly catchability parameter scales the natural mortality rate to reflect the amount of time an individual spends outside of their burrow. This is dependent on both sex and infection status, as described in Section 1.1 and Section 1.6.4. Natural mortality is therefore calculated using the equation:

$$M = Q^{l,s,p,t}m \tag{3.18}$$

Fishing mortality ($F^{l,s,p,t}$) is assumed to be the product of three main components: a quarterly catchability parameter $Q^{l,s,p,t}$ (as described above), a time dependent effort component (E^t) and a length dependent selectivity component (S^l) which accounts for gear selectivity. Fishing mortality is therefore calculated using the equation:

$$F^{\mathrm{l,s,p,t}} = c_1 Q^{l,s,p,t} E^t S^l \tag{3.19}$$

where 'c_1' is a scaling parameter.

Length dependent gear selectivity (S^l) ranges from 0 to 1 and represents the probability that an individual of length l is caught and retained by fishing gear. Fishing gear is often adjusted to select for larger individuals whilst allowing smaller, less marketable, individuals to escape unharmed. Length dependent gear selectivity is therefore represented by the two-parameter logistic curve:

$$S^l = \frac{1}{1 + e^{(-k_s(l - l_{50}))}} \tag{3.20}$$

where k_s is a slope parameter and l_{50} is the length at 50% selectivity.

Infected individuals experience increased mortality rates as a result of the infection. This is primarily caused by increased levels of exhaustion as well as a reduction in swimming ability (Stentiford et al. 2000). Reductions in swimming ability are likely to increase with infection severity. This increases the likelihood of heavily-infected individuals being captured by predators or caught in fishing gear. An additional disease mortality term (D^p) is therefore included in the model, where

$$D^p = dP \tag{3.21}$$

3.2.7 Catch, Landings and Discards

The number of individuals, of length 'l', sex 's' and parasite burden 'p' caught at each time step, $C_{l,s,p,t}$, is calculated using the Baranov catch equation:

$$C^{\,\mathrm{l,s,p,t}} = \frac{F^{\,\mathrm{l,s,p,t}}}{Z^{\,\mathrm{l,s,p,t}}} \left(1 - e^{-Z^{\,\mathrm{l,s,p,t}}}\right) N^{\,\mathrm{l,s,p,t}} \tag{3.22}$$

The catch is split into landings, $L^{\,\mathrm{l,s,p,t}}$, and discards, $D^{\,\mathrm{l,s,p,t}}$, according to the equation:

$$L^{\,\mathrm{l,s,p,t}} = C^{\,\mathrm{l,s,p,t}} - D^{\,\mathrm{l,s,p,t}} \tag{3.23}$$

The number of individuals discarded, $D^{l,s,p,t}$, is estimated using the equation:

$$D^{\,\mathrm{l,s,p,t}} = C^{\,\mathrm{l,s,p,t}} \times d^{\,\mathrm{l,p}} \tag{3.24}$$

where $d^{\,\mathrm{l,p}}$ represents the probability of discarding for individuals of length 'l' and parasite burden 'p'. Fishermen in the CSA are known to selectively discard individuals which show visible signs of *Hematodinium* infection (Albalat et al., 2016b). Fishermen are also known to selectively discard small individuals including those which fall below the Minimum Conservation Reference Size (MCRS) (Fox et al., 2020). Fish below the MCRS cannot be sold for human consumption and therefore have a reduced market value. The probability of discarding therefore depends on two main factors: length (l) and parasite burden (p), and is calculated using the equation:

$$d^{\,\mathrm{l,p}} = \begin{cases} 1 & \text{if } \frac{P}{V} > 50{,}000{,}000 \quad \text{i.e. individual is visibly-infected} \\ d^{\,\mathrm{l}} & \text{otherwise} \end{cases} \tag{3.25}$$

where P is the number of parasites, V is the volume of haemolymph and $d^{\,\mathrm{l}}$ is a function which describes the probability of discarding an individual of length 'l'. Individuals are

classified as visibly-infected if the concentration of parasites per ml haemolymph is greater than 50,000,000.

The probability of discarding individuals which show no signs of visible infection depends solely on length and is calculated using a two-parameter logistic function:

$$d^{\,l} = \frac{1}{1 + e^{(k_d(l - d_{50}))}} \tag{3.26}$$

where k_d is a slope parameter and d_{50} is the length at which 50% of individuals are discarded.

A proportion of discarded individuals are assumed to survive. For simplicity, the *Nephrops-Hematodinium* population model assumes a constant discard survival rate for all individuals. However, in reality, the survival rate of discarded individuals depends on a number of factors including size, infection status, trawling time and the location of animals within the cod-end (Albalat et al., 2016b).

The number of discarded individuals surviving, D_{Surv} is calculated using the equation:

$$D_{surv} = \psi \; D^{\,\mathrm{l,s,p,t}} \tag{3.27}$$

where ψ is the discard survival rate. Discarded individuals which survive are added back into their respective cohorts.

3.3 Model Implementation

The model is implemented in R. A copy of the R code used to run the model can be found in Appendix A. To improve the efficiency of the model, the system of ODEs (Equations 3.1 - 3.5) are converted into a set of coupled difference equations implemented with a daily time step, as shown below. Full details on this conversion can be found in Appendix B. To ensure the coupled difference equations converged to the same solutions as the original ODEs, the results were compared with a separate model in which the system of ODEs was solved using the ode45 method in the deSolve Package (R Development Core Team, 2014).

$$N_{i,t+1} = e^{-Z} N_{i,t} \tag{3.28}$$

$$W_{i,t+1} = \frac{e^{-(\mu+\delta)\left(1+\frac{ln(-(\mu+\delta)W_{i,t}+(\phi L_{i,t}^2-\gamma P_{i,t}))}{-(\mu+\delta)}\right)} - (\phi L_{i,t}^2 - \gamma P_{i,t})}{-(\mu+\delta)} \tag{3.29}$$

$$E_{i,t+1} = \delta W_{i,t} + E_{i,t} \tag{3.30}$$

$$P_{i,t+1} = e^g P_{i,t} \tag{3.31}$$

The efficiency of the model was also improved by setting a maximum number of cohorts. After this maximum number of cohorts is reached, the creation of a new cohort results in the cohort with the fewest individuals being overwritten, and the new cohort taking its place. The maximum number of cohorts is carefully set to minimize the loss of individuals from the model, with separate values used for infected and uninfected cohorts. New uninfected cohorts are created annually. Infected cohorts, on the other hand, are created at each distinct moult event. Consequently, the maximum number of infected cohorts must be substantially greater than the maximum number of uninfected cohorts. In the baseline *Nephrops-Hematodinium* population model the maximum number of uninfected cohorts is set at 20 and the maximum number of infected cohorts is set at 400.

3.4 Model Output

Each model run begins by first 'spinning up' an infection-free population to an equilibrium state in the absence of fishing mortality. This ensures that a viable fishery-free/infection-free equilibrium is attained as a minimum constraint to the model. Following this, fishing mortality is introduced and the population is allowed to settle to a new equilibrium. Infection is then introduced into the model via a pulse of spores. The number of spores in this initial pulse is determined by the parameter, X_0. Following this, the population is once again allowed to settle to a new equilibrium.

Model output during this final period is stored for further analysis and for comparison with real-world data. Several key metrics are calculated from the model including the abundance of individuals in the model, the weight of individuals landed and discarded, the length distribution of individuals in the population and the length distribution of individuals landed and discarded. Key information is also stored about the prevalence of *Hematodinium* in the population. This includes the background level of infection in the population, as well as the proportion of individuals diagnosed with infection according to different *Hematodinium* diagnostic tests.

The majority of these metrics can be calculated directly from the model output. Some metrics, however, require further processing of model output. This includes the length distribution of individuals and the prevalence of *Hematodinium* infection as determined by different diagnostic tests. The post-processing procedures required to obtain these metrics are outlined below.

3.4.1 Redistributing Length Classes

The *Nephrops* DEB growth model causes individuals to transition from one length to another at specified moult events, with all individuals moving along the same growth trajectory. Consequently, there are certain length classes in the model that do not (and cannot) contain any individuals. For example, upon moulting a female with an initial carapace length 29 mm gains a new carapace with a length of 32 mm. The model therefore does not contain any females with a carapace length of 30 or 31 mm. This results in a 'patchy' length distribution, in which individuals of certain lengths are completely absent from the population. An example of such a length distribution is shown in Figure 3.2 (a).

To counteract this, individuals in occupied length classes are redistributed using a normal distribution with μ equal to the length of the occupied length class and a constant variance of 10 %. An example of a length distribution after this redistribution process has been applied can be seen in Figure 3.2 (b). The redistribution process spreads the population out across all length classes. This allows for an improved fit between model and observed length distributions. This also removes the assumption that all individuals grow identically and allows for an element of stochastic growth.

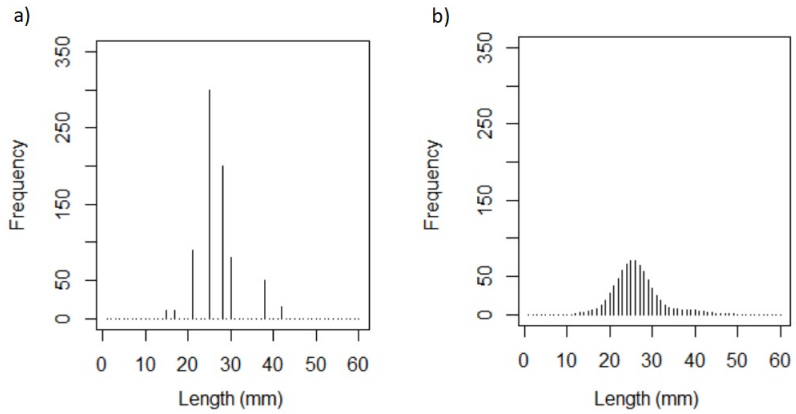

Figure 3.2: Diagram showing a hypothetical example of (a) a typical model length distribution and (b) a model length distribution after the length classes have been redistributed.

3.4.2 *Hematodinium* Prevalence

Hematodinium infection in *Nephrops* is diagnosed via a number of different diagnostic methods. This includes the body colour method, the pleopod method, western blot immunoassay, ELISA and PCR. More detail on each of these diagnostic methods can be found in Section 1.5, alongside a table outlining the detection threshold of each method (see Table 1.1). The detection threshold of each method is based on the concentration of parasite cells in the haemolymph and ranges from 30 parasites per ml haemolymph for the most sensitive PCR method (Beevers, 2010) to 50,000,000 parasites per ml haemolymph for the least sensitive body colour method (Field et al., 1992).

Six separate prevalence values are extracted from the *Nephrops-Hematodinium* population model - one to correspond with each of the five main diagnostic tests and one which corresponds with the true level of *Hematodinium* prevalence. Prevalence values corresponding with each of the five main diagnostic tests are obtained from the *Nephrops-Hematodinium* population model by first calculating the concentration of parasitic cells in each individual in the model. This is achieved using the same process outlined in Equations 3.13 - 3.14. All individuals with a concentration level above the required detection threshold are classified as 'infected'. Individuals with a concentration level below the required detection threshold, on the other hand, are classified as 'uninfected'. Modelled estimates of parasite prevalence can then be compared with observational data collected using the corresponding diagnostic method. This allows for a fair comparison of model output with real-world observational data.

3.5 Conclusion

In conclusion, this chapter has outlined the development of a population model of *Nephrops* and *Hematodinium* in the CSA. This includes a detailed description of the key processes and equations which make up the model, the key metrics that are output from the model, as well as the post-processing procedures required to obtain these metrics. In the following chapter, the *Nephrops-Hematodinium* population model is parameterised by comparing model output to data on *Nephrops* and *Hematodinium* in the CSA. Finally, in Chapters 5-7, the model is used to further our understanding of this important host-parasite system and to examine the potential effects of altering fishing management strategies on the CSA *Nephrops* population.

Chapter 4

Parameterisation and Sensitivity Analysis

4.1 Introduction

The *Nephrops-Hematodinium* population model set out in the previous chapter contains a total of 29 parameters. Directly estimating the value of these parameters, however, is difficult due to the lack of experimental data. In this chapter, values for each of the model parameters are derived using a three-stage approach. Firstly, parameter values are obtained directly from the literature where possible. Following this, a small number of parameters are derived from empirical data. Finally, parameters for which no value could be obtained or derived, are treated as free-fitting parameters. Values for free-fitting parameters are obtained by fitting the *Nephrops-Hematodinium* population model to observational data on *Nephrops* and *Hematodinium* in the CSA. Observational data used in this process falls into three broad categories: (i) fisheries-related data, (ii) data on parasite prevalence and (iii) data on parasite growth.

Nephrops fishery data in the CSA is collected by Marine Scotland. It is important to note, however, that the Firth of Clyde and the Sound of Jura form a single Functional Unit. As a result, fisheries data are combined for both regions and cannot be easily separated. We therefore parameterise our population model to fisheries data for the whole Functional Unit. These data include annual estimates of the total weight of *Nephrops* landed and discarded within the region, as shown in Figures 4.1 (a) and (b) respectively. Other available fisheries related data include the length distribution of individuals landed and discarded, as well as annual estimates of *Nephrops* abundance. *Nephrops* abundance is estimated using an underwater TV survey to count the number of burrow openings on the seabed. The time series of abundance estimates is shown in Figure 4.1 (c). The

annual weight of landings and discards and the annual abundance estimates are publicly available and can be downloaded from ICES (2019). The length distribution of landings and discards, on the other hand, are not currently publicly available. This data can, however, be obtained directly from Marine Scotland Science.

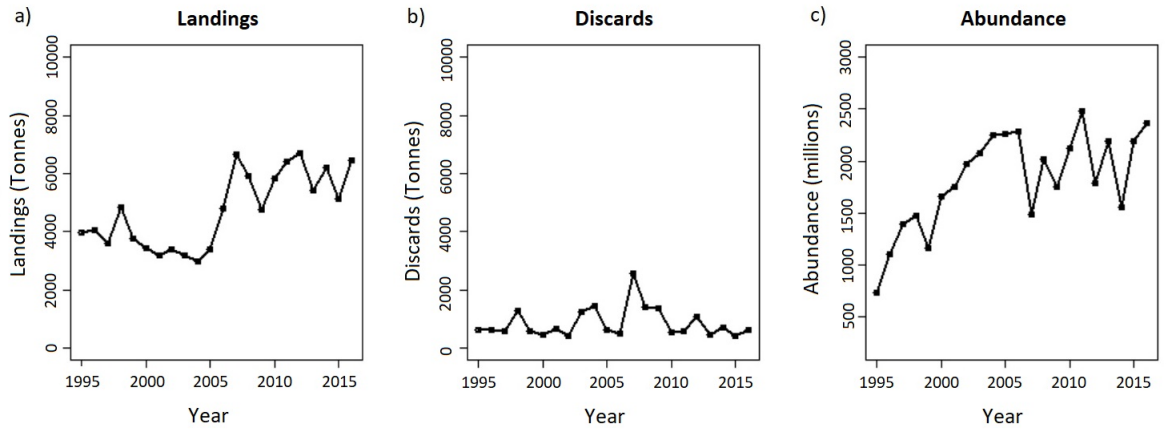

Figure 4.1: Figures (a) and (b) show the weight of *Nephrops* landed and discarded in the Firth of Clyde and Sound of Jura. Figure (c) shows the estimated abundance of *Nephrops* in the Firth of Clyde and Sound of Jura.

Two main sources of *Hematodinium* data were used to parameterise the model. The first dataset was collected by Stentiford et al. (2001b) and records the monthly prevalence of *Hematodinium* in the CSA from February 1998 to August 2000, as shown in Figure 1.9. It is important to note that the prevalence values within this dataset were collected using the relatively insensitive pleopod method of diagnosis. This dataset therefore only records the prevalence of high-level 'patent' infection. This dataset does, however, highlight the clear seasonal patterns in patent *Hematodinium* infection. The second source of *Hematodinium* data used to parameterise the model was collected by Appleton (1996). This dataset provides repeated measurements of the concentration of *Hematodinium* in the haemolymph of three infected individuals over time. This dataset therefore provides crucial information on the rate of parasite growth.

In this chapter, the fit of the model is optimised to the various sources of data described above. Following this, a sensitivity analysis of the optimised parameters is performed using a one-at-a-time sensitivity analysis method. This outlines the reliability of model results by highlighting the influence of parameter uncertainty on model output.

4.2 Parameter Estimation

Values for model parameters were obtained using a three-stage approach, as shown in the following sections. Firstly, parameter values were obtained directly from the literature where possible. Following this a small number of parameters were derived from empirical data. Finally, parameters for which no information could be found, were determined by fitting the model to observational data of *Nephrops* and *Hematodinium* in the CSA.

4.2.1 Parameters Obtained Directly from the Literature

A small number of parameters were obtained directly from the literature, as shown in Table 4.1. This includes fishing effort, E_t which was taken to be 130,000 hours fished per annum (ICES, 2009). This is the average value over the time period used in model parameterisation (1998-2000).

Other parameters obtained directly from the literature include the egg survival rate, κ_1, which was taken to be 0.65 (Briggs and McAliskey, 2002). Similarly, the survival rate of *Nephrops* larvae was obtained from a study carried out by Dickey-Collas et al. (2000). This study records a larval mortality rate of 0.033 per day for *Nephrops* larvae in the Eastern Irish Sea and a mean larval duration of 70 days. This provides an overall mortality rate for larvae of 95%. The survival rate of *Nephrops* larvae, κ_2, is therefore 0.05.

The survival rate of discarded *Nephrops* was also obtained directly from the literature. The survival rate of discarded *Nephrops* depends on a number of factors including size, infection status, trawling time and the location of animals within the cod-end (Albalat et al., 2016b). However, for simplicity, the *Nephrops-Hematodinium* population model assumes a constant discard survival rate (ψ) for all individuals. The baseline *Nephrops-Hematodinium* population model assumes a discard survival rate (ψ) of 25%. This value is reported in numerous studies including Wileman et al. (1999) and Chapman (1980) and is commonly used in *Nephrops* stock assessments (ICES, 2019). It is important to note, however, that some recent studies have reported substantially higher rates of discard survival. For example, Fox et al. (2020) estimated the discard survival rate of *Nephrops* to be around 60%. Albalat et al. (2016b), on the other hand, estimated the survival rate of discarded *Nephrops* to be as high as 90%. The consequences of altering the discard survival rate from the chosen baseline value of 25% are explored fully in Chapter 7.

Finally, the 'weight to haemolymph volume conversion factor', h, was obtained directly from Harris and Andrews (2005) and was set at 0.33.

4.2.2 Parameters Derived from Empirical Data

Parameters that could not be obtained directly from the literature were derived from data, as shown below.

Discards - Size Selectivity

The values for the discard selectivity parameters were estimated by analysing data on the length frequency of the catch and the length frequency of discards as obtained from Marine Scotland (see Figure 4.2) The logistic function (Eq 3.26) was optimised to fit the data using the optim package in R (R Core Team 2014). This produced values of 0.38 and 23.05 for k_d and d_{50} respectively.

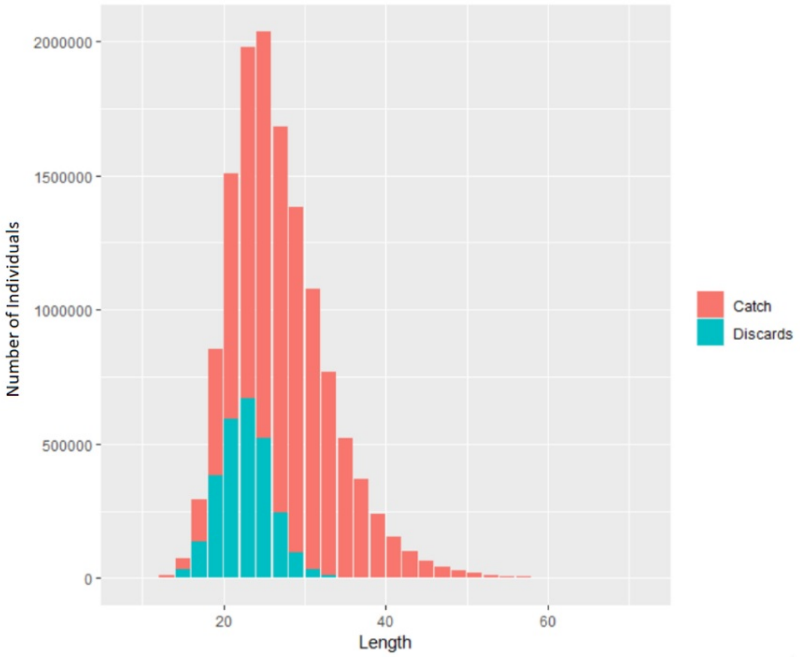

Figure 4.2: Length frequency of the catch and discards combined across all available years (1981-2017).

Energetic Cost of Egg Production

The energetic cost of egg production, c_e, was determined by comparing the amount of energy invested in reproduction by individuals of different lengths with the commonly used length dependent equation for potential fecundity:

$$\text{Potential Fecundity} = aL^b \tag{4.1}$$

where L is the carapace length (mm) and 'a' and 'b' are constants. Values for 'a' and 'b' were taken to be 0.191 and 2.644 respectively for *Nephrops* in the CSA (Smith, 1987).

The energetic cost of producing a single egg, c_e, could therefore be calculated from the amount of energy invested in reproduction, E, using the equation:

$$c_e = \frac{E}{aL^b} \tag{4.2}$$

This produced a value of 0.001 for c_e.

Catchability

The burrow emergence patterns of *Nephrops* are known to differ substantially between males and females and between infected and uninfected individuals. This was incorporated into the model via a catchability parameter ($Q_{l,s,p,t}$). In order to determine suitable values for this parameter, the differing burrow emergence patterns between males and females were assessed by examining the sex ratio of individuals in the catch throughout the year. Quarterly catch data were obtained from Marine Scotland detailing the number of males and females caught from 1980 – 2017 at 1 mm length intervals. The data were separated by maturity status (with individuals > 27 mm classified as mature), and used to determine the proportion of immature and mature females in the catch as shown in Figure 4.3.

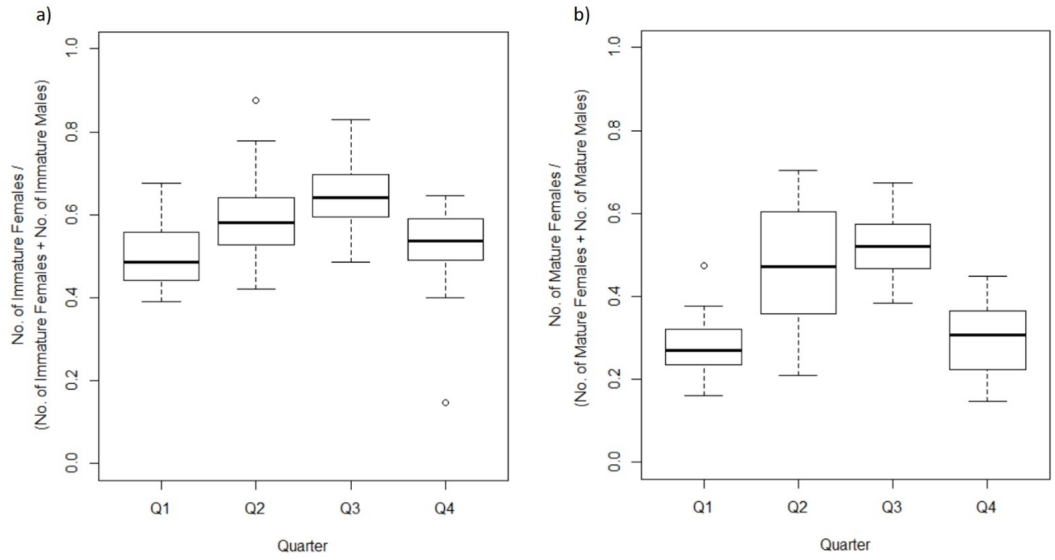

Figure 4.3: The proportion of (a) immature and (b) mature females in the catch separated by quarter for combined years 1981-2017.

The proportion of immature females in the catch was found to be roughly 0.5 across all quarters, with a slight increase in Q2 and Q3. This indicates that immature females are equally as likely to be captured by the fishery as immature males. The proportion of mature females in the catch, however, varies substantially throughout the year. The proportion of mature females in the catch is roughly 0.5 during Q2 and Q3 but falls significantly to 0.27 in Q1 and 0.3 in Q4. Mature females are therefore less likely to be captured by the fishery during the winter (Q4 and Q1) in comparison to mature males, but equally as likely to be captured during the summer (Q2 and Q3). This is thought to be caused by mature females spending more time inside their burrows during the winter months whilst they are incubating eggs.

In addition to differing patterns between males and females, burrow emergence patterns also differ between infected and uninfected individuals. Infected individuals spend significantly more time on the sediment surface in comparison to uninfected individuals (Field et al., 1998; Stentiford et al., 2001a,c). This is thought to be caused by the high energy demands of *Hematodinium* infection, which forces infected individuals to spend more time out of their burrow hunting for food. Consequently, infected individuals are more available to the fishery in comparison to their uninfected counterparts.

The complex burrow emergence patterns of *Nephrops* were incorporated into the model via a quarterly dependent catchability parameter $Q_{l,s,p,t}$. This parameter represents the relative catchability of each group in comparison to infected males and infected immature females, since this group spends the greatest amount of time outside of their burrows. The catchability of each group is shown in Table 4.1. q_1 $(0 < q_1 < 1)$ accounts for the reduced catchability of infected individuals in comparison to their uninfected counterparts. q_2 $(0 < q_2 < 1)$, on the other hand, accounts for the reduced catchability of mature females during the winter months. The values of both q_1 and q_2 are estimated within the model. A graphical depiction of these values are shown in Figure 4.4.

Quarter	**Infected Males and Immature Females**	**Uninfected Males and Immature Females**	**Infected Mature Females**	**Uninfected Mature Females**
1	1	q_1	q_2	$q_1 q_2$
2	1	q_1	1	q_1
3	1	q_1	1	q_1
4	1	q_1	q_2	$q_1 q_2$

Table 4.1: Quarterly catchability parameters, $Q_{l,s,p,t}$, describing the amount of time different groups spend out of the burrow relative to infected males and immature females.

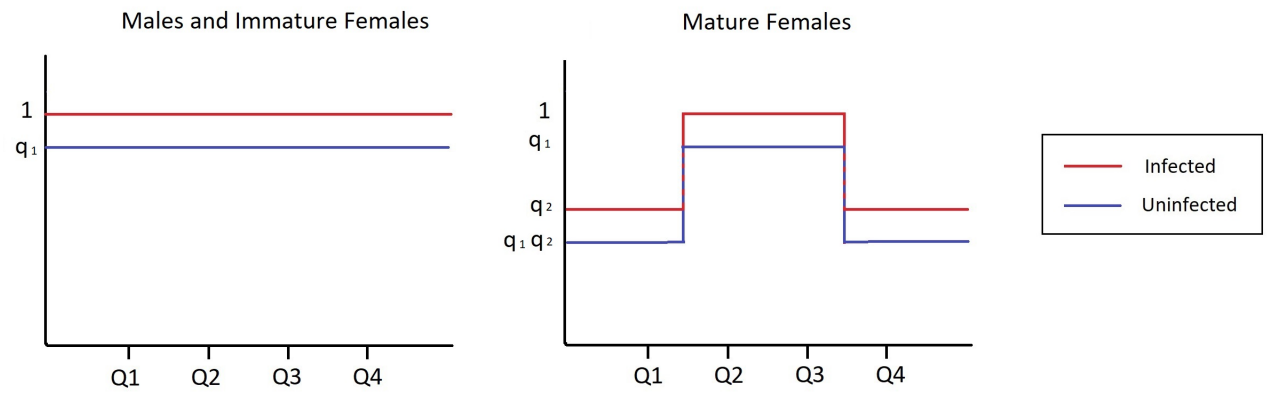

Figure 4.4: Graphical representation of the quarterly catchability parameter, $Q_{l,s,p,t}$, as shown in Table 4.1.

4.2.3 Free-fitting Parameters

Parameters for which no information could be obtained directly from the literature or derived from empirical data were treated as free-fitting parameters. Fitting parameters were found by fitting the model output to various sources of observational data on *Nephrops* and *Hematodinium* in the CSA. These observational data were grouped into three main categories: (i) fisheries-related data, (ii) data on parasite prevalence and (iii) data on parasite growth. The model was fitted by selecting the set of unknown model parameters (Ω) which minimized the following error:

$$\text{Error} = \min_{\Omega}(E_1 + E_2 + E_3) \tag{4.3}$$

where E_1, E_2 and E_3 are the error associated with fisheries data, *Hematodinium* prevalence data and parasite growth data respectively.

E_1, E_2 and E_3 are each made up of a number of sub-components as set out in the following sections. It is important to note that some sub-components are scaled to reduce their dominance (see Equations 4.4 - 4.6). The weighting of individual sub-components was developed through a process of trial and error. Early attempts to parameterise the model without the application of scaling factors led to a parameter set which was able to closely match the fisheries related data (in particular the weight of landings and discards and the abundance of *Nephrops*) but was much poorer at replicating the data on *Hematodinium* prevalence and growth. Consequently, a new optimisation process was developed in which

the weight of landings and discards and the abundance of *Nephrops* are scaled to reduce their dominance (see Equation 4.4). This allowed the model to produce a good fit to all of the different sources of data used in the parameterisation process.

Model fitting was carried out using the optim package in R (R Core Team 2014). The selected method of optimisation was 'L-BFGS-B'. This method is described fully in Byrd et al. (1995). In brief, this is a quasi-Newton optimisation method that uses function values and gradients to build up a picture of the surface being optimized.

Fisheries Related Data

Firstly, the model is fitted to various sources of fisheries related data. This includes annual estimates of the total weight of *Nephrops* landed and discarded in the CSA, length distributions of individuals landed and discarded, and an estimate of total *Nephrops* abundance from underwater TV (UWTV) surveys. These data sets covers a long time period covering 1990-2019. However, here we restrict ourselves to data collected from 1998-2000, in order to match the time period over which data on *Hematodinium* prevalence is also available.

Nephrops abundance, landings weight, and discard weight were averaged over this three year period. The mean values were then used for model fitting. Annual length distributions of landings and discards over the three year period were combined and normalized. This produced two separate length distributions (one for landings and one for discards) which were then used for model fitting. The error associated with fisheries related data, E_1, is therefore represented by Equation 4.4. It is important to note that some components of this equation are scaled to reduce the dominance of individual components and allow the model to fit to all components equally. It is also important to note that UWTV surveys estimate abundance by counting burrows on the seabed. Juvenile *Nephrops* are thought to reside in the burrows of older individuals. Hence, UWTV estimates are thought to be an estimate of individuals >17mm as opposed to a true estimate of population abundance. Model output was modified to reflect this assumption in order to allow for a fair comparison.

$$E_1 = \left(\frac{\text{Mean Modelled Abundance} - \text{Mean Observed Abundance}}{\text{Mean Observed Abundance}}\right)^2 +$$
$$\left(\frac{\text{Mean Modelled Landings Weight} - \text{Mean Observed Landings Weight}}{\text{Mean Observed Landings Weight}}\right)^2 +$$
$$\left(\frac{\text{Mean Modelled Discard Weight} - \text{Mean Observed Discard Weight}}{\text{Mean Observed Discard Weight}}\right)^2 +$$
$$(\text{Modelled Cumulative Length Distribution of Landings (l)} -$$
$$\text{Observed Cumulative Length Distribution of Landings (l)})^2 +$$
$$(\text{Modelled Cumulative Length Distribution of Discards (l)} -$$
$$\text{Observed Cumulative Length Distribution of Discards (l)})^2 \quad (4.4)$$

where l = carapace length which is increased in millimetre intervals from 1 to 80 mm.

Data on *Hematodinium* Prevalence

Secondly, the model is also fitted to observational data on *Hematodinium* prevalence in the CSA. The most complete record of parasite prevalence in the CSA covers the period from 1998-2000, as shown in Figure 1.9. Prevalence values were averaged over this three year period to produce a typical annual cycle. This cycle was then summarised using four summary statistics: maximum prevalence, minimum prevalence, the time at which maximum prevalence occurs and the time at which minimum prevalence occurs. These key summary statistics were then used in the model fitting process. It is important to note that the prevalence values within this dataset were collected using the relatively insensitive pleopod method of diagnosis. This dataset therefore only records the prevalence of high-level 'patent' infection. Model output was therefore modified, following the method outlined in Section 3.4.2, to extract 'pleopod-derived' prevalence values from the model, and to ensure a fair comparison. The error associated with *Hematodinium* prevalence data, E_2, is therefore represented by Equation 4.5.

$$E_2 = (\text{Max Modelled Parasite Prevalence} - \text{Max Observed Parasite Prevalence})^2 +$$
$$(\text{Min Modelled Parasite Prevalence} - \text{Min Observed Parasite Prevalence})^2 +$$
$$(\text{Time of Max Modelled Parasite Prevalence} - \text{Time of Max Observed Parasite Prevalence})^2 +$$
$$(\text{Time of Min Modelled Parasite Prevalence} - \text{Time of Min Observed Parasite Prevalence})^2 \quad (4.5)$$

Data on Parasite Growth

Finally, the model is fitted to experimental data collected by Appleton (1996). This dataset provides repeated measurements of the concentration of *Hematodinium* in the haemolymph of three infected individuals over time. Individuals were held in the laboratory in seawater tanks with a temperature of 10 °C. This temperature is typical of the average temperature experienced in the CSA. This dataset therefore provides detailed information on the rate of *Hematodinium* growth in the CSA. The number of parasite cells per ml haemolymph within each individual, as recorded by Appleton (1996), is shown in Figure 4.5. During the experiment, one of the individuals was observed to undergo sporulation. This is likely to have had a significant impact on the number of dinoflagellate cells within the host. We therefore exclude any measurements made following sporulation from the study.

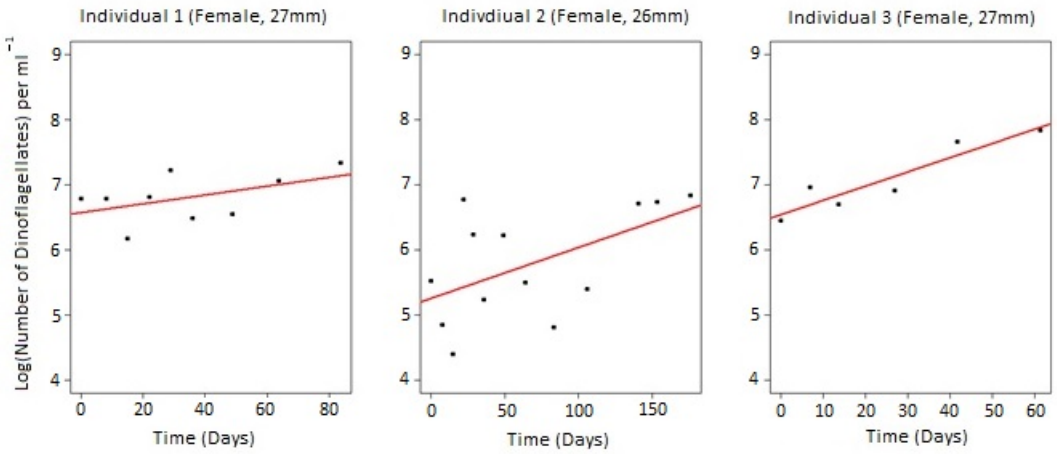

Figure 4.5: Data showing the logged estimates of the number of dinoflagellates per ml haemolymph over the course of several months for three separate individuals as determined by Appleton (1996). The red line shows the line of best fit through the data points as determined by linear regression.

The initial concentration of parasites within each individual was determined by fitting a linear regression line to the logged estimate of the total parasites per ml haemolymph, as shown in Figure 4.5. This produced the regression equation:

$$\text{Number of dinoflagellates per ml haemolymph} = 10^{(d_1+d_2t)} \tag{4.6}$$

where 't' is time (days) and 'd_1' and 'd_2' are regression coefficients. The values of 'd_1' and 'd_2' for each individual are shown in Table 4.2. Consequently, the number of parasites

in each individual at the beginning of the experiment is $10^{6.573}$, $10^{5.2629}$, and $10^{5.5418}$, for individuals 1, 2 and 3 respectively.

Individual	**1**	**2**	**3**
d_1	6.573	5.2629	6.5418
d_2	0.0068	0.0078	0.022

Table 4.2: Parameter estimates of d_1 and d_2 for each individual.

This information was used to parameterise the population model. This process, however, was carried out independently of the population model. Three individuals were created 'in-silico', with length and initial parasite burdens equal to those of the three individuals in Appleton's experiment. These individuals were allowed to grow according to the growth model, set out in the previous chapter. Similarly, the parasite burden of each individual was also assumed to increase according to the parasite growth model, set out in the previous chapter. The concentration of parasites in each individual was then determined at time points corresponding to those used in Appleton's experiments. The error associated with parasite growth, E_3, is therefore represented by the equation:

$$\begin{aligned} E_3 = (&\text{Modelled Parasite Concentration of Individual 1} - \\ &\text{Observed Parasite Concentration of Individual 1})^2 + \\ &(\text{Modelled Parasite Concentration of Individual 2} - \\ &\text{Observed Parasite Concentration of Individual 2})^2 + \\ &(\text{Modelled Parasite Concentration of Individual 3} - \\ &\text{Observed Parasite Concentration of Individual 3})^2 \end{aligned} \quad (4.7)$$

4.3 Optimised Model Output

The model was parameterised using the method described in the previous section. The best fitting values for all parameters are shown in Table 4.3. Plots showing the fit of the optimised model to observational data are shown in Figure 4.6 to 4.10. The model shows a good fit to all three data categories: fisheries related data, data on *Hematodinium* prevalence and data on parasite growth.

In particular, Figure 4.9 shows that the assumptions made regarding parasite transmission are conducive to the production of the observed seasonal cycle with high levels of

patent infection in the winter and spring and low levels of patent infection throughout the summer. This provides further support to the idea that moulting plays an important role in parasite transmission.

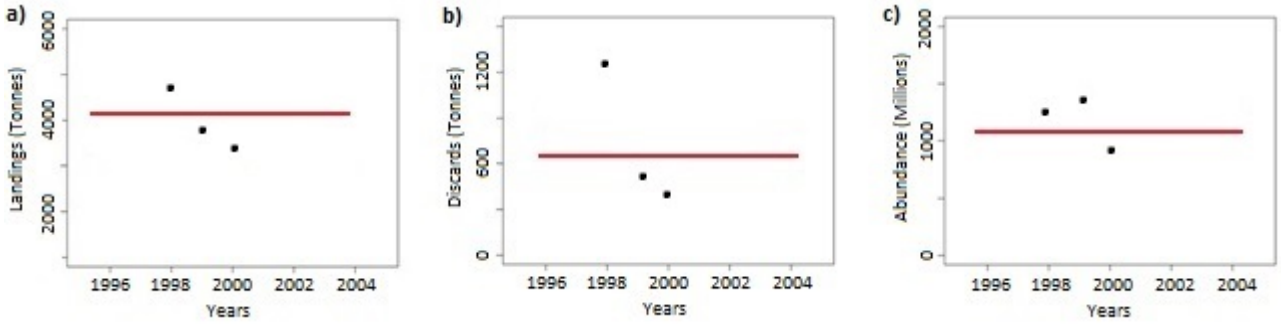

Figure 4.6: The fit of the model to (a) the weight of landings (b) the weight of discards and (c) the abundance of *Nephrops* as determined by UWTV surveys. Black dots represent observed data points and red lines represent model output.

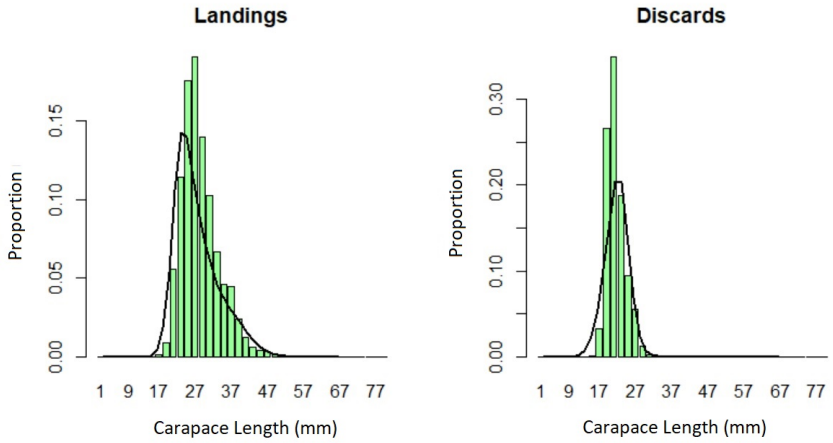

Figure 4.7: The fit of the model to the length distribution of individuals landed and discarded. Green bars represent observational data and black lines represent model output.

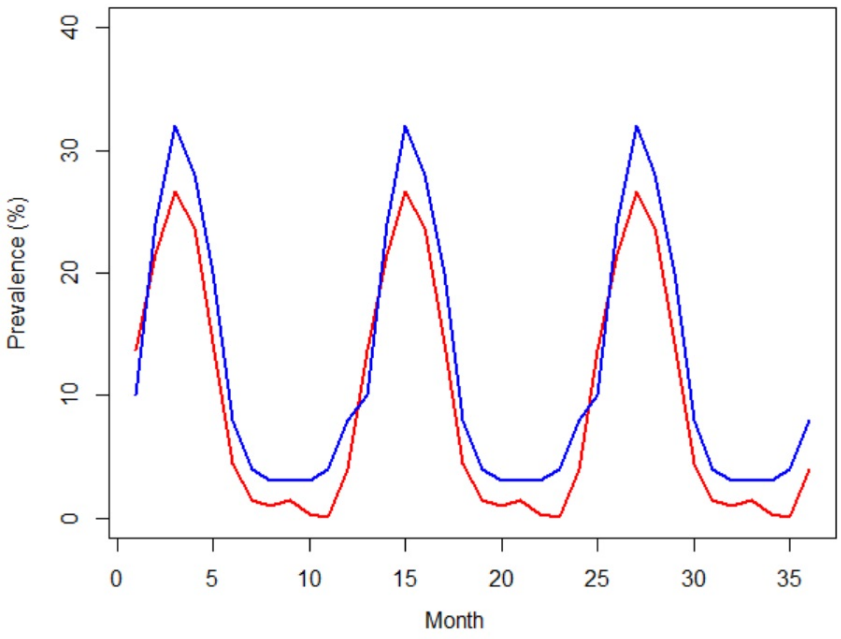

Figure 4.8: The fit of the model to the annual cycle of *Hematodinium* prevalence determined using the pleopod method of diagnosis. The blue line represents observational data and the red line represents model output.

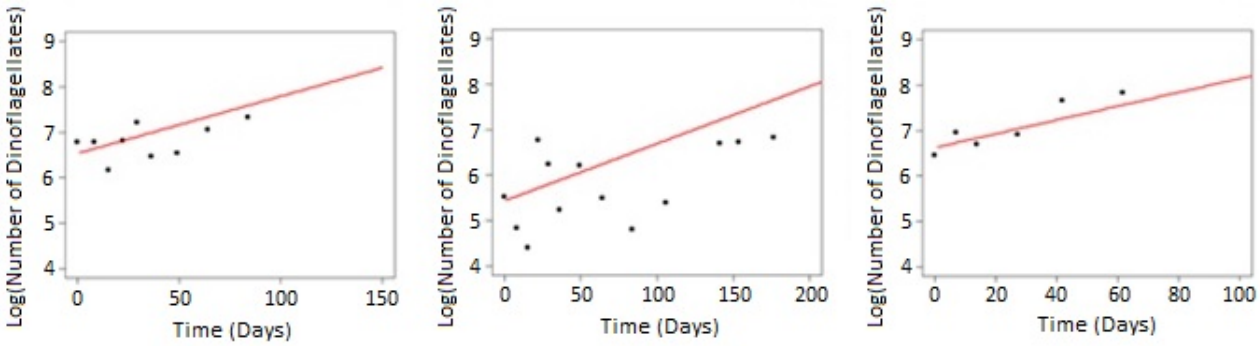

Figure 4.9: The fit of the model to *Hematodinium* growth data (number of dinoflagellates per ml haemolymph) for three different individuals collected by Appleton (1996).

Name	Description	Value	Units	Estimation Method
ϕ	Energy Intake	Males = 0.00005, Immature Females = 0.00007, Mature Females = 0.00007	day^{-1}	Estimated as part of growth model. See Table 2.3
μ	Energy spent on metabolism	Males = 0.00025, Immature Females = 0.002, Mature Females = 0.002	day^{-1}	Estimated as part of growth model. See Table 2.3
δ	Energy spent on reproduction	Males = 0, Immature Females = 0, Mature Females = 0.0003	day^{-1}	Estimated as part of growth model. See Table 2.3
γ	Energy consumed by the parasite	1e-15	day^{-1}	Free-fitting
c	Increase in weight which triggers moulting in males and immature females	Males = 1.37 Immature Females = 1.24		Estimated as part of growth model. See Section 2.5.1
a	Weight-length parameter	Males = 0.00028 Females = 0.00074		Fixed (Howard, 1989)
b	Weight-length parameter	Males = 3.24 Females = 2.91		Fixed (Howard, 1989)
w_0	Initial weight	0.1	grams	Estimated as part of growth model. See Table 2.3
q_1	Catchability parameter	0.9		Free fitting
q_2	Catchability parameter	0.8		Free fitting
m	Natural mortality	0.00068	day^{-1}	Free fitting
c_1	Fishing mortality conversion factor	4.4e-08		Free fitting
E_t	Effort	130000	hrs per annum	Fixed. (ICES, 2009)
k_s	Size selectivity	0.7		Free fitting
L_{50}	Size selectivity	29	mm	Free fitting
d	Disease mortality	1e-15		Free fitting
k_1	Egg Survival Rate	0.65		Fixed (Briggs and McAliskey, 2002)
k_2	Larval Survival Rate	0.05		Fixed (Dickey-Collas et al. 2000)
c_e	Cost of egg production	0.001		Derived. See Section 4.2.2
B_0	Population carrying capacity	8e+10		Free fitting
g	Parasite growth rate	0.032	day^{-1}	Free fitting
β	Parasite transmission rate	1e-18		Free fitting
λ	Spore decay rate	0.016	day^{-1}	Free fitting
k_c	Sporulation probability curve	0.1		Free fitting
C_{50}	Sporulation probability curve	283333333		Free fitting
h	Weight to heamolymph volume conversion factor	0.33		Fixed (Harris and Andrews, 2005)
k_d	Discard selectivity curve	0.38		Derived. See Section 4.2.2
d_{50}	Discard selectivity curve	23.05	mm	Derived. See Section 4.2.2
ψ	Discard survival rate	25	%	Fixed (Chapman, 1980)

Table 4.3: Table showing the optimised parameters used in the baseline *Nephrops-Hematodinium* population model.

4.4 Sensitivity Analysis

One of the main challenges in the development of mathematical models of biological systems is the precise estimation of parameter values. This is particularly true for the *Nephrops-Hematodinium* population model. The process of parameterising the *Nephrops-Hematodinium* population model is described fully in Section 4.2. This process involved the estimation of parameter values directly from literature where possible. These values, however, are often based on limited data and therefore have a high degree of uncertainty associated with them. Parameters for which no information could be obtained from literature were treated as free-fitting parameters. The values of these parameters were determined solely by fitting the output of the model to observational data on *Nephrops* and *Hematodinium* in the CSA. These free-fitting parameters therefore also have a high degree of uncertainty associated with them. In this section, a one-at-a-time sensitivity analysis is carried out to investigate the effect of changes to the optimised parameter values (see Table 4.3) on the fit of the model to observational data. Examining the influence of parameter uncertainty on the behaviour of the model is crucial for determining the reliability of associated model output.

A one-at-a-time sensitivity analysis was carried out by varying model parameters $\pm 10\%$ and recording the percentage change in associated model output. Five key statistics were chosen to summarise the model output. This includes population size, the annual weight of individuals landed, the annual weight of individuals discarded, the maximum prevalence of the parasite in the catch as determined by the pleopod method and the timing at which this maximum prevalence occurs. These five values cover the wide range of observational data used in the parameterisation process (see Figures 4.6 - 4.8). Data on parasite growth (see Fig 4.9) was not included in the sensitivity analysis. The fit of the model to observational data on parasite growth is governed solely by the parasite growth parameter (g).

The results of the one-at-a-time sensitivity analysis are shown in Figures 4.10 - 4.14. Parameter values which comprise the *Nephrops* growth model (i.e. $\phi, \mu, \delta, \gamma, c, a, b, w_0$) are excluded from these plots. Instead the sensitivity analysis focuses on the remaining model parameters which relate solely to the *Nephrops-Hematodinium* population model. A brief description of the role of each of these parameters can be found in Table 4.3.

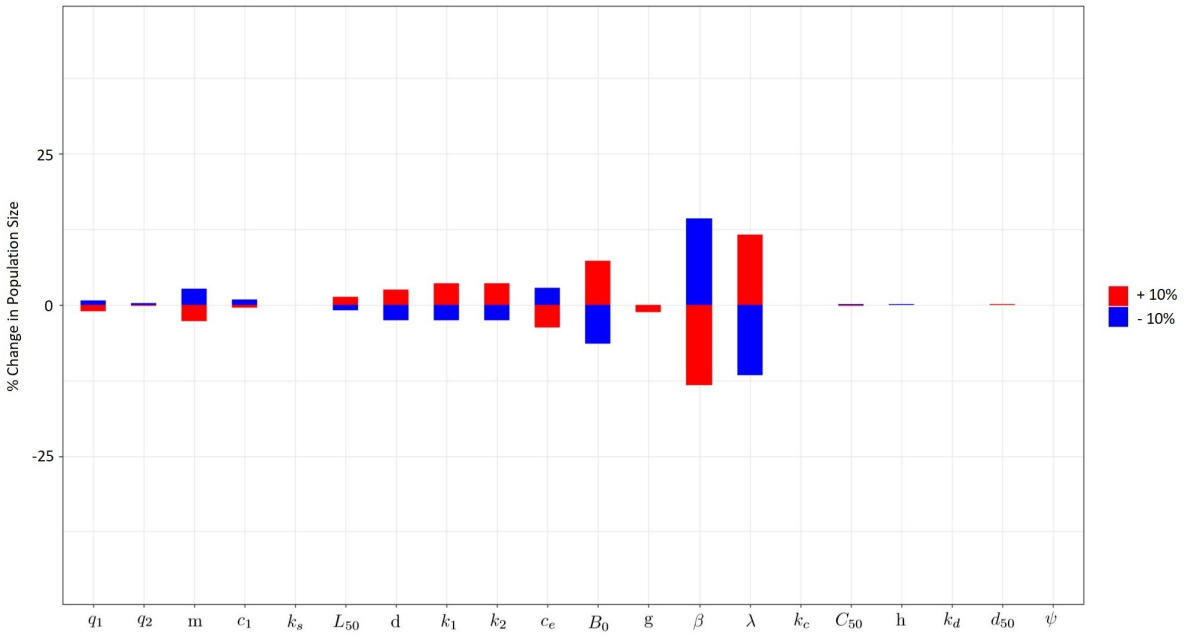

Figure 4.10: One-at-a-time sensitivity analysis of model parameters on the mean annual population size. Each parameter is adjusted ± 10% and predicted mean population size is compared to the modelled mean population size given by the baseline parameterisation.

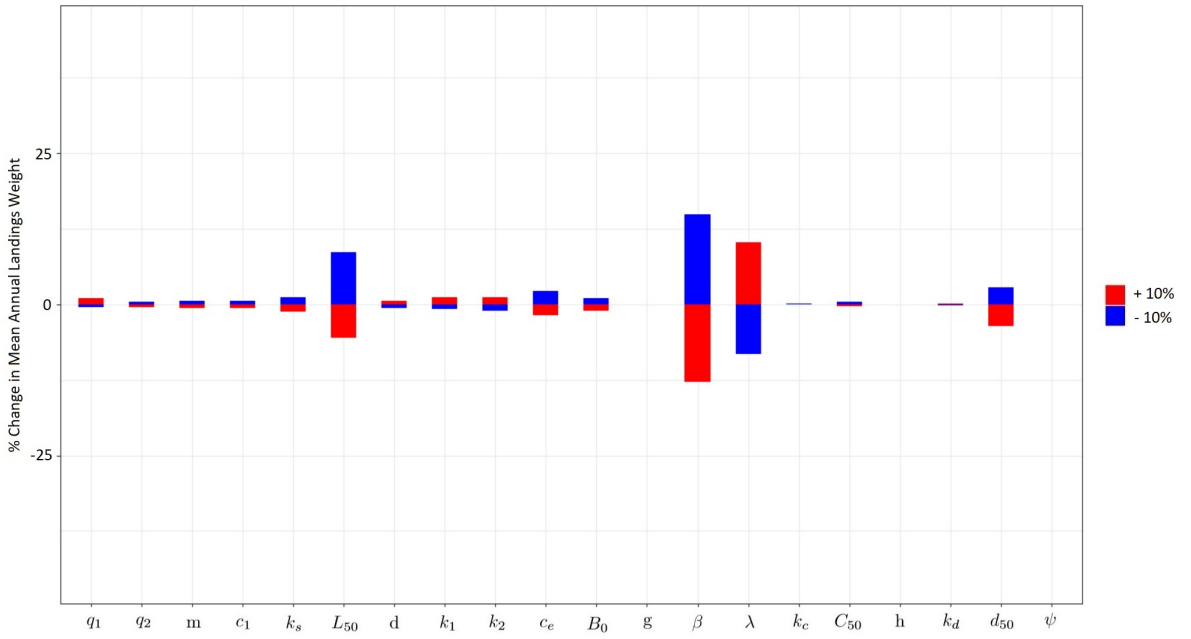

Figure 4.11: One-at-a-time sensitivity analysis of model parameters on the mean annual weight of landings. Each parameter is adjusted ± 10% and the predicted mean annual weight of landings is compared to the modelled mean annual weight of landings given by the baseline parameterisation.

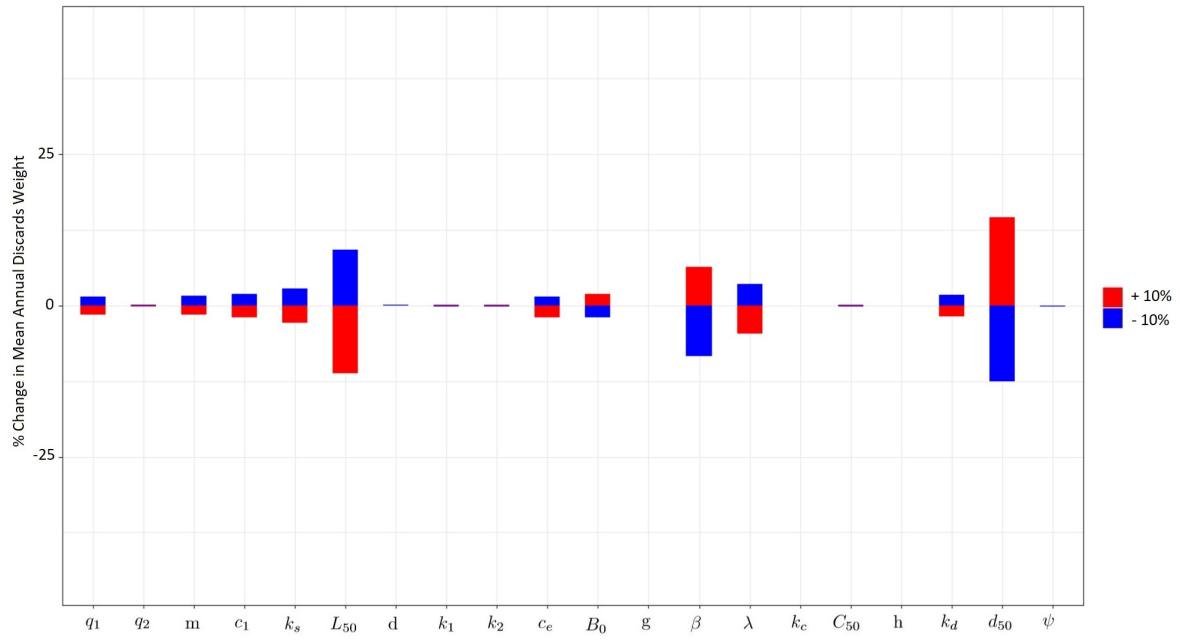

Figure 4.12: One-at-a-time sensitivity analysis of model parameters on the mean annual weight of discards. Each parameter is adjusted ± 10% and predicted mean annual weight of discards is compared to the modelled mean annual weight of discards given by the baseline parameterisation.

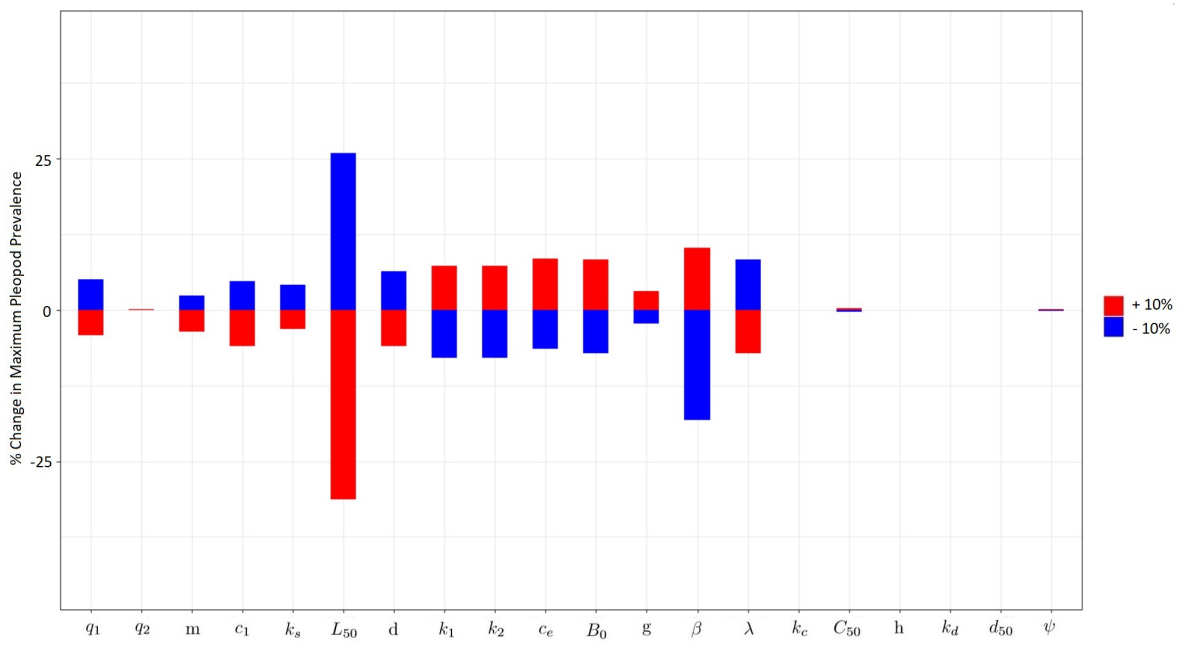

Figure 4.13: One-at-a-time sensitivity analysis of model parameters on maximum *Hematodinium* prevalence as determined by the pleopod method. Each parameter is adjusted ± 10% and predicted maximum pleopod prevalence of individuals in the catch is compared to the modelled maximum pleopod prevalence given by the baseline parameterisation.

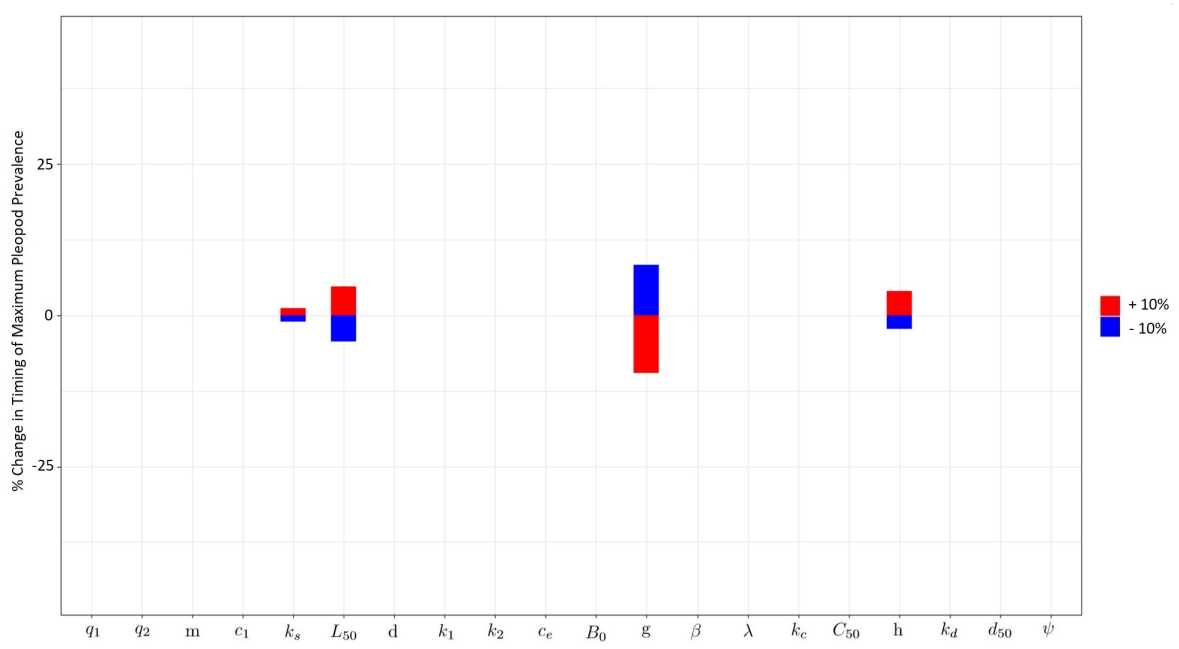

Figure 4.14: One-at-a-time sensitivity analysis of model parameters on the timing of peak *Hematodinium* prevalence. Each parameter is adjusted ± 10% and predicted timing (day of the year) of maximum pleopod prevalence in the catch is compared to the modelled predicted timing of maximum pleopod prevalence given by the baseline parameterisation.

Sensitivity analysis of model parameters showed that the population size of *Nephrops* is most sensitive to parameters β and λ (see Figure 4.10). These parameters represent the transmission rate of the parasite and the decay rate of parasitic spores respectively. Increasing the parasite transmission rate (β) by +10% results in a 13% decrease in population size. Infected individuals have a higher mortality rate in comparison to their uninfected counterparts. Increasing the transmission rate therefore increases the number of infected individuals which in turn reduces the overall population size. Increasing the spore decay rate (λ) by +10%, on the other hand, results in a 11% increase in population size. Increasing the spore decay rate reduces the number of spores in the environment and therefore reduces the number of infected individuals in the population.

Figure 4.11 shows that the mean annual weight of landings is also sensitive to the parameters β and λ. β and λ affect the population size and the proportion of infected individuals in the population as outlined above. This in turn impacts the annual weight of landings since the model assumes that fishermen discard heavily-infected individuals which show visible signs of infection. Furthermore, the mean annual weight of landings was also shown to be sensitive to the size selectivity parameter L_{50}. This parameter controls the size distribution of individuals captured by fishermen which in turn impacts the weight of the landings. Finally, the mean annual weight of landings was also shown to be sensitive

to the discard size selectivity parameter d_{50}.

Similarly, the mean annual weight of individuals discarded by fishermen is also sensitive to the parameters β, λ, L_{50} and d_{50} as shown in Figure 4.12. The weight of discards was found to be most sensitive to the discard selectivity parameter d_{50}. Increasing d_{50} causes fishermen to discard larger individuals and consequently leads to a substantial increase in the weight of discards.

The maximum prevalence of patent *Hematodinium* infection was found to be sensitive to a whole host of parameters (q_1, m, c_1, k_s, L_{50} d, k_1, k_2, c_e, B_0, g, β and λ), as shown in Figure 4.13. The maximum prevalence of patent infection in the catch was found to be most sensitive to the size selectivity parameter L_{50}. This parameter governs the size distribution of individuals in the catch. Increasing L_{50} increases the mean size of individuals in the catch. This leads to a decrease in *Hematodinium* prevalence due to the increased rate of infection amongst smaller individuals. Increasing parameter L_{50} by +10% was found to cause a 31% decrease in the maximum prevalence of patent *Hematodinium* infection in the catch.

The timing of the peak in maximum patent *Hematodinium* prevalence is governed by just four parameters (k_s, L_{50}, g and h), as shown in Figure 4.14. The timing of maximum patent prevalence is found to be most sensitive to the parasite growth parameter (g). Increasing the parasite growth rate causes the peak of patent *Hematodinium* infection to occur earlier in the year.

Finally, the parasite growth data was not included in the sensitivity analysis. The fit of the model to observational data on parasite growth is governed solely by the parasite growth parameter (g). Increasing parameter 'g' in the model increases the rate of parasite growth. The value of parameter 'g' is based on experimental data collected by Appleton (1996) during which repeated measurements of parasite concentration were obtained from infected individuals held in laboratory tanks. The sample size of these experiments, however, is noticeably small. Regular measurements of parasite concentrations are obtained from just 3 individuals. Hence, it is important to note, that a great degree of uncertainty surrounds the value of this parameter.

4.5 Conclusion

In conclusion, this chapter has outlined the process used to parameterise the *Nephrops-Hematodinium* population model. Parameter values were obtained directly from liter-

ature where possible. Any remaining parameters were treated as free-fitting parameters. Values for these parameters were obtained by comparing output from the *Nephrops-Hematodinium* population model to a range of observational data. This includes fisheries-related data, data on the prevalence of patent *Hematodinium* infection and data on parasite growth. Optimised parameter values were found to show a good fit to available sources of observational data. The effect of parameter uncertainty on model output was then examined using a one-at-a-time sensitivity analysis. This process outlines the effect of minor changes in parameter values on the fit of the model to observational data.

Chapter 5

Comparison of Model Output with Observational Data on *Hematodinium* Prevalence

5.1 Introduction

The population dynamics of *Nephrops* and *Hematodinium* in the CSA show a number of distinctive patterns, as described fully in Section 1.6. This includes clear seasonal patterns in patent *Hematodinium* prevalence measured using the pleopod and body colour methods of diagnosis, as well as distinct seasonality in high level sub-patent infection measured using the western blot immunoassay method. The exact timing of these seasonal infection patterns depends on the diagnostic test used. Prevalence estimates obtained using the body colour method and pleopod method show a short sharp peak in infection prevalence during late winter/spring with an absence of detectable infection throughout the summer and autumn months (Stentiford et al., 2001c). The western blot immunoassay method, on the other hand, detects infection over a longer period (October-June). However, like the body colour and pleopod method, the western blot immunoassay method also fails to detect infection during the summer months (Stentiford et al., 2001b). These distinct seasonal patterns in patent *Hematodinium* prevalence are accompanied by a lack of seasonality in low-level sub-patent infection measured using highly sensitive ELISA and PCR methods of diagnosis. Prevalence estimates obtained using ELISA and PCR detect infected individuals throughout the whole year, without any clear seasonal patterns in infection prevalence (Beevers et al., 2012).

This chapter examines the ability of the *Nephrops-Hematodinium* population model to replicate the key patterns of *Hematodinium* prevalence produced by different diagnostic

methods. Furthermore, where possible, prevalence estimates obtained from the *Nephrops-Hematodinium* population model are compared with observational data on *Hematodinium* prevalence in the CSA. The *Nephrops-Hematodinium* population model is parameterised using infection prevalence data as determined by the pleopod method of diagnosis (Stentiford et al., 2001b). Model parameters have therefore been chosen specifically to show a good fit to this data, as highlighted in Figure 4.8. This chapter focuses on the ability of the *Nephrops-Hematodinium* population model to replicate the patterns of *Hematodinium* prevalence observed using other key diagnostic tests not included in the parameterisation process. This includes prevalence data measured using the western blot immunoassay (Stentiford et al., 2001c), ELISA (Beevers, 2010) and PCR methods of diagnosis (Beevers, 2010). No suitable data on *Hematodinium* prevalence in the CSA measured using the body colour method could be obtained. This chapter therefore focuses specifically on the fit of the *Nephrops-Hematodinium* population model to data on sub-patent infection prevalence.

Estimates of *Hematodinium* prevalence in the CSA are obtained by measuring the level of infection in a small subset of the population caught using standard *Nephrops* trawl nets. This work is generally carried out aboard commercial *Nephrops* trawlers. Regulations governing the mesh size of trawl nets used by commercial *Nephrops* trawlers in the CSA have, however, changed substantially over time (McIntyre et al., 2012). New regulations introduced in 2008 forced fishermen to switch from trawl nets with a mesh size of 70 mm to trawl nets with a mesh size of 80 mm. It is important to note, however, that many fishermen switched mesh size prior to this official legislation being brought in. These changes in mesh size have important implications for recorded levels of *Hematodinium* prevalence in the CSA. Prevalence estimates obtained by Stentiford et al. (2001b) and Stentiford et al. (2001c) using the pleopod and western blot immunoassay methods span the period October 1999 to September 200 and were obtained using trawl nets with a mesh size of 70 mm. Prevalence estimates made by Beevers (2010) using ELISA and PCR, on the other hand span the period September 2007 to September 2008 and were obtained using trawl nets with a mesh size of 80 mm. Samples obtained using nets with larger mesh sizes typically record lower levels of *Hematodinium* prevalence in comparison to samples obtained using nets with a smaller mesh size due to the increased prevalence due to the increased prevalence of *Hematodinium* amongst smaller individuals (see Section 1.6.4 for more details). In this chapter, changes in the mesh size of trawl nets are simulated within the *Nephrops-Hematodinium* population model by altering the size selectivity parameter L_{50}. This allows for a fair comparison to be made between model output and observational data on the prevalence of *Hematodinium* in the CSA.

Finally, *Nephrops-Hematodinium* population dynamics show a number of other unique infection patterns in addition to the distinct seasonal patterns outlined above. This includes a marked difference in the prevalence of *Hematodinium* between males and females and between individuals of different size classes (see Section 1.6.4 for more details). In brief, the prevalence of *Hematodinium* is higher amongst females and amongst smaller individuals (Field et al., 1992, 1998; Stentiford et al., 2001b,c; Briggs and McAliskey, 2002). This chapter examines the ability of the *Nephrops-Hematodinium* population model to replicate these distinctive infection patterns. This chapter focuses specifically on the ability of the *Nephrops-Hematodinium* population model to replicate the general patterns of infection prevalence recorded across a number of different studies (Field et al., 1992, 1998; Stentiford et al., 2001b,c; Briggs and McAliskey, 2002), rather than the ability of the model to closely fit the output of a single chosen dataset.

5.2 Methods

Differences in the seasonal patterns of *Hematodinium* prevalence produced by different diagnostic tests were examined by running the baseline *Nephrops-Hematodinium* population model to a steady state, using the optimised set of model parameters shown in Table 4.3. The baseline *Nephrops-Hematodinium* population model assumes a net mesh size of 70 mm. Monthly averaged estimates of *Hematodinium* prevalence were extracted from the model using the methods set out in Section 3.4.2. Five separate estimates of parasite prevalence were extracted – one to correspond with each of the five main diagnostic methods (body colour method, pleopod method, western blot immunoassay, ELISA and PCR).

Model estimates of *Hematodinium* prevalence were then compared to observational data collected near the Isle of Cumbrae in the CSA. Prevalence data collected using the western blot immunoassay method was obtained from Stentiford et al. (2001c). This data set spans the period from October 1999 to September 2000 and was collected using trawl nets with a mesh size of 70 mm. Prevalence data collected by Stentiford et al. (2001c) could therefore be compared directly to the estimate of western blot immunoassay prevalence predicted by the baseline *Nephrops-Hematodinium* population model.

Prevalence data collected using the ELISA and PCR methods of diagnosis were obtained from Beevers (2010). These data sets span the period September 2007 - September 2008 and were collected using trawl nets with a mesh size of 80 mm. It is important to note that this time period is slightly before the official introduction of new regulations in 2008 requiring all fishermen to use nets with a mesh size of 80 mm (McIntyre et al., 2012).

However, it is thought that many fishermen switched mesh size prior to the introduction of new legislation. For simplicity, we assume a complete switch to nets with a mesh size of 80 mm by all fishermen prior to data collection. This allows changes in mesh size to be simulated within the model by altering the size selectivity parameter L_{50}. The value of L_{50} in the baseline *Nephrops-Hematodinium* population model is 29 mm, as shown in Table 4.3. This value was increased to 33.15 mm. Note that this represents a 14.3% increase in L_{50}, which is comparable to the 14.3% increase in net mesh size from 70 to 80 mm. Before applying this change the baseline *Nephrops-Hematodinium* population model was run to a steady state as described above. Following this, the L_{50} parameter value was increased, and the model was allowed to reach a new steady state. Note that the timing of new legislation makes it extremely unlikely that the system would have reached a new steady state prior to the collection of observational data by (Beevers, 2010). However, this complexity is not included in the current model. Instead, the *Nephrops-Hematodinium* population model was allowed to reach a new steady state after which prevalence estimates corresponding with the ELISA and PCR methods of diagnosis were obtained from the model. These estimates were then compared with the observational data collected by Beevers (2010).

Differences in the prevalence of *Hematodinium* between males and females and between individuals of different length classes were examined using the baseline *Nephrops - Hematodinium* population model (i.e. assuming a net mesh size of 70 mm). The *Nephrops-Hematodinium* population model was run to a steady state, as described above. Yearly averaged estimates of *Hematodinium* prevalence were then extracted from the model. Separate estimates were made for males and females in the population and for individuals in a range of different size classes: 0-10, 10-20, 20-30, 30-40 and 40-50 mm CL. *Hematodinium* prevalence was separated into three separate categories: patent infection, detectable sub-patent infection and undetectable sub-patent infection. Patent infections were classified as having a parasite burden greater than the detection threshold for the pleopod method (i.e. individuals with a parasite burden greater than 2,400,000 parasites per ml haemolymph). Detectable sub-patent infection was classified as having a parasite burden greater than the detection threshold for the PCR method but lower than the detection threshold for the pleopod method (i.e. individuals with a parasite burden between 30 and 2,400,000 parasites per ml haemolymph). Undetectable sub-patent infection was classified as having a parasite burden less than the detection threshold for the PCR method (i.e. individuals with a parasite burden less than 30 parasites per ml haemolymph).

5.3 Results

5.3.1 *Hematodinium* Prevalence: Seasonal Patterns Produced by Key Diagnostic Tests

Monthly averaged estimates of *Hematodinium* prevalence, as extracted from the baseline *Nephrops-Hematodinium* population model, are shown in Figure 5.1. Five separate prevalence estimates are shown, one corresponding with each of the five main diagnostic methods: body colour method, pleopod method, western blot immunoassay, ELISA and PCR. Prevalence levels corresponding with the body colour and pleopod methods show a relatively short sharp peak around April/May with exceptionally low prevalence throughout the summer and autumn months. Prevalence levels corresponding with the western blot immunoassay method show a longer peak, with infected individuals first appearing in the catch in August/September. However, like the body colour and pleopod methods, prevalence levels corresponding with the western blot immunoassay method also show relatively low prevalence throughout the summer months. Prevalence levels corresponding with the ELISA and PCR methods of diagnosis show a distinct lack of seasonality with levels remaining relatively constant throughout the entire year. Mean levels of ELISA and PCR prevalence were estimated to be 32% and 45% respectively. Figure 5.1 also highlights the rapid development of the infection, from levels which are detectable by western blot immunoassay (> 200,000 parasites per ml haemolymph) to levels detectable by the body colour method (> 50,000,000 parasites per ml haemolymph), within a relatively short time frame (2-3 months).

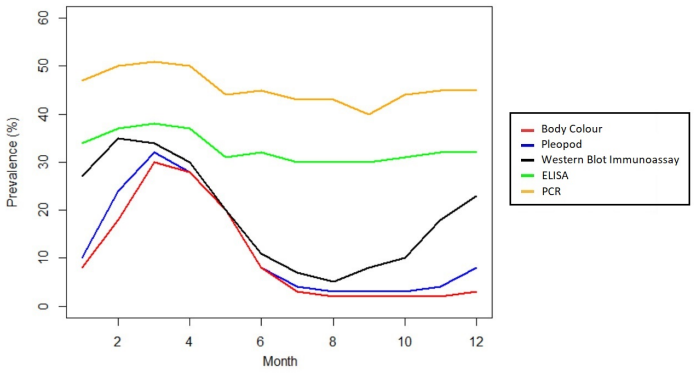

Figure 5.1: Plot showing the monthly averaged prevalence of *Hematodinium* in the catch for each of the five main diagnostic methods as extracted from the baseline *Nephrops-Hematodinium* population model (i.e. assuming a net mesh size of 70 mm).

Figure 5.2 shows the fit of prevalence estimates obtained from the *Nephrops-Hematodinium* population model to observational data on sub-patent *Hematodinium* prevalence in the

CSA collected using the western blot immunoassay, ELISA and PCR methods of diagnosis. It is important to note that model estimates of ELISA and PCR prevalence differ between Figures 5.1 and 5.2. Model estimates of ELISA and PCR prevalence in Figure 5.2 have been modified to account new legislation which led to an increase in the mesh size of trawl nets used by fishermen in the CSA. This increased mesh size (80 mm) was also used in the collection of ELISA and PCR observational data by Beevers (2010). The *Nephrops-Hematodinium* population model shows a good fit to the western blot immunoassay prevalence data collected by Stentiford et al. (2001c), as shown in Figure 5.2 (a). The *Nephrops-Hematodinium* population model also captures the key features of ELISA and PCR prevalence data, including a distinct lack of seasonality. The *Nephrops-Hematodinium* population model, however, overestimates the level of ELISA and PCR prevalence as measured by Beevers (2010).

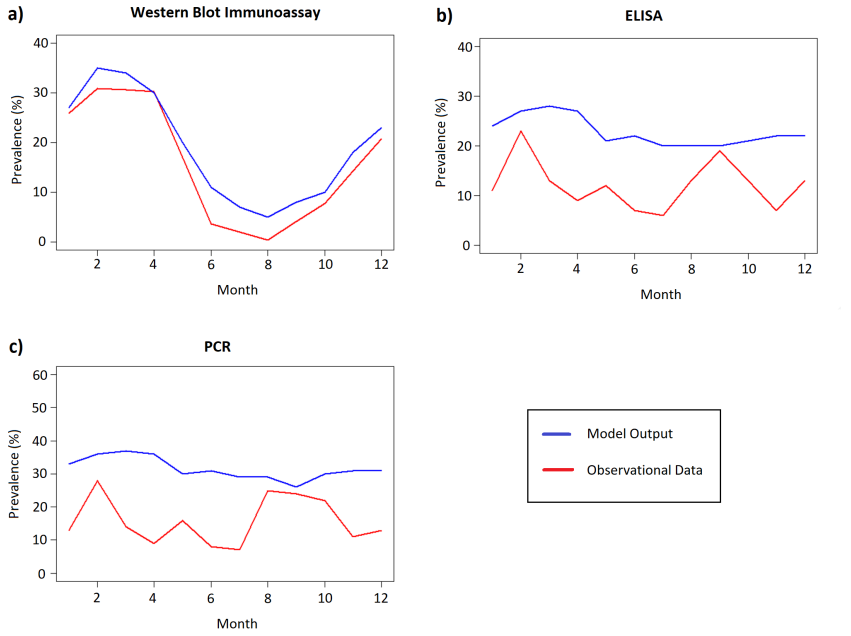

Figure 5.2: Plot showing the fit of prevalence estimates obtained from the *Nephrops-Hematodinium* population model to observational data from the CSA obtained using (a) Western blot immunoassay, (b) ELISA and (c) PCR methods of diagnosis. Western blot immunoassay data was collected by Stentiford et al. (2001c) and spans the period October 1999 - September 2000. During this time, fishermen in the CSA used nets with a mesh size of 70 mm. ELISA and PCR data was collected by Beevers (2010) and spans the period September 2007 - September 2008. During this time, the majority of fishermen in the CSA used nets with a mesh size of 80 mm. Model output shown in (a) was therefore obtained from the baseline *Nephrops-Hematodinium* population model which assumes a net mesh size of 70 mm. Model output shown in (b) and (c) was obtained from a modified version of the *Nephrops-Hematodinium* population model which assumes a net mesh size of 80 mm.

5.3.2 *Hematodinium* Prevalence: Length and Sex

The *Nephrops-Hematodinium* population model shows distinct differences in infection prevalence between males and females, as shown in Figure 5.3. Females were found to have higher levels of overall infection (patent infection + detectable sub-patent infection + undetectable sub-patent infection). The baseline *Nephrops-Hematodinium* population model predicts that 64% of females in the population are infected with *Hematodinium*, compared to just 41% of males. Females were also found to have higher levels of patent *Hematodinium* infection. 22% of females in the population are patently infected compared to just 11% of males.

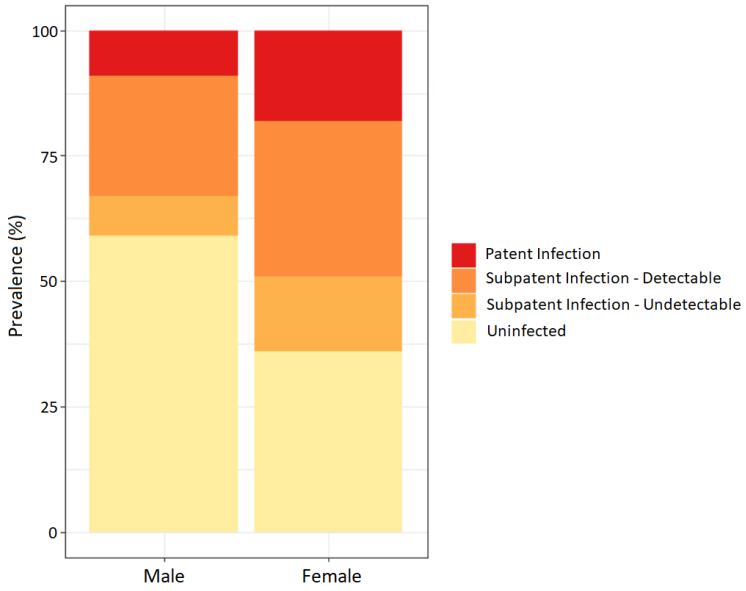

Figure 5.3: Yearly averaged estimates of patent, detectable sub-patent and undetectable sub-patent infection prevalence for males and females, as extracted from the baseline *Nephrops-Hematodinium* population model.

Furthermore, the *Nephrops-Hematodinium* population model also shows distinct differences in infection prevalence as carapace length increases, as shown in Figure 5.4. The baseline *Nephrops-Hematodinium* population model records relatively low levels of infection prevalence in the smallest size class (0-10 mm CL). This is followed by a sharp rise in infection prevalence. Overall infection prevalence is highest in individuals with a carapace length of 10-20 mm. The model then shows a steady decline in the level of overall infection prevalence as carapace length increases.

Patterns of patent infection prevalence were found to differ slightly to the patterns of overall infection prevalence outlined above. The level of patent *Hematodinium* infection was

found to be highest amongst individuals of 20-30 mm CL. The *Nephrops-Hematodinium* population model also shows a distinct absence of patently infected individuals in the smallest size class (0-10 mm CL).

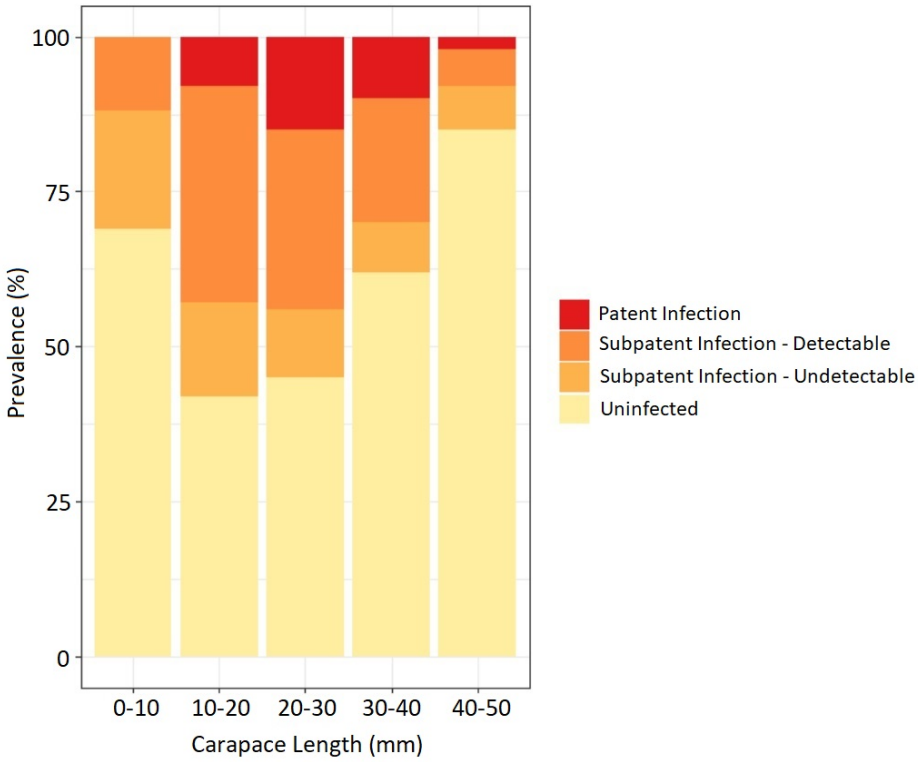

Figure 5.4: Yearly averaged estimates of patent, detectable sub-patent and undetectable sub-patent infection prevalence for individuals of different length classes, as extracted from the baseline *Nephrops-Hematodinium* population model.

5.4 Discussion

This chapter has highlighted the ability of the *Nephrops-Hematodinium* population model to successfully replicate the key features of *Nephrops-Hematodinium* population dynamics. This includes clear seasonal patterns in patent and high-level sub-patent infection prevalence measured using the body colour, pleopod and western blot immunoassay methods of diagnosis. This is accompanied by a lack of seasonality in low-level sub-patent infection prevalence measured using highly sensitive ELISA and PCR methods of diagnosis. Furthermore, this chapter also examined the fit of prevalence estimates from the *Nephrops-Hematodinium* population model to observational data on infection prevalence in the CSA. Particular attention was given to the fit of the model to data on sub-patent infection prevalence since this data was not directly used for model parameterisation. Model estimates of western blot immunoassay prevalence were found to closely replicate

western blot immunoassay prevalence data collected by Stentiford et al. (2001b). Model estimates of ELISA and PCR prevalence, however, were found to overestimate ELISA and PCR prevalence data collected by Beevers (2010).

The *Nephrops-Hematodinium* population model was adjusted to account for the different mesh sizes used by fishermen in the CSA. Western blot immunoassay data was collected by Stentiford et al. (2001c) and spans the period October 1999 - September 2000. During this time, fishermen in the CSA used nets with a mesh size of 70 mm. ELISA and PCR data was collected by Beevers (2010) and spans the period September 2007 - September 2008. During this time, the majority of fishermen in the CSA used nets with a mesh size of 80 mm. Changes in mesh size were incorporated into the model by altering the size selectivity parameter L_{50}. Increasing mesh size (increasing L_{50}) led to a significant reduction in the perceived level of *Hematodinium* prevalence. This can be seen by comparing estimates of ELISA and PCR prevalence obtained from the baseline *Nephrops-Hematodinium* population model which assumes a mesh size of 70 mm (see Figure 5.1) with estimates of ELISA and PCR prevalence obtained from the model following a switch to trawl nets with a mesh size of 80 mm (see Figure 5.2). Increasing the mesh size of trawl nets, however, does not lower the model prevalence levels enough to closely replicate the observational data collected by Beevers (2010). This suggests that other important factors may be involved, which are not currently included in the model. It is important to note, however, that modelled estimates of ELISA and PCR prevalence successfully capture the key features of observational data. This includes a distinct lack of seasonality, with ELISA and PCR positive individuals present throughout the whole year.

The *Nephrops-Hematodinium* population model is also able to successfully replicate observed differences in infection prevalence between males and females and between different length classes. The *Nephrops-Hematodinium* population model shows higher levels of infection prevalence amongst females as required. The *Nephrops-Hematodinium* population model also records distinct changes in infection prevalence between length classes. The model records relatively low levels of infection prevalence in the smallest length class (0-10 mm CL). This is followed by a sharp rise in infection prevalence in individuals in the length class 10-20 mm CL, after which infection prevalence steadily decreases with increasing carapace length. Observational studies in the CSA generally record a decrease in infection prevalence as carapace length increases (Field et al., 1992, 1998; Stentiford et al., 2001b,c; Briggs and McAliskey, 2002). These studies, however, are based solely on individuals in the catch. Individuals in the smallest length class (0-10 mm) are not captured by fishing gear and therefore do not appear in observational studies. Restricting the output of the *Nephrops-Hematodinium* population model to individuals of 'catchable'

size allows the output of the *Nephrops-Hematodinium* population model to replicate the observed patterns of infection prevalence.

Furthermore, this chapter also highlights the distinct absence of patently infected individuals in the smallest length class (0-10 mm CL). This can be seen clearly in Figure 5.4. *Hematodinium* infection takes a relatively long time to reach patent infection levels (> 1 year) (more information on this can be found in the following chapter). Consequently, individuals in the smallest length class (0-10 mm CL) do not develop patent *Hematodinium* infection.

In conclusion, this chapter has highlighted the ability of the *Nephrops-Hematodinium* population model to successfully replicate the key features of *Nephrops-Hematodinium* population dynamics with regards to seasonality, sex and carapace length. It is important to note that these features are not pre-ordained by design but instead develop as emergent properties of the model. The *Nephrops-Hematodinium* population model is primarily based on two assumptions, namely that moulting plays an important role in both the release of spores from infected individuals and the susceptibility of individuals to contracting the disease (see Section 1.8 for more detail). The ability of the *Nephrops-Hematodinium* population model to successfully replicate all of the key features of *Nephrops-Hematodinium* population dynamics provides further support to both of these key assumptions.

Chapter 6

Nephrops-Hematodinium Population Dynamics

6.1 Introduction

Certain aspects of *Nephrops-Hematodinium* population dynamics are difficult to study directly in the field. This includes, for example, the length of time required for the parasite burden within newly infected individuals to reach the detection thresholds of key diagnostic tests, the level of 'undetectable' sub-patent infection in the population, and the number of parasitic spores in the environment. In this chapter, the *Nephrops-Hematodinium* population model is used to estimate the value of these key statistics. This will provide new insights into the population dynamics of *Nephrops* and *Hematodinium* in the CSA and will help further our understanding of this commercially important parasite-host relationship.

Firstly, the *Nephrops-Hematodinium* population model is used to calculate the length of time required for the parasite burden within newly infected individuals to reach the detection thresholds of each of the five main diagnostic tests: body colour method, pleopod method, western blot immunoassay, ELISA and PCR. Particular attention is given to the length of time required to reach the detection threshold of the pleopod method. This corresponds with the point at which infection classification changes from 'sub-patent' to 'patent'. The length of time from initial infection to patency has been the subject of debate amongst researchers, as outlined in Section 1.6. Examination of the peaks in sub-patent infection (as measured by the western blot immunoassay method) and patent infection (as measured by the pleopod method) led Stentiford et al. (2001c) to conclude that infection, sub-patency and patency must all occur within a single year. The development of more sensitive diagnostic tests, however, revealed the presence of low-level

sub-patent infection throughout the whole year (Beevers et al. 2010). The presence of low-level sub-patent infection during late winter/early spring (at the time of peak patent prevalence) points towards the possibility that infection may persist at a low level for a relatively long period (> 1 year) before eventually manifesting as patent infection. In this chapter, the *Nephrops-Hematodinium* population model is used to provide further insight into the development time of patent *Hematodinium* infection.

Secondly, the *Nephrops-Hematodinium* population model is also used to estimate the current level of undetectable background infection in the CSA *Nephrops* population. Current estimates of *Hematodinium* prevalence are obtained by measuring the prevalence of infection in a small sub-sample of the population caught using *Nephrops* trawl nets. Estimates of *Hematodinium* prevalence obtained in this way, however, are subject to a number of biases. Firstly, this method fails to account for low level sub-patent infection which cannot be detected by current methods of *Hematodinium* diagnosis. Secondly, this method also fails to account for differences in infection prevalence between the proportion of the population captured by fishermen and the population as a whole. Individuals infected with *Hematodinium* are known to spend significantly more time outside of their burrows in comparison to their uninfected counterparts (Field et al., 1992). Infected individuals are therefore more likely to be captured by fishing gear. Consequently, the prevalence of *Hematodinium* in the catch may actually over-estimate the true level of infection in the population.

The level of infection prevalence in the catch also depends significantly on the mesh size of the trawl net. This is because higher levels of infection prevalence occur amongst smaller individuals (see Section 1.6.4). Nets with a smaller mesh size therefore capture a higher proportion of infected individuals. In this chapter, the *Nephrops-Hematodinium* population model is used to explore the effect of mesh size on reported levels of infection prevalence in the catch. Furthermore, the *Nephrops-Hematodinium* population model is also used to explore the distinct differences in infection prevalence between the population, catch, landings and discards obtained with historically used mesh sizes in the CSA. This allows for an examination into the extent to which estimates of *Hematodinium* prevalence obtained from the catch differ from the true level of infection prevalence in the *Nephrops* population as a whole.

Finally, the *Nephrops-Hematodinium* population model is also used to investigate seasonal patterns in the number of parasitic spores in the environment. This is accompanied by an investigation into the timing of moulting (and hence sporulation) in immature males, mature males, immature females and mature females. This provides further insight into the

potential driving factors behind the distinct seasonal patterns in patent *Hematodinium* prevalence.

6.2 Methods

The number of days required for the parasite burden within newly infected individuals to reach the detection threshold for each of the five main diagnostic tests (body colour method, pleopod method, western blot immunoassay, ELISA and PCR) was determined using the detection thresholds outlined in Table 1.1. The detection threshold of each test is based on the concentration of parasite cells in the haemolymph and ranges from 30 parasites per ml haemolymph for the most sensitive PCR method (Beevers, 2010) to 50,000,000 parasites per ml haemolymph for the least sensitive body colour method (Field et al., 1992). The length of time required to reach the detection threshold of each test therefore depends on the volume of haemolymph within the infected host. Haemolymph volume is related to weight (see Equation 3.14), which in turn, is related to carapace length (see Equation 2.6). Consequently, the number of days required to reach the detection threshold of each test varies with the initial carapace length of the infected individual. The number of days also varies with sex due to the differing growth patterns between males and females (see Chapter 2 for more details).

The number of days required to reach the detection threshold of each diagnostic test was therefore calculated separately for males and females with carapace lengths ranging from 5-55 mm at the point of infection. Following initial infection, the length (and weight) of each individual increased according to the *Nephrops* DEB growth model set out in Chapter 2. Individuals were initially infected by a single parasitic cell, after which the number of parasitic cells increased exponentially as set out in Equation 3.4, with the optimised parasite growth parameter g=0.032. The concentration of parasite cells in the haemolymph was calculated at daily time intervals using Equations 3.13 - 3.14. The day on which individuals reached the required detection threshold of each diagnostic test was extracted and stored for further analysis.

Differences in the prevalence of *Hematodinium* infection in the population, catch, landings and discards were examined for two different trawl mesh sizes historically used in the CSA (70 mm and 80 mm). Changes in mesh size are simulated within the model by altering the size selectivity parameter L_{50}. The baseline *Nephrops-Hematodinium* population model, set out in Chapters 3-4, assumes a mesh size of 70 mm and has a corresponding L_{50} of 29 mm. The baseline *Nephrops-Hematodinium* population model was run to a

steady state after which yearly averaged prevalence values were extracted from the model for the population, catch, landings and discards. Following this, the L_{50} parameter was increased to 33.15 mm, corresponding with a switch to trawl nets with a mesh size of 80 mm. The model was then allowed to reach a new steady state, after which a second set of prevalence values were extracted from the model. Infected individuals were separated into three separate categories: patent infection, detectable sub-patent infection and undetectable sub-patent infection. Patent infections were classified as having a parasite burden greater than the detection threshold for the pleopod method (i.e.individuals with a parasite burden greater than 2,400,000 parasites per ml haemolymph). Detectable sub-patent infection was classified as having a parasite burden greater than the detection threshold for the PCR method but lower than the detection threshold for the pleopod method (i.e. individuals with a parasite burden between 30 and 2,400,000 parasites per ml haemolymph). Undetectable sub-patent infection was classified as having a parasite burden less than the detection threshold for the PCR method (i.e. individuals with a parasite burden less than 30 parasites per ml haemolymph).

Finally, seasonal patterns in moulting and spore production were examined using the baseline *Nephrops-Hematodinium* population model. The model was allowed to reach a steady state after which a number of key statistics were extracted. This includes daily estimates of the number of parasitic spores in the environment, as well as the proportion of immature females, mature females, immature males and mature males moulting on each day of the year.

6.3 Results

6.3.1 Time to Reach the Detection Thresholds of Key Diagnostic Tests

The number of days required for the parasite burden within newly infected hosts to reach the detection thresholds of each of the five main diagnostic tests (body colour method, pleopod method, western blot immunoassay, ELISA and PCR) are shown in Figure 6.1 for individuals with initial carapace lengths ranging from 5-55 mm at the point of infection. Detailed values for individuals with initial carapace lengths of 10, 20, 30, 40 and 50 mm are shown in Tables 6.1 and 6.2 for males and females respectively.

The number of days required for the parasite burden to reach the detection threshold of

each diagnostic test increases as the initial carapace length of the host increases. Individuals with an initial carapace length of 10 mm CL were found to take around 80 days to reach the detection threshold of the most sensitive PCR method and 605 days to reach the detection threshold of the least sensitive body colour method. Individuals with an initial carapace length of 40 mm CL, on the other hand, were found to take around 210 days to reach the detection threshold of the PCR method and 690 days to reach the detection threshold of the body colour method.

The number of days required for the parasite burden to reach patent infection levels corresponds with the number of days required for the parasite to develop from initial infection to the threshold level required for detection using the pleopod method of diagnosis. The number of days required to reach patency is therefore around 520 days for individuals with an initial carapace length of 10 mm and 600 days for individuals with an initial carapace length of 40 mm.

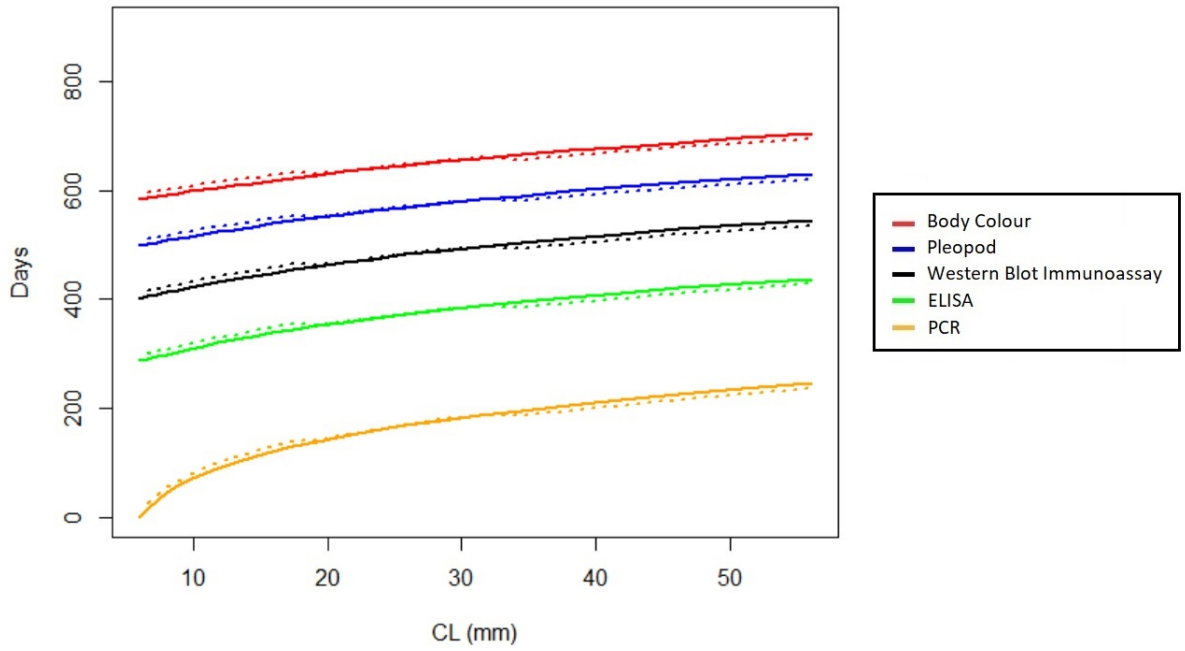

Figure 6.1: Plot showing the number of days required for the parasite burden within a newly infected host to reach the detection thresholds of key *Hematodinium* detection tests following initial infection by a single parasitic spore. Males and females are represented by solid and dotted lines respectively.

Initial CL (mm)	PCR	ELISA	Western Blot Immunoassay	Pleopod	Body Colour
10	79	314	426	519	601
20	139	351	461	550	628
30	187	388	496	580	659
40	216	412	520	606	680
50	235	430	537	622	696

Table 6.1: Table recording the number of days required for newly infected males of different initial carapace lengths to reach the detection thresholds of five commonly used *Hematodinium* diagnostic tests.

Initial CL (mm)	PCR	ELISA	Western Blot Immunoassay	Pleopod	Body Colour
10	89	324	436	529	611
20	140	352	462	551	629
30	188	389	497	584	660
40	206	407	510	596	670
50	225	420	527	612	686

Table 6.2: Table recording the number of days required for newly infected females of different initial carapace lengths to reach the detection thresholds of five commonly used *Hematodinium* diagnostic tests.

6.3.2 Infection Prevalence: Population, Catch, Landings and Discards

The prevalence of patent, detectable sub-patent and undetectable sub-patent infection in the population, catch, landings, and discards are shown in Figure 6.2. Plots (a) and (b) show the prevalence levels obtained following the use of trawl nets with a mesh size of 70 mm and 80 mm respectively. Mesh size was found to have a significant effect on the prevalence of infection in the proportion of the population captured by fishing gear (i.e. "the catch"). The level of overall infection prevalence (patent + detectable sub-patent + undetectable sub-patent) in the catch was 68% following the use of nets with a mesh size of 70 mm and 47% following the use of nets with a mesh size of 80 mm. Mesh size was also found to a have a significant effect on the prevalence of infection in the population as a whole. The level of overall infection in the population was found to be 55% and 61% following the use of nets with a mesh size of 70 and 80 mm respectively.

Furthermore, Figure 6.2 also highlights the extent to which the PCR method of diagnosis underestimates the true prevalence of infection. Roughly 10% of individuals in the catch were estimated to have undetectable sub-patent infection. Figure 6.2 also highlights the extent to which estimates of *Hematodinium* prevalence obtained by measuring the prevalence of detectable infection in the catch differ from the true prevalence of *Hematodinium* infection in the population. The level of detectable infection in the catch was found to be 57% following the use of nets with a mesh size of 70 mm. This is 2% more than the overall level of infection prevalence in the population (55%). On the other hand, the level of detectable infection in the catch was found to be 40% following the use of nets with a mesh size of 80 mm. This is 21% less than the overall level of infection prevalence in the population (61%).

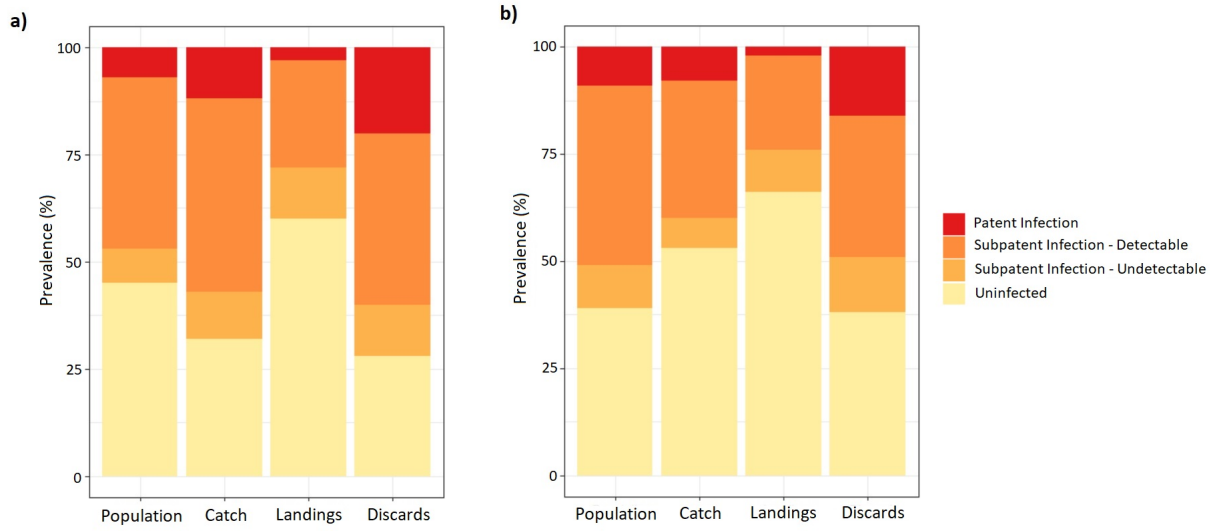

Figure 6.2: Yearly averaged estimates of patent, detectable sub-patent and undetectable sub-patent infection prevalence in the population, catch, landings and discards, as extracted from the *Nephrops-Hematodinium* population model. Plots (a) and (b) show the infection prevalence levels obtained using trawl nets with a mesh size of 70 and 80 mm respectively.

Finally, Figure 6.2 also highlights the large difference between the proportion of infected individuals in the landings and the proportion of infected individuals in the discards. This is accompanied by a stark contrast in the proportion of patently infected individuals. Using trawl nets with a mesh size of 70 mm resulted in an overall infection prevalence of 40% in the landings and 72% in the discards. Similarly, 3% of individuals in the landings were patently infected compared to 18% of individuals in the discards. The *Nephrops-Hematodinium* population model assumes that fishermen selectively discard

visibly-infected individuals i.e. all individuals with a parasite burden greater than the detection threshold for the body colour method are automatically discarded by fishermen regardless of size. This accounts for the high percentage of patently infected individuals discarded by fishermen. Patently infected individuals landed by fishermen are restricted to those with a parasite burden above the detection threshold for the pleopod method but below the detection threshold for the body colour method. Consequently, the prevalence of patently infected individuals in the landings is exceptionally low.

6.3.3 Seasonal Patterns in Moulting and Sporulation

The *Nephrops-Hematodinium* population model shows distinct patterns in the number of individuals moulting each day. In the model all mature females are assumed to moult annually on a fixed date, as shown in 6.3 (b). This fixed date is taken to be May 1st (see Section 2.2.3 for more details). Males and immature females, on the other hand, moult, sporadically throughout the year, as shown in Figure 6.3 (a)(c-d).

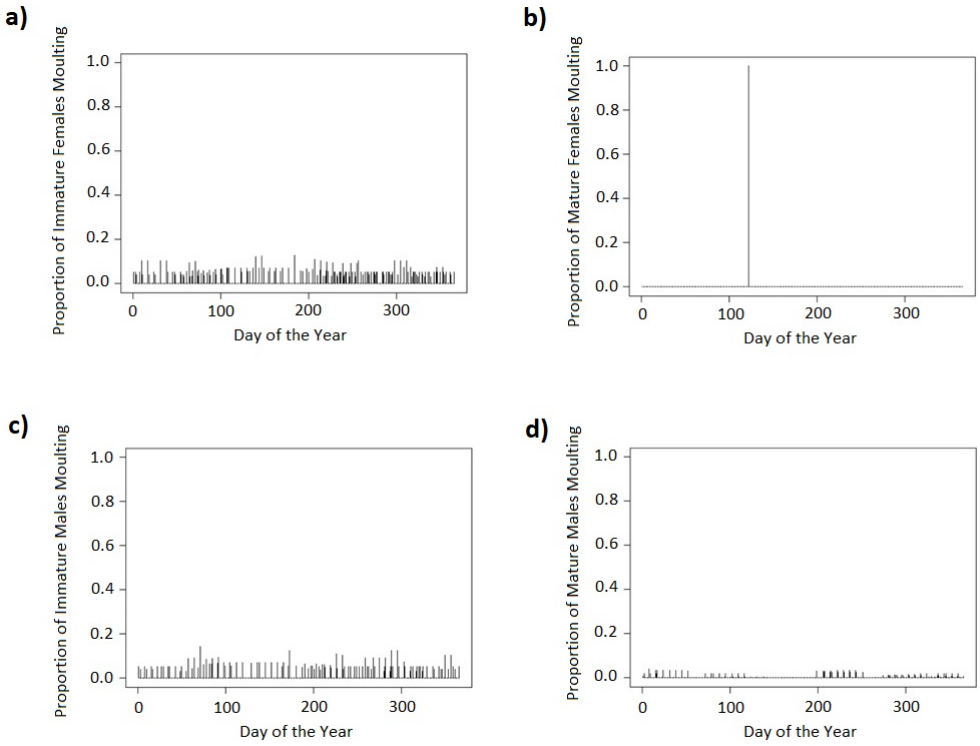

Figure 6.3: Plots showing the proportion of (a) immature females, (b) mature females, (c) immature males and (d) mature males moulting on each day of the year as predicted by the *Nephrops-Hematodinium* population model.

Sporulation (the release of spores from infected individuals) is directly linked to moulting, as set out in Section 3.2.5. The *Nephrops-Hematodinium* population model therefore also shows distinct seasonal patterns in the number of parasitic spores in the environment, as shown in Figure 6.4. The model records a dramatic increase in the number of parasitic spores in the environment on 1st May. This date coincides with the annual moult of mature females.

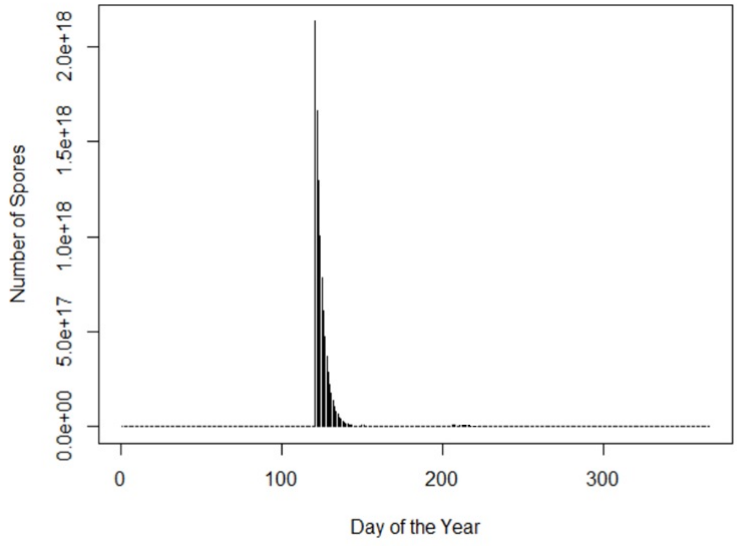

Figure 6.4: Plot showing the number of parasitic spores present in the environment on each day of the year as predicted by the *Nephrops-Hematodinium* population model.

6.4 Discussion

In this chapter, the *Nephrops-Hematodinium* population model has been used to further our understanding of *Nephrops-Hematodinium* population dynamics in the CSA. This has included the estimation of key statistics which are difficult to measure directly in the field. One statistic of great importance is the length of time required for the parasite burden within newly infected individuals to reach patent infection levels. In this chapter, the *Nephrops-Hematodinium* population model has shown that the length of time from initial infection to patency ranges from 519-620 days depending on the carapace length of the infected individual. The *Nephrops-Hematodinium* population model therefore provides further support to the idea of a multi-year infection pathway, as first suggested by Beevers (2010), rather than earlier claims by Stentiford et al. (2001c) which pointed to the likelihood of a single year infection pathway. In the previous chapter, the *Nephrops-Hematodinium* population model was shown to successfully replicate the patterns of infection prevalence produced by each of the five main *Hematodinium* diagnostic

tests. This includes distinct seasonal patterns in patent *Hematodinium* prevalence alongside a lack of seasonality in low-level sub-patent infection prevalence (see Section 5.2.3 for more detail). The ability of the *Nephrops-Hematodinium* population model to replicate these distinctive infection patterns provides further support to the idea of a multi-year infection pathway.

Furthermore, the *Nephrops-Hematodinium* population model has also provided further insight into the differences between estimates of *Hematodinium* prevalence obtained from the catch and the true level of *Hematodinium* prevalence in the *Nephrops* population as a whole. The prevalence of detectable infection in the catch was found to be 57% when using trawl nets with a mesh size of 70 mm. This was marginally higher than the estimate of overall prevalence in the population (55%). Estimates of *Hematodinium* prevalence obtained via the sustained use of trawl nets with a mesh size of 70 mm, are therefore a relatively good measure of the level of *Hematodinium* prevalence in the population as a whole. Increasing the mesh size of trawl nets, however, reduces the prevalence of infection in the catch. This is because smaller individuals are more susceptible to *Hematodinium* infection. The sustained use of trawl nets with a mesh size of 80 mm was found to result in an estimate of detectable infection prevalence in the catch of 40%. This was significantly lower than the estimate of overall prevalence in the population (61%). Estimates of *Hematodinium* prevalence obtained via the sustained use of trawl nets with a mesh size of 80 mm, therefore significantly underestimate the true level of *Hematodinium* prevalence in the population as a whole.

Finally, the *Nephrops-Hematodinium* population model has also provided further insight into the driving factors behind the distinct seasonal patterns in patent *Hematodinium* infection. Mature females in the CSA are known to moult annually each spring. In the *Nephrops-Hematodinium* population model this occurs on a fixed date, which is taken to be 1st May. Males and immature females, on the other hand, moult sporadically throughout the year. This results in a large peak in the total number of individuals moulting at the beginning of May, with relatively small numbers of individuals moulting throughout the rest of the year. The timing of sporulation is directly linked to the timing of moult events. Consequently, the peak in the number of individuals moulting in May leads to a distinct peak in the number of parasitic spores in the environment at this time. This in turn leads to an increase in the number of uninfected individuals contracting the infection since individuals must be in the soft-shelled recently moulted condition in order to contract the infection. The annual moult cycle of mature females is therefore responsible for driving the large increase in spores. This, in turn, leads to a large increase in the number of newly infected individuals. Newly infected individuals take 519-620 days to reach the

detection threshold of the pleopod method, as outlined above. Individuals infected at the beginning of May therefore reach patency the following February/March. The parasite burden within infected individuals then increases rapidly over the following months in response to the release of nutrients related to the pre-moult condition (Stentiford et al., 2001b). The timing of sporulation therefore coincides closely with the next moult event thereby continuing the seasonal cycle.

Chapter 7

Scenario Analysis: Changing Fishing Management Practices

7.1 Introduction

Changing current fishing practices in the CSA could impact the prevalence of *Hematodinium*, as outlined in Section 1.7. Predicting the exact effect of altering fishing management strategies, however, is difficult due to the large number of complex factors and feedback loops involved. Understanding and quantifying these complex interactions, in such a way as to provide useful advice for fisheries management, requires the use of population modelling. In this chapter, the newly developed *Nephrops-Hematodinium* population model is used to assess the potential impact of altering fishing management practices on the population dynamics of *Nephrops* and *Hematodinium* in the CSA. This chapter focuses specifically on the following three scenarios:

1) Changing fishing intensity
2) Preventing the discard of visibly-infected individuals
3) Altering the size distribution of discarded individuals.

These scenarios are all predicted to play an important role in determining the prevalence of *Hematodinium* in the CSA. Increasing fishing intensity, for example, is predicted to cause a reduction in the mean size of individuals in the population (Stentiford et al., 2001a). Smaller individuals are known to be more vulnerable to *Hematodinium* infection (Stentiford et al., 2001b). Increasing fishing intensity may therefore lead to a population structure which is more vulnerable to *Hematodinium* infection. This, in turn, could lead to an increase in *Hematodinium* prevalence. However, increasing fishing intensity to relatively high levels is also predicted to cause a decrease in the population size of

Nephrops in the CSA. The transmission of *Hematodinium* is thought to be density dependent. Decreasing population size is therefore expected to cause a reduction in the rate of *Hematodinium* transmission. Consequently, increasing fishing intensity may instead lead to a reduction in the overall prevalence of *Hematodinium*.

Changing current discard practices could also have a significant impact on the prevalence of *Hematodinium*. The EU landing obligation, introduced in 2015, requires fishermen to retain and land all species which are subject to quotas. This legislation applies to *Nephrops* fisheries in the CSA. However, some exemptions are available for this fishery due to the high survivability of discarded *Nephrops* (ICES, 2019). This allows *Nephrops* fisheries in the CSA to discard a small proportion of their catch. Fishermen in the CSA are known to selectively discard heavily-infected individuals which show visible signs of *Hematodinium* infection (Albalat et al., 2016b). Fishermen also selectively discard small individuals including those which fall below the Minimum Conservation Reference Size (MCRS) (Fox et al., 2020). Fish below the MCRS cannot be sold for human consumption and therefore have a reduced market value. Altering these selective discarding practices could have a significant impact on the prevalence of *Hematodinium*. For example, preventing the discarding of visibly-infected individuals will reduce the proportion of heavily-infected individuals in the population and is therefore predicted to cause a reduction in the overall prevalence of *Hematodinium*. Similarly, preventing the selective discarding of small individuals which are known to be more vulnerable to *Hematodinium* infection could also lead to a reduction in *Hematodinium* prevalence. Stopping fishermen from discarding small individuals, however, will prevent the discarding of immature females which have not yet had a chance to reproduce and could therefore have a detrimental effect on overall stock density.

In this chapter, the *Nephrops-Hematodinium* population model is used to explore the impact of altering current fishing management practices on *Nephrops-Hematodinium* population dynamics in the CSA. Particular attention is given to factors such as the overall prevalence of *Hematodinium*, the abundance of *Nephrops*, and the weight of marketable individuals landed by fishermen (i.e. *Nephrops* yield). This information will help aid fisheries management by highlighting strategies which reduce the prevalence of *Hematodinium* whilst maintaining or improving *Nephrops* yield.

Finally, this chapter concludes with an exploration of a hypothetical infection-free scenario. This allows for an investigation into the population dynamics of *Nephrops* in the CSA in the absence of *Hematodinium* infection. This will help highlight the negative impact of *Hematodinium* infection on *Nephrops* fisheries in the CSA. Furthermore, the

exploration of an infection-free scenario also highlights the significant benefits that could be gained by *Nephrops* fisheries in the CSA following the successful eradication of *Hematodinium* infection in this region.

7.2 Methods

Each scenario was examined in turn. In all cases, the baseline *Nephrops-Hematodinium* population model was first run to a steady state, using the optimised set of model parameters shown in Table 4.3. Changes were then made to parameter values or model equations in order to simulate the changes in fishery management practices described by each scenario. More detail on the changes applied in each specific scenario are provided in the sub-sections below. Following this the *Nephrops-Hematodinium* population model was restarted and allowed to reach a new steady state. Key statistics were then extracted from the model to summarise *Nephrops-Hematodinium* population dynamics. This includes the overall prevalence of *Hematodinium*, the prevalence of patent *Hematodinium* infection, the annual biomass of *Nephrops* landed by fishermen, the mean carapace length of *Nephrops* and the total number of *Nephrops* in the population. More detail on extracting these key statistics from the *Nephrops-Hematodinium* population model can be found in Section 3.4.

Scenario 1: Changing Fishing Intensity

Changing fishing intensity was simulated by altering the effort parameter (E_t). This parameter represents the annual number of hours which fishermen in the CSA actively spend trawling. The baseline *Nephrops-Hematodinium* population model assumes an annual effort of 130,000 hours per annum. This chapter examines the impact of a range of different levels of fishing intensity starting from no fishing (0 hours of effort per annum) and ranging to exceptionally high levels of fishing intensity (600,000 hours of effort per annum).

Scenario 2: Preventing The Discard of Visibly-Infected Individuals

Preventing the discard of visibly-infected individuals was simulated within the model by altering the discard rules. The discard rules used in the baseline *Nephrops-Hematodinium* population model are shown in Equation 3.25. The baseline *Nephrops-Hematodinium* population model assumes that fishermen automatically discard all visibly-infected individuals regardless of their size. This chapter examines the impact of reversing this rule to simulate a scenario in which discard policies are changed to require fishermen to land individuals which show visible signs of *Hematodinium* infection. This was simulated by

altering Equation 3.25, to become:

$$d^{\,\mathrm{l,p}} = \begin{cases} 0 & \text{if } \frac{P}{V} > 50{,}000{,}000 \quad \text{i.e. individual is visibly-infected} \\ d^{\,\mathrm{l}} & \text{otherwise} \end{cases} \tag{7.1}$$

where $d^{\,\mathrm{l,p}}$ represents the probability of discarding individuals of length 'l' and parasite burden 'p' and d^{l} is a size selectivity curve which determines the probability of fishermen discarding individuals based on size (see Equation 3.26 for more details).

The impact of altering discard policies on *Nephrops-Hematodinium* population dynamics is highly dependent on the survival rate of discarded individuals. The baseline *Nephrops-Hematodinium* population model assumes a discard survival rate of 25%, as estimated by Chapman (1980) and commonly used in *Nephrops* stock assessments (ICES, 2019). Other studies, however, have estimated the discard survival rate of *Nephrops* to be anywhere from 20% (Charuau et al., 1982; Sangster et al., 1997; Wileman et al., 1999) to 100% (Harris and Ulmestrand, 2004). A recent study on the survival rate of discarded *Nephrops* on the west coast of Scotland estimated discard survival to be between 47% and 62% (Fox et al., 2020). This chapter therefore examines the effect of changing discard policies under a range of different discard survival rates (0-100%).

Scenario 3: Altering the Size Distribution of Discarded Individuals

Changes to the size distribution of discarded individuals were simulated within the model by altering the discard size-selectivity parameter d_{50}. Parameter d_{50} corresponds with the length at which 50% of individuals are discarded by fishermen. Lowering d_{50} causes fishermen to discard a higher proportion of smaller individuals. Conversely, increasing the value of d_{50} causes fishermen to discard a higher proportion of larger individuals. The value of d_{50} in the baseline *Nephrops-Hematodinium* population model is 23.05 mm. This chapter examines the impact of altering parameter d_{50} within the range 10-40 mm. The effect of altering the size distribution of discards on *Nephrops-Hematodinium* population dynamics is highly dependent on the survival rate of discarded individuals. This chapter therefore examines the effect of changing the size distribution of discards under a range of different discard survival rates (0-100%).

Scenario 4: *Hematodinium*-Free Population Dynamics

A hypothetical infection-free scenario was investigated by setting the parasite transmission rate (β) to zero. This eliminates *Hematodinium* infection from the population and

therefore allows for an investigation into the population dynamics of *Nephrops* in the absence of *Hematodinium* infection. This chapter examines the infection-free population dynamics of *Nephrops* under a range of different fishing intensities. This is achieved by altering the effort parameter E_t as described above. This allows for comparisons to be made between *Nephrops* population dynamics with and without the presence of *Hematodinium* in order to highlight the negative impact of parasitic infection on the CSA *Nephrops* population.

7.3 Scenario Analysis: Results

7.3.1 Scenario 1: Changing Fishing Intensity

Changing the level of fishing intensity was found to affect the mean carapace length of *Nephrops* in the population. Increasing fishing intensity caused a decrease in the mean carapace length of *Nephrops*, as shown in Figure 7.1. In the absence of fishing, the mean carapace length of males and females was predicted to be 34.9 mm and 28.2 mm respectively. At high fishing intensities of 600,000 hours per annum, the mean carapace length of males and females was predicted to be 26.1 mm and 23.6 mm respectively.

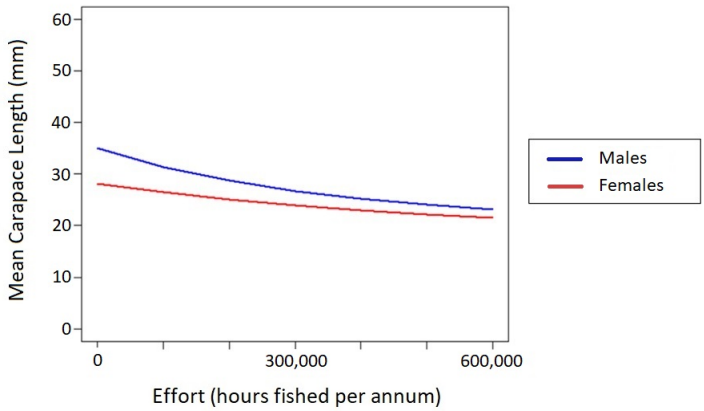

Figure 7.1: Plot showing the mean carapace length of *Nephrops* in the population under a range of different fishing intensities.

Changing fishing intensity was also found to have a significant effect on the weight of *Nephrops* landed by fishermen in the CSA. Figure 7.2 shows the weight (tonnes) of *Nephrops* obtained from the CSA across a range of fishing intensities. In the absence of fishing, the weight of *Nephrops* landed by fishermen was 0 tonnes as expected. The highest yield of *Nephrops* was obtained at relatively low levels of fishing intensity (205,000

hours per annum). Increasing fishing intensity beyond this point results in a decrease in the weight of *Nephrops* landed by fishermen. The *Nephrops-Hematodinium* population model predicts that the weight of *Nephrops* landings will fall to 0 tonnes for fishing intensities greater than 620,000 hours per annum.

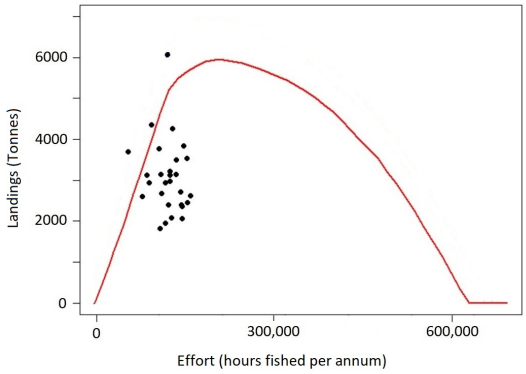

Figure 7.2: Plot showing the weight (tonnes) of *Nephrops* landed by fishermen in the CSA under a range of different fishing intensities. Black points show historical landings-effort data for the period 1980-2007 as obtained from ICES(2009).

Finally, changing the level of fishing intensity was also found to have a significant effect on the prevalence of *Hematodinium* in the population, as shown in Figure 7.3. Increasing fishing intensity (i.e. increasing the number of hours fished) results in a decrease in the overall prevalence of *Hematodinium*. In the absence of any fishing, the prevalence of *Hematodinium* in the population is predicted to be 58%. At high fishing intensities of 600,000 hours per annum, the prevalence of *Hematodinium* in the CSA *Nephrops* population is predicted to be just 21 %.

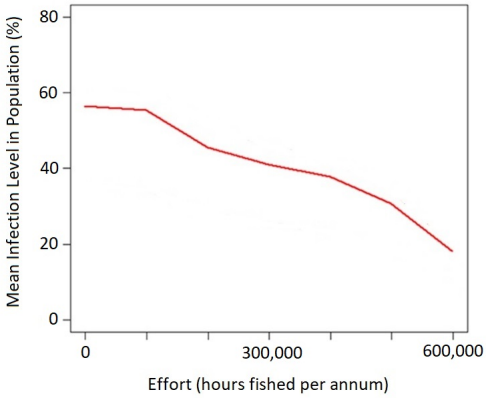

Figure 7.3: Plot showing the percentage of *Nephrops* in the population infected with *Hematodinium* under a range of different fishing intensities.

7.3.2 Scenario 2: Preventing the Discard of Visibly-Infected Individuals

Changing discard policies to prevent the discard of visibly-infected individuals leads to a decrease in the prevalence of *Hematodinium*, as shown in Figure 7.4. The effect of altering discard policies on *Hematodinium* prevalence is dependent on the survival rate of discarded individuals. The baseline *Nephrops-Hematodinium* population model assumes a discard survival rate of 25%. At 25% discard survival, there is very little difference between the overall prevalence of *Hematodinium* in a scenario in which fishermen discard all visibly-infected individuals (58%) and a scenario in which discard policies are changed to force fishermen to land all visibly-infected individuals (56%). Increasing the discard survival rate, however, progressively increases the difference between these two scenarios. Increasing the discard survival rate to 100% resulted in an overall infection prevalence of 63% for a scenario in which all visibly-infected individuals were discarded and an infection prevalence rate of 56.4% for a scenario in which all visibly-infected individuals were landed by fishermen.

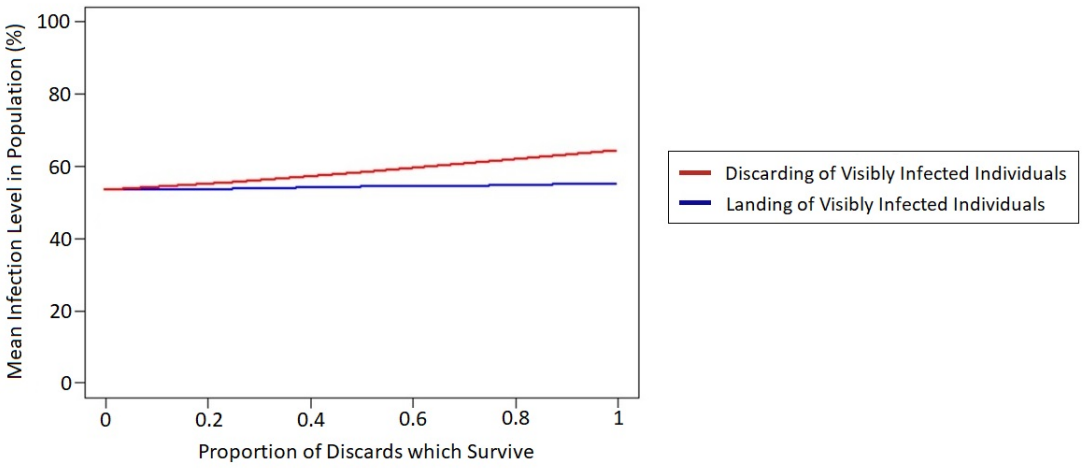

Figure 7.4: Plot showing the mean prevalence level of infection in the population (%) for two alternate discard policies under a range of different discard survival rates.

Preventing the discard of visibly-infected individuals was also found to cause an increase in the yield of *Nephrops* obtained by fishermen, as shown in Figure 7.5. Using a baseline discard survival rate of 25% resulted in an annual *Nephrops* yield of 4120 tonnes for a scenario in which all visibly-infected individuals were discarded compared to an annual *Nephrops* yield of 4335 tonnes for a scenario in which all visibly-infected individuals were landed by fishermen. Increasing the survival rate to 100% resulted in an annual *Nephrops*

yield of 3957 tonnes for a scenario in which all visibly-infected individuals were discarded and an annual *Nephrops* yield of 4402 tonnes for a scenario in which all visibly-infected individuals were landed by fishermen.

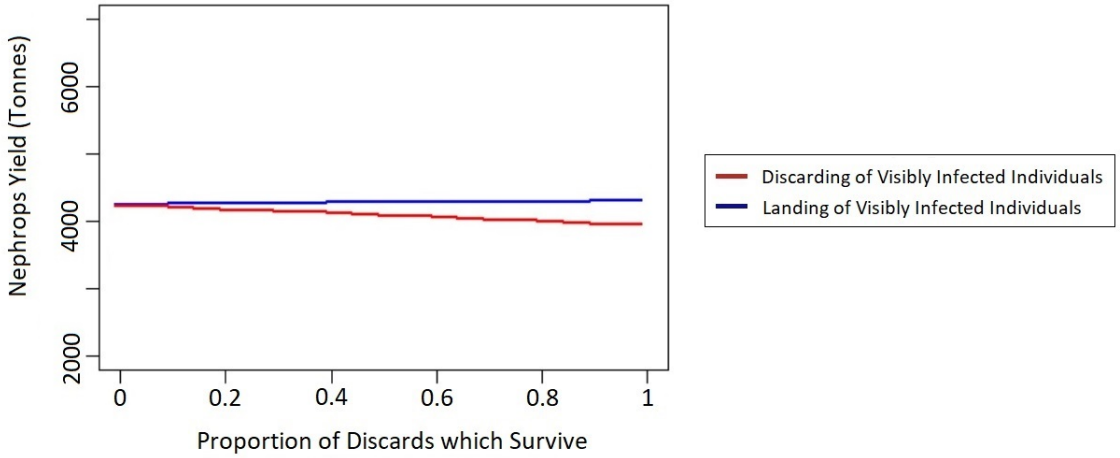

Figure 7.5: Plot showing the annual yield of *Nephrops* (tonnes) obtained by fishermen for two alternate discard policies under a range of different discard survival rates.

7.3.3 Scenario 3: Altering the Size Distribution of Discarded Individuals

Lowering d_{50} was found to reduce the overall prevalence of *Hematodinium* in the CSA, as shown in Figure 7.6. The effect of changing the size distribution of discards is highly dependent on the survival rate of discarded individuals. At the baseline discard survival rate of 25%, there is very little difference between the overall prevalence of *Hematodinium* in a scenario in which d_{50} is 40 mm (58%) and a scenario in which d_{50} is 10 mm (55%). Increasing the discard survival rate, however, increases the difference between these two scenarios. Increasing the survival rate to 100% resulted in an overall infection prevalence of 66% for a scenario in which d_{50} was 40 mm and an overall infection prevalence of 56% for a scenario in which d_{50} was 10 mm.

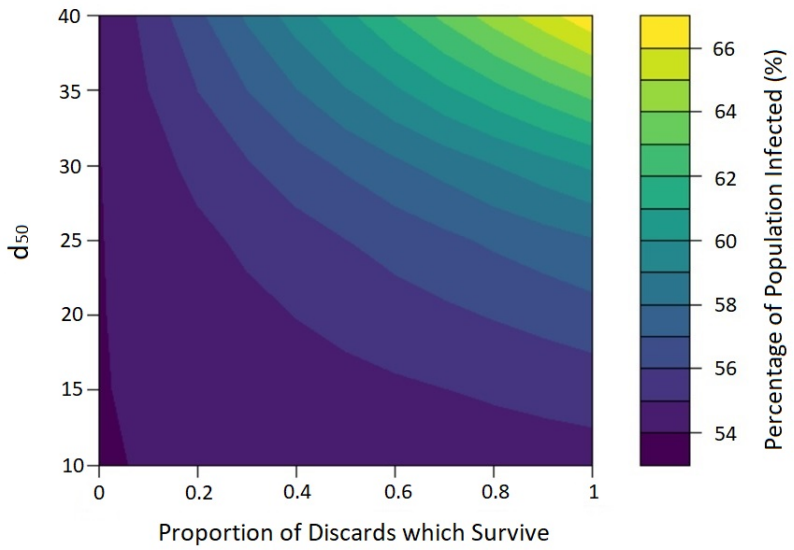

Figure 7.6: Contour plot showing the effect of altering parameter d_{50} and discard survival rate on the prevalence of *Hematodinium* in the CSA.

Lowering d_{50} was also found to lead to a reduction in the yield of *Nephrops* obtained by fishermen. Figure 7.7 shows the annual yield of *Nephrops* obtained by fishermen assuming a baseline discard survival rate of 25%. The annual yield of *Nephrops* obtained by fishermen was found to be 4020 tonnes for a scenario in which d_{50} was 10 mm and 4370 tonnes for a scenario in which d_{50} was 40 mm.

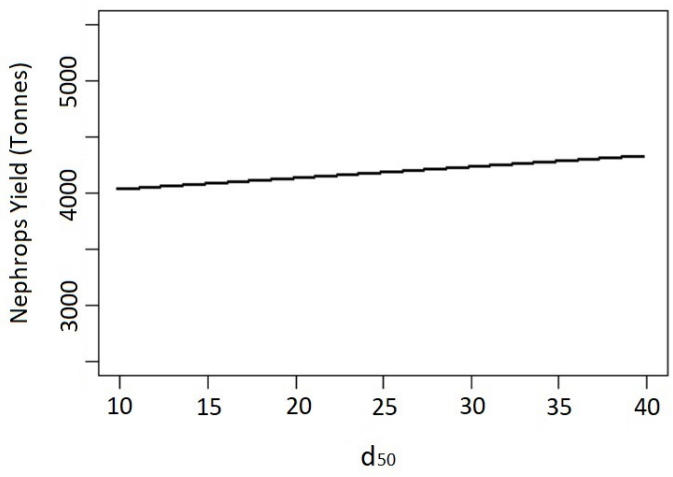

Figure 7.7: Plot showing the effect of altering the discard selectivity parameter d_{50} on the annual yield of *Nephrops* obtained by fishermen. This plot assumes a discard survival rate of 25%.

7.3.4 Scenario 4: *Hematodinium*-Free Population Dynamics

Eradicating *Hematodinium* infection has significant benefits for *Nephrops* fisheries in the CSA, as shown in Figure 7.8. This figure shows the weight of *Nephrops* landed by fishermen under a range of fishing intensities for two scenarios: one in which *Hematodinium* infection is present in the population and another in which the population is completely free of *Hematodinium* infection. The weight of *Nephrops* landed by fishermen was found to be substantially greater in the infection-free scenario compared to weight of *Nephrops* landed by fishermen in the scenario in which *Hematodinium* infection is present in the population. This is true across all levels of fishing intensity.

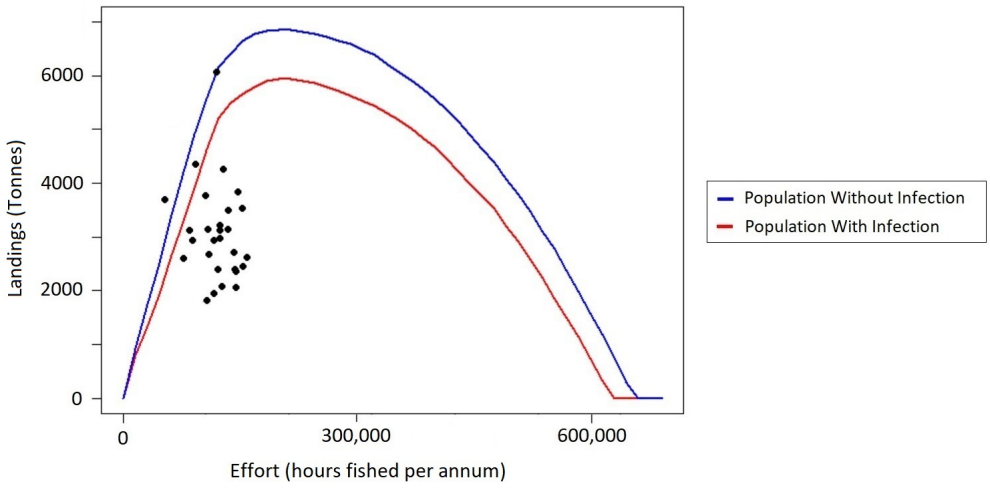

Figure 7.8: Plot showing the weight (tonnes) of *Nephrops* landed by fishermen in the CSA under a range of different fishing intensities for two different scenarios: one in which *Hematodinium* infection is present in the population and another in which *Hematodinium* infection is absent from the population. Black points show historical landings-effort data for the period 1980-2007 as obtained from ICES(2009).

7.4 Discussion

In this chapter, the *Nephrops-Hematodinium* population model has been used to explore the impact of altering current fishing management practices on the population dynamics of *Nephrops* and *Hematodinium* in the CSA. This chapter has focused specifically on the impact of three distinct scenarios, each of which was initially selected due to its expected importance on the prevalence of *Hematodinium* in the CSA *Nephrops* population. These scenarios include changing the current level of fishing intensity, preventing the discard of visibly-infected individuals and altering the size distribution of discarded individuals. This chapter examines the suitability of each strategy for managing *Hematodinium* in the

CSA by examining a range of factors including the prevalence of *Hematodinium* infection and the overall yield of *Nephrops* obtained by fishermen.

Altering the level of fishing intensity was found to have an important impact on *Nephrops-Hematodinium* population dynamics in the CSA. Increasing fishing intensity led to a significant reduction in the mean carapace length of *Nephrops* in the population, as shown in Figure 7.1. Smaller individuals are known to be more vulnerable to *Hematodinium* infection (Stentiford et al., 2001b). Increasing fishing intensity therefore leads to a population with a size distribution which is more vulnerable to *Hematodinium* infection. However, despite this, the results of the *Nephrops-Hematodinium* population model show that there is an overall decrease in the prevalence of *Hematodinium* in the population as fishing intensity increases. This suggests that the prevalence of *Hematodinium* infection is predominantly governed by other factors, including density dependent *Hematodinium* transmission. Increasing fishing intensity causes a decrease in population size and consequently leads to an overall reduction in the prevalence of *Hematodinium*.

However, it is important to note that this reduction in *Hematodinium* prevalence is accompanied by a significant reduction in the weight of *Nephrops* landed by fishermen. The highest yield of *Nephrops* is obtained at relatively low levels of fishing intensity (205,000 hours per annum). At this level of intensity the prevalence of *Hematodinium* in the population was estimated to be 54%. Increasing fishing intensity beyond this point leads to a decrease in the weight of *Nephrops* landed by fishermen despite the decreasing levels of *Hematodinium* prevalence in the population. Reducing *Hematodinium* prevalence in the CSA by increasing fishing intensity would therefore come at the expense of a significant reduction in yield. This strategy will therefore have an overall detrimental effect on *Nephrops* fisheries in the CSA.

Furthermore, increasing the level of fishing intensity does not lead to the successful eradication of *Hematodinium* infection in the CSA *Nephrops* population. Increasing the level of fishing intensity has been suggested as an effective control strategy in a number of other aquatic host-parasite systems (Dobson and May, 1987; Wood et al., 2010; Ben-Horin et al., 2015). These studies argue that increasing the level of fishing intensity could drive host populations below the density required for parasite transmission. As a result, increasing fishing intensity could lead to the parasite effectively being 'fished out' of the population. However, this strategy only works if the level of fishing intensity required to reduce parasite transmission does not lead to over-exploitation of the host stock i.e. the threshold density for transmission is lower than the maximum sustainable yield. The results of the present study suggest that *Nephrops* stocks in the CSA will collapse prior

to the successful eradication of the parasite. Increasing fishing intensity is therefore not a successful method of controlling or eliminating *Hematodinium* infection in the CSA.

Scenarios which involve altering discard policies (i.e preventing the discard of visibly-infected individuals and changing the size distribution of discarded individuals) were also found to affect the prevalence of *Hematodinium* in the CSA. The effectiveness of these strategies, however, is highly dependent on the survival rate of discarded *Nephrops*. The baseline *Nephrops-Hematodinium* population model assumes a discard survival rate of 25%. This is based on experimental studies carried out by Chapman (1980). Other studies, however, have estimated the discard survival rate of *Nephrops* to be anywhere from 20% (Charuau et al., 1982; Sangster et al., 1997; Wileman et al., 1999) to 100% (Harris and Ulmestrand, 2004). A recent study on the survival rate of discarded *Nephrops* on the west coast of Scotland estimated discard survival to be between 47% and 62% (Fox et al., 2020). Increasing the discard survival rate significantly increases the impact of altering discard policies on *Nephrops-Hematodinium* population dynamics. Further research is therefore required to determine the true survival rate of discarded *Nephrops* in the CSA. This in turn will determine the effectiveness of changing current discard policies on reducing *Hematodinium* prevalence in the CSA.

Preventing the discard of visibly-infected individuals led to a slight reduction in *Hematodinium* prevalence, as shown in Figure 7.4. This decrease in *Hematodinium* prevalence was accompanied by a slight increase in the yield of *Nephrops* obtained by fishermen in the CSA. Preventing the discard of visibly-infected individuals therefore has an overall positive effect on *Nephrops* fisheries in the CSA. Lowering d_{50} (and hence lowering the size distribution of individuals discarded by fishermen) was also found to lead to a small reduction in the overall prevalence of *Hematodinium*, as shown in Figure 7.6. However, reducing d_{50} increases the proportion of immature females which are removed from the population. This reduces the abundance of *Nephrops* in the CSA and consequently leads to a reduction in the yield of *Nephrops* obtained by fishermen. The selective discarding of smaller individuals by fishermen is partly driven by current legislation including the Minimum Conservation Reference Size (MCRS). Fish below the MCRS cannot be sold for human consumption and therefore have a reduced market value. Altering MCRS is therefore likely to influence the behaviour of fishermen and could lead to changes in the size distribution of discarded individuals. However, the results of this study show that reducing the size distribution of discards, and consequently reducing MCRS, is not an effective method of controlling *Hematodinium* infection in the CSA.

In conclusion, preventing the discard of visibly-infected individuals was the only scenario

predicted to cause a decrease in *Hematodinium* prevalence whilst also causing a slight increase in the yield of *Nephrops* obtained by fishermen. It is therefore recommended that stricter discard rules are enforced in the CSA to prevent fishermen from discarding visibly-infected individuals. It is important to note, however, that this strategy is only predicted to lead to a minor reduction in *Hematodinium* prevalence. The other scenarios investigated in this chapter (increasing fishing intensity and reducing the size distribution of discards) were found to lead to a greater reduction in *Hematodinium* prevalence. These strategies, however, were are also found to cause a reduction in the yield of *Nephrops* obtained by fishermen and are therefore not considered to be effective methods of controlling *Hematodinium* infection in the CSA. Finally, this chapter has also highlighted the clear benefits to *Nephrops* fisheries in the CSA following the successful eradication of *Hematodinium* infection. The yield of marketable *Nephrops* obtained by fishermen was substantially greater in the absence of *Hematodinium* infection across all levels of fishing intensity, as highlighted in Figure 7.8. It is therefore imperative that further research is carried out to identify possible strategies which could substantially reduce or eliminate *Hematodinium* infection in the CSA, without having a detrimental effect on *Nephrops* fisheries in the region.

Part II

The Distribution and Dispersal Patterns of *Nephrops* in the Clyde Sea Area

Chapter 8

The Spatial Distribution of *Nephrops*

8.1 Introduction

The *Nephrops-Hematodinium* population model set out in the previous section makes a number of simplifying assumptions. One of the primary assumptions of this model is that *Nephrops* growth rates, population density and fishing intensity are the same across the entire region. In reality, however, these factors all vary substantially across the CSA. In general, the northern sea-lochs and upper regions of the CSA contain a low density of large individuals and are primarily targeted by creel fisheries. The lower regions of the CSA, on the other hand, typically contain a higher density of small individuals and are primarily targeted by high intensity bottom trawlers (Tuck et al., 1997). Fishing intensity, population density and *Nephrops* growth rates all impact *Hematodinium* transmission, as outlined in the previous section. Fully understanding the population dynamics of *Nephrops* and *Hematodinium* in the CSA therefore requires the development of a spatial population model capable of accounting for spatial variability across the region.

The creation of a full spatial population model is beyond the scope of this thesis. In this section, however, I lay the groundwork for the creation of such a model. The first step in extending the *Nephrops-Hematodinium* population model to the spatial domain involves mapping the distribution of *Nephrops* across the CSA. In this chapter a new method for predicting *Nephrops* habitat is developed and used to create an updated high-resolution map of suitable *Nephrops* habitat across the west coast of Scotland. The variability in burrow density across areas of predicted suitable *Nephrops* habitat is then explored. Finally, in Chapter 9, the movement of *Nephrops* larvae between areas of suitable habitat is explored using a high-resolution hydrodynamic model. In addition to

laying the groundwork for the creation of a spatial *Nephrops-Hematodinium* population model, this work also furthers our knowledge of the distribution and dispersal patterns of *Nephrops* in the CSA. Improving our understanding of these factors is essential for the effective management of this commercially important host-parasite system.

8.2 Mapping Suitable *Nephrops* habitat

Nephrops are restricted to regions of muddy seabed sediment suitable for the construction of elaborate burrow systems, as discussed in Section 1.1. Suitable *Nephrops* habitat on the west coast of Scotland, as categorised by Marine Scotland, is shown in Figure 8.1. A large, continuous patch of suitable sediment is located in the Firth of Clyde, which surrounds the Isle of Arran and extends into the Clyde estuary and northern sea-lochs. Smaller patches of suitable sediment can also be found in the Sound of Jura and the South Minch.

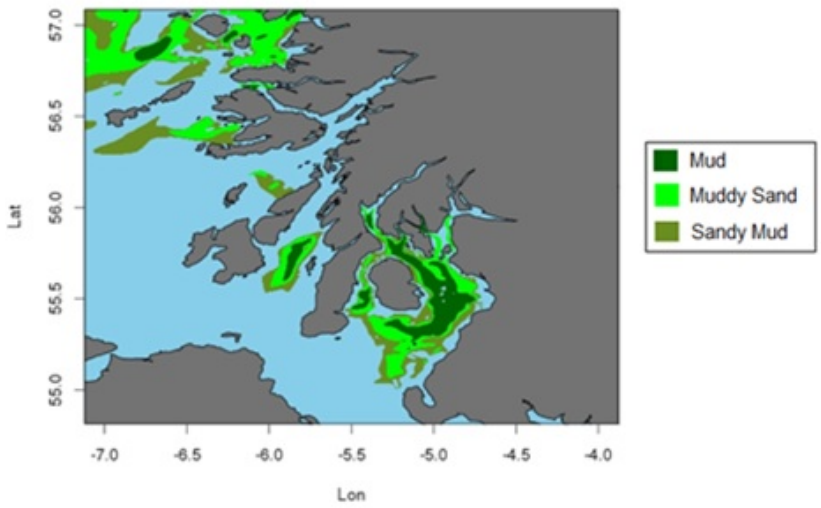

Figure 8.1: Suitable *Nephrops* habitat on the west coast of Scotland as classified by Marine Scotland. The map distinguishes between three different sediment classifications: mud, muddy sand and sandy mud. All three sediment classifications are assumed to be suitable *Nephrops* habitat.

Patches of suitable *Nephrops* habitat were identified by interpolating British Geological Survey (BGS) seabed sediment data. This dataset records the percentages of mud, sand and gravel at numerous sampling locations throughout British territorial waters. Suitable *Nephrops* habitat was classified as mud, muddy sand and sandy mud as determined by Folk sediment classification (Folk, 1954). Patches of suitable sediment identified via the interpolation of BGS data were then compared with the distribution of Vessel Monitoring System (VMS) pings. VMS pings show the distribution of fishing activity and can

therefore be used as an indicator of the presence of *Nephrops*. Areas which showed a high density of VMS pings but were not classified as suitable sediment by the interpolated BGS data were added in as additional patches of suitable sediment by drawing a convex hull around the VMS data points, as described in the ICES Working Group Report (2013).

However, this process is likely to have led to an under-representation of suitable *Nephrops* habitat, particularly in the northern regions of the CSA. Firstly, the sediment data obtained from BGS do not provide uniform coverage of the entire region. Predicting sediment composition using statistical interpolation is therefore unreliable in areas of low quality spatial sediment data. Furthermore, VMS data are only available for trawlers greater than 12 m. Relying on VMS data to validate suitable *Nephrops* habitat severely underestimates the presence of suitable sediment in the inner Clyde and northern sea lochs, which are predominantly targeted by small fishing vessels.

In this chapter, a new map of suitable *Nephrops* habitat across the west coast of Scotland is developed. Updated predictions about habitat suitability are determined via the creation of high-resolution maps of seabed sediment composition across the region. Seabed sediment composition is determined using a novel method, initially developed by Wilson et al. (2018). This method combines interpolation in areas of high data density with random forest modelling in areas of low data density.

Random forest modelling is a flexible statistical technique capable of 'learning' patterns in data in order to predict an associated value (Breiman, 2001). Random forest models have become one of the most powerful and widely used statistical learning tools, with high predictive accuracy across a wide range of disciplines, including the prediction of seabed sediment composition (Stephens and Diesing, 2015; Diesing et al., 2014; Huang et al., 2012).

However, predictions made using random forest models are often less reliable than interpolated values in areas of high data density. The most accurate picture of seabed sediment composition is therefore achieved by combining random forest modelling in areas of low data density with interpolation in areas of high data density. This combined approach has already been used to successfully predict seabed sediment composition across the entire north-west European Shelf (Wilson et al., 2018). Here the focus is specifically on the west coast of Scotland. This allows for the creation of high resolution maps of mud, sand and gravel across this region. These maps in turn are used to improve predictions about the location of suitable *Nephrops* habitat.

8.3 Methods

8.3.1 Data Sources

The study area was defined as the region bounded by 53.75 to 56.5 °N and -6.8 to -4 °W. This area extends from the Isle of Mull in the north to the central part of the Irish Sea in the south. Data on seabed sediment composition within the region were obtained from two sources (i) BGS sediment data and (ii) Marine Scotland sediment data. This provided a combined total of 2691 sampling sites across the region, comprised of 1998 BGS sampling locations and 693 Marine Scotland sampling locations. The locations of all sampling sites are shown in Figure 8.2.

BGS data were downloaded from the BGS website using the GeoIndex tool (http://www.bgs.ac.uk/geoindex/wms.htm). BGS sediment data were collected using a variety of equipment including day grabs, shipek grabs, corers and diver collected samples. To produce a consistent measure of seabed sediment composition, the analysis was restricted to grab samples. Marine Scotland sediment data were obtained directly from Marine Scotland. This data was collected as part of the Marine Scotland annual underwater television (UWTV) survey. The primary aim of this survey is to estimate *Nephrops* abundance by counting the number of burrow complexes on the seabed (see Section 8.6 for more details). However, additional data on seabed sediment composition is also collected. During the UWTV survey, a van veen grab was deployed at the end of each camera tow, with an additional day grab deployed if the van veen grab was unsuccessful.

The procedure for analysing sediment samples differs considerably between BGS and Marine Scotland. The gravel component is removed from the Marine Scotland sediment data prior to analysis. As a result, the mud and sand percentages sum to 100% within the Marine Scotland dataset and no information is provided about the percentage of gravel. BGS, on the other hand, retain the gravel component and consequently mud, sand and gravel percentages sum to 100% within the BGS dataset. These data must therefore be carefully processed in order to incorporate information from both data sources, as shown in Section 8.3.2.

Data were also obtained from BGS on the distribution of rock across the west coast of Scotland (http://www.bgs.ac.uk/discoverymetadata/13605550.html). This dataset outlines areas of exposed rock as well as areas of rock covered by less than 0.5 m of sediment. The distribution of rock, as categorised by the BGS dataset, is shown in Figure 8.3.

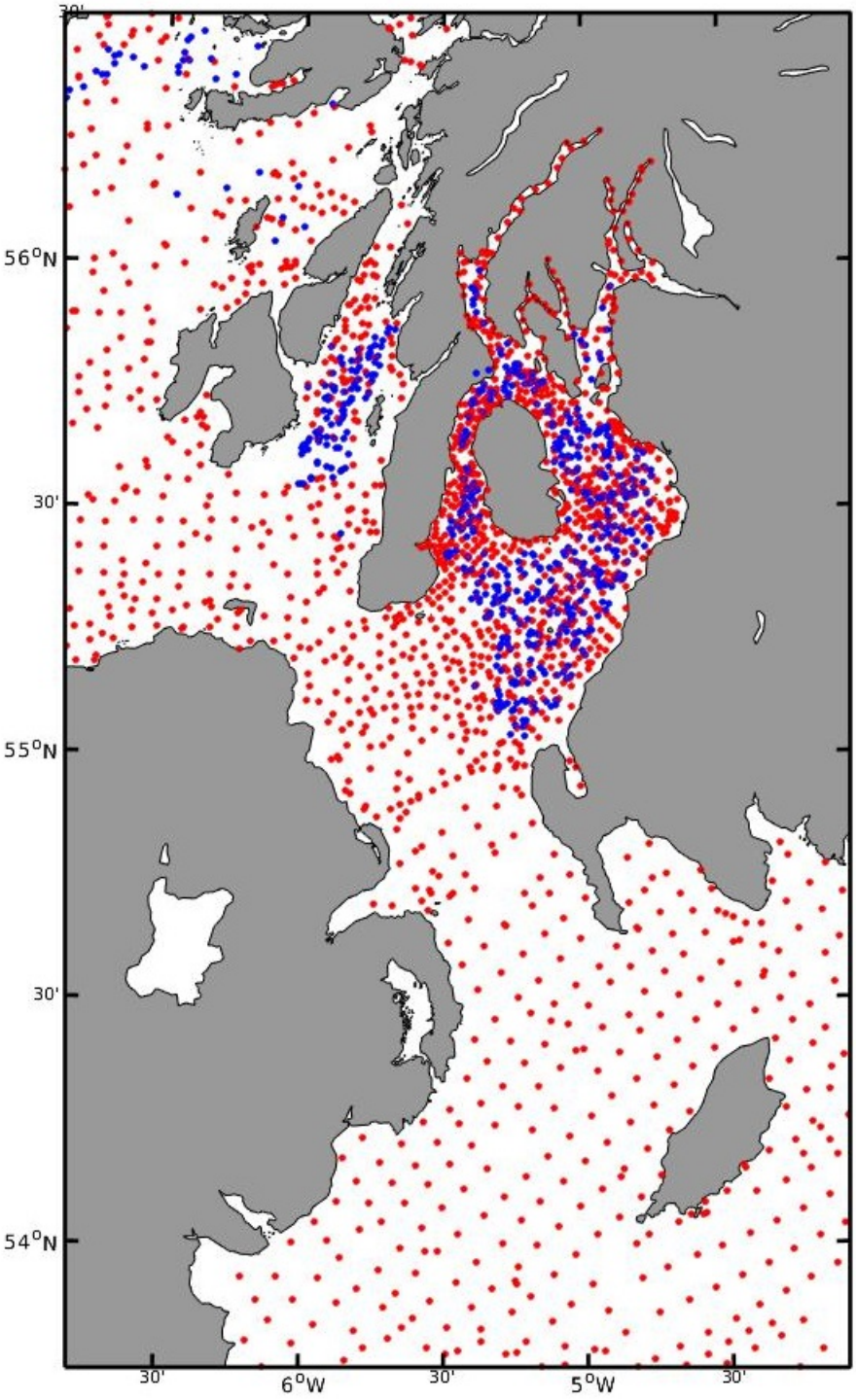

Figure 8.2: Sediment composition sampling locations included within the analysis. BGS sampling locations are shown in red and Marine Scotland sampling locations are shown in blue.

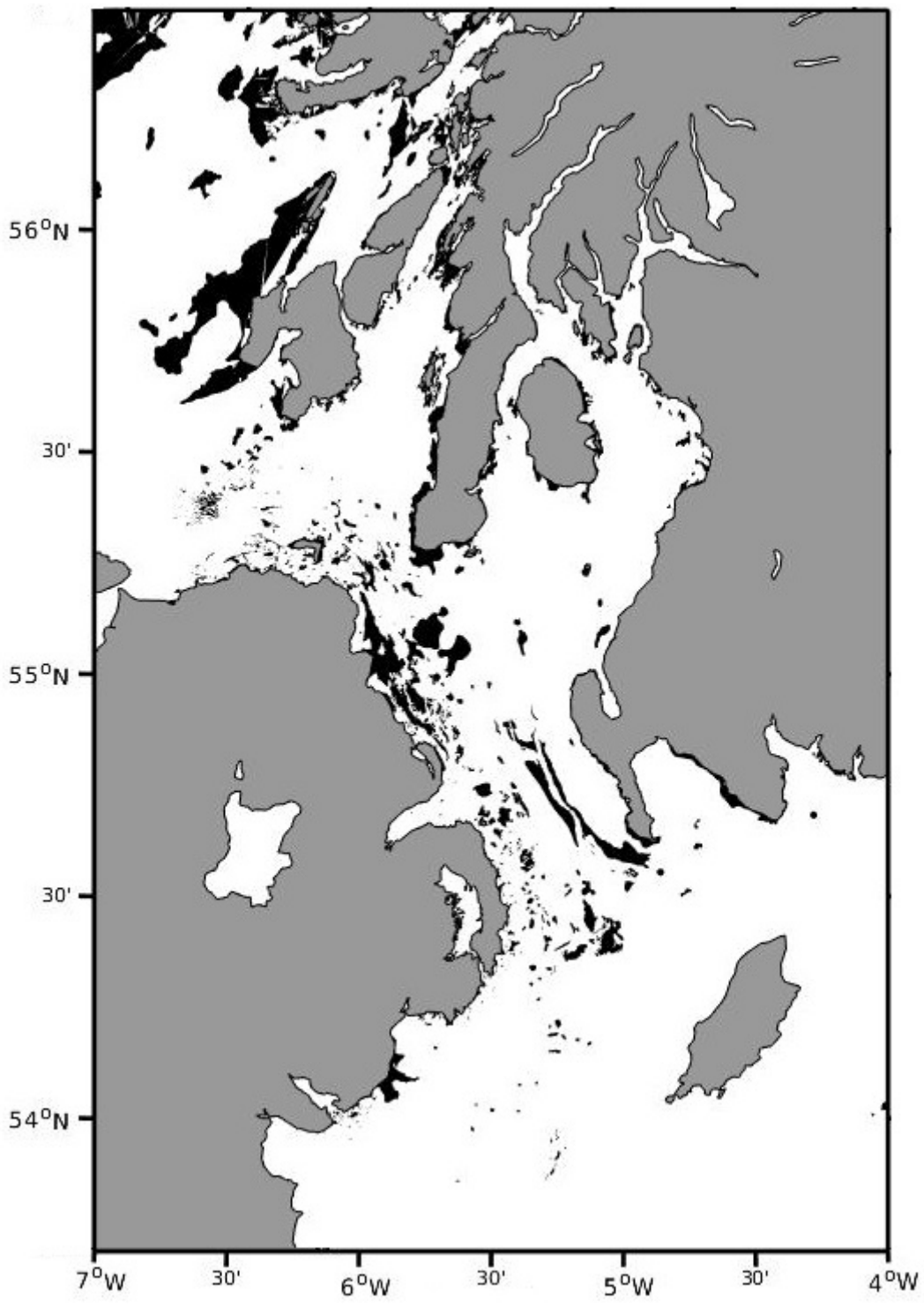

Figure 8.3: Distribution of rock across the west coast of Scotland, as categorised by BGS (http://www.bgs.ac.uk/discoverymetadata/13605550.html). Black represents areas classified as rock and white represents areas classified as non-rock.

8.3.2 Data Processing

The sediment data were transformed onto an additive log-ratio scale, following the method set out in Stephens and Diesing (2015). Equations (6.1) and (6.2) were used to couple the sediment fractions and ensure that the predicted values of mud, sand and gravel always sum to 100%.

$$alrs = ln\left(\frac{Sand}{Mud}\right) = ln(Sand) - ln(Mud) \tag{8.1}$$

$$alrg = ln\left(\frac{Gravel}{Mud}\right) = ln(Gravel) - ln(Mud) \tag{8.2}$$

Transforming the sediment data onto the additive log-ratio scale makes it possible to reconcile the BGS and Marine Scotland datasets. This is achieved by specifically choosing mud as the denominator. The calculation of 'alrs' deals with the ratio of sand to mud and is therefore insensitive to the inclusion or removal of the gravel fraction prior to analysis. As a result, values for 'alrs' can be calculated at both BGS and Marine Scotland sampling locations. Values of 'alrg', however, can only be calculated at BGS sampling locations.

8.3.3 Predicting 'alrs' and 'alrg'

A grid of equally spaced points was created across the study region, with a total of over 45,000 points. Predictions of 'alrs' and 'arlg' were then made at each point. Values for 'alrs' and 'alrg' were predicted using interpolation in areas of high data density and random forest modelling in areas of low data density. No predictions about seabed sediment were made at locations classified as rock.

Regions with a high density of data were identified by creating an alphahull around the sampling locations using the R package alphahull (Pateiro-Lopez and Rodriguez-Casal, 2010). An alphahull is a convex envelope which characterizes the shape of a set of points. The alphahull excludes areas outside of the sampled regions as well as excluding large holes in the data coverage. The parameter α controls the size and level of detail included in each polygon. Different values of α were tested and a value of $\alpha = 0.01$ was found to produce optimal results. Separate alphahulls were created for 'alrs' and 'alrg' since values of 'alrg' are only available at BGS sampling locations whilst values of 'alrs' are available at both BGS and Marine Scotland sampling locations. High density sampling areas are shown in Figure 8.4 (a) and (b) for 'alrs' and 'alrg' respectively.

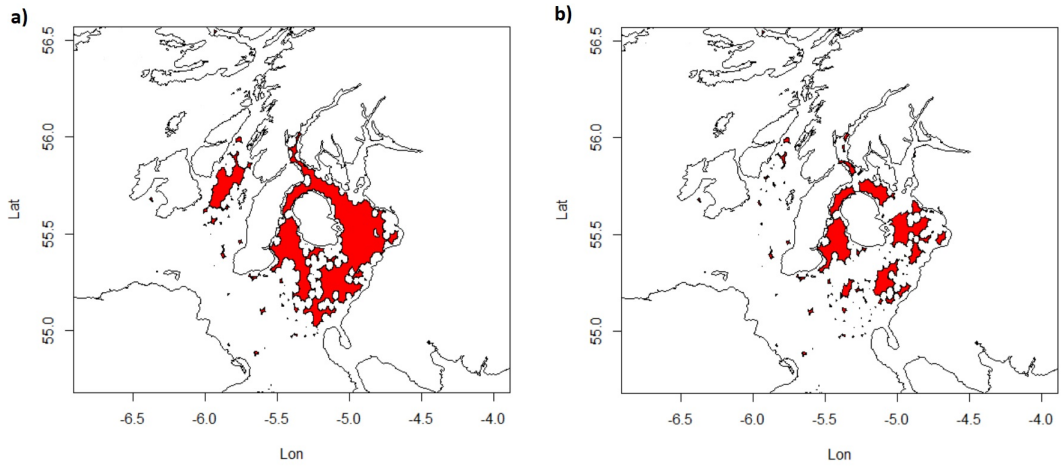

Figure 8.4: Plots a) and b) show high density sampling areas for 'alrs' and 'alrg' respectively. Points within these areas are predicted using interpolation. Points which fall outside of these areas are predicted using random forest modelling.

8.3.4 Random Forest Modelling

Random forest modelling is a machine-learning approach. Predictions are made by averaging the outputs of a large number of regression trees, each of which is built from a random subset of predictor variables (Breiman, 2001). Random forest models are extremely versatile and have a number of advantages over other statistical techniques. Firstly, random forest models do not require any prior assumptions about the distribution of variables. They can also handle complex, non-linear relationships between predictor and response variables. Finally, random forest models are insensitive to the inclusion of noisy or irrelevant features.

Random forest models were created using the ranger package in R (Wright and Ziegler, 2017). A suite of environmental variables were used to predict 'alrs' and 'alrg', as shown in Table 8.1. Predictor variables were selected based on their expected importance for explaining the distribution of seabed sediment. Predictor variables include depth, distance from the coast, slope, terrain ruggedness (rugosity), depth-averaged velocity and bed shear stress. Maps showing the spatial variance of each predictor variable are shown in Figure 8.5.

Predictor	Units	Reference
Depth	m	GEBCO and Seazone
Distance from Coast	km	Calculated using the Geosphere package in R
Slope	degrees	Calculated using the spatial analyst toolbox in ArcGIS
Rugosity	unitless	Calculated using the spatial analyst toolbox in ArcGIS
Mean and Maximum Velocity	ms^{-1}	Sabatino (2016)
Mean and Maximum Bed Stress	$N\ m^{-2}$	Sabatino (2016)

Table 8.1: Environmental predictors used in the random forest model.

Seabed depth is expected to influence sediment composition, with deeper areas generally composed of finer grained sediment. High resolution bathymetric data for the west coast of Scotland were obtained by combining data from the General Bathymetric Chart of the Oceans (GEBCO) (Fisher et al., 1982) with SeaZone bathymetric data (see Sabatino (2016) for more information).

The supply of sediment from river discharge and coastal erosion also influences the composition of seabed sediment. Distance from the coast is therefore included as a model predictor. Shape files of the UK coastline were downloaded from the Global Self-consistent, Hierarchical, High-resolution Geography (GSHHG) Database (Wessel and Smith, 1996). Distance of each data point from the coast was then calculated using the R package geosphere (Hijmans et al., 2012).

Seabed terrain can influence disturbance and sediment accumulation. Seabed terrain is commonly described by two factors: slope and rugosity. Slope and rugosity were calculated from the bathymetry data using the spatial analyst toolbox in ArcGIS 10.1. Slope describes the rate of change in elevation over distance and ranges from 0 to 90 degrees. Rugosity, on the other hand, gives an indication of the complexity of the sea-floor by combining information on slope variability and aspect into a single measure. This parameter is unitless and ranges from 0 (no terrain variation) to 1 (complete terrain variation). In general, flat ocean bottom with low terrain rugosity tends to correspond with soft seabed substrate. High terrain rugosity, on the other hand, indicates the potential presence of a rocky outcrop.

Finally, tidal and wave energy levels at the seabed strongly influence sediment composition. Waves and currents cause erosion and are also responsible for the transportation and deposition of sediments. High bed shear stress is generally associated with an increase in average grain size and a reduction in mud content (Ward et al., 2015; Heath et al.,

2016). Depth-averaged velocity and bed shear stress were extracted from a high resolution Finite Volume Community Ocean Model (FVCOM) of the CSA (Sabatino, 2016). This model has been tested extensively against a number of validation datasets. This includes a comparison of predicted velocities with observational data on tidal currents collected by the British Oceanographic Data Centre. Model predictions of velocity were found to show a good fit to observational data collected at 40 sites across the region (see Sabatino (2016) for more information). The hydrodynamic model was run for a two year period (2005-2006). Note that these years are thought to represent typical hydrodynamic conditions within the CSA. Depth-averaged velocity and bed shear stress were output at hourly intervals over this period. Seabed composition is likely to be influenced by year-round tidal and wave energy levels as well as by individual high-energy events. Mean and maximum values for velocity and bed shear stress were therefore calculated and included as model predictors.

8.3.5 Calculating the Percentage of Mud, Sand and Gravel

Predictions of 'alrs' and 'alrg' were made at equally spaced points across the study region using either interpolation or random forest modelling, as described above. At the end of the process the data were transformed back to mud, sand and gravel percentages using the following transformation equations:

$$Sand(\%) = \frac{e^{alrs}}{1 + e^{alrs} + e^{alrg}} \text{ x100} \tag{8.3}$$

$$Gravel(\%) = \frac{e^{alrg}}{1 + e^{alrs} + e^{alrg}} \text{ x100} \tag{8.4}$$

$$Mud(\%) = \frac{1}{1 + e^{alrs} + e^{alrg}} \text{ x100} \tag{8.5}$$

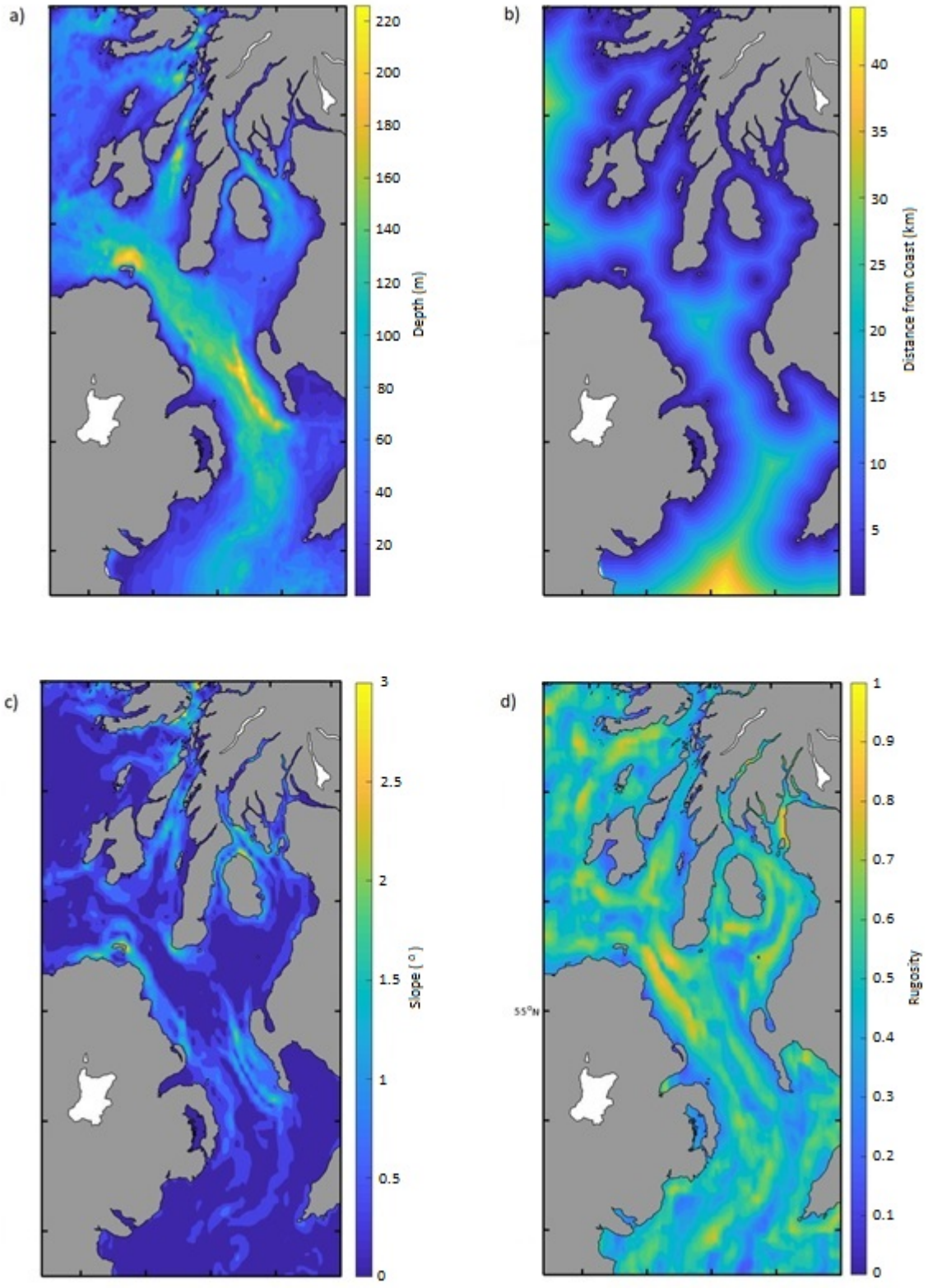
a)
220
200
180
160
140
120
100
80
60
40
20
Depth (m)
b)
40
35
30
25
20
15
10
5
Distance from Coast (km)
c)
3
2.5
2
1.5
1
0.5
0
Slope (°)
d)
55°N
1
0.9
0.8
0.7
0.6
0.5
0.4
0.3
0.2
0.1
0
Rugosity

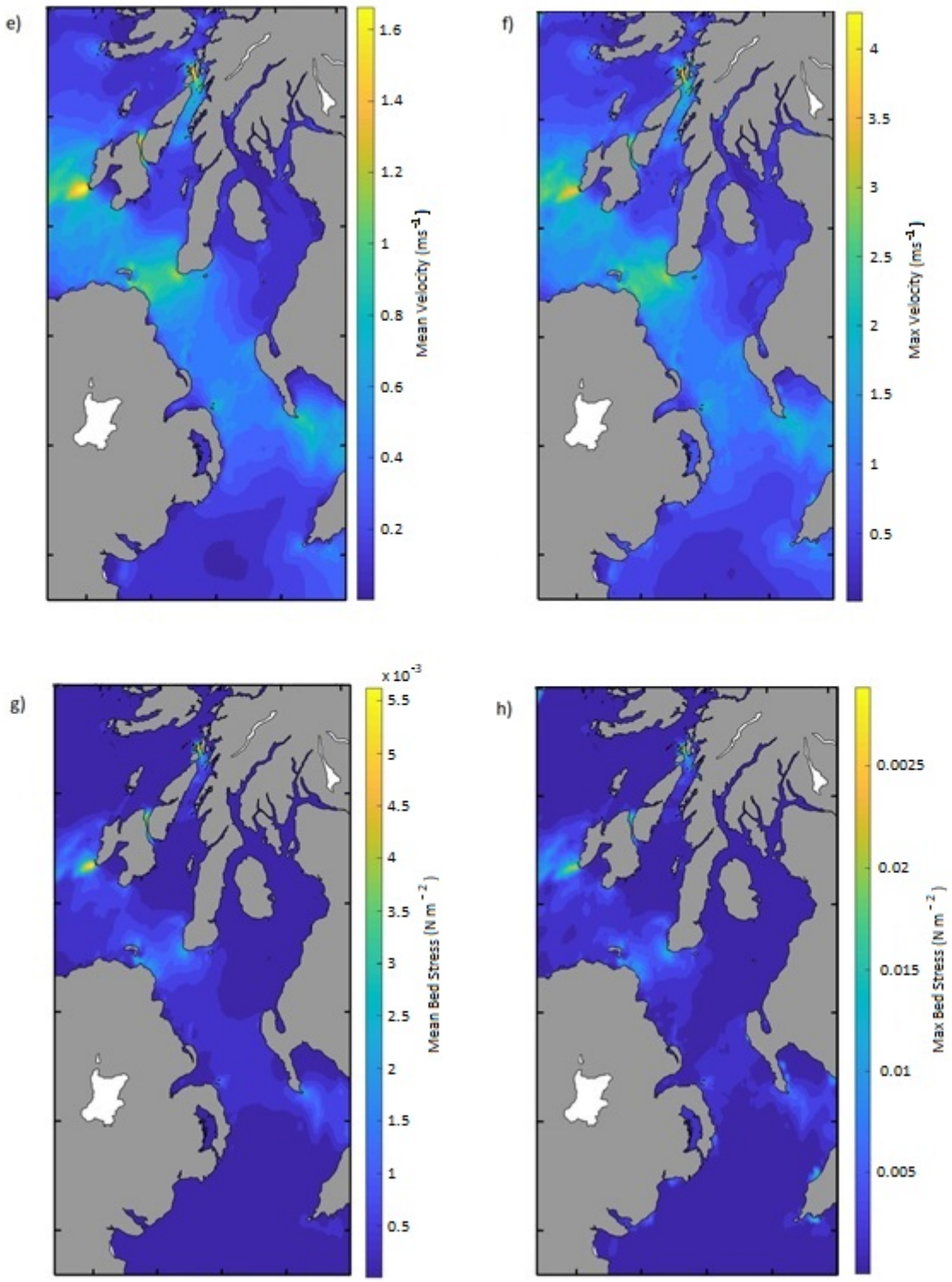

Figure 8.5: Plots showing the spatial variability of environmental variables used as predictors in the random forest model: a) Depth, b) Distance from Coast, c) Slope, d) Rugosity, e) Mean Velocity, f) Max Velocity g) Mean Bed Stress and h) Max Bed Stress.

8.3.6 Summary of Methods

In summary, seabed sediment composition across the west coast of Scotland was predicted according to the following steps

1. Sediment data were obtained from BGS and Marine Scotland and transformed onto an additive log ratio scale
2. Areas of high data density were identified using an alphahull
3. Values for 'alrs' and 'arlg' inside the alphahull were predicted using interpolation
4. Values for 'alrs' and 'alrg' outside the alphahull were predicted using a random forest model. The random forest model uses a number of environmental predictor variables including depth, distance from the coast, slope, rugosity, depth-averaged velocity and bed shear stress.
5. Predicted values of 'alrs' and 'alrg' were transformed back to mud, sand and gravel percentages

8.4 Seabed Sediment Composition

8.4.1 Model Results

Maps of predicted mud, sand and gravel percentages across the west coast of Scotland are shown in Figures 8.6 - 8.8. Muddy seabed sediment was found to dominate the outer regions of the CSA, with additional patches of mud in the Irish Sea and Sound of Jura. In contrast, sand was found to dominate coastal areas of the CSA, with high percentages of sand along the Ayrshire coast. Additional patches of sandy sediment were also predicted in the South Minch and the Irish Sea. The model predicted almost no gravel within the CSA. Hot spots of gravel, however, were predicted off the south west coast of the Mull of Kintyre and the west coast of Islay.

Figure 8.9 shows the relative importance of each of the eight predictor variables used in the random forest model in predicting 'alrs' and 'alrg'. Mean velocity was found to be the most important predictor for both 'alrs' and 'alrg'. On the other hand, seabed roughness (rugosity) and seabed slope were found to be the least important predictor for both 'alrs' and 'alrg'.

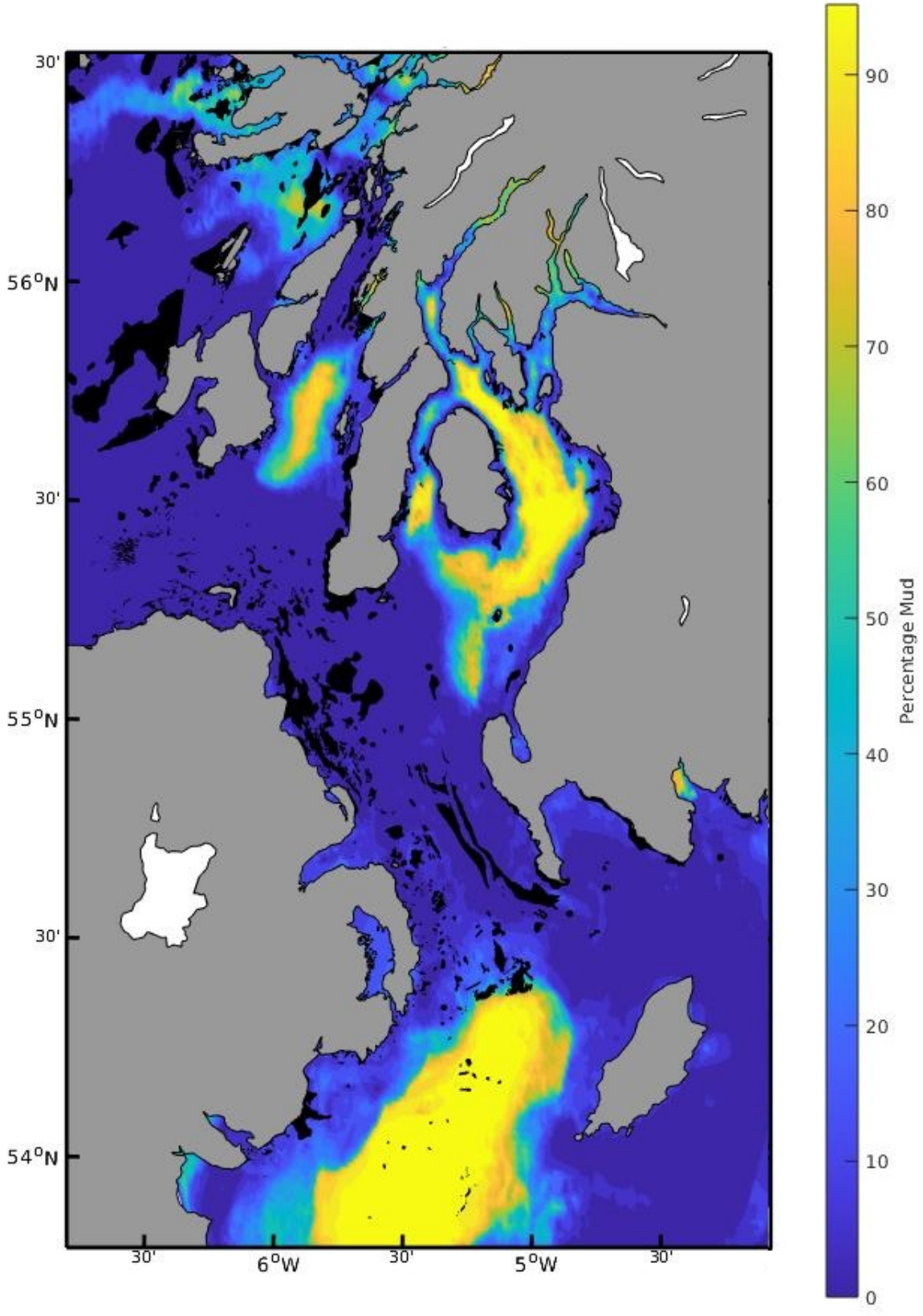

Figure 8.6: The percentage of mud in seabed sediment as predicted by the combined interpolation and random forest model. Black polygons show the distribution of rock at which no predictions about sediment composition were made.

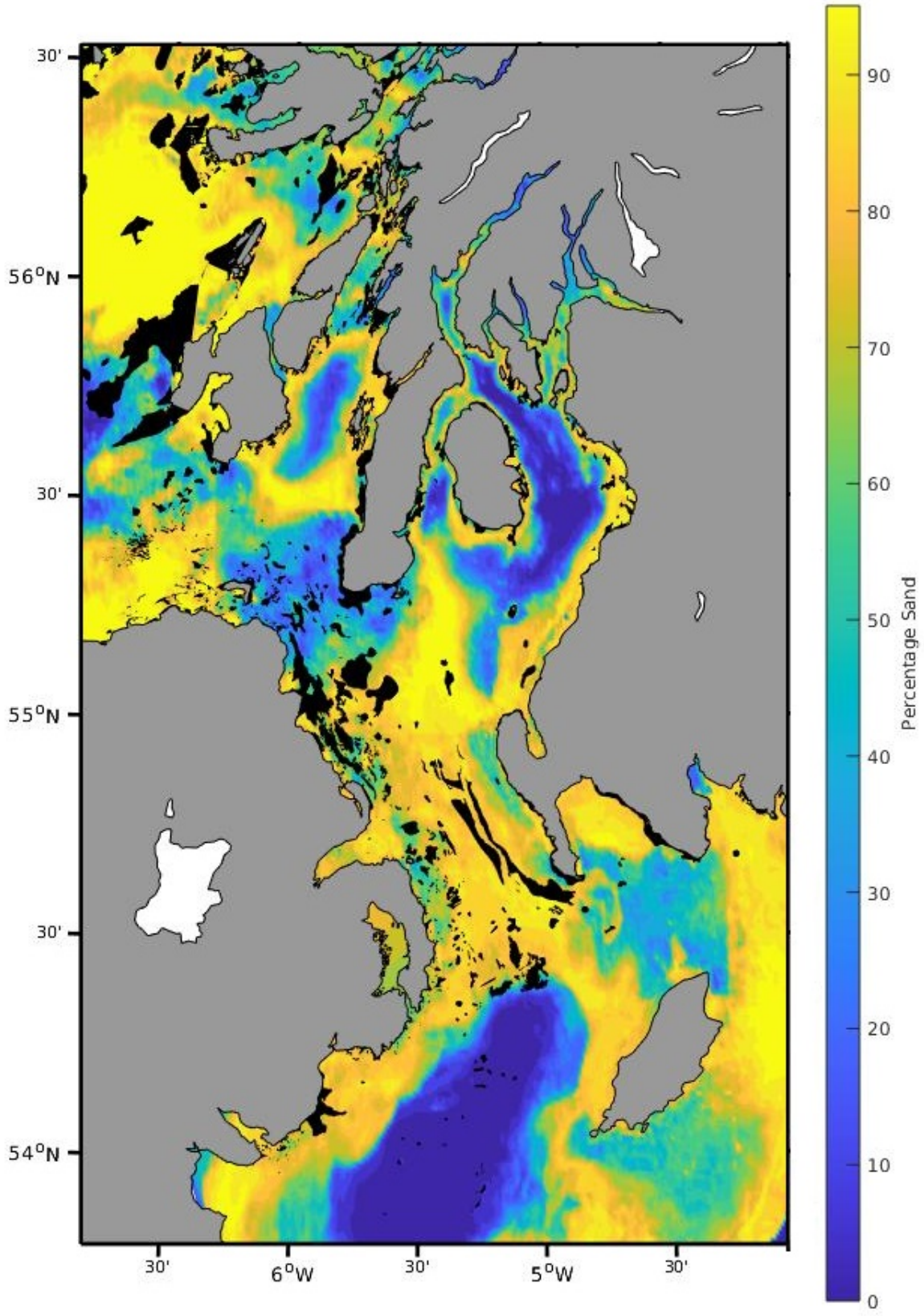

Figure 8.7: The percentage of sand in seabed sediment as predicted by the combined interpolation and random forest model. Black polygons show the distribution of rock at which no predictions about sediment composition were made.

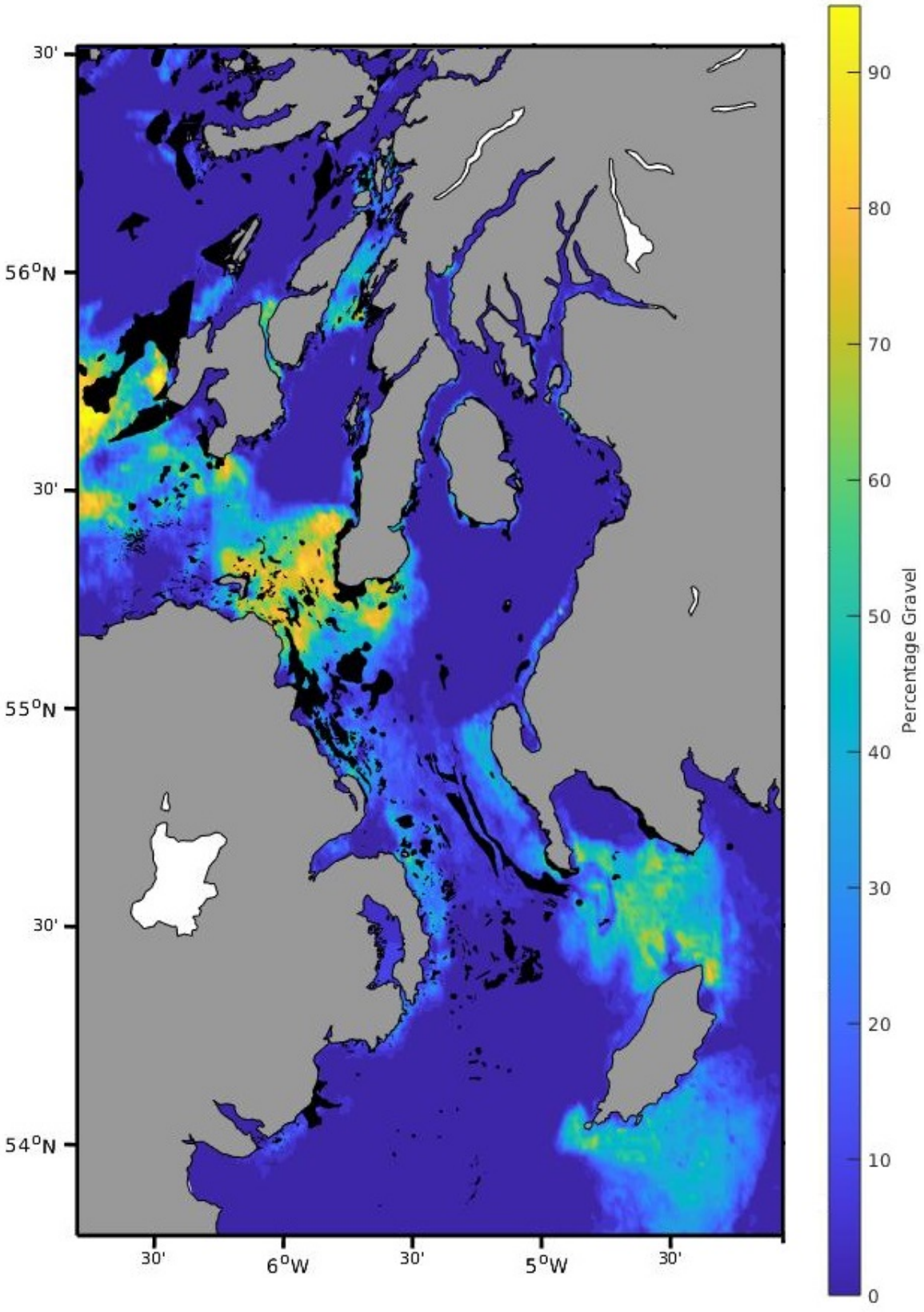

Figure 8.8: The percentage of gravel in seabed sediment as predicted by the combined interpolation and random forest model. Black polygons show the distribution of rock at which no predictions about sediment composition were made.

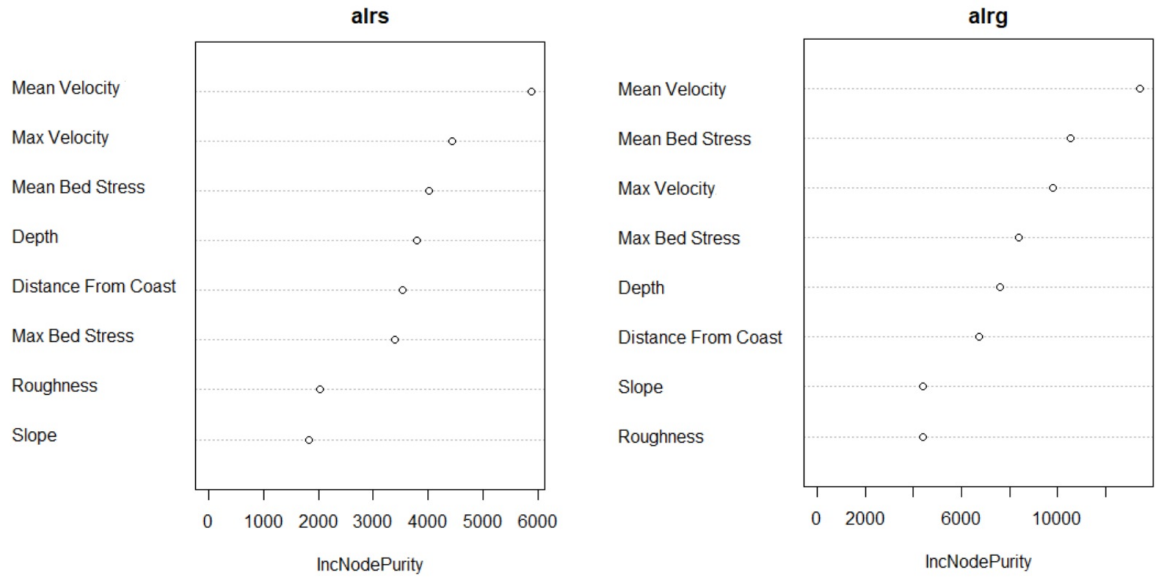

Figure 8.9: The importance of predictor variables used by the random forest algorithm. The x-axis indicates the average decrease in node sum of squares when variable is used.

8.4.2 Model Validation

Overall model performance was assessed using leave-one-out cross validation. This involves removing a single observation from the initial dataset. The remaining observations form the training set and are used for model development. A prediction is made at the location of the removed observation, and the squared error is calculated between the observed and predicted values. This process was repeated at 1000 randomly chosen locations. Leave-one-out cross validation provides a better measure of model performance in comparison to traditional cross validation methods since only one observation is excluded from model development each time.

Only BGS data were included in the validation process since the gravel component was removed from the Marine Scotland sediment data prior to analysis. Model predictions made at Marine Scotland sampling locations contain a gravel component and therefore cannot be compared to the original data. Consequently, the Marine Scotland dataset is used only for model development and not for validation purposes.

Leave-one-out cross validation yielded R^2 values of 0.76, 0.65 and 0.47 for mud, sand and gravel respectively. The model therefore captures the variation in mud and sand content relatively well. Predictions of gravel content, however, are considerably poorer.

8.5 Suitable *Nephrops* Habitat

In this section, predictions of seabed sediment composition (i.e. the percentages of mud, sand, and gravel) are used to identify patches of suitable *Nephrops* habitat. *Nephrops* require the presence of muddy seabed sediment suitable for the construction of burrows. Suitable *Nephrops* habitat was classified as sediment with a mud content $\geq 10\%$, as set out in Campbell et al. (2009). *Nephrops* cannot construct burrows on rocky outcrops or in areas where bedrock is covered by a thin layer of sediment. Areas of rock were therefore automatically classified as unsuitable sediment.

Areas identified as suitable *Nephrops* habitat are shown in Figure 8.10. The model predicts a large continuous patch of suitable sediment in the CSA, which surrounds the Isle of Arran and extends north into Loch Fyne and the Clyde Estuary. A number of other patches of suitable sediment were also identified including a large patch in the Irish Sea and several smaller patches in the Sound of Jura and the South Minch.

The model largely agrees with areas classified as suitable sediment by the original Marine Scotland map of suitable habitat (see Figure 8.1). The main differences lie in the inner regions of the CSA. This area is classified as suitable sediment by the model described above but not included in the original Marine Scotland map of suitable habitat. This region, however, is known to be frequented by small *Nephrops* fishing vessels. Hence, this area is highly likely to be suitable *Nephrops* habitat.

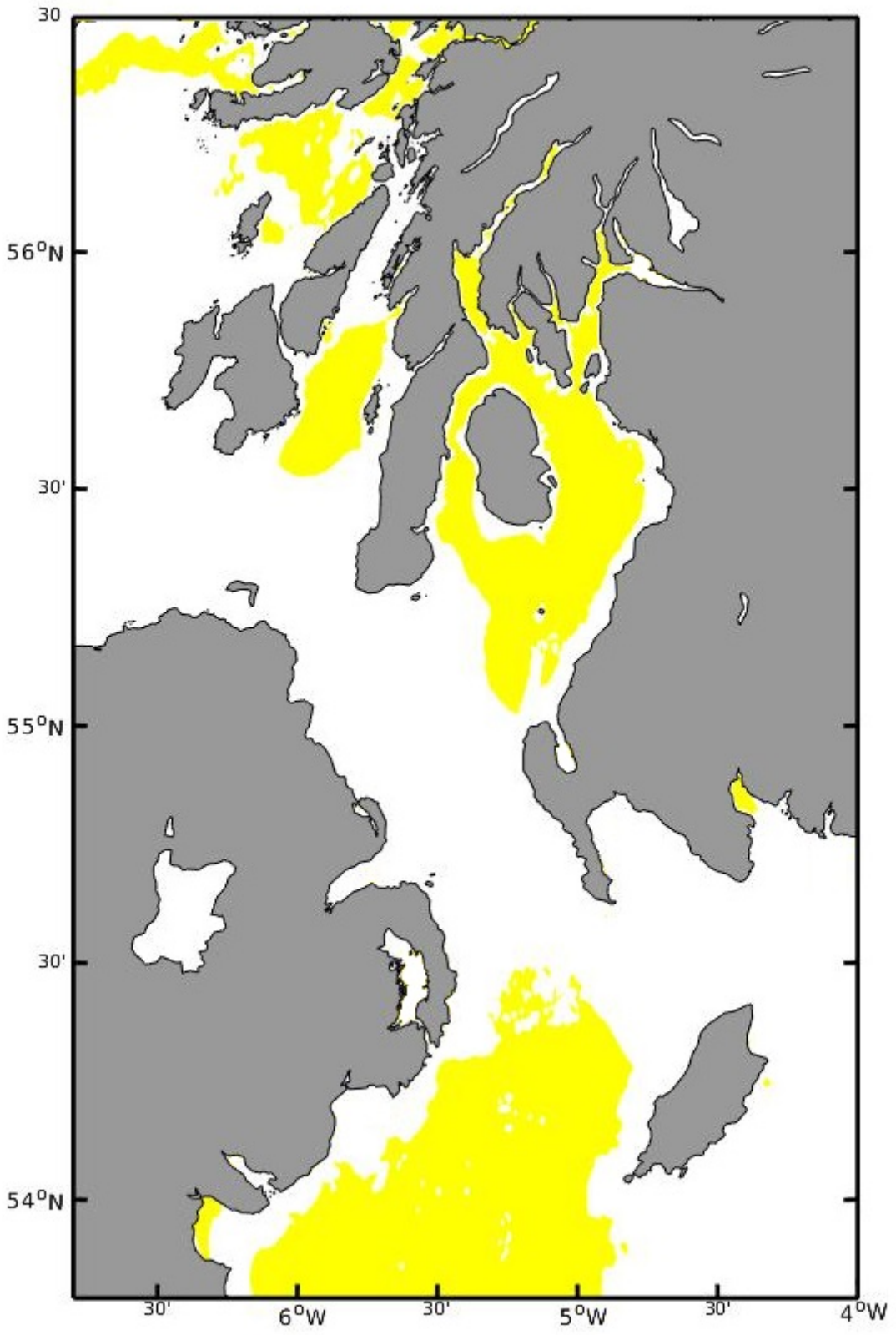

Figure 8.10: Areas of predicted suitable *Nephrops* habitat are shown in yellow.

8.6 Burrow Density

8.6.1 Introduction

Nephrops are not equally distributed across areas of suitable sediment. Southern regions of the CSA have been reported to contain a high density of small individuals whilst the northern sea-lochs and upper regions of the CSA are reported to contain a lower density of larger individuals (Bailey and Chapman, 1983). *Nephrops* are solitary animals, with each individual generally inhabiting a separate burrow complex. The density of burrow complexes on the seafloor therefore provides an estimate of the overall population density of *Nephrops*.

Seabed sediment composition is thought to play an important role in determining *Nephrops* burrow density. Afonso-Dias (1998) proposed a dome-shaped relationship between *Nephrops* burrow density and sediment grain size. Under this proposal, burrow density is thought to peak in medium-grained muddy sediment. In coarse, sandy sediments, the population density of *Nephrops* is expected to be relatively low. Coarse, sandy sediment is relatively unstable and so burrows made in this sediment are more likely to collapse. Population density is also thought to be low in exceptionally fine-grained muddy sediment. Fine-grained sediments allow individuals to build extensive burrow complexes. As a result, competition for space ultimately becomes a limiting factor on population density in these regions.

The burrow density of *Nephrops* across the west coast of Scotland is assessed annually by Marine Scotland using an underwater television (UWTV) survey method. During the UWTV survey, a sledge carrying a TV camera is towed along the seabed, as shown in Figure 8.11. The TV footage is watched by experienced burrow counters who record the number of *Nephrops* burrow complexes. In addition to a TV camera, the sledge also carries an odometer, which measures the distance covered, and a rangefinder, which measures the distance between the camera and the seabed, allowing the width of the field of view to be calculated. At designated survey stations, the sledge is towed for a period of 10 minutes, covering a distance of 140-200 m. The total number of burrow complexes at each survey station is recorded along with the area viewed (width of view multiplied by length of track). This information is combined to provide an estimate of population density.

In this section, I predict the burrow density of *Nephrops* across the west coast of Scotland using a generalised additive model (GAM). Furthermore, I also use the UWTV survey data to explore the relationship between seabed sediment composition and burrow den-

sity. Improving our understanding of the density of *Nephrops* across patches of suitable sediment is crucial for the effective management of this species.

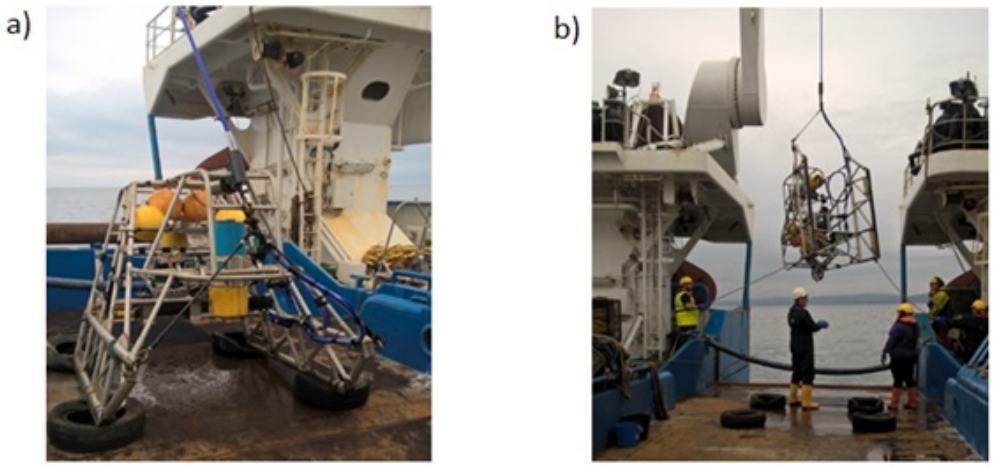

Figure 8.11: a) Photo of the underwater TV sledge b) Photo of the sledge being lowered into the sea during the 2016 UWTV *Nephrops* survey (Photos: H. Smith).

8.6.2 Methods

Raw *Nephrops* burrow density data for the west coast of Scotland were obtained from Marine Scotland for the period 2010 - 2017. The sampling locations of the burrow density data match with the Marine Scotland sediment sampling locations shown in Figure 8.2. Prior to analysis the raw burrow counts were multiplied by a correction factor, as described in ICES (2015). This accounts for factors such as edge effects and burrow misidentification.

A grid of equally spaced points was then created across the study region. Burrow density predictions were made at each point using a generalised additive model (GAM). Predictor variables used in the GAM include time (year survey was conducted) and seabed sediment composition (percentage of mud, sand and gravel). Note that samples of seabed sediment are obtained at each burrow density sampling location as part of the UWTV survey process. However, as discussed in Section 6.3.1, the gravel fraction is removed from these samples prior to analysis. Data on seabed sediment composition, obtained directly from the UWTV surveys, was therefore not used in the GAM. Instead the percentages of mud, sand and gravel were predicted at each burrow density sampling location using the sediment maps set out in Section 6.4. This allows the model results to be easily generalised across the whole region.

8.6.3 Results

The density of *Nephrops* burrows across the west coast of Scotland, as predicted by the model for the year 2017, is shown in Figure 8.12. The model predicts high burrow densities in the southern regions of the CSA and in the Sound of Jura. Low burrow densities are predicted in the northern regions of the CSA and in the South Minch. The model performed relatively well and was found to account for 51% of the variance in burrow density. Furthermore, the relationship between burrow density and seabed sediment composition (% mud) in the CSA was also examined (Figure 8.13).

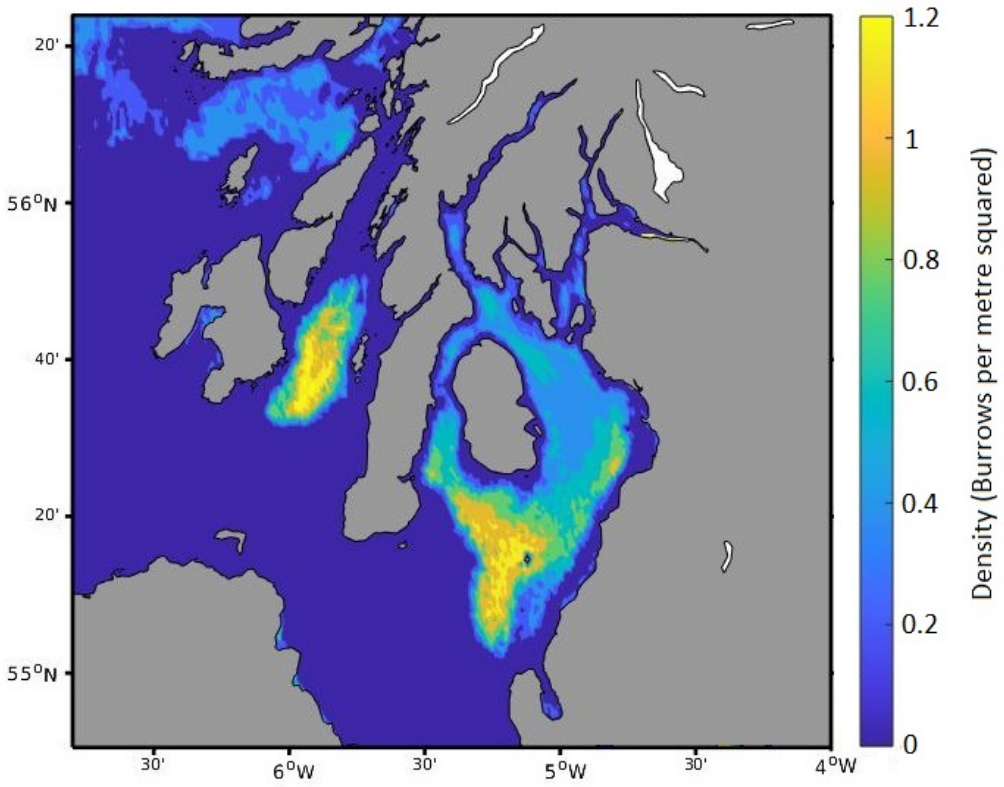

Figure 8.12: *Nephrops* burrow density across the West Coast of Scotland in 2017 as predicted by the generalised additive model.

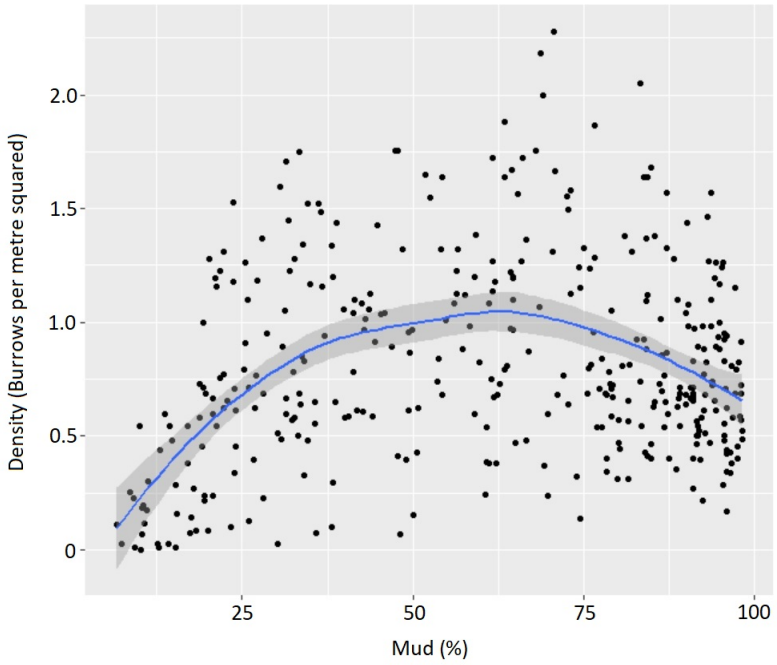

Figure 8.13: The relationship between *Nephrops* burrow density and percentage mud in the CSA. The blue line shows the line of best fit as determined by loess regression.

8.6.4 Discussion

In conclusion, the burrow density of *Nephrops* varies substantially across the CSA. Variation in burrow density can be partly attributed to seabed sediment composition, as shown in Figure 8.13. Burrow density and percentage mud were found to roughly follow the dome-shaped relationship initially proposed by Afonso-Dias (1998). However, large variations around this relationship were also observed. This variation occurs because *Nephrops* population density is not governed purely by sediment composition. The distribution of *Nephrops* also depends on factors such as the dispersal patterns of *Nephrops* larvae. Larval dispersal patterns of *Nephrops* in the CSA are explored in detail in the following chapter.

Chapter 9

Modelling the Dispersal of *Nephrops* Larvae

9.1 Introduction

Fully understanding the population dynamics of *Nephrops* in the CSA requires knowledge of the dispersal patterns of *Nephrops* larvae. Like many other marine organisms, *Nephrops* pass through a pelagic larval phase. The swimming speeds of pelagic *Nephrops* larvae are minimal in comparison to ocean current velocity, and so the dispersal patterns of *Nephrops* larvae are controlled primarily by local hydrodynamic flow-fields. Adult *Nephrops* live a sedentary life on the seabed, only leaving their burrow to undertake short foraging excursions (Bell et al., 2013). Consequently, the only opportunity for individuals to transfer between geographically distinct mud patches, or to re-locate within a large, continuous mud patch, occurs during the pelagic larval phase. Understanding the patterns of larval dispersal, and predicting the transfer of individuals between and within patches of suitable sediment, is important for forecasting population dynamics and can be used to inform fisheries management.

Hydrodynamic models are commonly used to predict the dispersal patterns of pelagic larvae. A small number of studies have been carried out to examine the dispersal of *Nephrops* larvae from populations located in the Irish Sea (O'Sullivan et al., 2015; Phelps et al., 2015) and off the coast of Portugal (Marta-Almeida et al., 2008). However, despite the commercial importance of *Nephrops* in the CSA, no studies have yet been undertaken to explore the dispersal patterns of *Nephrops* larvae within this region. This is likely due to the difficulties involved in creating a hydrodynamic model of this region. The CSA has an elaborate coastline, which features multiple islands, rivers and sea lochs, all of which increase the complexity of the hydrodynamic modelling process. Despite these

difficulties, a high resolution hydrodynamic model of the CSA was recently developed by Sabatino (2016). In this chapter, the dispersal patterns of *Nephrops* larvae are predicted by coupling this hydrodynamic model with a particle tracking model, which moves particles throughout the domain based on the hydrodynamic flow-fields.

Particles in the model are given behavioural characteristics which mimic those of *Nephrops* larvae. After hatching, *Nephrops* larvae ascend rapidly through the water column. They then pass through three distinct larval stages, the duration of which is highly dependent on water temperature (Powell and Erikkson, 2013). Larvae generally remain in surface waters throughout all three planktonic phases and are thought to undertake minimal diel vertical migration (Dickey-Collas et al., 2000). Towards the end of the third larval stage the larvae become negatively phototactic and descend to the seabed, where they then metamorphose into the adult form (Smith, 1987). Individuals which are dispersed to patches of muddy seabed sediment enter into existing burrow systems and assume a sedentary life on the seabed. Individuals dispersed to areas of unsuitable sediment, however, are unable to survive.

Key aspects of this *Nephrops* larval behaviour are incorporated into the particle tracking model via a biological sub-model. The biological sub-model is responsible for controlling the depth of model larvae in the water column. The biological sub-model is also responsible for estimating the duration of the pelagic larval phase; a factor which is known to significantly affect larval dispersal patterns (Simons et al., 2013). In order to improve predictions of larval duration, separate predictions are made for each individual in the model based on the temperatures it encounters along its drift trajectory. This makes it possible to gain an accurate picture of *Nephrops* larval dispersal patterns in the CSA.

In this chapter, the dispersal patterns of *Nephrops* larvae in the CSA are explored by focusing on four specific locations, thought to exemplify dispersal patterns across the whole region: one in Loch Fyne, one in the eastern region of the CSA, one in the southern region of the CSA and one in the Sound of Jura. Temporal and spatial changes in dispersal patterns are examined across these four key locations. The percentage of 'viable' larvae produced across the whole region is also examined. This will aid the management of *Nephrops* in the CSA by identifying key sites for protection and will also help inform the planning of Marine Protected Areas.

9.2 Methods

9.2.1 The Hydrodynamic Model

Water movement within the CSA was modelled using a Finite Volume Community Ocean Model (FVCOM), developed by Sabatino (2016). The model predicts water currents, temperature and salinity across the CSA using a system of differential equations (see Sabatino (2016) for more details). The model is forced by open tides and freshwater flow from eight major rivers, as well as by wind and heat exchange across the water surface. The model is run on an unstructured triangular grid composed of 30,644 nodes, 56,131 elements, and 11 terrain-following sigma layers. The computational grid extends from the Isle of Mull in the north to the central part of the Irish Sea in the south. The triangular grid elements vary in size, as shown in Figure 9.1. This allows areas with complex bathymetry to be modelled with increased accuracy and efficiency. The spatial resolution of the model ranges from 100 m in the northern sea lochs and the Clyde Estuary to approximately 7 km at the open boundaries. The hydrodynamic model has been tested extensively against a number of validation datasets. This includes a comparison of predicted velocities with observational data on tidal currents collected by the British Oceanographic Data Centre. Model predictions of velocity were found to show a good fit to observational data collected at 40 sites across the region (see Sabatino (2016) for more information).

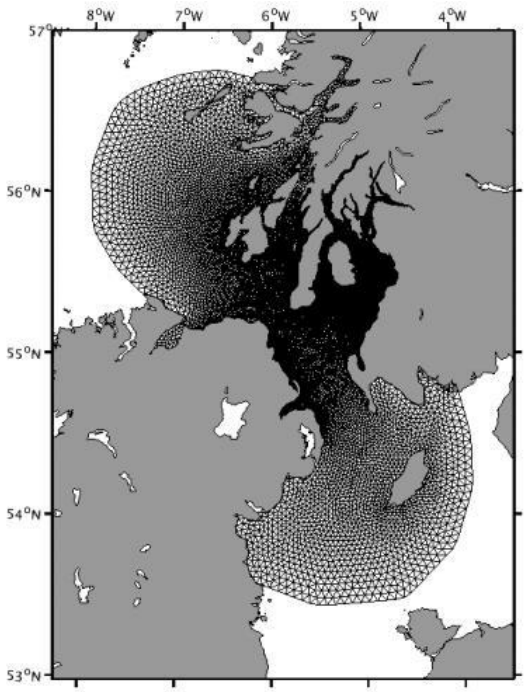

Figure 9.1: The computational grid used in the FVCOM (Sabatino, 2016).

The hydrodynamic model was run over two consecutive years: 2005 and 2006. These years are thought to represent typical hydrodynamic conditions within the CSA. The hydrodynamic model was used to predict hourly values of velocity across the region over this two-year period. This information is coupled with a particle tracking model which moves particles throughout the model domain based on the hydrodynamic flow-fields. Particles which are advected through the open boundaries, beyond the model domain, are removed from the system. The latitude, longitude, depth and temperature of each particle is recorded at hourly intervals and stored for further analysis.

9.2.2 Release Locations and Dates

140 release points were set up across patches of suitable *Nephrops* habitat in the CSA and Sound of Jura, as shown in Figure 9.2. Particles were not released from other patches of suitable sediment due to their close proximity to the boundary of the hydrodynamic model. Particles released from patches of suitable sediment in the South Minch and Irish Sea have a high probability of leaving the model domain. The resolution of the model is also dramatically reduced at the boundary making it difficult to reliably predict the movement of particles released from these patches.

Particles were released from each point on six chosen dates throughout May and June: 01/05, 11/05, 21/05, 01/06, 11/06 and 21/06. These release dates span the main *Nephrops* hatching season in the CSA, as shown in Figure 1.2. Particles were released in both 2005 and 2006, giving an overall total of 12 release dates.

In order to provide an overview of dispersal patterns across the whole region, 500 'larvae' were released from each release location on each chosen release date. Four locations, however, were selected for detailed analysis: one in the eastern region of the CSA (55.38^{o}N, -4.9^{o}W), one in the southern region of the CSA (55.12^{o}N, -5.22^{o}W), one in Loch Fyne in the upper regions of the CSA (55.75^{o}N, -5.16^{o}W) and one in the Sound of Jura (55.75^{o}N, -5.81^{o}W). The positions of these four sites are shown in Figure 9.2.

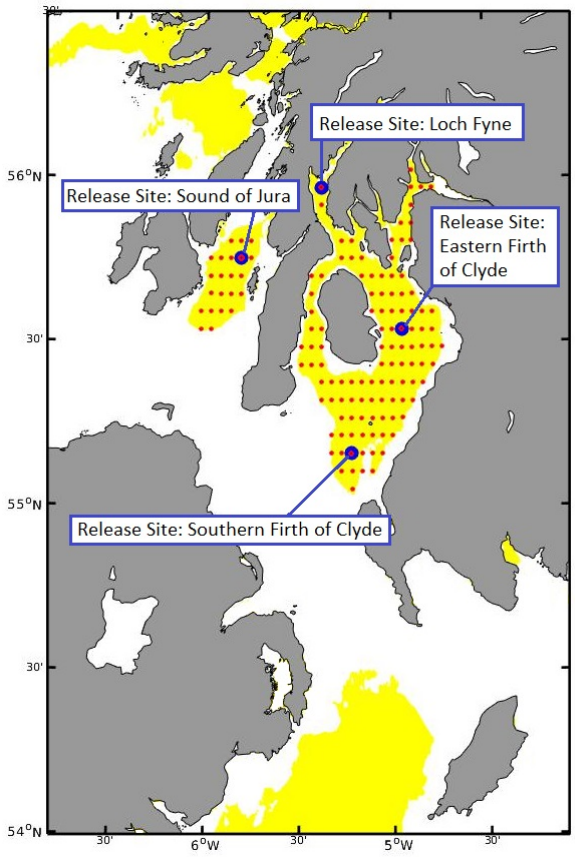

Figure 9.2: 500 'larvae' were released from all release locations (shown in red). Highlighted release locations show points which were selected for detailed analysis. Areas of suitable sediment, as predicted in Section 8.5, are shown in yellow.

9.2.3 The Biological Model

Modelled *Nephrops* larvae are held at a fixed depth of 20 m below the surface. This value is based on experimental studies by Smith (1987) conducted in the CSA, which showed the highest concentration of *Nephrops* larvae at this depth. In reality, however, *Nephrops* larvae do not remain at a single fixed depth. Instead larvae undertake diel vertical migration, ascending to the surface at nightfall and descending to deeper water at sunrise. Limited information is available on the timing and depth range of diel vertical migration in *Nephrops* larvae and so, for simplicity, diel vertical migration is excluded from the current study. Furthermore, in reality, *Nephrops* larvae are released from the seabed (from which they rise through the water column). *Nephrops* larvae also descend back to the seabed at the end of the third larval stage. However, for simplicity, these behaviours are not included within the model. Instead, larvae are held at a fixed depth of 20 m, or as close to this depth as possible, for the entire duration of the larval phase.

The duration of the larval phase is highly dependent on water temperature. The relationship between temperature and larval duration has been determined by experimental studies, involving the culture of *Nephrops* larvae within laboratory tanks (Dickey-Collas et al., 2000; Smith, 1987). These studies revealed that the duration, θ_i (days), of larval stage i (i = 1,2,3) can be approximated using the equation:

$$\theta_i = e^{(a_i - b_i T)} \tag{9.1}$$

where T represents seawater temperature (^{o}C), and a_i and b_i are coefficients which vary according to larval stage, as shown in Table 9.1.

Larval Stage (i)	a	b	
1	4.265	0.161	(Dickey-Collas et al., 2000)
2	4.646	0.175	(Dickey-Collas et al., 2000)
3	4.188	0.113	(Smith, 1987)

Table 9.1: Values of coefficients 'a' and 'b' for each larval stage. The parameter values of Dickey-Collas et al. (2000) were adopted for larval stages 1 and 2 and those of Smith (1987) were adopted for larval stage 3.

Equation (9.1) assumes that larvae remain at a constant temperature for the entire duration of each larval stage. However, in reality, seawater temperature varies both spatially and temporally. *Nephrops* larvae therefore encounter a wide range of temperatures as they are transported throughout the region. To account for this, Equation (9.1) is adapted following the method set out in Phelps et al. (2015) and Nicolle et al. (2013). This method calculates the larval duration of each individual separately based on the environmental conditions it encounters along its drift trajectory.

The seawater temperatures encountered by an individual larva depends on time (t) and on location (x), which is itself a function of time, i.e. x=x(t). This allows us to rewrite Equation (9.1) as a function of time (t):

$$\theta_i(t) = e^{(a_i - b_i T(t))} \tag{9.2}$$

Changes in the proportion of development, q, undergone by an individual can be approximated from the growth rate g (days^{-1}). Hence,

$$\frac{dq}{dt} = g(t) = \frac{1}{\theta_i(t)} = \frac{1}{e^{(a_i - b_i T(t))}} \tag{9.3}$$

At the beginning of each larval stage $t = t_0$, and $q(t_0) = 0$. As time progresses, the proportion of development (q) can be calculated using integration. The total duration of each larval stage can be found by determining the length of time taken for q to reach 1. Larval stage duration is therefore calculated by using a root finding function to solve for τ, in the equation:

$$0 = \int_{t_0}^{t_0+\tau} \frac{1}{e^{(a_i - b_i T(t))}} dt - 1 \tag{9.4}$$

The length of each of the three larval stages is calculated individually, and then summed to give an estimate of total larval duration. Metamorphosis is assumed to occur immediately after completion of the third larval stage. Settlement on the seabed is not directly included in the model. Instead, larvae are assumed to settle directly underneath the location at which they reach metamorphosis. Larvae are therefore considered to be 'viable' if they reach metamorphosis directly above an area of suitable *Nephrops* habitat.

9.3 Results

9.3.1 General Dispersal Patterns

In this section, the dispersal patterns of larvae from four chosen release sites (Eastern CSA (55.34^{o}N, -4.95^{o}W), Southern CSA (55.16^{o}N, -5.22^{o}W), Loch Fyne (55.97^{o}N, -5.38^{o}W) and the Sound of Jura (55.75^{o}N, -5.81^{o}W)) are examined across all 12 release dates. A specific focus is placed on the 'settling' location of larvae released from each site, defined as the location at which larvae reach the point of metamorphosis and 'settle' on the seabed. The 'settling' position must be located on suitable *Nephrops* habitat in order for the larvae to develop into adulthood. The 'settling' locations of larvae from each site are shown in Figures 9.3 - 9.6. Note that the colour scale of each figure differs in order to improve the readability of each individual plot.

Larval dispersal patterns were found to differ both spatially and temporally. Larval dispersal patterns changed significantly within a single year, but only showed minor variations across the two years tested. A large proportion of larvae released from the eastern region of the CSA were found to settle on patches of unsuitable sediment along the coast of Ayrshire (see Figure 9.3). A small proportion of larvae released from this site, however, manage to settle successfully on areas of suitable sediment throughout the CSA. On some release dates (e.g. 21st May) this release site was found to supply larvae across the entire CSA mud patch.

Larvae released from the southern region of the CSA are generally swept out of the region, as shown in Figure 9.4. Some of these larvae are swept northwards, with a small proportion managing to settle successfully on the Sound of Jura mud patch. The majority of larvae swept northwards, however, are swept north-west around the western coast of Islay, and hence do not settle on suitable sediment. A small proportion of larvae released from the southern region of the CSA are swept southwards, with some individuals managing to settle successfully on the large mud patch located in the Irish Sea.

Larvae released from Loch Fyne tend to remain within Loch Fyne, as shown in Figure 9.5. On some release dates (e.g. 1st May - 1st June 2005) all larvae released from this location settled within Loch Fyne. This area is therefore considered to be highly retentive. However, on some occasions, larvae manage to leak out of the Loch (e.g. June 11th and June 21st 2005). These larvae generally settle on suitable sediment in the western regions of the CSA.

Finally, larvae released from the Sound of Jura, generally move around the island of Islay before being swept northwards, as shown in Figure 9.6. On some occasions (e.g. May 1st and June 21st 2005) the region manages to successfully retain some larvae, which go on to settle within the Sound of Jura mud patch. However, the majority of larvae released from this location do not settle on patches of suitable sediment.

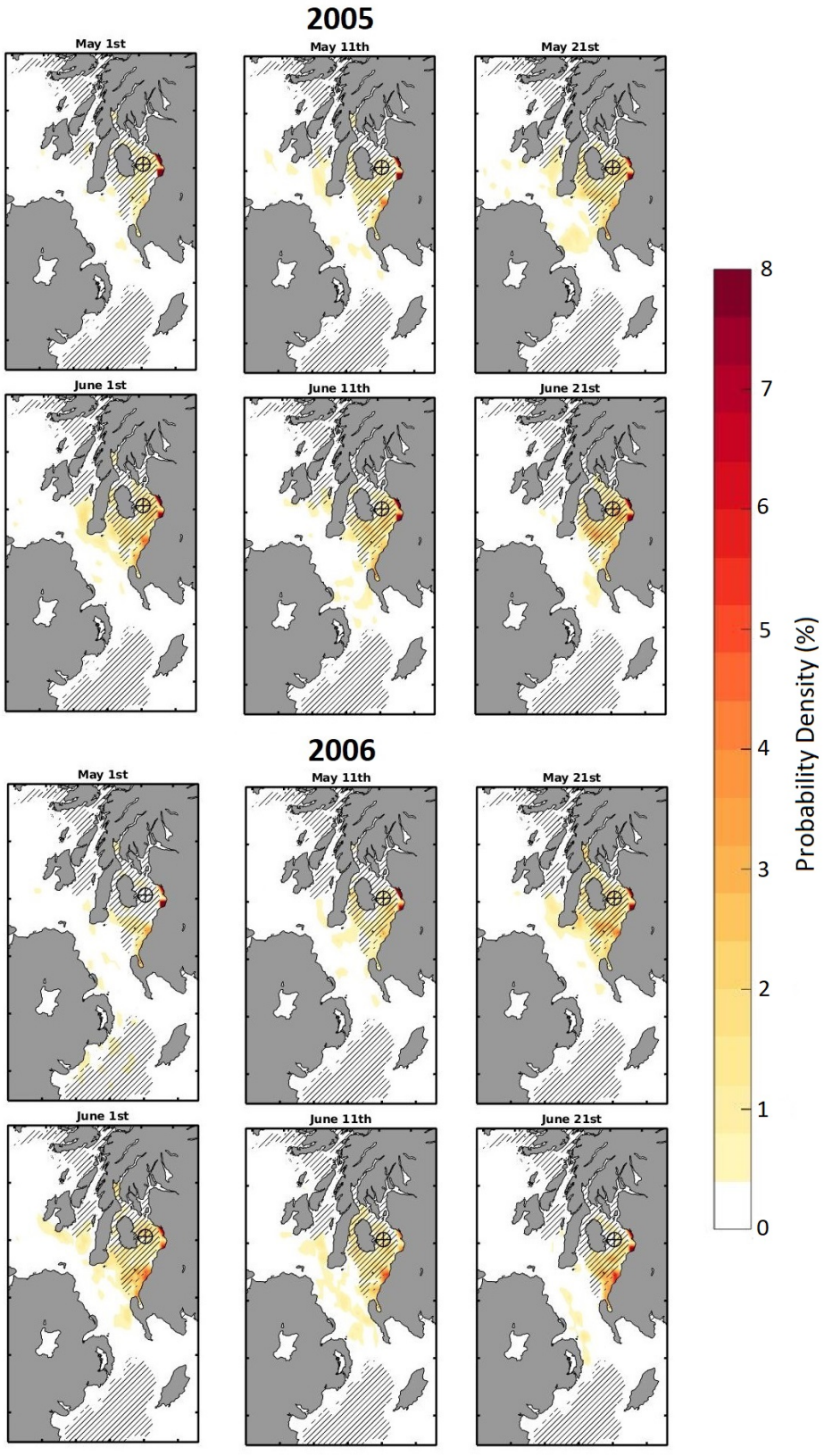

Figure 9.3: Probability density (%) of the final settling position of larvae released from the eastern region of the CSA on each release date. Hatched areas show patches of suitable sediment. The release point (55.34^{o}N, -4.95^{o}W) is represented by the black circle.

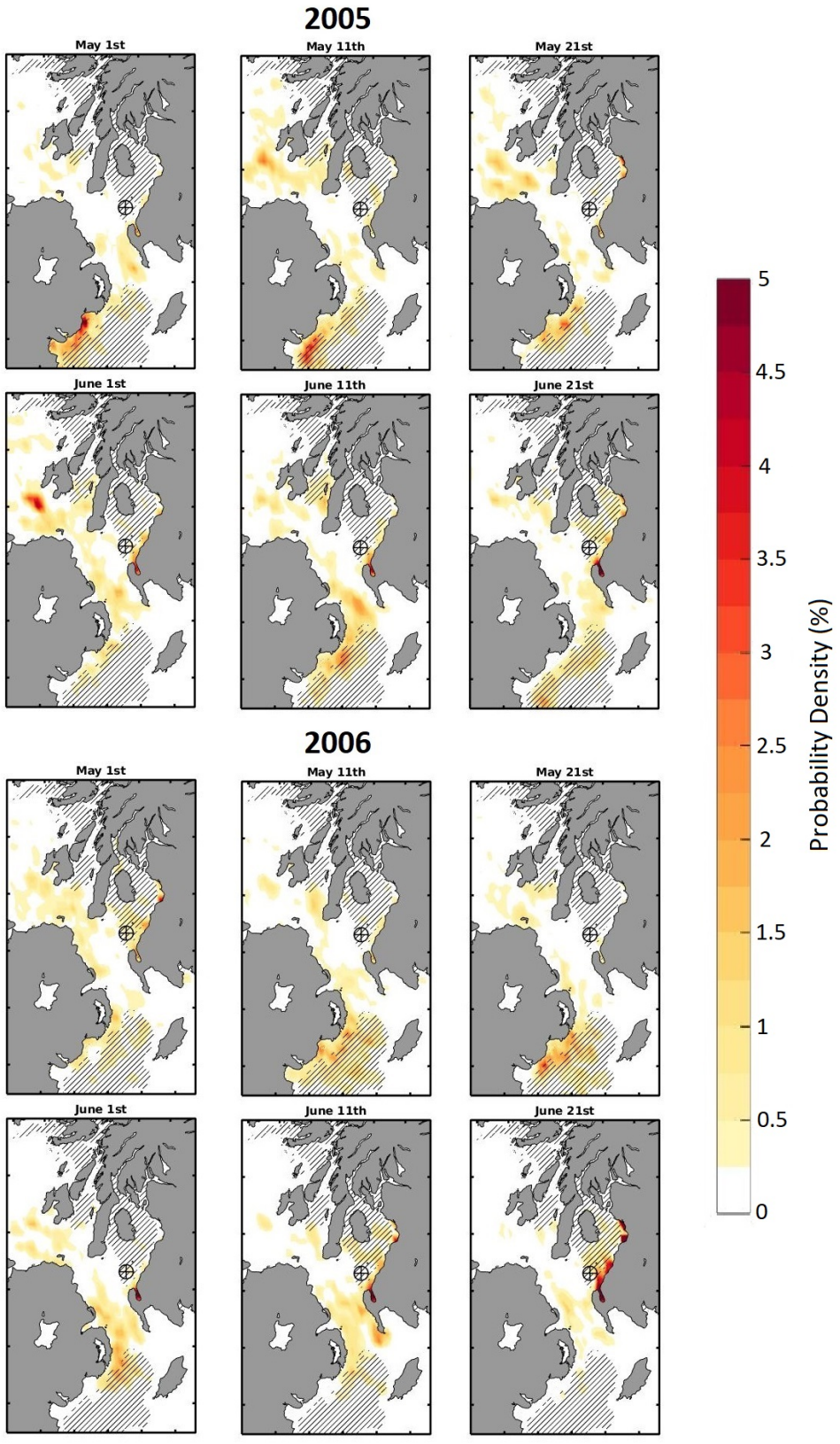

Figure 9.4: Probability density (%) of the final settling position of larvae released from the southern region of the CSA on each release date. Hatched areas show patches of suitable *Nephrops* habitat. The release point (55.16^{o}N, -5.22^{o}W) is represented by the black circle.

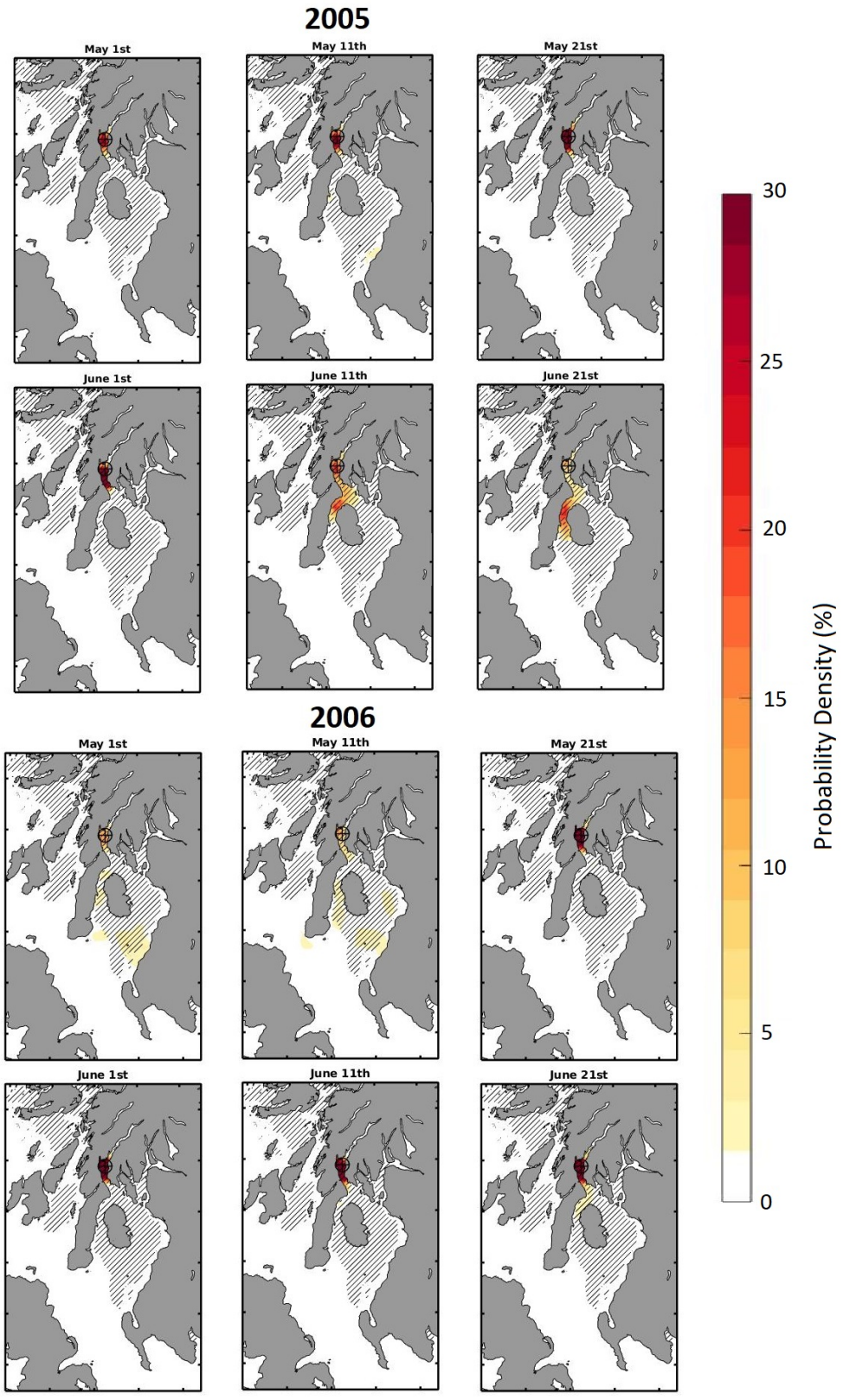

Figure 9.5: Probability density (%) of the final settling position of larvae released from the upper regions of the CSA (Loch Fyne) on each release date. Hatched areas show patches of suitable sediment. The release point (55.97^{o}N, -5.38^{o}W) is represented by the black circle.

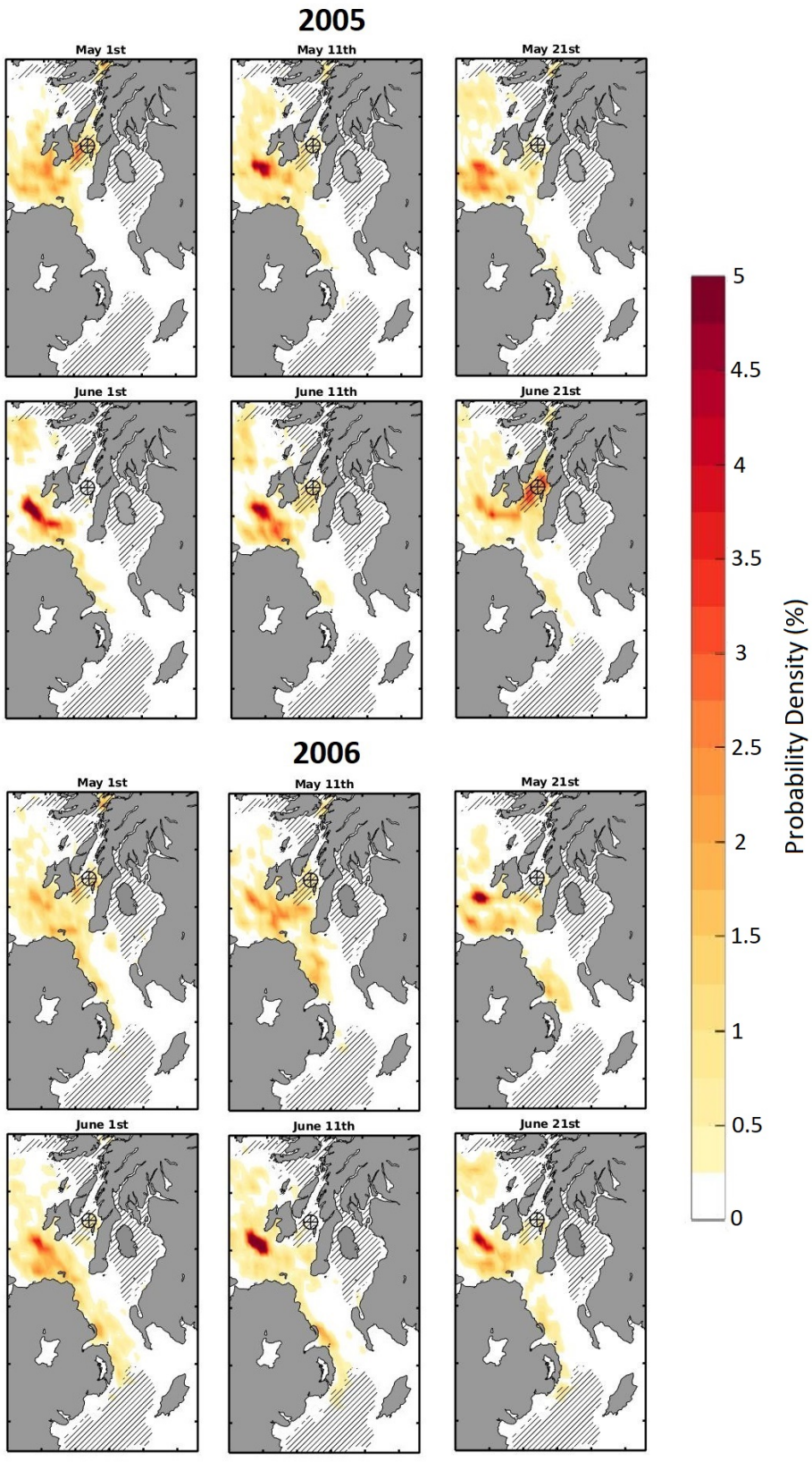

Figure 9.6: Probability density of the final settling position of larvae released from the Sound of Jura on each release date. Hatched areas show patches of suitable sediment. The release point (55.75^{o}N, -5.81^{o}W) is represented by the black circle.

9.3.2 Mean Distance Travelled

The distance between release location and the location at which larvae reach the point of metamorphosis differs across the region as shown in Figure 9.7. The mean distance (km) between release location and the location at which larvae reach the point of metamorphosis is calculated for all 12 release dates combined. The mean distance is calculated at all 140 release sites first and then interpolated across the whole region. Crucially, however, no distinction is made between larvae which settle on suitable sediment and those which do not. Instead, the mean distance is calculated across all larvae in the model regardless of larval viability.

This provides an overview of the level of retentiveness of each region. The upper regions of the Firth of Clyde were consistently found to be the most retentive. Larvae released from Loch Fyne and the Clyde Estuary reach the point of metamorphosis around 30 km or less from their initial release site. The southern tip of the Firth of Clyde mud patch was found to be the least retentive. Larvae released from this area were transported distances greater than 80 km prior to reaching the point of metamorphosis.

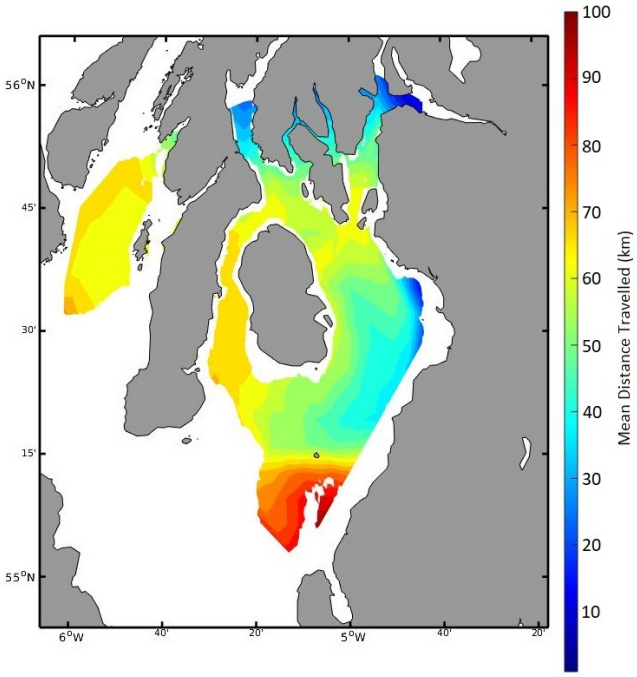

Figure 9.7: Mean distance (km) between release location and the location at which larvae reach the point of metamorphosis for all release dates combined. Note that mean distance is calculated at all release sites first and then interpolated across the whole area. White areas depict unsuitable sediment.

9.3.3 'Viable' Larvae

Larvae which reach the point of metamorphosis over an area of suitable *Nephrops* habitat are classified as 'viable'. In this section, the percentage of 'viable' larvae (i.e. the percentage of total larvae which settle on suitable substrate) is calculated for each release location and date. The results are then combined across both years, by taking the mean value of corresponding release dates. Finally, the results are interpolated to estimate the percentage of 'viable' larvae produced throughout the whole region, as shown in Figure 9.8.

Loch Fyne was found to consistently produce the highest percentage of viable larvae, whilst the Sound of Jura mud patch was found to consistently produce the lowest percentage of viable larvae. The percentage of viable larvae produced across the whole region, increased as the hatching season progressed.

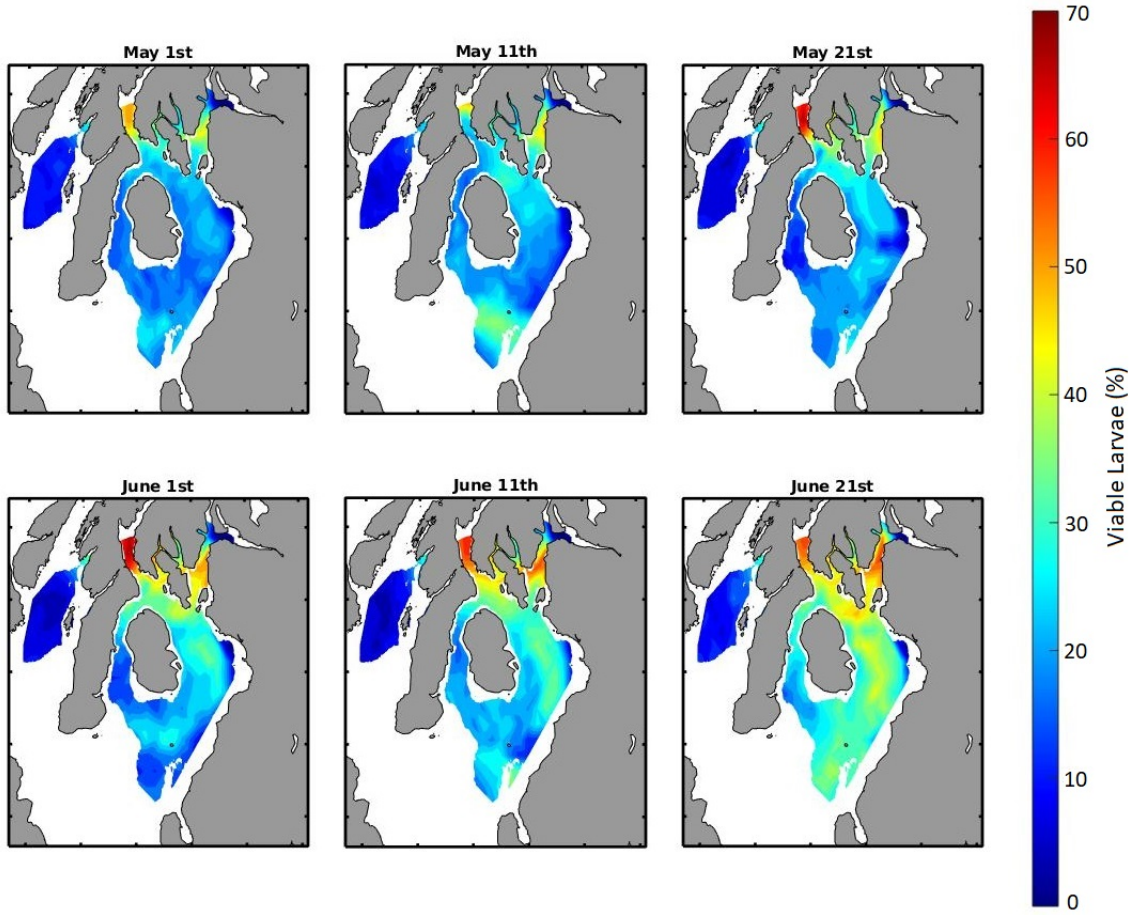

Figure 9.8: The percentage of viable larvae produced from each release location for 2005 and 2006 combined. Note that percentage of viable larvae is calculated at all release sites first and then interpolated across the whole area. White areas depict unsuitable sediment.

9.4 Discussion

In this chapter, the dispersal patterns of *Nephrops* larvae were predicted throughout the CSA using a coupled hydrodynamic and particle tracking model. The results of this study show that the dispersal patterns of *Nephrops* larvae depend on both release location and release date. The upper regions of the CSA, in particular Loch Fyne and the Clyde Estuary, were found to produce a high percentage of viable larvae (see Figure 9.8). However, these areas were also shown to be highly retentive (see Figure 9.7), which therefore indicates a high level of self-recruitment. Larvae released from the lower regions of the CSA and the Sound of Jura were dispersed over a much larger area, with large proportions of larvae settling on unsuitable sediment.

This study has identified connections between different mud patches across the region, including the movement of larvae from the lower regions of the CSA to the Sound of Jura. Larvae released from the lower region of the CSA were also capable of transferring to the Western Irish Sea mud patch. There is evidence to suggest that some of the larvae released in the Western Irish Sea may enter the CSA (Hill et al., 1996). A hydrodynamic modelling study of *Nephrops* larvae released from the Irish Sea estimated that around 5% of larvae released form the Western Irish Sea mud patch are transferred to the CSA (O'Sullivan et al., 2015).

Furthermore, the results show a clear increase in the percentage of 'viable' larvae produced throughout the CSA as the hatching season progresses. This may be caused by an increase in seawater temperature, which reduces the duration of the larval stage. As a result, larvae have less time to be swept out of the CSA, and away from the large patch of suitable sediment located in this region. In general, decreasing larval stage duration has been shown to increase the probability of survival and settlement upon suitable substrate (Cowen and Sponaugle, 2009). Understanding the impact of increasing temperatures, and hence decreasing larval duration, on the dispersal patterns of *Nephrops* larvae in the CSA is particularly important in the face of climate change, with global seawater temperature predicted to rise over the coming years.

This study provides a good first insight into larval dispersal patterns in the CSA. However, a number of biological simplifications were made in the model regarding *Nephrops* larval behaviour. Firstly, larvae were held at a fixed depth of 20 m for the entire duration of the larval phase. In reality *Nephrops* larvae undertake diel vertical migration (DVM) (Hillis, 1974). Diel vertical migration causes larvae to move in to and out of fast moving surface waters, and may therefore have a significant effect on dispersal patterns. The

inclusion of DVM has been shown to have a significant effect on dispersal patterns in particle tracking simulations across a wide range of areas and species (Robins et al., 2013; North et al., 2008; der Molen et al., 2007; Fox et al., 2006). In particular, Phelps et al. (2015), showed that the dispersal of *Nephrops* larvae in the Irish Sea differed under three different potential DVM behavioural scenarios. However, information on the timing and depth range of DVM in *Nephrops* larvae is currently limited. Therefore, it was chosen not to include DVM in the current model, but it is considered to be an important aspect for inclusion in future studies of *Nephrops* larval dispersal in the CSA.

Finally, the density of adult *Nephrops* differs dramatically throughout the CSA, as discussed in Section 8.6. Differences in population density, combined with density-dependent growth rates of *Nephrops*, result in variable larval production rates across the region. The densely populated lower regions of the CSA consist mainly of small individuals, which produce a relatively small number of eggs (Smith, 1987). The sparsely populated upper regions of the CSA, on the other hand, consist mainly of larger individuals, which produce a much greater number of eggs. In the model, an equal number of larvae were released across the whole region. However, release numbers which reflect population density, growth rates, and larval production rates are required to provide a deeper understanding of the effects of larval dispersal patterns on population dynamics. Population density is also likely to have a density-dependent effect on the survival rates of *Nephrops* post settlement.

In conclusion, although some simplifications have been made, this study provides a good first insight into the dispersal patterns of *Nephrops* larvae in the CSA. Despite the abundance of commercially important *Nephrops* fisheries based in the CSA, the dispersal of *Nephrops* larvae from this region has not previously been studied. Understanding larval dispersal patterns is essential for the prediction of future population trends. This model can be used to help inform fisheries management and ensure the sustainable exploitation of this commercially important species. Furthermore, understanding the dispersal patterns of *Nephrops* larvae within the CSA will help identify key sites for management and could also help inform the planning of Marine Protected Areas.

Chapter 10

Conclusions and Future Work

This thesis has furthered our understanding of *Nephrops-Hematodinium* population dynamics in the CSA. This has primarily been achieved through the development of a new mathematical model which simulates the coupled population dynamics of *Nephrops* and *Hematodinium*. Prior to this thesis, only limited modelling work had been undertaken in this area, with no published models of *Nephrops-Hematodinium* population dynamics currently available. This thesis therefore contains the first full-scale population model of this commercially important host-parasite relationship.

The *Nephrops-Hematodinium* population model developed in this thesis contains a number of novel components including a new 'dynamic energy budget' based approach for modelling *Nephrops* growth. The DEB *Nephrops* growth model includes distinct moult events which are crucial for accurately modelling *Hematodinium* transmission since the life-cycle of *Hematodinium* is closely synchronised with the moult cycle of *Nephrops*. Furthermore, the inclusion of distinct moult events also provides a more realistic method for modelling *Nephrops* growth in comparison to commonly used approaches such as the Von Bertalanffy growth curve. The DEB *Nephrops* growth model is embedded within an Escalator-Box-Car type representation which simulates the development of annual cohorts of individuals by combining information on mortality, reproduction and harvesting by fisheries. *Hematodinium* transmission is simulated within the model by allowing a proportion of each cohort to become infected at a moult event. The number of newly infected individuals is dependent upon the density of parasitic spores in the environment. Within the model, parasitic spores are released from infected individuals at a moult event, with the probability of sporulation dependent on the concentration of the parasite in the haemolypmh.

Following its development, the *Nephrops-Hematodinium* population model was used for two key purposes. Firstly, the model was used to further our understanding of *Nephrops-*

Hematodinium population dynamics. Comparing output from the model to observational data from the CSA led to a number of key insights and challenged previously held assumptions about *Nephrops-Hematodinium* population dynamics. For example, it was previously assumed that the parasite followed a single-year infection pathway with infection, sub-patency, patency and sporulation all occurring within a single year. However, the *Nephrops-Hematodinium* population model has shown that this assumption is unsustainable. The *Nephrops-Hematodinium* population model set out in this thesis has therefore led to a paradigm-shift in our understanding of the parasite life-cycle. The results reported in this thesis have shown that the life-cycle of *Hematodinium* can take up to 2 years or more, depending on the moulting rate of the host – which in turn depends on the size of the host at the point of infection.

Furthermore, the *Nephrops-Hematodinium* population model has also provided further insight into the impact of fishing gear size selectivity on the estimated level of *Hematodinium* prevalence in the population. The *Nephrops-Hematodinium* population model was used to compare estimates of *Hematodinium* prevalence obtained from the catch using trawl nets with different mesh sizes and the true level of *Hematodinium* prevalence in the *Nephrops* population as a whole. The prevalence of PCR detectable infection in the catch was found to be 57% following the sustained use of trawl nets with a mesh size of 70 mm. This was found to be marginally higher than the true level of *Hematodinium* prevalence in the population (55%). Estimates of *Hematodinium* prevalence obtained via PCR following the sustained use of trawl nets with a mesh size of 70 mm are therefore considered to be a relatively good measure of the level of *Hematodinium* prevalence in the *Nephrops* population as a whole. Increasing the mesh size of trawl nets, however, reduces the prevalence of infection in the catch. This is because smaller individuals are more susceptible to *Hematodinium* infection. Increasing the mesh size of trawl nets therefore leads to a significant difference between the level of detectable infection in the catch and the true level of *Hematodinium* infection in the population. Furthermore, estimates of *Hematodinium* prevalence obtained using other less sensitive diagnostic tests (eg the pleopod method and body colour method) were shown to significantly underestimate the true level of *Hematodinium* in the population.

The *Nephrops-Hematodinium* population model was also used to assess the impact of altering current fishing management practices on the population dynamics of *Nephrops* and *Hematodinium* in the CSA. This included an investigation into changing fishing intensity, preventing the discard of visibly-infected individuals and altering the size distribution of discarded individuals. The results of this work show that preventing the discard of visibly-infected individuals could lead to a small reduction in *Hematodinium* prevalence

combined with a slight increase in the yield of marketable *Nephrops* obtained by fishermen. It is therefore recommended that this small operational change is implemented in the CSA *Nephrops* fishery. Increasing fishing intensity and reducing the size distribution of discards were found to lead to a decrease in *Hematodinium* prevalence. These strategies, however, were also found to cause a reduction in the yield of *Nephrops* obtained by fishermen and are therefore not considered to be effective methods of controlling *Hematodinium* in the CSA.

The *Nephrops-Hematodinium* population model developed in this thesis is strictly non-spatial. However, a number of important factors are known to vary substantially across the CSA. This includes *Nephrops* growth rates, fishing intensity and *Hematodinium* prevalence. Fully understanding *Nephrops-Hematodinium* dynamics in the CSA therefore requires the development of a spatial population model, capable of accounting for these geographic variations. The final section of this thesis contains a number of supporting investigations which examine the spatial distribution and connectivity of *Nephrops* in the CSA. This lays the groundwork for the development of a spatial *Nephrops-Hematodinium* population model as well as improving our current understanding of the spatial distribution of *Nephrops* in the CSA.

Supporting investigations in this thesis include the development of a new method for predicting suitable *Nephrops* habitat across the west coast of Scotland, using a combined interpolation and random forest modelling approach. This new method was used to create an updated high-resolution map of suitable habitat across the CSA. This thesis also investigated differences in *Nephrops* burrow density across patches of suitable sediment in the CSA. This revealed areas of high burrow density in the southern regions of the Firth of Clyde. Furthermore, this thesis explored larval-transport connectivity between patches of suitable sediment using particle tracking methodology, driven by output from a high resolution hydrodynamic model of the CSA. The results of this study show a high rate of larval retention from patches in the northern regions of the Firth of Clyde. Patches of suitable sediment in the southern regions of the Firth of Clyde, on the other hand, were found to export a greater proportion of larvae, with some larvae from this region settling on suitable sediment in the Sound of Jura.

It is recommended that future work on *Nephrops-Hematodinium* population dynamics in the CSA focuses on the development of a spatial population model of *Nephrops* and *Hematodinium*. This can be achieved by implementing the *Nephrops-Hematodinium* population model set out in the first section of this thesis simultaneously in a number of spatially discrete patches. The size and shape of these discrete patches can be determined from

the burrow density patterns set out in the second section of this thesis. These discrete patches would be interconnected by the movement of *Nephrops* larvae and *Hematodinium* spores from one area to another. The probability of larval transport from one area to another can be identified from the particle tracking simulations set out in this thesis. A similar study could be carried out to identify the dispersal patterns of *Hematodinium* spores in the CSA. The number of larvae released from each area would be dependent on the density and size of *Nephrops* in each specified area. Likewise, the number of parasitic spores released from each area would be dependent on the density and size of infected *Nephrops*.

In conclusion, this thesis lays the groundwork for the development of a full-scale spatial population model of *Nephrops* and *Hematodinium* in the CSA. However, more research is required prior to the development of such a model. For example, particle tracking work is required in order to establish the dispersal patterns of *Hematodinium* spores in the CSA. This work is critical to the development of a spatial population model of *Nephrops* and *Hematodinium*. Further work is also required to collect up-to-date records of *Hematodinium* prevalence across the CSA. A particular focus should be given to recording spatial differences in *Hematodinium* prevalence across the region. This work is crucial in order to validate the output of a spatial *Nephrops-Hematodinium* population model. The creation of a full-scale spatial population model *Nephrops* and *Hematodinium* is required to investigate the driving factors behind observed spatial patterns in *Nephrops-Hematodinium* population dynamics. Improving our understanding of these factors is essential for the effective management of this commercially important host-parasite system.

Appendix A

Nephrops-Hematodinium Population Model - R Code

```
####################################
#### Nephrops-Model-Parameters #####
####################################

phi_male = 0.00005
mu_male = 0.00007
phi_female = 0.00025
mu_female = 0.002
delta_1 = 0.0003
gamma = 1e-15
c_male = 1.37
c_female = 1.24
alpha_Female = 0.00074
beta_Female = 2.91
alpha_Male = 0.00028
beta_Male = 3.24
W_Init = 0.1
L_Init_Female = Weight.to.Length.Female(W_Init)
L_Init_Male = Weight.to.Length.Male(W_Init)
Maturity = 27
q1 = 0.8
q2 = 0.9
m = 0.00068
c1 = 0.00000005
E1 = 130000
dc = 1e-12
ks = 0.7
L.50 = 29
kappa_1 = 0.65
kappa_2 = 0.05
ce = 0.002
B0 = 8e+10
Init.Spores = 1000000
g = 0.032
Beta = 0.000000000000000002
lambda = 0.25
I_Max = 1e+10
```

```
kc = 0.1
C.50 = 283333333
h = 0.33
kd = 0.5675287
D.50 = 23.2585312
ds = 0.25 # discard survival



##############################
#### Nephrops-Model-Main ####
##############################

# Initialise Information for the run
Max.Years = 800
Max.Time = Max.Years*365  # Days
Max.Uninfected.Cohorts = 20
Max.Infected.Cohorts = 400

# Create a counter which keeps track of the number of cohorts
No.of.Uninfected.Female.Cohorts = 1
No.of.Uninfected.Male.Cohorts = 1
No.of.Infected.Female.Cohorts = 0
No.of.Infected.Male.Cohorts = 0


#######################################

for (y in 1:Max.Years){

# Introduce fishing effort after model has reached a steady state
if(y <= 150){E <- 0
} else {E <-E1/365}


# Set up temporary results table
source('Nephrops_Model_Temp_Table_Initialisation.R')

####################################

for (d in 1:365){

t = y*365-365+d

# Impulse of spores after the population has reached steady state
if (t==(299*365+1)){No.of.Spores.Vector[t] = Init.Spores}

# Reset Counters
No.of.Spores <- 0

#######################################

# If infected female cohort is present
if(No.of.Infected.Female.Cohorts >= 1){

# Infected Females
L = Temp.Infected.Female.Length.Matrix[1:No.of.Infected.Female.Cohorts,d]
```

```
M = Temp.Infected.Female.Moult.Matrix[1:No.of.Infected.Female.Cohorts,d]
N0 = Temp.Infected.Female.Population.Matrix[1:No.of.Infected.Female.Cohorts,d]
W0 = Temp.Infected.Female.Weight.Matrix[1:No.of.Infected.Female.Cohorts,d]
E0 = Temp.Infected.Female.Reproduction.Matrix[1:No.of.Infected.Female.Cohorts,d]
I0 = Temp.Infected.Female.Parasite.Matrix[1:No.of.Infected.Female.Cohorts,d]


# Create a vector for delta
delta <- numeric(No.of.Infected.Female.Cohorts)
for (n in 1:No.of.Infected.Female.Cohorts){
if (L[n] < Maturity) {delta[n] <- 0
} else {
delta[n] <- delta_1
}
}

# Calculate fishing mortality for cohort
f = c1*E*Selectivity(L)

# Create a vector for catchability
Q_vector <- numeric(No.of.Infected.Female.Cohorts)
for (n in 1:No.of.Infected.Female.Cohorts) {
if (L[n] < Maturity) {
Q_vector[n] <- 1
} else if (L[n] >= Maturity &&  d <=90) {
Q_vector[n] <- q
} else if (L[n] >= Maturity &&  d >= 91 && d <= 181) {
Q_vector[n] <- 1
} else if (L[n] >= Maturity &&  d >= 182 && d <= 273) {
Q_vector[n] <- 1
} else if (L[n] >= Maturity &&  d >= 274 && d <= 365) {
Q_vector[n] <- q
}
}



# Calculate natural mortality
Z = Q_vector*(m+f) + dc * I0

# Solve Differential Equations

# Population Size
Temp.Infected.Female.Population.Matrix[1:No.of.Infected.Female.Cohorts,d+1] = N0 * exp(-Z)

# Weight
Integration.Constant = log(-(mu_female+delta)*W0 + (phi_female*L^2-gamma*I0))/(-(mu_female+delta))
Temp.Infected.Female.Weight.Matrix[1:No.of.Infected.Female.Cohorts,d+1] =
(exp(-(mu_female+delta)*(1+Integration.Constant)) -
(phi_female * L^2 - gamma*I0))/(-(mu_female+delta))

# Energy for Reproduction
Temp.Infected.Female.Reproduction.Matrix[1:No.of.Infected.Female.Cohorts,d+1] = delta*W0 + E0

# Parasite Growth
Temp.Infected.Female.Parasite.Matrix[1:No.of.Infected.Female.Cohorts,d+1] = I0 * exp(g)


for (n in 1:No.of.Infected.Female.Cohorts){
```

```
if (Temp.Infected.Female.Parasite.Matrix[n,d+1] > I_Max){
Temp.Infected.Female.Parasite.Matrix[n,d+1] <- I_Max}

# Determine the probability of sporulation
Prob.of.Sporulation <- Sporulation.Probability.Curve(Temp.Infected.Female.Parasite.Matrix[n,d]/
Volume.of.Haemolymph(Temp.Infected.Female.Weight.Matrix[n,d]))


# Moulting - Immature Individuals
if(L[n] < Maturity && Temp.Infected.Female.Weight.Matrix[n,d+1] >= Critical.Weight.Female[M[n]+1]){

L[n] = Critical.Length.Female[M[n]+1]
M[n] = M[n] + 1

No.of.Spores <- No.of.Spores + (Prob.of.Sporulation *
Temp.Infected.Female.Population.Matrix[n,d] *
Temp.Infected.Female.Parasite.Matrix[n,d])

# Sporulation results in death
Temp.Infected.Female.Population.Matrix[n,d+1] =
Temp.Infected.Female.Population.Matrix[n,d] - Prob.of.Sporulation *
Temp.Infected.Female.Population.Matrix[n,d]

}


# Moulting - Mature Individuals
if(L[n] >= Maturity && d==121){

L[n] = Weight.to.Length.Female(Temp.Infected.Female.Weight.Matrix[n,d+1])
M[n] = M[n] + 1
Temp.Infected.Female.Reproduction.Matrix[n,d+1] = 0

No.of.Spores <- No.of.Spores + (Prob.of.Sporulation *
Temp.Infected.Female.Population.Matrix[n,d] *
Temp.Infected.Female.Parasite.Matrix[n,d])

# Sporulation results in death
Temp.Infected.Female.Population.Matrix[n,d+1] <-
Temp.Infected.Female.Population.Matrix[n,d] - Prob.of.Sporulation *
Temp.Infected.Female.Population.Matrix[n,d]

}


# Egg Laying - Mature Individuals
if(L[n] >= Maturity && d==213){

Temp.Infected.Female.Reproduction.Matrix[n,d+1] = 0

}

}

Temp.Infected.Female.Length.Matrix[1:No.of.Infected.Female.Cohorts,d+1] = L
Temp.Infected.Female.Moult.Matrix[1:No.of.Infected.Female.Cohorts,d+1] = M
```

```
# Store information about females which are caught by the fishery
Temp.Infected.Female.Catch.Population.Matrix[1:No.of.Infected.Female.Cohorts,d] = (f/Z)*(1-exp(-Z))*
Temp.Infected.Female.Population.Matrix[1:No.of.Infected.Female.Cohorts,d]
Temp.Infected.Female.Catch.Weight.Matrix[1:No.of.Infected.Female.Cohorts,d] =
Temp.Infected.Female.Weight.Matrix[1:No.of.Infected.Female.Cohorts,d+1]
Temp.Infected.Female.Catch.Length.Matrix[1:No.of.Infected.Female.Cohorts,d] =
Temp.Infected.Female.Length.Matrix[1:No.of.Infected.Female.Cohorts,d+1]
Temp.Infected.Female.Catch.Moult.Matrix[1:No.of.Infected.Female.Cohorts,d] =
Temp.Infected.Female.Moult.Matrix[1:No.of.Infected.Female.Cohorts,d+1]
Temp.Infected.Female.Catch.Reproduction.Matrix[1:No.of.Infected.Female.Cohorts,d] =
Temp.Infected.Female.Reproduction.Matrix[1:No.of.Infected.Female.Cohorts,d+1]
Temp.Infected.Female.Catch.Parasite.Matrix[1:No.of.Infected.Female.Cohorts,d] =
Temp.Infected.Female.Parasite.Matrix[1:No.of.Infected.Female.Cohorts,d+1]


# Calculate the probability of the catch being discarded
Prob.of.Discard <-
Discard.Probability(Temp.Infected.Female.Catch.Length.Matrix[1:No.of.Infected.Female.Cohorts,d])

# Discards which survive are added back onto the original cohort
Temp.Infected.Female.Population.Matrix[1:No.of.Infected.Female.Cohorts,d+1] =
Temp.Infected.Female.Population.Matrix[1:No.of.Infected.Female.Cohorts,d+1] +
Temp.Infected.Female.Catch.Population.Matrix[1:No.of.Infected.Female.Cohorts,d] * Prob.of.Discard * ds

# Store information about females which are discarded by the fishery
Temp.Infected.Female.Discards.Population.Matrix[1:No.of.Infected.Female.Cohorts,d] =
Temp.Infected.Female.Catch.Population.Matrix[1:No.of.Infected.Female.Cohorts,d] * Prob.of.Discard
Temp.Infected.Female.Discards.Weight.Matrix[1:No.of.Infected.Female.Cohorts,d] =
Temp.Infected.Female.Weight.Matrix[1:No.of.Infected.Female.Cohorts,d+1]
Temp.Infected.Female.Discards.Length.Matrix[1:No.of.Infected.Female.Cohorts,d] =
Temp.Infected.Female.Length.Matrix[1:No.of.Infected.Female.Cohorts,d+1]
Temp.Infected.Female.Discards.Moult.Matrix[1:No.of.Infected.Female.Cohorts,d] =
Temp.Infected.Female.Moult.Matrix[1:No.of.Infected.Female.Cohorts,d+1]
Temp.Infected.Female.Discards.Reproduction.Matrix[1:No.of.Infected.Female.Cohorts,d] =
Temp.Infected.Female.Reproduction.Matrix[1:No.of.Infected.Female.Cohorts,d+1]
Temp.Infected.Female.Discards.Parasite.Matrix[1:No.of.Infected.Female.Cohorts,d] =
Temp.Infected.Female.Parasite.Matrix[1:No.of.Infected.Female.Cohorts,d+1]


# Store information about females which are landed by the fishery
Temp.Infected.Female.Landings.Population.Matrix[1:No.of.Infected.Female.Cohorts,d] =
Temp.Infected.Female.Catch.Population.Matrix[1:No.of.Infected.Female.Cohorts,d] -
Temp.Infected.Female.Catch.Population.Matrix[1:No.of.Infected.Female.Cohorts,d] * Prob.of.Discard
Temp.Infected.Female.Landings.Weight.Matrix[1:No.of.Infected.Female.Cohorts,d] =
Temp.Infected.Female.Weight.Matrix[1:No.of.Infected.Female.Cohorts,d+1]
Temp.Infected.Female.Landings.Length.Matrix[1:No.of.Infected.Female.Cohorts,d] =
Temp.Infected.Female.Length.Matrix[1:No.of.Infected.Female.Cohorts,d+1]
Temp.Infected.Female.Landings.Moult.Matrix[1:No.of.Infected.Female.Cohorts,d] =
Temp.Infected.Female.Moult.Matrix[1:No.of.Infected.Female.Cohorts,d+1]
Temp.Infected.Female.Landings.Reproduction.Matrix[1:No.of.Infected.Female.Cohorts,d] =
Temp.Infected.Female.Reproduction.Matrix[1:No.of.Infected.Female.Cohorts,d+1]
Temp.Infected.Female.Landings.Parasite.Matrix[1:No.of.Infected.Female.Cohorts,d] =
Temp.Infected.Female.Parasite.Matrix[1:No.of.Infected.Female.Cohorts,d+1]


}
```

```
################################################

# If infected male cohort is present
if(No.of.Infected.Male.Cohorts >= 1){

L = Temp.Infected.Male.Length.Matrix[1:No.of.Infected.Male.Cohorts,d]
M = Temp.Infected.Male.Moult.Matrix[1:No.of.Infected.Male.Cohorts,d]

N0 = Temp.Infected.Male.Population.Matrix[1:No.of.Infected.Male.Cohorts,d]
W0 = Temp.Infected.Male.Weight.Matrix[1:No.of.Infected.Male.Cohorts,d]
E0 = Temp.Infected.Male.Reproduction.Matrix[1:No.of.Infected.Male.Cohorts,d]
I0 = Temp.Infected.Male.Parasite.Matrix[1:No.of.Infected.Male.Cohorts,d]


# Create a vector for delta
delta <- rep(0,No.of.Infected.Male.Cohorts)

f = c1*E*Selectivity(L)

# Create a vector for catchability
Q_vector <- rep(1, No.of.Infected.Male.Cohorts)


# Calculate natural mortality
Z = Q_vector*(m+f) + dc * I0


# Solve Differential Equations

# Population Size
Temp.Infected.Male.Population.Matrix[1:No.of.Infected.Male.Cohorts,d+1] = N0 * exp(-Z)

# Weight
Integration.Constant = log(-(mu_male+delta)*W0 +
(phi_male*L^2-gamma*I0))/(-(mu_male+delta))
Temp.Infected.Male.Weight.Matrix[1:No.of.Infected.Male.Cohorts,d+1] =
(exp(-(mu_male+delta)*(1+Integration.Constant)) -
(phi_male * L^2 - gamma*I0))/(-(mu_male+delta))

# Energy for Reproduction
Temp.Infected.Male.Reproduction.Matrix[1:No.of.Infected.Male.Cohorts,d+1] = delta*W0 + E0

# Parasite Growth
Temp.Infected.Male.Parasite.Matrix[1:No.of.Infected.Male.Cohorts,d+1] = I0 * exp(g)


for (n in 1:No.of.Infected.Male.Cohorts){

if (Temp.Infected.Male.Parasite.Matrix[n,d+1] > I_Max){
Temp.Infected.Male.Parasite.Matrix[n,d+1] <- I_Max}


# Determine the probability of sporulation
Prob.of.Sporulation <- Sporulation.Probability.Curve(Temp.Infected.Male.Parasite.Matrix[n,d]/ Volume.of.Haemolymph(Temp.Infe
```

```
# Moulting
if(Temp.Infected.Male.Weight.Matrix[n,d+1] >= Critical.Weight.Male[M[n]+1]){

L[n] = Critical.Length.Male[M[n]+1]
M[n] = M[n] + 1

No.of.Spores <- No.of.Spores +
(Prob.of.Sporulation*Temp.Infected.Male.Population.Matrix[n,d]*
Temp.Infected.Male.Parasite.Matrix[n,d])

# Sporulation results in death
Temp.Infected.Male.Population.Matrix[n,d+1] <-
Temp.Infected.Male.Population.Matrix[n,d] - Prob.of.Sporulation *
Temp.Infected.Male.Population.Matrix[n,d]

}

}

Temp.Infected.Male.Length.Matrix[1:No.of.Infected.Male.Cohorts,d+1] = L
Temp.Infected.Male.Moult.Matrix[1:No.of.Infected.Male.Cohorts,d+1] = M


# Store information about males which are caught by the fishery
Temp.Infected.Male.Catch.Population.Matrix[1:No.of.Infected.Male.Cohorts,d] =
(f/Z)*(1-exp(-Z))*Temp.Infected.Male.Population.Matrix[1:No.of.Infected.Male.Cohorts,d]
Temp.Infected.Male.Catch.Weight.Matrix[1:No.of.Infected.Male.Cohorts,d] =
Temp.Infected.Male.Weight.Matrix[1:No.of.Infected.Male.Cohorts,d+1]
Temp.Infected.Male.Catch.Length.Matrix[1:No.of.Infected.Male.Cohorts,d] =
Temp.Infected.Male.Length.Matrix[1:No.of.Infected.Male.Cohorts,d+1]
Temp.Infected.Male.Catch.Moult.Matrix[1:No.of.Infected.Male.Cohorts,d] =
Temp.Infected.Male.Moult.Matrix[1:No.of.Infected.Male.Cohorts,d+1]
Temp.Infected.Male.Catch.Reproduction.Matrix[1:No.of.Infected.Male.Cohorts,d] =
Temp.Infected.Male.Reproduction.Matrix[1:No.of.Infected.Male.Cohorts,d+1]
Temp.Infected.Male.Catch.Parasite.Matrix[1:No.of.Infected.Male.Cohorts,d] =
Temp.Infected.Male.Parasite.Matrix[1:No.of.Infected.Male.Cohorts,d+1]


# Calculate the probability of the catch being discarded
Prob.of.Discard <-
Discard.Probability(Temp.Infected.Male.Catch.Length.Matrix[1:No.of.Infected.Male.Cohorts,d])

# Discards which survive are added back onto the original cohort
Temp.Infected.Male.Population.Matrix[1:No.of.Infected.Male.Cohorts,d+1] =
Temp.Infected.Male.Population.Matrix[1:No.of.Infected.Male.Cohorts,d+1] +
Temp.Infected.Male.Catch.Population.Matrix[1:No.of.Infected.Male.Cohorts,d] * Prob.of.Discard * ds

# Store information about males which are discarded by the fishery
Temp.Infected.Male.Discards.Population.Matrix[1:No.of.Infected.Male.Cohorts,d] =
Temp.Infected.Male.Catch.Population.Matrix[1:No.of.Infected.Male.Cohorts,d] * Prob.of.Discard
Temp.Infected.Male.Discards.Weight.Matrix[1:No.of.Infected.Male.Cohorts,d] =
Temp.Infected.Male.Weight.Matrix[1:No.of.Infected.Male.Cohorts,d+1]
Temp.Infected.Male.Discards.Length.Matrix[1:No.of.Infected.Male.Cohorts,d] =
Temp.Infected.Male.Length.Matrix[1:No.of.Infected.Male.Cohorts,d+1]
Temp.Infected.Male.Discards.Moult.Matrix[1:No.of.Infected.Male.Cohorts,d] =
Temp.Infected.Male.Moult.Matrix[1:No.of.Infected.Male.Cohorts,d+1]
Temp.Infected.Male.Discards.Reproduction.Matrix[1:No.of.Infected.Male.Cohorts,d] =
Temp.Infected.Male.Reproduction.Matrix[1:No.of.Infected.Male.Cohorts,d+1]
```

```
Temp.Infected.Male.Discards.Parasite.Matrix[1:No.of.Infected.Male.Cohorts,d] =
Temp.Infected.Male.Parasite.Matrix[1:No.of.Infected.Male.Cohorts,d+1]

# Store information about males which are landed by the fishery
Temp.Infected.Male.Landings.Population.Matrix[1:No.of.Infected.Male.Cohorts,d] =
Temp.Infected.Male.Catch.Population.Matrix[1:No.of.Infected.Male.Cohorts,d] -
Temp.Infected.Male.Catch.Population.Matrix[1:No.of.Infected.Male.Cohorts,d] * Prob.of.Discard
Temp.Infected.Male.Landings.Weight.Matrix[1:No.of.Infected.Male.Cohorts,d] =
Temp.Infected.Male.Weight.Matrix[1:No.of.Infected.Male.Cohorts,d+1]
Temp.Infected.Male.Landings.Length.Matrix[1:No.of.Infected.Male.Cohorts,d] =
Temp.Infected.Male.Length.Matrix[1:No.of.Infected.Male.Cohorts,d+1]
Temp.Infected.Male.Landings.Moult.Matrix[1:No.of.Infected.Male.Cohorts,d] =
Temp.Infected.Male.Moult.Matrix[1:No.of.Infected.Male.Cohorts,d+1]
Temp.Infected.Male.Landings.Reproduction.Matrix[1:No.of.Infected.Male.Cohorts,d] =
Temp.Infected.Male.Reproduction.Matrix[1:No.of.Infected.Male.Cohorts,d+1]
Temp.Infected.Male.Landings.Parasite.Matrix[1:No.of.Infected.Male.Cohorts,d] =
Temp.Infected.Male.Parasite.Matrix[1:No.of.Infected.Male.Cohorts,d+1]

}



########################################

# Impulse of spores from moulting is added to the number of spores already in the environment
No.of.Spores.Vector[t+1] = No.of.Spores.Vector[t] * exp(-lambda) + No.of.Spores

########################################

# Uninfected Females

L = Temp.Uninfected.Female.Length.Matrix[1:No.of.Uninfected.Female.Cohorts,d]
M = Temp.Uninfected.Female.Moult.Matrix[1:No.of.Uninfected.Female.Cohorts,d]

N0 = Temp.Uninfected.Female.Population.Matrix[1:No.of.Uninfected.Female.Cohorts,d]
W0 = Temp.Uninfected.Female.Weight.Matrix[1:No.of.Uninfected.Female.Cohorts,d]
E0 = Temp.Uninfected.Female.Reproduction.Matrix[1:No.of.Uninfected.Female.Cohorts,d]
I0 = Temp.Uninfected.Female.Parasite.Matrix[1:No.of.Uninfected.Female.Cohorts,d]


# Create a vector for delta
delta <- numeric(No.of.Uninfected.Female.Cohorts)
for (n in 1:No.of.Uninfected.Female.Cohorts){
if (L[n] < Maturity) {delta[n] <- 0
} else {
delta[n] <- delta_1
}
}

# Calculate fishing mortality for cohort
f = c1*E*Selectivity(L)


# Create a vector for catchability
Q_vector <- numeric(No.of.Uninfected.Female.Cohorts)

for (n in 1:No.of.Uninfected.Female.Cohorts) {
if (L[n] < Maturity) {
```

```
Q_vector[n] <- 0.9
} else if (L[n] >= Maturity &&  d <=90) {
Q_vector[n] <- 0.9*q
} else if (L[n] >= Maturity &&  d >= 91 && d <= 181) {
Q_vector[n] <- 0.9
} else if (L[n] >= Maturity &&  d >= 182 && d <= 273) {
Q_vector[n] <- 0.9
} else if (L[n] >= Maturity &&  d >= 274 && d <= 365) {
Q_vector[n] <- 0.9*q
}
}

# Calculate natural mortality
Z = Q_vector*(m+f) + dc*I0


# Solve Differential Equations

# Population Size
Temp.Uninfected.Female.Population.Matrix[1:No.of.Uninfected.Female.Cohorts,d+1] = N0 * exp(-Z)

# Weight
Integration.Constant = log(-(mu_female+delta)*W0 +
(phi_female*L^2-gamma*I0))/(-(mu_female+delta))
Temp.Uninfected.Female.Weight.Matrix[1:No.of.Uninfected.Female.Cohorts,d+1] =
(exp(-(mu_female+delta)*(1+Integration.Constant)) -
(phi_female * L^2 - gamma*I0))/(-(mu_female+delta))

# Energy for Reproduction
Temp.Uninfected.Female.Reproduction.Matrix[1:No.of.Uninfected.Female.Cohorts,d+1] = delta*W0 + E0

# Parasite Growth
Temp.Uninfected.Female.Parasite.Matrix[1:No.of.Uninfected.Female.Cohorts,d+1] = I0 * exp(g)


for (n in 1:No.of.Uninfected.Female.Cohorts){

# Moulting individuals are susceptible to infection
# A proportion of moulting individuals will become infected
# Create a new infected cohort to store these individuals

# Moulting - Immature Individuals
if(L[n] < Maturity && Temp.Uninfected.Female.Weight.Matrix[n,d+1] >= Critical.Weight.Female[M[n]+1]){

L[n] = Critical.Length.Female[M[n]+1]
M[n] = M[n] + 1

# Create new infected cohort
if((Temp.Uninfected.Female.Population.Matrix[n,d+1]*(1-exp(-Beta*No.of.Spores.Vector[t]))) > 0){

# Identify the cohort to be replaced
if(No.of.Infected.Female.Cohorts<Max.Infected.Cohorts){
Infected.Female.Cohort.Marker <- No.of.Infected.Female.Cohorts+1
}else{
Infected.Female.Cohort.Marker <- which.min(Temp.Infected.Female.Population.Matrix[1:Max.Infected.Cohorts,d+1])}

Temp.Infected.Female.Population.Matrix[Infected.Female.Cohort.Marker,d+1] <-
(Temp.Uninfected.Female.Population.Matrix[n,d+1]*(1-exp(-Beta*No.of.Spores.Vector[t])))
```

```
Temp.Infected.Female.Weight.Matrix[Infected.Female.Cohort.Marker,d+1] <-
Temp.Uninfected.Female.Weight.Matrix[n,d+1]
Temp.Infected.Female.Length.Matrix[Infected.Female.Cohort.Marker,d+1] <- L[n]
Temp.Infected.Female.Moult.Matrix[Infected.Female.Cohort.Marker,d+1] <- M[n]
Temp.Infected.Female.Reproduction.Matrix[Infected.Female.Cohort.Marker,d+1] <-
Temp.Uninfected.Female.Reproduction.Matrix[n,d+1]
Temp.Infected.Female.Parasite.Matrix[Infected.Female.Cohort.Marker,d+1] <- 1

No.of.Infected.Female.Cohorts <- No.of.Infected.Female.Cohorts + 1

if(No.of.Infected.Female.Cohorts > Max.Infected.Cohorts){No.of.Infected.Female.Cohorts = Max.Infected.Cohorts}

# Calculate the number of individuals in the uninfected cohort to
# account for individuals which have become infected
Temp.Uninfected.Female.Population.Matrix[n,d+1] = Temp.Uninfected.Female.Population.Matrix[n,d+1] -
(Temp.Uninfected.Female.Population.Matrix[n,d+1]*(1-exp(-Beta*No.of.Spores.Vector[t])))

}}


# Moulting - Mature Individuals
if(L[n] >= Maturity && d==121){

L[n] = Weight.to.Length.Female(Temp.Uninfected.Female.Weight.Matrix[n,d+1])
M[n] = M[n] + 1

# Create New infected cohort
if((Temp.Uninfected.Female.Population.Matrix[n,d+1]*(1-exp(-Beta*No.of.Spores.Vector[t]))) > 0){

# Identify the cohort to be replaced
if(No.of.Infected.Female.Cohorts<Max.Infected.Cohorts){
Infected.Female.Cohort.Marker <- No.of.Infected.Female.Cohorts+1
}else{
Infected.Female.Cohort.Marker <- which.min(Temp.Infected.Female.Population.Matrix[1:Max.Infected.Cohorts,d+1])}


Temp.Infected.Female.Population.Matrix[Infected.Female.Cohort.Marker,d+1] <-
(Temp.Uninfected.Female.Population.Matrix[n,d+1]*(1-exp(-Beta*No.of.Spores.Vector[t])))
Temp.Infected.Female.Weight.Matrix[Infected.Female.Cohort.Marker,d+1] <-
Temp.Uninfected.Female.Weight.Matrix[n,d+1]
Temp.Infected.Female.Length.Matrix[Infected.Female.Cohort.Marker,d+1] <- L[n]
Temp.Infected.Female.Moult.Matrix[Infected.Female.Cohort.Marker,d+1] <- M[n]
Temp.Infected.Female.Reproduction.Matrix[Infected.Female.Cohort.Marker,d+1] <-
Temp.Uninfected.Female.Reproduction.Matrix[n,d+1]
Temp.Infected.Female.Parasite.Matrix[Infected.Female.Cohort.Marker,d+1] <- 1

No.of.Infected.Female.Cohorts <- No.of.Infected.Female.Cohorts + 1

if(No.of.Infected.Female.Cohorts > Max.Infected.Cohorts){No.of.Infected.Female.Cohorts = Max.Infected.Cohorts}


# Calculate the number of individuals in the uninfected cohort to
# account for individuals which have become infected
Temp.Uninfected.Female.Population.Matrix[n,d+1] = Temp.Uninfected.Female.Population.Matrix[n,d+1] -
(Temp.Uninfected.Female.Population.Matrix[n,d+1]*(1-exp(-Beta*No.of.Spores.Vector[t])))

}}
```

```
# Egg Laying - Mature Individuals
if(L[n] >= Maturity && d==213){

Temp.Uninfected.Female.Reproduction.Matrix[n,d+1] = 0

}
}

Temp.Uninfected.Female.Length.Matrix[1:No.of.Uninfected.Female.Cohorts,d+1] = L
Temp.Uninfected.Female.Moult.Matrix[1:No.of.Uninfected.Female.Cohorts,d+1] = M

# Store Information about Females which are caught by the fishery
Temp.Uninfected.Female.Catch.Population.Matrix[1:No.of.Uninfected.Female.Cohorts,d] =
(f/Z)*(1-exp(-Z))*Temp.Uninfected.Female.Population.Matrix[1:No.of.Uninfected.Female.Cohorts,d]
Temp.Uninfected.Female.Catch.Weight.Matrix[1:No.of.Uninfected.Female.Cohorts,d] =
Temp.Uninfected.Female.Weight.Matrix[1:No.of.Uninfected.Female.Cohorts,d+1]
Temp.Uninfected.Female.Catch.Length.Matrix[1:No.of.Uninfected.Female.Cohorts,d] =
Temp.Uninfected.Female.Length.Matrix[1:No.of.Uninfected.Female.Cohorts,d+1]
Temp.Uninfected.Female.Catch.Moult.Matrix[1:No.of.Uninfected.Female.Cohorts,d] =
Temp.Uninfected.Female.Moult.Matrix[1:No.of.Uninfected.Female.Cohorts,d+1]
Temp.Uninfected.Female.Catch.Reproduction.Matrix[1:No.of.Uninfected.Female.Cohorts,d] =
Temp.Uninfected.Female.Reproduction.Matrix[1:No.of.Uninfected.Female.Cohorts,d+1]
Temp.Uninfected.Female.Catch.Parasite.Matrix[1:No.of.Uninfected.Female.Cohorts,d] =
Temp.Uninfected.Female.Parasite.Matrix[1:No.of.Uninfected.Female.Cohorts,d+1]


# Calculate the probability of the catch being discarded
Prob.of.Discard <-
Discard.Probability(Temp.Uninfected.Female.Catch.Length.Matrix[1:No.of.Uninfected.Female.Cohorts,d])

# Discards which survive are added back onto the original cohort
Temp.Uninfected.Female.Population.Matrix[1:No.of.Uninfected.Female.Cohorts,d+1] =
Temp.Uninfected.Female.Population.Matrix[1:No.of.Uninfected.Female.Cohorts,d+1] +
Temp.Uninfected.Female.Catch.Population.Matrix[1:No.of.Uninfected.Female.Cohorts,d] * Prob.of.Discard * ds

# Store Information about females which are discarded by the fishery
Temp.Uninfected.Female.Discards.Population.Matrix[1:No.of.Uninfected.Female.Cohorts,d] =
Temp.Uninfected.Female.Catch.Population.Matrix[1:No.of.Uninfected.Female.Cohorts,d] * Prob.of.Discard
Temp.Uninfected.Female.Discards.Weight.Matrix[1:No.of.Uninfected.Female.Cohorts,d] =
Temp.Uninfected.Female.Weight.Matrix[1:No.of.Uninfected.Female.Cohorts,d+1]
Temp.Uninfected.Female.Discards.Length.Matrix[1:No.of.Uninfected.Female.Cohorts,d] =
Temp.Uninfected.Female.Length.Matrix[1:No.of.Uninfected.Female.Cohorts,d+1]
Temp.Uninfected.Female.Discards.Moult.Matrix[1:No.of.Uninfected.Female.Cohorts,d] =
Temp.Uninfected.Female.Moult.Matrix[1:No.of.Uninfected.Female.Cohorts,d+1]
Temp.Uninfected.Female.Discards.Reproduction.Matrix[1:No.of.Uninfected.Female.Cohorts,d] =
Temp.Uninfected.Female.Reproduction.Matrix[1:No.of.Uninfected.Female.Cohorts,d+1]
Temp.Uninfected.Female.Discards.Parasite.Matrix[1:No.of.Uninfected.Female.Cohorts,d] =
Temp.Uninfected.Female.Parasite.Matrix[1:No.of.Uninfected.Female.Cohorts,d+1]

# Store information about females which are landed by the fishery
Temp.Uninfected.Female.Landings.Population.Matrix[1:No.of.Uninfected.Female.Cohorts,d] =
Temp.Uninfected.Female.Catch.Population.Matrix[1:No.of.Uninfected.Female.Cohorts,d] -
Temp.Uninfected.Female.Catch.Population.Matrix[1:No.of.Uninfected.Female.Cohorts,d] * Prob.of.Discard
Temp.Uninfected.Female.Landings.Weight.Matrix[1:No.of.Uninfected.Female.Cohorts,d] =
Temp.Uninfected.Female.Weight.Matrix[1:No.of.Uninfected.Female.Cohorts,d+1]
Temp.Uninfected.Female.Landings.Length.Matrix[1:No.of.Uninfected.Female.Cohorts,d] =
Temp.Uninfected.Female.Length.Matrix[1:No.of.Uninfected.Female.Cohorts,d+1]
```

```
Temp.Uninfected.Female.Landings.Moult.Matrix[1:No.of.Uninfected.Female.Cohorts,d] =
Temp.Uninfected.Female.Moult.Matrix[1:No.of.Uninfected.Female.Cohorts,d+1]
Temp.Uninfected.Female.Landings.Reproduction.Matrix[1:No.of.Uninfected.Female.Cohorts,d] =
Temp.Uninfected.Female.Reproduction.Matrix[1:No.of.Uninfected.Female.Cohorts,d+1]
Temp.Uninfected.Female.Landings.Parasite.Matrix[1:No.of.Uninfected.Female.Cohorts,d] =
Temp.Uninfected.Female.Parasite.Matrix[1:No.of.Uninfected.Female.Cohorts,d+1]

################################

# Uninfected Males

L = Temp.Uninfected.Male.Length.Matrix[1:No.of.Uninfected.Male.Cohorts,d]
M = Temp.Uninfected.Male.Moult.Matrix[1:No.of.Uninfected.Male.Cohorts,d]

N0 = Temp.Uninfected.Male.Population.Matrix[1:No.of.Uninfected.Male.Cohorts,d]
W0 = Temp.Uninfected.Male.Weight.Matrix[1:No.of.Uninfected.Male.Cohorts,d]
E0 = Temp.Uninfected.Male.Reproduction.Matrix[1:No.of.Uninfected.Male.Cohorts,d]
I0 = Temp.Uninfected.Male.Parasite.Matrix[1:No.of.Uninfected.Male.Cohorts,d]


# Create a vector for delta
delta <- rep(0,No.of.Uninfected.Male.Cohorts)

f = c1*E*Selectivity(L)

# Create a vector for catchability
Q_vector <- rep(0.9, No.of.Uninfected.Male.Cohorts)

# Calculate natural mortality
Z = Q_vector*(m+f) + dc*I0


# Solve Differential Equations

# Population Size
Temp.Uninfected.Male.Population.Matrix[1:No.of.Uninfected.Male.Cohorts,d+1] = N0 * exp(-Z)

# Weight
Integration.Constant = log(-(mu_male+delta)*W0 +
(phi_male*L^2-gamma*I0))/(-(mu_male+delta))
Temp.Uninfected.Male.Weight.Matrix[1:No.of.Uninfected.Male.Cohorts,d+1] =
(exp(-(mu_male+delta)*(1+Integration.Constant)) -
(phi_male * L^2 - gamma*I0))/(-(mu_male+delta))

# Energy for Reproduction
Temp.Uninfected.Male.Reproduction.Matrix[1:No.of.Uninfected.Male.Cohorts,d+1] = delta*W0 + E0

# Parasite Growth
Temp.Uninfected.Male.Parasite.Matrix[1:No.of.Uninfected.Male.Cohorts,d+1] = I0 * exp(g)


for (n in 1:No.of.Uninfected.Male.Cohorts){

if (Temp.Uninfected.Male.Weight.Matrix[n,d+1] > W_Max_Male){
Temp.Uninfected.Male.Weight.Matrix[n,d+1] <- W_Max_Male}

# Moulting
if(Temp.Uninfected.Male.Weight.Matrix[n,d+1] >= Critical.Weight.Male[M[n]+1]){
```

```
L[n] = Critical.Length.Male[M[n]+1]
M[n] = M[n] + 1

# Create new infected cohort
if((Temp.Uninfected.Male.Population.Matrix[n,d+1]*(1-exp(-Beta*No.of.Spores.Vector[t]))) > 0){

# Identify the cohort to be replaced
if(No.of.Infected.Male.Cohorts<Max.Infected.Cohorts){
Infected.Male.Cohort.Marker <- No.of.Infected.Male.Cohorts+1
}else{
Infected.Male.Cohort.Marker <- which.min(Temp.Infected.Male.Population.Matrix[1:Max.Infected.Cohorts,d+1])}

Temp.Infected.Male.Population.Matrix[Infected.Male.Cohort.Marker,d+1] <-
(Temp.Uninfected.Male.Population.Matrix[n,d+1]*(1-exp(-Beta*No.of.Spores.Vector[t])))
Temp.Infected.Male.Weight.Matrix[Infected.Male.Cohort.Marker,d+1] <-
Temp.Uninfected.Male.Weight.Matrix[n,d+1]
Temp.Infected.Male.Length.Matrix[Infected.Male.Cohort.Marker,d+1] <- L[n]
Temp.Infected.Male.Moult.Matrix[Infected.Male.Cohort.Marker,d+1] <- M[n]
Temp.Infected.Male.Reproduction.Matrix[Infected.Male.Cohort.Marker,d+1] <-
Temp.Uninfected.Male.Reproduction.Matrix[n,d+1]
Temp.Infected.Male.Parasite.Matrix[Infected.Male.Cohort.Marker,d+1] <- 1

No.of.Infected.Male.Cohorts <- No.of.Infected.Male.Cohorts + 1

if(No.of.Infected.Male.Cohorts > Max.Infected.Cohorts){No.of.Infected.Male.Cohorts = Max.Infected.Cohorts}

# Calculate the number of individuals in the uninfected cohort to account for individuals who have become infected
Temp.Uninfected.Male.Population.Matrix[n,d+1] = Temp.Uninfected.Male.Population.Matrix[n,d+1] -
(Temp.Uninfected.Male.Population.Matrix[n,d+1]*(1-exp(-Beta*No.of.Spores.Vector[t])))

}}

}

Temp.Uninfected.Male.Length.Matrix[1:No.of.Uninfected.Male.Cohorts,d+1] = L
Temp.Uninfected.Male.Moult.Matrix[1:No.of.Uninfected.Male.Cohorts,d+1] = M

# Store Information about Males which are caught by the fishery
Temp.Uninfected.Male.Catch.Population.Matrix[1:No.of.Uninfected.Male.Cohorts,d] =
(f/Z)*(1-exp(-Z))*Temp.Uninfected.Male.Population.Matrix[1:No.of.Uninfected.Male.Cohorts,d]
Temp.Uninfected.Male.Catch.Weight.Matrix[1:No.of.Uninfected.Male.Cohorts,d] =
Temp.Uninfected.Male.Weight.Matrix[1:No.of.Uninfected.Male.Cohorts,d+1]
Temp.Uninfected.Male.Catch.Length.Matrix[1:No.of.Uninfected.Male.Cohorts,d] =
Temp.Uninfected.Male.Length.Matrix[1:No.of.Uninfected.Male.Cohorts,d+1]
Temp.Uninfected.Male.Catch.Moult.Matrix[1:No.of.Uninfected.Male.Cohorts,d] =
Temp.Uninfected.Male.Moult.Matrix[1:No.of.Uninfected.Male.Cohorts,d+1]
Temp.Uninfected.Male.Catch.Reproduction.Matrix[1:No.of.Uninfected.Male.Cohorts,d] =
Temp.Uninfected.Male.Reproduction.Matrix[1:No.of.Uninfected.Male.Cohorts,d+1]
Temp.Uninfected.Male.Catch.Parasite.Matrix[1:No.of.Uninfected.Male.Cohorts,d] =
Temp.Uninfected.Male.Parasite.Matrix[1:No.of.Uninfected.Male.Cohorts,d+1]


# Calculate the probability of the catch being discarded
Prob.of.Discard <-
Discard.Probability(Temp.Uninfected.Male.Catch.Length.Matrix[1:No.of.Uninfected.Male.Cohorts,d])

# Discards which survive are added back onto the original cohort
Temp.Uninfected.Male.Population.Matrix[1:No.of.Uninfected.Male.Cohorts,d+1] =
```

```
Temp.Uninfected.Male.Population.Matrix[1:No.of.Uninfected.Male.Cohorts,d+1] +
Temp.Uninfected.Male.Catch.Population.Matrix[1:No.of.Uninfected.Male.Cohorts,d] * Prob.of.Discard * ds

# Store information about males which are discarded by the fishery
Temp.Uninfected.Male.Discards.Population.Matrix[1:No.of.Uninfected.Male.Cohorts,d] =
Temp.Uninfected.Male.Catch.Population.Matrix[1:No.of.Uninfected.Male.Cohorts,d] * Prob.of.Discard
Temp.Uninfected.Male.Discards.Weight.Matrix[1:No.of.Uninfected.Male.Cohorts,d] =
Temp.Uninfected.Male.Weight.Matrix[1:No.of.Uninfected.Male.Cohorts,d+1]
Temp.Uninfected.Male.Discards.Length.Matrix[1:No.of.Uninfected.Male.Cohorts,d] =
Temp.Uninfected.Male.Length.Matrix[1:No.of.Uninfected.Male.Cohorts,d+1]
Temp.Uninfected.Male.Discards.Moult.Matrix[1:No.of.Uninfected.Male.Cohorts,d] =
Temp.Uninfected.Male.Moult.Matrix[1:No.of.Uninfected.Male.Cohorts,d+1]
Temp.Uninfected.Male.Discards.Reproduction.Matrix[1:No.of.Uninfected.Male.Cohorts,d] =
Temp.Uninfected.Male.Reproduction.Matrix[1:No.of.Uninfected.Male.Cohorts,d+1]
Temp.Uninfected.Male.Discards.Parasite.Matrix[1:No.of.Uninfected.Male.Cohorts,d] =
Temp.Uninfected.Male.Parasite.Matrix[1:No.of.Uninfected.Male.Cohorts,d+1]


# Store information about males which are landed by the fishery
Temp.Uninfected.Male.Landings.Population.Matrix[1:No.of.Uninfected.Male.Cohorts,d] =
Temp.Uninfected.Male.Catch.Population.Matrix[1:No.of.Uninfected.Male.Cohorts,d] -
Temp.Uninfected.Male.Catch.Population.Matrix[1:No.of.Uninfected.Male.Cohorts,d] *
Prob.of.Discard
Temp.Uninfected.Male.Landings.Weight.Matrix[1:No.of.Uninfected.Male.Cohorts,d] =
Temp.Uninfected.Male.Weight.Matrix[1:No.of.Uninfected.Male.Cohorts,d+1]
Temp.Uninfected.Male.Landings.Length.Matrix[1:No.of.Uninfected.Male.Cohorts,d] =
Temp.Uninfected.Male.Length.Matrix[1:No.of.Uninfected.Male.Cohorts,d+1]
Temp.Uninfected.Male.Landings.Moult.Matrix[1:No.of.Uninfected.Male.Cohorts,d] =
Temp.Uninfected.Male.Moult.Matrix[1:No.of.Uninfected.Male.Cohorts,d+1]
Temp.Uninfected.Male.Landings.Reproduction.Matrix[1:No.of.Uninfected.Male.Cohorts,d] =
Temp.Uninfected.Male.Reproduction.Matrix[1:No.of.Uninfected.Male.Cohorts,d+1]
Temp.Uninfected.Male.Landings.Parasite.Matrix[1:No.of.Uninfected.Male.Cohorts,d] =
Temp.Uninfected.Male.Parasite.Matrix[1:No.of.Uninfected.Male.Cohorts,d+1]


##################################################


# Reproduction:

if (d==213){

No.of.Uninfected.Female.Cohorts.Laying.Eggs <-  No.of.Uninfected.Female.Cohorts
No.of.Infected.Female.Cohorts.Laying.Eggs <-  No.of.Infected.Female.Cohorts

Uninfected.No.of.Eggs <- numeric()
Infected.No.of.Eggs <- numeric()

for (n in 1:No.of.Uninfected.Female.Cohorts.Laying.Eggs){
Uninfected.No.of.Eggs[n] <- Temp.Uninfected.Female.Reproduction.Matrix[n,d]/ce}

for (n in 1:No.of.Infected.Female.Cohorts.Laying.Eggs){
Infected.No.of.Eggs[n] <- Temp.Infected.Female.Reproduction.Matrix[n,d]/ce}

}


if (y>1 && d==182 && (sum(Uninfected.No.of.Eggs)+sum(Infected.No.of.Eggs)) > 0){
```

```
# Calculate the amount of eggs produced
Uninfected.Egg.Production <- numeric()
Infected.Egg.Production <- numeric()

for (n in 1:No.of.Uninfected.Female.Cohorts.Laying.Eggs){
Uninfected.Egg.Production[n] <- Temp.Uninfected.Female.Population.Matrix[n,d-60]*Uninfected.No.of.Eggs[n]
}

for (n in 1:No.of.Infected.Female.Cohorts.Laying.Eggs){
Infected.Egg.Production[n] <- Temp.Infected.Female.Population.Matrix[n,d-60]*Infected.No.of.Eggs[n]
}


Total.Egg.Production = sum(Uninfected.Egg.Production)+sum(Infected.Egg.Production)

Total.Larval.Production = kappa_1 * Total.Egg.Production

Potential.Recruits = kappa_2 * Total.Larval.Production

# Calculate Total Biomass
Total.Biomass <- sum(Temp.Uninfected.Female.Weight.Matrix[1:Max.Uninfected.Cohorts,d]*
Temp.Uninfected.Female.Population.Matrix[1:Max.Uninfected.Cohorts,d], na.rm=TRUE) +
sum(Temp.Uninfected.Male.Weight.Matrix[1:Max.Uninfected.Cohorts,d]*
Temp.Uninfected.Male.Population.Matrix[1:Max.Uninfected.Cohorts,d], na.rm=TRUE) +
sum(Temp.Infected.Female.Weight.Matrix[1:Max.Infected.Cohorts,d]*
Temp.Infected.Female.Population.Matrix[1:Max.Infected.Cohorts,d], na.rm=TRUE) +
sum(Temp.Infected.Male.Weight.Matrix[1:Max.Infected.Cohorts,d]*
Temp.Infected.Male.Population.Matrix[1:Max.Infected.Cohorts,d], na.rm=TRUE)


Actual.Recruits = (Potential.Recruits * exp(-Total.Biomass/B0))


# Females

# Identify cohort to be replaced
if(No.of.Uninfected.Female.Cohorts<Max.Uninfected.Cohorts){
Uninfected.Female.Cohort.Marker <- No.of.Uninfected.Female.Cohorts+1
}else{
Uninfected.Female.Cohort.Marker <- which.min(Temp.Uninfected.Female.Population.Matrix[1:Max.Uninfected.Cohorts,d+1])}

Temp.Uninfected.Female.Population.Matrix[Uninfected.Female.Cohort.Marker,d+1] <- Actual.Recruits/2
Temp.Uninfected.Female.Weight.Matrix[Uninfected.Female.Cohort.Marker,d+1] <- W_Init
Temp.Uninfected.Female.Length.Matrix[Uninfected.Female.Cohort.Marker,d+1] <- L_Init_Female
Temp.Uninfected.Female.Moult.Matrix[Uninfected.Female.Cohort.Marker,d+1] <- 1
Temp.Uninfected.Female.Reproduction.Matrix[Uninfected.Female.Cohort.Marker,d+1] <- 0
Temp.Uninfected.Female.Parasite.Matrix[Uninfected.Female.Cohort.Marker,d+1] <- 0

No.of.Uninfected.Female.Cohorts <- No.of.Uninfected.Female.Cohorts + 1
if(No.of.Uninfected.Female.Cohorts > Max.Uninfected.Cohorts){No.of.Uninfected.Female.Cohorts = Max.Uninfected.Cohorts}



# Males

# Identify cohort to be replaced
if(No.of.Uninfected.Male.Cohorts<Max.Uninfected.Cohorts){
```

```
Uninfected.Male.Cohort.Marker <- No.of.Uninfected.Male.Cohorts+1
}else{
Uninfected.Male.Cohort.Marker <- which.min(Temp.Uninfected.Male.Population.Matrix[1:Max.Uninfected.Cohorts,d+1])}

Temp.Uninfected.Male.Population.Matrix[Uninfected.Male.Cohort.Marker,d+1] <- Actual.Recruits/2
Temp.Uninfected.Male.Weight.Matrix[Uninfected.Male.Cohort.Marker,d+1] <- W_Init
Temp.Uninfected.Male.Length.Matrix[Uninfected.Male.Cohort.Marker,d+1] <- L_Init_Male
Temp.Uninfected.Male.Moult.Matrix[Uninfected.Male.Cohort.Marker,d+1] <- 1
Temp.Uninfected.Male.Reproduction.Matrix[Uninfected.Male.Cohort.Marker,d+1] <- 0
Temp.Uninfected.Male.Parasite.Matrix[Uninfected.Male.Cohort.Marker,d+1] <- 0

No.of.Uninfected.Male.Cohorts <- No.of.Uninfected.Male.Cohorts + 1
if(No.of.Uninfected.Male.Cohorts > Max.Uninfected.Cohorts){No.of.Uninfected.Male.Cohorts = Max.Uninfected.Cohorts}


}}


# Extract relevant information (varies with model run) and re-load temporary matrices for the following year.
source('Data_Extraction.R')
source('Reload_Temp_Table.R')

}
```

Appendix B

Converting ODEs to Coupled Difference Equations

B.1 Cohort Size

The number of individuals in each cohort, N, is tracked using Equation 3.1 (shown again below for convenience):

$$\frac{dN}{dt} = -ZN$$

This is a first order separable ODE, which can be solved as follows

$$\begin{aligned} \int \frac{1}{N} dN &= -\int Z dt \\ \ln(N) &= -Zt + c \\ N &= e^{-Zt+c} \end{aligned}$$

When t=0, $N = N_0$. Therefore,

$$\begin{aligned} N_0 &= e^{-Z(0)+c} \\ N_0 &= e^c \\ \ln(N_0) &= c \end{aligned}$$

Hence

$$\begin{aligned} N &= e^{-Zt+\ln(N_0)} \\ N &= N_0 e^{-Zt} \end{aligned}$$

The ODE can therefore be rewritten as a difference equation:

$$N_{t+1} = N_t e^{-Z}$$

where N_t and N_{t+1} are the number of individuals at time step 't' and 't+1' respectively.

B.2 Weight

The weight of individuals, W, is tracked using Equation 3.3 (shown again below for convenience):

$$\frac{dw}{dt} = \phi L_n^2 - \mu w - \delta w - \gamma P$$

We can treat this as a first order separable ODE by assuming that the number of parasites, I, and the length of individuals, L, remain constant over time. Hence

$$\int \frac{1}{(\phi L_n^2 - \gamma P) - (\mu + \delta)W} dW = \int 1 dt$$

$$\frac{-1}{(\mu + \delta)} \ln((\phi L_n^2 - \gamma P) - (\mu + \delta)W) = t + c$$

$$\ln((\phi L_n^2 - \gamma P) - (\mu + \delta)W) = -(\mu + \delta)(t + c)$$

$$(\phi L_n^2 - \gamma P) - (\mu + \delta)W = e^{-(\mu+\delta)(t+c)}$$

$$(\mu + \delta)W = e^{-(\mu+\delta)(t+c)} - (\phi L_n^2 - \gamma P)$$

$$W = \frac{e^{-(\mu+\delta)(t+c)} - (\phi L_n^2 - \gamma P)}{(\mu + \delta)}$$

When t=0, $W = W_0$, $P = P_0$, and $L = L_0$. Hence,

$$W_0 = \frac{e^{-(\mu+\delta)(c)} - (\phi L_n^2 - \gamma P_0)}{(\mu + \delta)}$$

$$(\mu + \delta)W_0 = e^{-(\mu+\delta)(c)} - (\phi L_n^2 - \gamma P_0)$$

$$(\mu + \delta)W_0 + (\phi L_n^2 - \gamma P_0) = e^{-(\mu+\delta)(c)}$$

$$\ln((\mu + \delta)W_0 + (\phi L_n^2 - \gamma P_0)) = -(\mu + \delta)(c)$$

$$c = \frac{\ln((\mu + \delta)W_0 + (\phi L_n^2 - \gamma P_0))}{-(\mu + \delta)}$$

Hence

$$W = \frac{e^{-(\mu+\delta)\left(t+\frac{ln(-(\mu+\delta)W_0+(\phi L_t^2-\gamma P_0))}{-(\mu+\delta)}\right)} - (\phi L_0^2 - \gamma P_0)}{-(\mu+\delta)}$$

In reality, the number of parasites, I, and the length of individuals, L, change significantly over time. However, by implementing a relatively short time step of 1 day, the ODE can be written as the following coupled difference equation:

$$W_{t+1} = \frac{e^{-(\mu+\delta)\left(1+\frac{ln(-(\mu+\delta)W_t+(\phi L_t^2-\gamma P_t))}{-(\mu+\delta)}\right)} - (\phi L_t^2 - \gamma P_t)}{-(\mu+\delta)}$$

where W_{t+1} is the weight of individuals at time step 't+1' and W_t, L_t and P_t are the weight, length and parasite burden of of individuals at time step 't'.

B.3 Energy for Reproduction

The amount of energy invested in reproduction, E, is tracked using Equation 3.3 (shown again below for convenience):

$$\frac{dE}{dt} = \delta W$$

We can treat this as a first order separable ODE, by making the simplifying assumption that weight, W, remains constant over time. Hence

$$\int 1 dE = -\int \delta W dt$$
$$E = \delta W t + c$$

When t=0, $E = E_0$ and $W = W_0$. Hence,

$$E_0 = c$$

Therefore

$$E = \delta W_0 t + E_0$$

In reality, weight, W, changes continuously over time. However, by implementing a relatively short time step of 1 day, the ODE can be written as the following coupled difference

equation:

$$E_{t+1} = \delta W_t + E_t$$

where E_{t+1} is the amount of energy invested in reproduction at time 't+1' and W_t, E_t are the weight and amount of energy invested in reproduction at time step 't'.

B.4 Parasite Growth

The number of parasites in each individual, I, is tracked using Equation 3.4 (shown again below for convenience):

$$\frac{dP}{dt} = gP$$

This is a first order separable ODE, which can be solved as follows

$$\int \frac{1}{P} dP = -\int g dt$$
$$ln(P) = gt + c$$
$$P = e^{gt+c}$$

When t=0, $P = P_0$. Therefore

$$P_0 = e^{g(0)+c}$$
$$P_0 = e^c$$
$$\ln(P_0) = c$$

Hence

$$P = e^{gt+\ln(P_0)}$$
$$P = P_0 e^{gt}$$

The ODE can therefore be rewritten as a difference equation:

$$P_{t+1} = P_t e^g$$

where P_t and P_{t+1} are the number of parasites at time step 't' and 't+1' respectively.

Bibliography

Afonso-Dias, M. (1998), Variability of *Nephrops norvegicus* (L.) populations in Scottish waters in relation to the sediment characteristics of the seabed, PhD thesis, University of Aberdeen.

Albalat, A., Collard, A., McAdam, B., Coates, C. and Fox, C. (2016b), 'Physiological condition, short-term survival, and predator avoidance of discarded Norway lobsters *Nephrops norvegicus*', *Journal of Shellfish Research* **35**, 1–13.

Albalat, A., Gornik, S., Beevers, N., Atkinson, R., Miskin, D. and Neil, D. (2012), '*Hematodinium sp.* infection in Norway lobster *Nephrops norvegicus* and its effect on meat quality', *Diseases of Aquatic Organisms* **100**, 105–112.

Albalat, A., Nadler, L., Foo, N., Dick, J., Watts, A., Philip, H., Neil, D. and Monroig, O. (2016a), 'Lipid composition of oil extracted from wasted Norway lobster (*Nephrops norvegicus* heads and comparison with oil extracted from antarctic krill (*Euphasia superba*)', *Marine Drugs* **14**.

Appleton, P. (1996), Investigation on the cytology and life cycle of the parasitic dinoflagellate *Hematodinium sp.* associated with mortality of *Nephrops norvegicus*, PhD thesis, University of Glasgow.

Appleton, P. and Vickerman, K. (1998), '*In vitro* cultivation and developmental cycle in culture of a parasitic dinoflagellate (*Hematodinium sp.*) associated with mortality of Norway lobster (*Nephrops norvegicus*) in British waters', *Paristology* **116**, 115–130.

Bailey, N. and Chapman, C. (1983), 'A comparison of density, length composition and growth of two *Nephrops* populations off the west coast of Scotland', *ICES CM* .

Beevers, N. (2010), Prevalence and life cycle studies on the parasitic dinoflagellate *Hematodinium sp.* from *Nephrops norvegicus* (L.), PhD thesis, University of Glasgow.

Beevers, N., Kilbride, E., Atkinson, R. and Neil, D. (2012), '*Hematodinium* infection seasonality in the Firth of Clyde (Scotland) *Nephrops norvegicus* population: a re-evaluation', *Diseases of Aquatic Organisms* **100**, 95–104.

Bell, M., Tuck, I. and Dobby, H. (2013), *Nephrops Species. Lobsters: Biology, Management, Aquaculture and Fisheries*, 2 edn, Wiley-Blackwell, West Sussex.

Ben-Horin, T., Lafferty, K., Bidegain, G. and Lenihan, H. (2015), 'Fishing diseased abalone to promote yield and conservation', *Philosophical Transactions Royal Society* **371**.

Breiman, L. (2001), *Random Forest. Machine Learning*, 45 edn, 5-32, https://doi.org/10.1023/A:1010933494324.

Briggs, R. and McAliskey, M. (2002), 'The prevalence of *Hematodinium* in *Nephrops norvegicus* from the western Irish Sea', *Journal of the Marine Biological Association of the United Kingdom* **82**, 427–433.

Brylawski, B. and Miller, T. (2006), 'Temperature-dependent growth of the blue crab *Callinectes Sapidus*: a moult process approach', *Canadian Journal of Fisheries and Aquatic Sciences* **63**, 1298–1308.

Butler, M., Tiggelaar, J., Shields, J. and Butler, M. (2014), 'Effects of the parasitic dinoflagellate *Hematodinium perezi* on blue crab (*Callinectes sapidus*) behaviour and predation', *Journal of Experimental Marine Biology and Ecology* **461**, 381–388.

Butler, W. (2007), Modelling the host-parasite interaction between the Norway lobster (*Nephrops norvegicus*) and its dinoflagellate parasite of the genus *Hematodinium*, PhD thesis, University of Glasgow.

Byrd, R., Lu, P., Nocedal, J. and Zhu, C. (1995), 'A limited memory algorithm for bound constrained optimization', *SIAM Journal on Scientific Computing* **16**, 1190–1208.

Campbell, N., Allan, L., Weetman, A. and Dobby, H. (2009), 'Investigating the link between *Nephrops norvegicus* burrow density and sediment composition in Scottish waters', *ICES Journal of Marine Science* **66**, 2052–2059.

Castro, M. (1992), 'A methodology for obtaining information on the age structure and growth rates of the Norway lobster, *Nephrops norvegicus*(L.)(Decapoda. Nephropidae).', *Crustaceana* **63**, 29–43.

Chang, E. and Mykles, D. (2011), 'Regulation of crustacean molting: A review and our perspectives', *General and Comparative Endocrinology* **172**, 323–330.

Chang, Y., Sun, C., Chen, Y. and Yeh, S. (2012), 'Modelling the growth of crustacean species', *Reviews in Fish Biology and Fisheries* **22**, 157–187.

Chapman, C. (1980), Ecology of juvenile and adult *Nephrops*. the biology and management of lobsters, Technical report, London.

Chapman, C. (1982), '*Nephrops* tagging experiments in Scottish waters', *ICES CM* .

Chatton, E. and Poisson, R. (1931), 'Sur l'existence dans le sang des crabes de peridiniencs parasites: Hematodinium perezi n.h., n.sp. (syndinidae)', *Comptes Rendus des Seances Societe de Biologie* **105**, 553–557.

Cowen, R. and Sponaugle, S. (2009), 'Larval dispersal and marine population connectivity', *Annual Review of Marine Science* **1**, 443–466.

de Roos, A. (1988), 'Numerical methods for structured population models: the escalator boxcar train', *Numerical Methods for Partial Differential Equations* **4**, 173–195.

der Molen, J. V., Rogers, S., Ellis, J., Fox, C. and McCloghrie, P. (2007), 'Dispersal patterns of the eggs and larvae of spring-spawning fish in the Irish Sea, UK', *Journal of Sea Research* **58**, 313–330.

Dickey-Collas, M., McQuaid, N., Armstrong, M., Allen, M. and Briggs, R. (2000), 'Temperature-dependent stage duration of Irish Sea *Nephrops* larvae', *Journal of Plankton Research* **22**, 749–760.

Diesing, M., Green, S., Stephens, D., Lark, R., Stewart, H. and Dove, D. (2014), 'Mapping seabed sediments: Comparison of manual, geostatistical, object-based image analysis and machine learning approaches', *Continental Shelf Research* **84**, 107–119.

Dobby, H. (2003), 'Investigating a size-transition matrix approach to the assessment of *Nephrops*', *Working Document for the Working Groups on Nephrops Stocks* .

Dobby, H. (2004), 'More thoughts on a length-based approach to the assessment of Firth of Forth *Nephrops*: incorporation of auxiliary data', *Report of the Working Group on Nephrops Stocks* pp. 407–421.

Dobson, A. and May, R. (1987), 'The effects of parasites on fish populations - theoretical aspects', *International Journal of Parasitology* **17**, 363–370.

Field, R. and Appleton, P. (1995), 'A *Hematodinium*-like dinoflagellate infection of the Norway lobster *Nephrops norvegicus*: observation on pathology and progression of infection', *Diseases of Aquatic Organisms* **22**, 115–128.

Field, R., Chapman, C., Taylor, A., Neil, D. and Vickerman, K. (1992), 'Infection of the Norway lobster *Nephrops norvegicus* by a *Hematodinium*-like species of dinoflagellate on the west coast of Scotland', *Diseases of Aquatic Organisms* **13**, 1–15.

Field, R., Hills, J., Atkinson, R., Magill, S. and Shanks, A. (1998), 'Distribution and seasonal prevalence of the Norway lobster (*Nephrops norvegicus*) around the west coast of Scotland', *ICES Journal of Marine Science* **55**, 846–858.

Fisher, R., Jantsch, M. and Comer, R. (1982), *General Bathymetric chart of the Oceans (GEBCO)*, Canadian Hydrographic Service, Ottowa, Canada.

Fox, C., Albalat, A., Valentinsson, D., Nilsson, H., F. Armstrong, P. R. and Catchpole, T. (2020), 'Survival rates for *Nephrops norvegicus* discarded from Northern European trawl fisheries', *ICES Journal of Marine Science* **77**, 1698–1710.

Fox, C., McCloghrie, P., Young, E. and Nash, R. (2006), 'The importance of individual behaviour for successful settlement of juvenile plaice (*Pleuronectes platessa* L.): a modelling and field study in the eastern Irish Sea', *Fisheries Oceanography* **15**, 301–313.

Frischer, M., Lee, R., Sheppard, M., Mauer, A., Rambow, R., Neumann, M., Brofft, J., Wizenmann, T. and Danforth, J. (2006), 'Evidence for a free-living stage of the blue crab parasitic dinoflagellate, *Hematodinium sp.*', *Harmful Algae* **5**, 548–557.

Gonzalez-Gurriaran, E., Freire, J., Farina, A. and Fernandez, A. (1998), 'Growth at moult and intermoult period in the Norway lobster *Nephrops norvegicus* from Galician waters', *ICES Journal of Marine Science* **55**, 924–940.

Gornik, S., Cassin, A., MacRae, J., Ramaprasad, A., Rchiad, Z., McConville, M., Bacic, A., McFadden, G., Pain, A. and R.F, W. (2015), 'Endosymbiosis undone by stepwise elimination of the plastid in a parasitic dinoflagellate', *Proceedings of the National Academy of Sciences* **112**, 5767–5772.

Gurney, W. and Nisbet, R. (1998), *Ecological Dynamics*, Oxford University Press, Oxford.

Hanif, A., Dyson, W., Bowers, H., Pitula, J., Messick, G., Jagus, R. and Schott, E. (2013), 'Variation in spatial and temporal incidence of the crustacean pathogen *Hematodinium perezi* in environmental samples from Atlantic coastal bays', *Aquatic Biosystems* **9**, 1–13.

Harris, R. and Andrews, M. (2005), 'Physiological changes in the Norway lobster *Nephrops norvegicus* (L.) escaping and discarded from commercial trawls on the west coast of Scotland, 1. Body fluid volumes and haemolymph composition after capture and during recovery', *Journal of Experimental Marine Biology and Ecology* **320**, 179–193.

Haynes, P., Browne, P., Fullbrook, L., Graham, C., Hancox, L., Johnson, M., Lauria, V. and Power, A. (2016), 'Growth in *Nephrops norvegicus* from a tag-recapture experiment', *Scientific Reports* **6**, 35143–35153.

Heath, M., Sabatino, A., Serpetti, N., McCaig, C. and Murray, R. O. (2016), 'Modelling the sensitivity of suspended sediment profiles to tidal current and wave conditions', *Ocean Coastal Management* **147**, 49–66.

Heath, M. and Speirs, D. (2012), 'Changes in species diversity and size composition in the Firth of Clyde demersal fish community (1927-2009)', *Proceedings of the Royal Society of London B.* **279**, 543–552.

Hijmans, R., Williams, E. and Vennes, C. (2012), 'Geosphere: Spherical Trigonometry', *R Project, CRAN* **R Package version 1.2-28**.

Hill, A., Brown, J. and Fernald, L. (1996), 'The western Irish Sea gyre: a retention system for Norway lobster (*Nephrops norvegicus*)?', *Oceanologica Acta* **19**, 357–368.

Hillis, J. (1974), 'Field observations on larvae of the Dublin Bay prawn *Nephrops norvegicus* (L.) in the western Irish Sea', *Irish Fisheries Investigation* **13**, 1–24.

Howard, F. (1989), The Norway lobster, Technical report.

Howard, F. and Hall, W. (1983), 'Some observations on the biometrics of *Nephrops norvegicus* (L.) in Scottish waters', *ICES, Doc. Shellfish Comm.* **CM 1983/K:36**.

Howarth, L., Roberts, C., Thurstan, R. and Stewart, B. (2014), 'The unintended consequences of simplifying the sea: making the case for complexity', *Fish and Fisheries* **15**, 690–711.

Huang, Z., Nichol, S., Siwabessy, J., Daniell, J. and Brooke, B. (2012), 'Predictive modelling of seabed sediment parameters using multibeam acoustic data: a case study on the Carnarvon Shelf, Western Australia', *International Journal of Geographical Information Science* **26**, 283–307.

ICES (2009), Report of the Benchmark Workshop on Nephrops (WKNEPH), Technical report.

ICES (2015), Report of the Working Group on the Celtic Sea Eco-region (WGCSE), Technical report.

ICES (2019), Norway lobster (*Nephrops norvegicus*) in Division 6.a, Functional Unit 13 (West of Scotland, the Firth of Clyde, and the Sound of Jura), Technical report.

Kilada, R. and Driscoll, J. (2017), 'Age determination in crustaceans: a review', *Hydrobiologia* **799**, 21–36.

Li, C., Wheeler, K. and Shields, J. (2011), 'Lack of transmission of *Hematodinium sp.* in the blue crab *Callinectes sapidus* through cannibalism', *Diseases of Aquatic Organisms* **96**, 249–258.

Marta-Almeida, M., J. Dubert, A. P., dos Santos, A. and Queiroga, H. (2008), 'A modelling study of the Norway lobster *Nephrops norvegicus* larval dispersal in southern Portugal: predictions of larval wastage and self-recruitment in the Algarve stock', *Canadian Journal of Fisheries and Aquatic Sciences* **65**, 2253–2268.

McIntyre, F., Fernandes, P. and Turrell, W. (2012), 'Clyde Ecosystem Review', *Scottish Marine and Freshwater Science Report* **3**, 1–123.

Meyers, T., Koeneman, T., Botelho, C. and Short, S. (1987), 'Bitter crab disease: A fatal dinoflagellate infection and marketing problem for Alaskan tanner crab *Chionoecetes bairdi*', *Diseases of Aquatic Organisms* **9**, 37–43.

Milligan, R., Alalbat, A., Atkinson, R. and Neil, D. (2009), 'The effects of trawling on the physical condition of the lobster *Nephrops norvegicus* in relation to the seasonal cycles in the Clyde Sea Area', *ICES Journal of Marine Science* **66**, 488–494.

Nicolle, A., Dumas, F., Foveau, A., Foucher, E. and Thiebaut, E. (2013), 'Modelling larval dispersal of the king scallop (*Pecten maximus*) in the English Channel: examples from the Bay of Saint-Brieuc and the Bay of Seine', *Ocean Dynamics* **63**, 661–678.

North, E., Schlag, Z., Hood, P., Li, M., Zhong, L., Gross, T. and Kennedy, V. (2008), 'Vertical swimming behaviour influences the dispersal patterns of simulated oyster larvae in a coupled particle-tracking and hydrodyanamic model of Chesapeake Bay', *Marine Ecology Progress Series* **359**, 99–115.

O'Sullivan, D., Lordan, C., Doyle, J., Berry, A. and Lyons, K. (2015), 'Metapopulation connectivity via larval transport of the Norway lobster *Nephrops norvegicus* in waters around Ireland: a modelled approach', *Marine Ecology Progress Series* **534**, 95–106.

Pagenkopp-Lohan, K., Reece, K., Miller, T., Wheeler, K., Small, H. and Shields, J. (2012), 'The role of alternate hosts in the ecology and life history of *Hematodinium sp.*, a parasitic dinoflagellate of the blue crab (*Callinectes sapidus*)', *Journal of Parasitology* **98**, 73–84.

Pateiro-Lopez, B. and Rodriguez-Casal, A. (2010), 'Generalizing the convex hull of a sample', *The R Package Alphahull* **34**, 1–28.

Phelps, J., Polton, J., Souza, A. and Robinson, L. (2015), 'Behaviour influences larval dispersal in shelf sea gyres: *Nephrops norvegicus* in the Irish Sea', *Marine Ecology Progress Series* **518**, 177–191.

Powell, A. and Erikkson, S. (2013), *Reproduction: Life Cycle, Larvae and Larviculture. The Ecology and Biology of Nephrops norvegicus*, eds. M.L. Johnson and M.P. Johnson edn, Academic Press, Oxford.

Punt, A., Deng, R., Dichmont, C., Kompas, T., Venables, W., Zhou, S., Pascoe, S., Hutton, T., Kenyon, R., van der Velde, T. and Kienzle, M. (2010), 'Integrating size-structured assessment and bio-economic management advice in Australia's northern prawn fishery', *ICES Journal of Marine Science* **67**, 1785–1801.

Punt, A., Hobday, D., Gerhard, J. and Troynikov, V. (2006), 'Modelling growth of rock lobsters, *Jasus edwardsii*, off Victoria, Australia using models that allow for individual variation in growth parameters', *Fisheries Research* **82**, 119–130.

R Core Team (2014), *R: A Language and Environment for Statistical Computing*, R Foundation for Statistical Computing, Vienna, Austria.
URL: *http://www.R-project.org/*

Robins, P., Neill, S., Gimenez, L., Jenkins, S. and Malham, S. (2013), 'Physical and biological controls on larval dispersal and connectivity in a high energetic shelf sea', *Limnology and Oceanography* **58**, 505–524.

Rowley, A., Smith, A. and Davies, C. (2015), 'How does the dinoflagellate parasite *Hematodinium* outsmart the immune system of its crustacean hosts?', *PLoS pathogens* **11**, 1–9.

Sabatino, A. (2016), Modelling the physical oceanography of the Clyde Sea and of the East Coast of Scotland, PhD thesis, University of Strathclyde.

Sadykova, D., Skurdal, J., Sadykov, A., Taugbol, T. and Hessen, D. (2009), 'Modelling crayfish population dynamics using catch data: A size-structured model', *Ecological Modelling* **220**, 2727–2733.

Shields, J. (1994), 'The parasitic dinoflagellates of marine crustaceans', *Annual Review of Fish Diseases* **4**, 241–271.

Siddeek, M., Zheng, J., Punt, A. and Vanek, V. (2016), 'Estimation of size-transition matrices with and without moult probability for Alaska golden crab using tag-recapture data', *Fisheries Research* **180**, 161–168.

Simons, R., Siegel, D. and Brown, K. (2013), 'Model sensitivity and robustness in the estimation of larval transport: A study of particle tracking parameters', *Journal of Marine Systems* **119-120**, 19–29.

Small, H., Wilson, S., Neil, D., Hagan, P. and Coombs, G. (2002), 'Detection of the parasitic dinoflagellate *Hematodinium* in the Norway lobster *Nephrops norvegicus* by elisa', *Diseases of Aquatic Organisms* **52**, 175–177.

Smith, R. (1987), The biology of larval and juvenile *Nephrops norvegicus* (L.) in the Firth of Clyde, PhD thesis, University of Glasgow.

Stentiford, G., Neil, D., Albalat, A., Milligan, R. and Bailey, N. (2015), 'The effect of parasitic infection by *Hematodinium sp.* on escape swimming and subsequent recovery in the Norway lobster, *Nephrops norvegicus* (L.)', *Journal of Crustacean Biology* **35**, 1–10.

Stentiford, G., Neil, D. and Atkinson, R. (2001a), 'Alteration of burrow related behaviour of the Norway lobster, *Nephrops norvegicus*, during infection by the parasitic dinoflagellate *Hematodinium*', *Marine and Freshwater Behaviour and Physiology* **34**, 139–156.

Stentiford, G., Neil, D. and Atkinson, R. (2001b), 'The relationship of *Hematodinium* infection prevalence in a Scottish *Nephrops norvegicus* population to season, moulting and sex', *ICES Journal of Marine Science* **58**, 814–823.

Stentiford, G., Neil, D., Atkinson, R. and Bailey, N. (2000), 'An analysis of swimming performance in the Norway lobster, *Nephrops norvegicus* L. infected by a parasitic dinoflagellate of the genus *Hematodinium*', *Journal of Experimental Marine Biology and Ecology* **24**, 169–181.

Stentiford, G., Neil, D. and Coombs, G. (2001c), 'Development and application of an immunoassay diagnostic technique for studying *Hematodinium* infections in *Nephrops norvegicus* populations', *Diseases of Aquatic Organisms* **46**, 223–229.

Stentiford, G. and Shields, J. (2005), 'A review of the parasitic dinoflagellates *Hematodinium* species and *Hematodinium*-like infection in marine crustaceans', *Diseases of Aquatic Organisms* **66**, 47–70.

Stephens, D. and Diesing, M. (2015), 'Towards quantitative spatial models of seabed sediment composition', *PLoS ONE* **10**.

Talbot, S., Widdicombe, S., Hauton, C. and Bruggeman, J. (2019), 'Adapting the dynamic energy budget (DEB) approach to include non-continuous growth (moulting) and provide better predictions of biological performance in crustaceans', *ICES Journal of Marine Science* **76**, 192–205.

Tew, K. H. I., Atkinsona, R. and Roberts, E. (2011), 'Occurrence of the parasite genus *Hematodinium* (Alveolata: Syndinea) in the water column', *Journal of Eukaryotic Microbiology* **58**, 446–451.

Thurstan, R. and Roberts, C. (2010), 'Ecological meltdown in the Firth of Clyde, Scotland: two centuries of change in a coastal marine ecosystem', *Plos One* **7**, e11767.

Tuck, I., Chapman, C. and Atkinson, R. (1997), 'Population biology of the Norway lobster *Nephrops norvegicus* (L.) in the Firth of Clyde, Scotland - I: Growth and Density', *ICES Journal of Marine Science* **54**, 125–135.

Ulmestrand, M. and Eggert, H. (2001), 'Growth of Norway lobster, *Nephrops norvegicus* (Linnaeus 1758), in the Skagerrak, estimated from tagging experiments and length frequency data', *ICES Journal of Marine Science* **58**, 1326–1334.

Verdoit, M., Pelletier, D. and Talidec, C. (1999), 'A growth model that incorporates individual variability for the Norway lobster population (*Nephrops norvegicus*, L. 1758) from the Bay of Biscay', *ICES Jounral of Marine Science* **56**, 734–745.

Von-Bertalanffy, L. (1938), 'A quantitative theory of organic growth', *Human Biology* **10**, 181–213.

Walker, A., Lee, R. and Frischer, M. (2009), 'Transmission of the parasitic dinoflagellate *Hematodinium sp.* infection in blue crabs *Callinectes sapidus* by cannibalism', *Diseases of Aquatic Organisms* **85**, 193–197.

Ward, S., Neill, S., Landeghem, K. V. and Scourse, J. (2015), 'Classifying seabed sediment type using simulated tidal-induced bed shear stress', *Marine Geology* **367**, 94–104.

Watts, A., Alalbat, A., Smith, I., Atkinson, R. and Neil, D. (2016), 'Seasonal nutritional status in Norway lobsters, *Nephrops norvegicus* (L.): are females nutritionally compromised over the winter?', *Marine Biology Research* .

Wessel, P. and Smith, W. (1996), 'A global, self-consistent, hierarchical, high-resolution shoreline', *Journal of Geophysical Research* **101**, 8741–8743.

Wileman, D., Sangster, G., Ulmestrand, M., Soldal, A. and Harris, R. (1999), 'Roundfish and *Nephrops* survival after escape from commercial fishing gear', *Final report to European Commission, Brussels, FAIR-CT95-0753* .

Wilson, R., Speirs, D., Sabatino, A. and Heath, M. (2018), 'A synthetic map of the northwest European Shelf sedimentary environment for application in Marine Science', *Earth System Science Data* **10**, 109–130.

Wood, C., Lafferty, K. and Micheli, F. (2010), 'Fishing out marine parasites? impacts of fishing on rates of parasitism in the ocean', *Ecology Letters* **13**, 761–775.

Wright, M. and Ziegler, A. (2017), 'Ranger: A fast implementation of random forests for high dimensional data in C++ and R', *Journal of Statistical Software* **77**.

Zheng, J., Murphy, M. and Kruse, G. (1994), 'A length-based population model and stock-recruitment relationships for red king crab, *Paralithodes camtschaticus*, in Bristol Bay, Alaska', *Canadian Journal of Fisheries and Aquatic Sciences* **52**, 1229–1246.